Late Holocene aeolian activity and landscape development in a northern German inland dune system

An approach to spatially reconstruct past landscape dynamics using geoarchaeological records and scientific visualization techniques

Dissertation
zur Erlangung des Doktorgrades
der Mathematisch-Naturwissenschaftlichen Fakultät
der Christian-Albrechts-Universität zu Kiel

vorgelegt von
Uta Lungershausen

Mainz, 2016

Erster Gutachter: Prof. Dr. Rainer Duttmann
Zweiter Gutachter: Prof. Dr. Hans-Rudolf Bork

Tag der mündlichen Prüfung: 13. September 2016
Zum Druck genehmigt: 13. September 2016

gez. Prof. Dr. Natascha Oppelt (Dekanin)

Eidesstattliche Erklärung

Die vorgelegte Arbeit »*Late Holocene Aeolian activity and landscape development in a northern German inland dune system - An approach to spatially reconstruct past landscape dynamics using geoarchaeological records and scientific visualization techniques*« ist nach Inhalt und Form meine eigene, abgesehen von der Beratung meiner Betreuerinnen und Betreuer. Der vorliegende Text wurde nicht und auch nicht zum Teil einer anderen Stelle im Rahmen eines Prüfungsverfahren vorgelegt, veröffentlicht oder zur Veröffentlichung eingereicht. Diese Arbeit wurde unter Einhaltung guter wissenschaftlicher Praxis nach den Regeln der Deutschen Forschungsgemeinschaft erstellt.

.....

Uta Lungershausen

Für Edgar

Abstract

Aeolian processes, characterised by erosion, transport and deposition of sediment of the Earth´s surface, occur as natural land-forming processes in most arid and semi-arid region, but are locally also a phenomenon of temperate climate areas. Within Northern-central Europe cover sands of cold-climate aeolian origin as well as drifting sands of anthropogenic origin are found widespread within the European Sand Belt (ESB). Cover sands mainly formed during the Late Pleistocene (Older and Younger Dryas) until widespread and ongoing stabilization took place with the onset of the Holocene climate amelioration and re-vegetation. From the Neolithic Period until present several re-sedimentations of the Pleistocene sand sheet deposits as drift sands occurred, which was induced by human activities such as woodland clearings, agricultural land-use and grazing. Holocene aeolian dynamics thus consist of complex phases of Aeolian activity and landscape stabilization, respectively, which are attributed primarily to changing patterns of human impact.

The purpose of this thesis is to investigate and spatially reconstruct long-term aeolian landscape dynamics using a small inland dune system in Northern Germany as a case study. Against the background of the dune formation of the Kuhharder Hill dune (KHD), this thesis investigated the timing, causes, effects and magnitude of phases of aeolian activity since the beginning of the Holocene. In order to reconstruct past landscape changes and palaeo-environmental conditions, a multidisciplinary approach was chosen that combined pedological and geomorphologic analysis of aeolian sediments and past dune surfaces, chronology (^{14}C and OSL dating), detailed stratigraphy, as well as palaeo-botanical records of charcoal and pollen.

Four phases of aeolian sedimentation, and each with increasing magnitude, have been identified for the last ~ 2500 years, which have been linked to the historical settlement and land-use. Human activities during Roman Iron Age Period had only low impacts on the landscape, and provided the lowest deposition rate. Since the ~ 700 AD medieval deforestation and overexploitation of the land resulted in rapid dune-building and the highest aeolian accumulation rates (< 800 years for ~ 45 % of the total net sediment mass) in the KHD record since the deposition of aeolian sands began during the Late Pleistocene. The end of the medieval deposition phase occurs surprisingly abrupt

and is coincident with the simultaneous abandonment of the nearby village Hyoldelunt. The observed feedback structures of human-environmental interactions appear to be cyclical: Due to poor land-use management in historic as well as recent times severe drifting of sand and the accumulation of dunes occurred, forcing the local farmers to abandon theirs field and even their settlement, and finally, after a phase of recovery, adapting more extensive land management practices.

Anthracological analysis within this thesis contributed to the reconstruction of local vegetation of the different dune surfaces and gave insights into the wood species composition prior erosional events. Due to the ecological characteristics of the woody species that occur, two different local and extra-local/regional source areas of charcoal were differentiated. The taxonomical selection of datable charcoal turned out to be indispensable for the development and interpretation of the dune stratigraphy.

On the basis of palaeo-environmental results, and the creation of digital elevation models of buried dune surfaces, 3D visualisation techniques were used in order to visually reconstruct the past environmental conditions and local dune development. A visualization model was developed which to account of the varying quality concerning temporal and spatial resolution of the geoarchaeological data. Photorealistic landscape visualizations of local and regional scale landscape reconstruction were developed using Autodesk® 3ds Max® 8 and Visual Nature Studio™2.86. Additionally, interactive visualization techniques were used that implements features such as flexible navigation, queries of attribute data. This technique ensures the interactive exploration of surface structures and is complemented by high spatial and palaeoenvironmental landscape accuracy. By merging geoarchaeological records with scientific visualization techniques this thesis supports researchers as well as educators to gain deeper insights into human-induced changes of landscapes in the past.

Zusammenfassung

Äolische Prozesse treten als natürliche Phänomene in den ariden und semi-ariden Regionen der Erde auf, lassen sich aber auch lokal in humideren Gebieten beobachten. Der äolische Formenschatz Europas im sogenannten European Sand Belt (ESB) umfasst neben Flugsanddecken (cover sands) pleistozänen Ursprungs auch jüngere Flugsand- und Dünenbildungen (drift sand), die auf eine anthropogen bedingte äolische Aktivität zurückzuführen sind. Die Morphogenese des äolischen Reliefs im Holozän zeichnet sich durch zeitlich alternierende Stabilität- und Aktivitätsphasen, wobei innerhalb der Stabilitätsphasen die Etablierung einer mehr oder minder geschlossenen Vegetationsdecke mit entsprechender Bodenbildung erfolgt, hingegen – während der Aktivitätsphasen – durch anthropogene Eingriffe die anstehenden verwehungsfähigen Substrate reaktiviert werden.

Am Beispiel der Entwicklung einer Binnendünenlandschaft in Norddeutschland sollen in der vorliegenden Arbeit die langfristige äolische Dynamik und ehemalige Mensch-Umwelt-Interaktionen räumlich rekonstruiert wie auch quantifiziert werden. Im Mittelpunkt steht die Erörterung der Ursachen sowie die Untersuchung der Auswirkungen und Intensität von Phasen äolischer Aktivität und Winderosionsereignissen seit dem Holozän im Raum Joldelund. Zur Rekonstruktion vergangener Umweltzustände und Landschaftsveränderungen wurde ein multidisziplinärer Ansatz gewählt, der bodenkundliche sowie geomorphologische Analysen der äolischen Sedimente und begrabenen Dünenoberflächen, Datierungsmethoden (^{14}C und OSL Datierung), detaillierte Stratigraphie sowie paläobotanische Methoden (Holzkohle- und Pollenanalyse) verbindet.

Es konnten vier Aufwehungsphasen mit zunehmender Intensität innerhalb der letzten ~ 2500 Jahren im Untersuchungsgebiet nachgewiesen werden. Die früheste Phase anthropogen bedingter äolischer Aktivität mit Flugsandsedimentation datiert in die Römische Eisenzeit. Menschliche Eingriffe in die Landschaften hatten nur lokalen Einfluss, was sich in den geringsten Depositionsraten widerspiegelt. Weiträumige Entwaldung und Intensivierung der Landwirtschaft seit ~ 700 n. Chr. führte zu einer Destabilisierung der vorher stabilen Oberflächen und einem signifikanten Anstieg der äolischen Aktivität. Die Reaktivierung der zuvor festgelegten Sande hatte die Bildung mächtiger Dünensedimente unter höchsten Depositi-

onsraten zur Folge (~ 45 % der Netto-Sedimentmasse in weniger als 800 Jahren). Das Ende der mittelalterlichen Äktivitätsphase tritt überraschend abrupt auf und fällt zeitlich dem Wüstfallen des nahegelegenen Dorfes Hyoldelunt zusammen. Die beobachteten Feedback-Strukturen der Mensch-Umwelt-Interaktionen scheinen im Untersuchungsgebiet zyklisch aufzutreten: Unangepasste Landnutzung löste verstärkt Bodenerosion durch Wind aus; die damit verbundene Reaktivierung äolischer Sande führte zur Ablagerung weitläufiger Flugsanddecken und Dünen. Die sozioökonomischen Auswirkungen der Winderosionsereignisse zwangen die lokale Bevölkerung, Ackerflächen und Siedlung aufzugeben und, nach einer erneuten Stabilisierung der Landschaft, schließlich nachhaltige Landnutzungsformen einzusetzen.

Anthrakologische Untersuchungen im Rahmen der Arbeit trugen zur Rekonstruktion der lokalen Vegetationsgeschichte bei und gaben Einblicke in die Zusammensetzung der Wälder vor den Erosionsereignissen. Auf Grund der ökologischen Charakteristiken der identifizierten Holzarten, konnten lokale und extra-lokale/regionale Auswehungsgebiete der Holzkohle unterschieden werden. Zudem war die taxonomische Selektion von datierbaren Holzkohlen unverzichtbar für die Auswertung der dünenstratigraphischen Befunde.

Basierend auf den geoarchäologischen Befunden und digitalen Geländemodellen der ehemaligen Dünenoberflächen wurde ein Visualisierungsmodell entwickelt, mit dem Ziel, einerseits wissenschaftlich belastbare 3D-Landschaftsvisualisierungen zu erstellen und andererseits, geoarchäologische Befunde der breiten Öffentlichkeit verständlich zu präsentieren. Mit unterschiedlicher Visualisierungssoftware (Autodesk® 3ds Max®, Visual Nature Studio™2.86, a3Dc) wurden Szenarien der Landschafts- und Dünengenese datenangepasst auf unterschiedlichen geographischen Skalen visualisiert. Über die Integration einer 3D-Echtzeit-Umgebung sowie einer multimedialen Lernumgebung fördert unser Visualisierungsmodell die Interpretation historischer Umweltdaten und den Dialog zwischen Wissenschaft und Öffentlichkeit.

Danksagung

Es ist ein seltsames Gefühl, nach über acht Jahren Promotionszeit nichts mehr schreiben zu müssen als die Danksagung. Vieles geht einem durch den Kopf: die Zweifel, ob die Arbeit gelungen ist, die Sorge, das ein oder andere Kapitel doch noch überarbeiten zu müssen, und die Erleichterung, dieses Projekt ›Doktorarbeit‹ nun loslassen zu dürfen. Umso schöner ist es, sich jetzt, in dieser Danksagung, den Menschen widmen zu dürfen, die mich bei dieser Arbeit auf unterschiedliche Weise unterstützt haben. Zunächst möchte ich herzlichst meinem Doktorvater Herrn Prof. Dr. Rainer Duttmann für seine wissenschaftliche Betreuung und seine Geduld während meiner langen Promotionsphase danken. Auf seine Anregung hin hatte ich mich um ein Stipendium an der damals neugegründeten Graduiertenschule Human Development in Landscapes beworben, die diese Arbeit finanziell gefördert hat. Mein besonderer Dank gilt auch meinem zweiten Betreuer Prof. Dr. Hans-Rudolf Bork für die Begeisterung und das Engagement, mit dem er meine Arbeit betreut hat.

Ich danke Carina Heinrich, Claus-Christian Hinrichs und Sven Köllner für ihren unerschütterlichen (und kälteresistenten) Support bei meinen Geländearbeiten von November bis März (und ja, 2008/09 war ein wirklich kalter Winter!) sowie Antje Berger, Ursula Bock und Julia Becker für ihre Hilfe bei der Bodenanalytik. Für all die zahlreichen Denkanstöße, fachlichen Diskussionen und Unterstützung im Verlauf dieser Arbeit möchte ich zudem meiner ehemaligen Kollegin am Geographischen Institut der CAU, Kirstin Marx, danken. Für eine wunderbare gemeinsame Zeit als office mates danke ich Yang Wang: Thank you for becoming such a great friend! Dass ich überhaupt zur 3D-Visualisierung gekommen bin, habe ich vor allem Rolf Gabler-Mieck zu verdanken. Ohne ihn wäre vieles im Rahmen dieser Arbeit nicht möglich gewesen, wie z. B. die tachymetrischen Vermessung der rezenten Dünenoberfläche oder die interaktiven Visualisierungen mit der Echtzeitumgebung a3Dc. Ich bin zutiefst traurig, dass ich ihm meinen Dank nicht mehr persönlich übermitteln kann.

Die Möglichkeit, diese Arbeit trotz meiner Tätigkeit an der Hochschule Ludwigshafen innerhalb von wenigen Monaten fertigzustellen, habe ich dem Verständnis und der Unterstützung von Imke Buß zu verdanken (ich weiß, Du magst das nicht mehr hören, aber dennoch: Ich hätte es nicht ohne diese Hilfe geschafft!). Mein besonderer Dank gilt auch meinem Kol-

legen und Freund Georg Emunds – meinem persönlichen ClipArt-Master und Latein-Coach. Dass Du Dich ein Wochenende lang mit Uta der Übersetzung einer mittellateinischen Schrift und der Bedeutung des Wortes ›Ellumzuzel‹ gewidmet hast, vergess' ich Dir nie!
Annegret: Merci! Tausend Dank! Dafür, dass wir so ein tolles Paper geschrieben haben, dass Du nicht müde geworden bist, an den Erfolg dieser Arbeit (und an mich) zu glauben, dass Du mit so ansteckender Begeisterung Wissenschaftlerin bist! Katinka: Danke für Deine wunderbare Freundschaft, und dass Du mich bei allen wichtigen Entscheidungen unterstützt! Gerry: ♥! Paps, Mutsch, Anni, Tina: Ihr seid sowieso die Besten!

Table of Content

List of Figures

List of Tables

1 Introduction

Landscapes are dynamic systems that respond to changes in the environment, whether they are due to natural processes within the climate system or a result of human interference. The latter refers particularly to sustainable changes of landscapes occurred as a result of accelerated soil erosion since the Neolithic land acquisition and use (Warren and Bärring 2003). By reducing and removing vegetation cover for land-use purposes, the soil surface remained uncovered for longer periods, becoming prone to soil erosion processes. During times of erosive rainfalls or strong winds, top soil may be detached, transported and deposited downhill or across open space over considerable distances. Accelerated soil erosion can have important on-sites (e.g. loss of soil and organic matter, nutrient loss, decrease of soil fertility) and off-sites (e.g. sedimentation in water bodies, eutrophication, and loss in biodiversity) effects (Pimentel et al. 1995), causing valuable land to become unproductive and often eventually abandoned (Pimentel 2006). Soil erosion can be occurring as both, a very slow process that continues relatively unnoticed or at an alarming rate, causing serious loss of topsoil and soil degradation over a very short period of time. In central Europe, landscapes have experienced long-term histories of human-induced landscape changes that occurred in several stages (e.g. Neolithic period, Bronze Age, Iron Age, Medieval Times, Modern Times) from the beginning of the Holocene until present times, and which have left erosional forms and sediments related to past land-use (Bork et al. 1998). To understand our present day landscape a historic perspective is needed: on past soil erosion processes and land-use changes, the magnitude and rates of those changes and how they may influence present and future trajectories of geomorphic response. Investigating anthropogenic sediments – using them as palaeo-archives for human-environmental interaction – is a long tradition of interdisciplinary research (Lang and Bork 2003), since these sediments »contain cultural artifacts, biological evidence of former ecosystems (pollen, macrofossils, etc.) or geochemical and mineralogical signals that record the sources of sediment and the character of land-use before and after contact« (James 2013, p. 16). In terms of past wind erosion, the investigation on sedimentary records of aeolian deposits, such as inland dunes and aeolian drift sands, can provide valuable information on past human-envi-

ronmental interactions and past land-use changes in aeolian landscapes. Aeolian sediments are especially sensitive to environmental and land-use changes, mainly because their geomorphic response to human impact often occurs relatively fast. The geoarchaeological, geomorphological and pedological analysis of soil-sediment-sequences of inland dunes in combination with modern dating methods may thus provide valuable information on the recurrence and intensity of human- or climate-driven phases of dune instability and stability over time. Additionally, this multidisciplinary approach provides the possibility to temporally and spatially reconstruct past landscape dynamics at least on a local scale. Landscapes reconstructions that derived from geoarchaeological approaches are important to facilitate and improve predictions about the current and future state of the landscape as well as enable scenarios for future conditions (Marcucci 2000). By merging scientific visualization techniques with geoarchaeological landscape reconstructions, past landscape conditions can be transformed into visual information that, on the one hand, helps to enhance geoarchaeological interpretation and contributes to a wider academic discourse among scientists, on the other hand can be more easily understood by non-scientists. The latter is particularly important for sustainable landscape planning at the local level, where landscape changes are important relative to conservation planning (Bender et al. 2005).

Aims & Objectives

2

2.1 Research aims

The overall aim of this thesis is to contribute to a better understanding of the landscape development of inland dune areas of Weichselian sandy outwash plain of Northern Germany and its interactions with the local settlement and land-use history. It aims to investigate and spatially reconstruct the long-term aeolian landscape dynamics using a small inland dune system in Northern Frisia (Schleswig-Holstein) as a case study. Against the background of the dune formation, this thesis seeks to investigate the timing, causes, effects and magnitude of phases of aeolian activity since the beginning of the Holocene.

In order to understand aeolian processes, a range of related questions concerning vegetation cover and composition, as well as land-use changes need to be investigated. Additionally, to enhance and support geoarchaeological interpretation on long-term landscape changes, this thesis aims to establish highly detailed, local 3D landscape reconstructions and scenarios of past landscape surface changes based on geoarchaeological records and using scientific visualization techniques. The investigations were realized within the Graduate School *Human development in Landscapes* (GSHDL) of the Kiel University.

2.2 Structure of thesis

The structure of the thesis is designed so that major questions concerning the topics discussed above are presented in chapter 3 (State of the Art). Chapter 4 (Research methods) provides an overview of the approach and shortly summarizes all methods applied in this study. More detailed descriptions of the methods are given in chapters 6–8. The research area and the regional setting, including an overview of the Late Quaternary and Holocene landscape is presented in chapter 5 (Regional setting).

Chapter 6, a manuscript soon to be submitted to the *Journal of Quaternary Science*, aims to understand how and to what extent changes initiated by human activities have affected aeolian landscape dynamics and examines the intensity of geomorphological processes reflected as deposition rate in the dune record. In addition, the study seeks to find out what

feedbacks were associated with these changes on human socio-cultural systems. This multidisciplinary study aims to combine multiple data sets derived from e.g. botanical, geomorphic/sedimentological, pedological records, historical and archaeological data and dating methods (^{14}C and OSL dating) in order to spatially reconstruct past environmental conditions and human-related interferences.

In order to better understand past landscape and vegetation changes and the processes of dune formation, information on the local vegetation history is necessary. Chapter 7, which is published in *Quaternary International*, aims to reconstruct small-scale, local vegetation cover by wood species analysis from sediment charcoal fragments. This approach is also chosen in order to complement vegetation history previously only reconstructed from pollen records. Finally, this study aims to find out how taxonomic charcoal assemblages can support the geoarchaeological interpretation of dune record and whether aeolian sediments may serve as archives of former occurrences of woody species.

The objective of chapter 8, published in *Kartographische Nachrichten*, is to develop a visualization model that includes 3D scenarios of geoarchaeological landscape reconstructions on different geographical scales that addresses the different scientific requirements as well as the expectations of public users. This study asked how geoarchaeological results can be turned into reliable photorealistic 3D landscape visualization including different temporal and spatial resolutions and how 3D visualization techniques can support scientific discussion on the acquired field data, palaeo-botanical analyses, laboratory and dating results as well as improve geoarchaeological interpretation on landscape changes.

The thesis concludes with a summary of key research results, given as three separate chapters and highlights what is distinctive about it.

State of the Art 3

3.1 Origin and development of aeolian sand deposits in the European Sand Belt

Aeolian sands deposits are widespread throughout the north-western and central European Lowlands, collectively forming the European Sand Belt (ESB). This sand belt extends from Great Britain (Bateman 1998), where is occurs only in patches, and continues on the European continent from the Netherlands and Belgium in the west across to Denmark, Germany and Poland and finally into Belorussia and Russia (Kolstrup 1991, Koster 1988, Kozarski and Nowaczyk 1991, Manikowska 1991, Pyritz 1972, Zeeberg 1998) (Figure 3.1). The northern edges of the ESB are marked by marine deposits of the Post-glacial transgression of the North Sea, while in Jutland, Denmark, as well as in Germany and Poland the boundaries follow roughly with the glacial limits of the Last Glacial Maximum (Koster 2005). To the south the sand belt coincides more or less with the northern loess boundary of the Rhine River (Hilgers 2007) (Figure 3.1).

According to Koster (2005) aeolian sand sheets (cover sands) are the dominant landform in the western part of the ESB, where they have a much greater areal extent compared to the inland dune fields. In contrast, large inland dune fields are found in the eastern parts of the ESB, probably a result of the climate gradient from the Atlantic to more continental climate associated with increasing aridity (Böse 1991, Schirmer 1999). According to Kasse (1997, p. 308) the following four factors are considered essential for the sand-sheet formation:

a) The presence of unconsolidated sandy deposits providing source material for aeolian transport,

b) Low regional relief, generally not exceeding 200 m,

c) Sparse vegetation cover, and

d) Low sand availability due to the periodically wet, frozen or cemented depositional surface.

Three main categories are distinguished in the terminology of Aeolian deposits: sand dunes, sand sheets and loess blankets (Pye and Tsoar 2009). Aeolian sand dunes are mounds or ridges of loose sand formed by wind deposition and ranging in size from

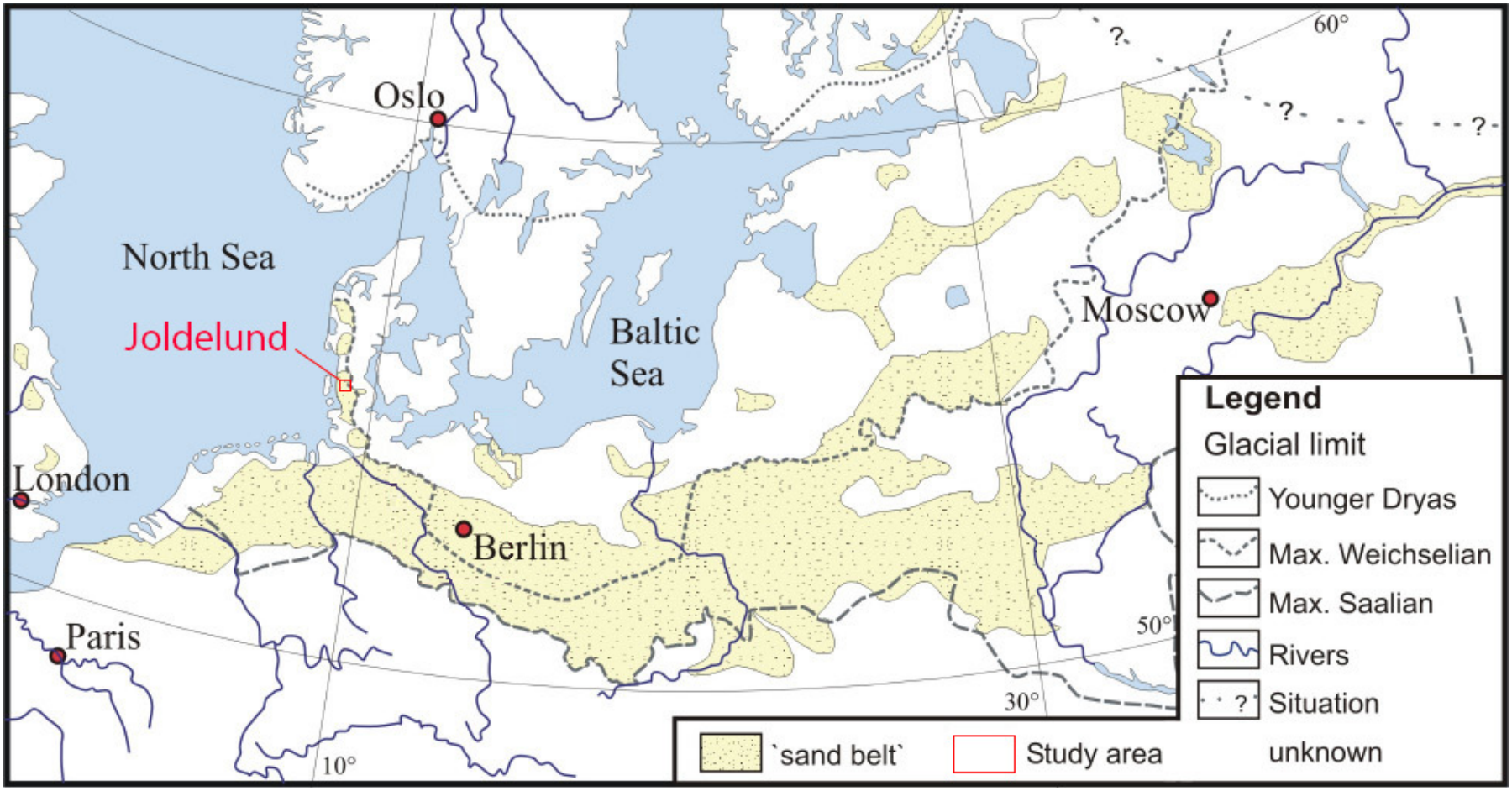

Figure 3.1: Distribution of aeolian sand deposits in the the European Sand Belt (ESB), Pleistocene glacial limits and location of the study area (Source: Hilgers 2007, modified; according to Zeeberg 1998)

less than 1 m to several kilometers (Pye and Tsoar 2009, p. 2). Sand sheets are defined as accumulations of sand characterized by a relatively flat to gently undulating relief without significant dune topography, and loess blankets principally consists of silt that is formed by the accumulation of windblown dust, often mantling a pre-existing land surface.

In western Europe, the term »cover sand« is commonly used and has a stratigraphical as well as a geomorphological meaning (Koster 1982). In this study the following definitions and terms proposed by Castel et al. (1989) and Koster (2005) are adopted. Cover sands are essentially cold-climate aeolian deposits, which formed during the last glacial period and »are not directly related to present or former coastlines or river courses« (Koster 2009, p. 95). The term »drift sand« is used for aeolian deposits which resulted from reactivation or reworking of Pleistocene cover sands by human impact during the Late Holocene period.

Research on these aeolian sediments has a long tradition and numerous studies have been carried out on their lithology and sedimentology, age and interpretation in terms of palaeoenvironmental reconstruction (Kasse 2002, Hilgers 2007). Phases of strong aeolian activity since the last glacial period in western and central Europe are therefore well-known (Schirmer 1999, Kasse 2002, Koster 2005).

The majority of aeolian deposits within the ESB originate from phases of increased aeolian activity during the Late Pleniglacial, Older Dryas and Younger Dryas, separated by periods of surface stabilization with soil formation during the Bølling and Allerød (e.g. Hoesel et al. 2012, Kaiser and Clausen 2005, Kasse 1999, 2002, Kaiser et al. 2009, Kolstrup 1991, Schirmer 1999). Age determinations and chronostratigraphy of the aeolian sequences were made using relative age determinations (e.g. lithostratigraphic, morphostratigraphic and pollen analysis) and absolute dating techniques such as thermoluminescence (TL) of sandy sediment and AMS radiocarbon measurements of palaeosols and organic materials (e.g. peat, charcoal, wood pieces) (Kozarski and Nowaczyk 1991). Comprehensive overviews on the areal distribution of the aeolian deposits and local to regional activity models in Europe are provided within Kozarski (1991), Kasse (1997), Schirmer (1999), Koster (2005) and Tolksdorf and Kaiser (2012).

Numerous studies have addressed the issue of human-triggered reactivation of aeolian sandy deposits and formation of drift sands throughout Northern and Northern-Central Europe, e.g. Denmark (Boas 1997, Mikkelsen et al. 2007), Netherlands (Castel 1991, Koster et al. 1993, Wallinga et al. 2007, van Mourik et al. 2010, Sevink et al. 2013), Belgium (e.g. Derese et al. 2010) the UK (Bateman and Godby 2004) and Poland (Kozarski and Nowaczyk 1991). On the basis of a synopsis of 189 luminescence ages and more than 300 ^{14}C-dates from palaeo-surfaces Tolksdorf and Kaiser (2012) recently identified several phases of aeolian sedimentation and landscape stabilization during the Holocene, beginning with distinct aeolian activity during the early Holocene: The Mesolithic Period (~ 6500 yrs BP), Late Neolithic Peri-

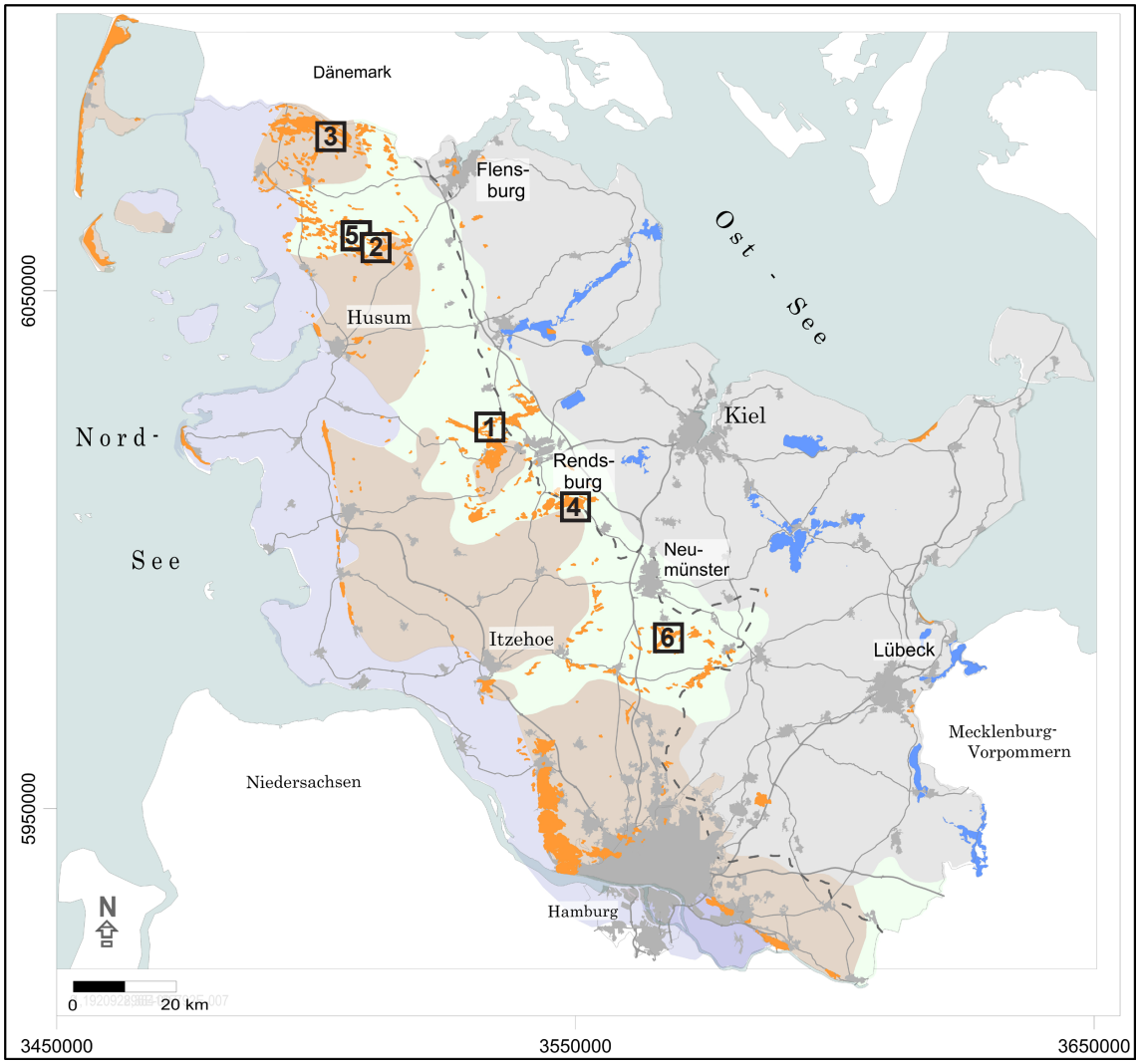

No. of location	Location	Number of dates	Dating method	Stratigraphical position	Reference
1	Föhrden	2	14C	buried soil	Kaiser et al. 1989
2	Joldelund	3	14C	buried soil / slag pit	Richter 1965
3	Jadelund	3	OSL	aeolian sand	
4	Brammerau	2	14C	charcoal layer in aeolian sand / buried soil	Mauz et al. 2005
		4	OSL	aeolian sand/buried soil	
5	Riesbriek	1	14C	buried soil	Fleige et al. 2006
2	Joldelund	15	14C	charcoal layer in aeolian sand / buried soil	Jansen et al. 2013
6	Boostedt	2	14C	buried soil	Grube 2016
2	Joldelund	5	14C	charcoal layer in aeolian sand / settlement pit	Lungershausen 2016
		6	OSL	aeolian sand	

Figure 3.2: Location of thus-far investigated dune areas and amount of published AMS and OSL datings for Schleswig-Holstein (map based on Grube 2016)

od (~ 4000 yrs BP), Late Bronze Age/ early Pre-Roman Iron Age (~ 2700 yrs BP), Early to High Medieval Ages (600–1200 AD), and Late Medieval Ages to Modern Times (1200–1600 AD). For Germany, the first comprehensive study on the morphogenesis, provenance, age and sediment characteristic of inland dunes in Lower Saxony was provided by Pyritz (1972), who differentiated between (pre-Holocene) older inland dunes (»Altdünen«) and (Holocene) younger inland dunes (»Jungdünen«) and

pointed out that human-induced reactivation of aeolian sand dunes during the late Holocene has been much greater than previously assumed. Further detailed investigations on the formation of Late Holocene aeolian deposits in Germany have been largely carried out in Lower Saxony (Alisch 1995), Brandenburg (de-Boer 1995, Hilgers 2007, Nicolay 2014), Mecklenburg-Western Pomerania (Kaiser et al. 2002, Küster et al. 2014) and Schleswig-Holstein (Müller 1999, Mauz et al. 2005, Grube 2016). However, the precise timing of phases of aeolian sedimentation and geomorphic stabilization is not easy to determine, due to the limited number of well-dated sequences and the influence of local depositional processes (García-Hidalgo et al. 2007, Tolksdorf and Kaiser 2012). This holds particular true for the region of Schleswig-Holstein.

Within Schleswig-Holstein specifically, only limited research with coarse temporal and spatial resolution has been undertaken thus far on inland dunes, especially for the Holocene period (Tolksdorf and Kaiser 2012, Küster et al. 2014). Palaeoenvironmental and climatic reconstructions have therefore been based on the chronostratigraphy of only very local dune areas (Kaiser et al. 1989, Richter 1965, Müller 1999, Mauz et al. 2005, Grube 2016). As recently stressed by Küster et al. (2014, p. 65): »in these locations mainly morphogenetic and lithofacial approaches on Holocene dune formation were discussed, with chronological classifications hitherto based on palynological and only a few AMS and OSL datings.« Figure 3.2 summarizes the locations with previously investigated inland dune areas in the Schleswig-Holstein region and associated chronological data.

3.2 Inland dunes as archives of past landscape and vegetation dynamics

In central Europe, soils have been exploited for agricultural purposes from the Neolithic onwards, and as a consequence, anthropogenic soil degradation is as old as agriculture itself (Zuazo and Pleguezuelo 2009). Following the general conceptual model of Bork et al. (1998) which incorporates the long-term interaction between past soil erosion and land-use change, it is assumed that during the whole Holocene the climate conditions and quality of soils allowed the development of dense vegetation which stabilizes erosive processes, with the exceptions of riparian systems, coastlines, and alpine systems (Dotterweich 2008, Dotterweich and Dreibrodt 2011). Many landscapes were therefore relatively stable systems, providing ideal conditions for human land-use (Dotterweich 2008). The opening of a closed vegetation cover through human activity may potentially cause an interruption of the Holocene surface stability, accelerating soil erosion either by water or wind, with the products accumulating as colluvial deposits on slopes and alluvial sediments in floodplains (Trimble and Lund 1982, Hooke 2000), and as aeolian drift sand areas (sheets or dunes) (Koster 2005), and can thus be closely linked to the settlement and land-use history (Bork et al. 1998, Niller 1998, Schatz 2000, Dreibrodt et al. 2010, Küster et al. 2014). Due to their wide distribution and continuous

presence for at least 7000 years these anthropogenic sediments serve as valuable geo-bio-archives to reconstruct the evolution and land-use of past landscapes, and especially human-environmental interactions (Bork et al. 1998, Leopold and Völkel 2007, Dreibrodt et al. 2010, Tolksdorf and Kaiser 2012).

3.2.1 Dunes as archives of past landscape dynamics

The analysis of aeolian sediment sequences preserved within inland dunes along the ESB offer the possibility to reconstruct long-term geomorphic dynamics (Küster et al. 2014). In order to determine a »post quem« age of aeolian (drift) sand formation, radiocarbon ages of the topmost part of intercalated palaeo-surfaces (e.g. organic (peat) layer and palaeosols) have traditionally been used (Castel 1991, Kolstrup 1991, Koster et al. 1993, deBoer 1995, Schirmer 1999, van Mourik et al. 2010). An important problem with this approach is the accurate dating of aeolian sediments and landforms, and the duration of the »effective« aeolian periods (Koster 2010). Establishing whether periods were dominated by active drift sand deposition or soil formation is often not possible using this approach. Since palaeo-surfaces represent phases of geomorphic stability »the possibility of a hiatus (non-depositional or erosional) at the transition of the peat layer or soil profile and the overlying drift sand cannot be excluded« (Koster 2010, p. 39). A ^{14}C and OSL dating based chronology of a drift sand sequence in southern Netherlands showed that radiocarbon ages of buried humic horizons are not always reliable for the chronology of drift sand sequences (van Mourik et al. 2010). Despite luminescence dating techniques proving very useful for the chronology of aeolian landscape evolution, only a few studies have examined luminescence dates from aeolian sands throughout the Holocene to the present (Radtke 1998, Bateman and Godby 2004, Mauz et al. 2005, Hilgers 2007, van Mourik et al. 2012, Willemse and Groenewoudt 2012). This study aims to address this discussion by providing a high resolution chronology for the Holocene aeolian sedimentation of a northern-German inland dune sequence that is based on both ^{14}C and OSL dating techniques.

3.2.2 Dunes as archives of local vegetation dynamics

Dunes often preserve buried peat and soil horizons from which pollen has been successfully analysed in several studies (Kaiser et al. 1989, Castel 1991, Brande et al. 1999, Kowalkowski et al. 1999). However, selective degradation / preservation of organic matter and pollen, and relocation of pollen within permeable dune sands, can diminish the reliability of pollen results from such sediments and their use in reconstructing past vegetation (deBoer 1995, Tomescu 2005, Twiddle 2012). Pollen analysis from buried peat layers, if existent, is much better suited to reveal vegetation change on a local and regional level. However, there are potential complications when it comes to the reconstruction of spatially precise species occurrence and composition (Nelle et al.

2010). To overcome this, analysis of wood charcoal can provide additional site-related information of wood species occurrence and woodland composition. So far, many studies have used charcoal from soil profiles to reconstruct fire and vegetation history (Poschlod and Baumann 2010, Talon 2010, Robin et al. 2011). However, only few anthracological studies have been performed on sandy sediments, especially dunes (Keit and Mothes 1942). Thus, the application of charcoal analysis as part of dune investigations is not yet well developed, although charcoal layers are mentioned in publications on dune development (Seppälä 1995, Schlaak 1999), and are routinely used for radiocarbon dating of layers within profiles (Seppälä 1995, Kowalkowski et al. 1999, Schirmer 1999, Loope and Arbogast 2000, Ivester and Leigh 2003). This study aims to examine the potential of inland dunes to provide geo-bio-archives for anthracology. It also attempts to reveal whether taxonomic information on dune charcoal can support the sedimentological/geomorphological interpretation by indicating potential provenances of dune sands (chapter 7).

3.2.3 Dunes as archives for quantifying past human impact on landscapes

The formation and stabilization of inland dunes in the ESB have been intimately linked to sediment availability, climate change and human-induced changes (e.g. Schirmer 1999, Koster 2005, chapter 3.1). The analysis of soil-sediment-sequences in inland dune archives in combination with bio-archives (soil charcoal and pollen) enable the reconstruction of palaeoenvironmental conditions and history of aeolian activity. Although aeolian sediments are known as sensitive indicator for soil erosion induced by land-use (Tolksdorf et al. 2013), comparable quantitative studies on past erosion and deposition rates still remain elusive for drift sand deposits. This is mainly because wind transport processes are highly variable in space and time (Hassenpflug 1998) and the reconstruction of clear spatial boundaries, i.e. the location and size of both sediment source and accumulation is highly complex or even impossible. Within these broad limitations, this study attempts to quantify spatio-temporal changes in the dune topography and aims to compare deposition rates of past aeolian sedimentation phases in order to assess human impact on the aeolian landscape evolution.

3.3 Three-dimensional landscape visualization of (pre)historic environmental data

Communication of science to the research community and beyond to the general public is increasingly recognized as a responsibility of all scientists (Leshner 2003). New research results are usually presented using conferences or via journal papers, while the wider communication is usually an afterthought (Royal Society 2006). In this context, a crucial step in scientific research is to communicate research results to both the scientific community and the public, either as written or oral reports or

in the form of data visualization such as charts, diagrams, maps, graphics, and 3D computer models (Sheppard 2005c). Most of the research results are contained within 2D and 3D representations with a relative high level of abstraction and simplification. Besides traditional visualizations, such as sketches, perspective drawings or photomontages, in this study visualization refers to computer-generated landscape visualizations (Lange 2002), which attempt to represent actual places and on-the-ground conditions with 3D perspective views from different viewpoints, with varying degrees of realism (abstract to photo-realistic) (Sheppard and Salter 2004, Bishop and Lange 2005). Landscape visualization as a branch of geovisualization is a relatively new research discipline that has been gradually establishing itself in the spatial sciences since the 1990s (Gabler-Mieck and Duttmann 2007). It integrates scientific computing, cartography, image analysis, information analysis, exploratory data analysis and geographic information systems (GIS) to provide theory, methods, and tools for the visual exploration, analysis, synthesis, and presentation of geospatial data (MacEachren and Kraak 2001). Depending on the visualization technique, the presentation of landscape visualizations can be static or dynamic on different levels of interactivity and on immersive or non-immersive displays (Lange 2002, Bishop and Lange 2005). Appleton et al. (2002) discuss three broad approaches which combine visualization and geographic information systems (GIS): i) *image draping*, where images are draped on a 3D terrain to produce still images or animation; ii) *photorealistic rendering*, where vegetation and other landscape features can be incorporated in the landscape scene to provide a more realistic representation of an area and iii) *virtual reality*, where a virtual simulation environment can be interactively and immersively explored by the users.

Based on a growing volume of geodata with a high degree of geometrical resolution, such as digital elevation models, topographical data, and aerial or satellite images (Traub and Kohlus 2006, Gabler-Mieck and Duttmann 2007), visualization environments are now capable of rendering landscapes in three dimensions with photorealistic effects (Figure 3.3). These visualizations are more illustrative; enabling the rather abstract information contained in maps and plans to be communicated in a format that is more easily understood (Lange 2001).

Today, methods to visualize landscapes and landscape processes in three dimensions are increasingly used, not only in urban and regional planning (e.g. Sheppard 2005c, Paar 2006), but also in the field of geography (e.g. Lange 2001, Buhmann 2002, Kääb et al. 2003, Boldt et al. 2005) and archaeology (e.g. Kramer 2007, Teichmann 2010). In particular, 3D visualization is being increasingly utilized in planning where it can support consensus building on public issues by transforming large amounts of rather abstract data into understandable images (Bishop and Lange 2005), and serves as an engagement and communication medium within the broader context of participatory decision making (Stock et al. 2008, Wu et al. 2010, Pettit 2011). Moreover, it is considered a powerful tool to communicate existing

Figure 3.3: Three-dimensional landscape visualization of the present situation of the study area (Source: R. Gabler-Mieck)

conditions and alternative landscape scenarios, past and present, for research, education, and consultation (Priestnall and Hampson 2008), and may substantially improve the awareness-building process on issues associated with climate change (e.g. local renewable energy and flood protection) (Sheppard 2005a). Duttmann et al. (2012) highlight a number of advantages 3D landscape visualization techniques for geographical purposes: the improvement of spatial visualization through 3D representations of landscapes features, the illustration of abstract information via realistic landscape images, and the possibility of creating scenarios and virtual scenes of present and historic landscapes in order to support environmental education. With respect to geoarchaeological research, the potential of 3D landscape visualization techniques for the presentation and reconstruction of past landscapes and landscape change dynamics are still far from being exploited. Only a few studies represent the outcomes of landscape and vegetation reconstructions using photorealistic 3D landscape visualization techniques (Fuest and Schnirch 2003, de Boer 2009, Siart et al. 2011, Szücs 2014). A major challenge is to create 3D landscape visualizations that meet various expectations of the scientific and public communities and to create reliable 3D scenarios of past landscape surfaces on different geographical scales. This study presents a visualization model which aims to i) create reliable

3D visualizations based on geodata, ii) to integrate knowledge from multiple disciplines to support an interdisciplinary dialogue and iii) to link scientific knowledge transfer and public outreach to improve communication between scientists and non-scientists.

Approach & Methods

4

This chapter shortly summarizes all methods used for this study. Methods are described in detail in chapter 6 (Lungershausen et al. 2016, unpublished), chapter 7 (Jansen et al. 2013) and chapter 8 (Lungershausen et al. 2013).

4.1 General approach

Geoarchaeology is a cross-disciplinary research area interfacing earth-science and past human activity (Rapp and Hill 1998, Roberts 2001, Butzer 2008). In order to examine and reconstruct past environmental changes and the impact of human activities on the development of landscapes, geoarchaeological research makes use of a large number of methods and techniques in the field of geomorphology, soil science, palaeoecology and environmental history (Rapp and Hill 1998, Goldberg and Macphail 2006, Fouache 2013). GIS and 3D visualization techniques are also used to display photorealistic landscape scenarios that include the impact on, and response of, humans to environmental changes during the Holocene (Ghilardi and Desruelles 2008, Siart et al. 2011).
The methods applied in this study are largely adopted from the landscape reconstruction approach presented by Bork et al. (1998) which was developed by the Task Force of the European Society for Soil Conservation (ESSC) on long-term effects of land use on soil erosion. This geoarchaeological approach focuses on the reconstruction of past soil erosion events and their causes by using bio-geo-archives as important sources of information on local to meso-scales (Bork et al. 1998, Bork et al. 2001, Dotterweich 2003a, Dotterweich 2004, Schmidtchen and Bork 2003). Figure 4.1 shows a overview of the approach and the steps undertaken in this study, with the methods used briefly described in the following sections.

4.2 Field work

4.2.1 Site selection

A preliminary field survey was carried out in August (25–30/08/2008) and September 2008 (30/09/2008). In order to get a general idea of the present soil varieties and to gain an overview of the predominant substrate and soil conditions, natural and artificial outcrops were studied and 60 auger corings of up to 2 m were carried out throughout different parts of

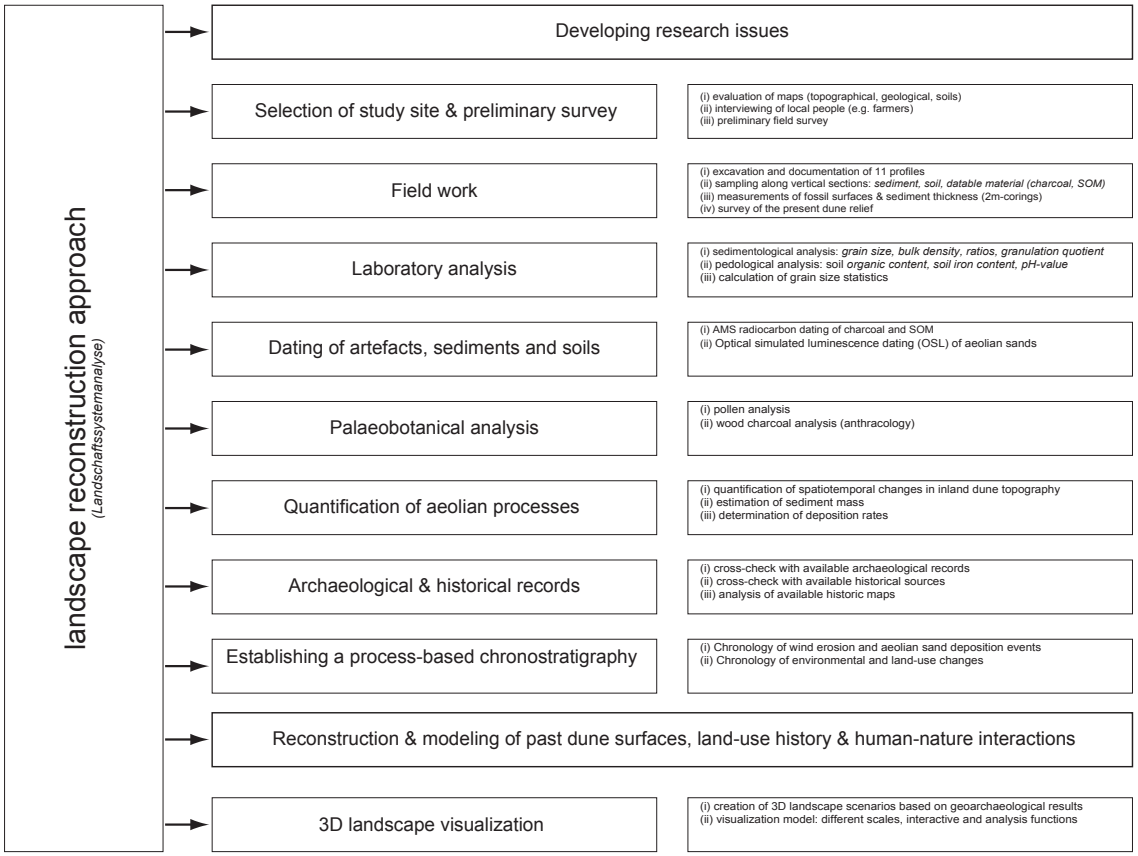

Figure 4.1: Overview of the various methods included in the landscape reconstruction approach (according to Bork 2006, modified)

the ~ 80 ha large inland dune field (Figure 4.2). The soil overview map (BÜK 200) of Schleswig-Holstein as well as the results of the forestry site mapping from 1990 (provided by the Lower Forest Authority) and of the General soil inventory from the 1930s (»Reichsbodenschätzung«) provided an initial basis for site selection. Criteria for the selection of the study site were: i) the absence of disturbed layers due to e.g. previous archaeological excavations, cultural layers, forest path, or marl pits; ii) the presence of a distinct sequence of soils and/or humic layers and aeolian sediments, and iii) a site covered with forest (soil and sediment preservation). The Kuhharder Hill dune (KHD, german: Kuhharder Berg) in the western part of the inland dune field was chosen as a case study because it met these criteria, and in particular pedo-sedimentological sequences found in auger corings at the site were deemed to have high environmental reconstruction potential. The Kuhharder hill dune complex has an area of ~ 2 ha and is covered with forest (municipal forest of Joldelund). Moreover, in the course of the preliminary field survey disturbed layers were not found.

4.2.2 Dune profiles and sampling

A detailed field study was conducted on the selected study site from November 2008 until May 2009. At the ~ 2-ha large

Preliminary field survey
Overview of selected land parcels of Joldelund community

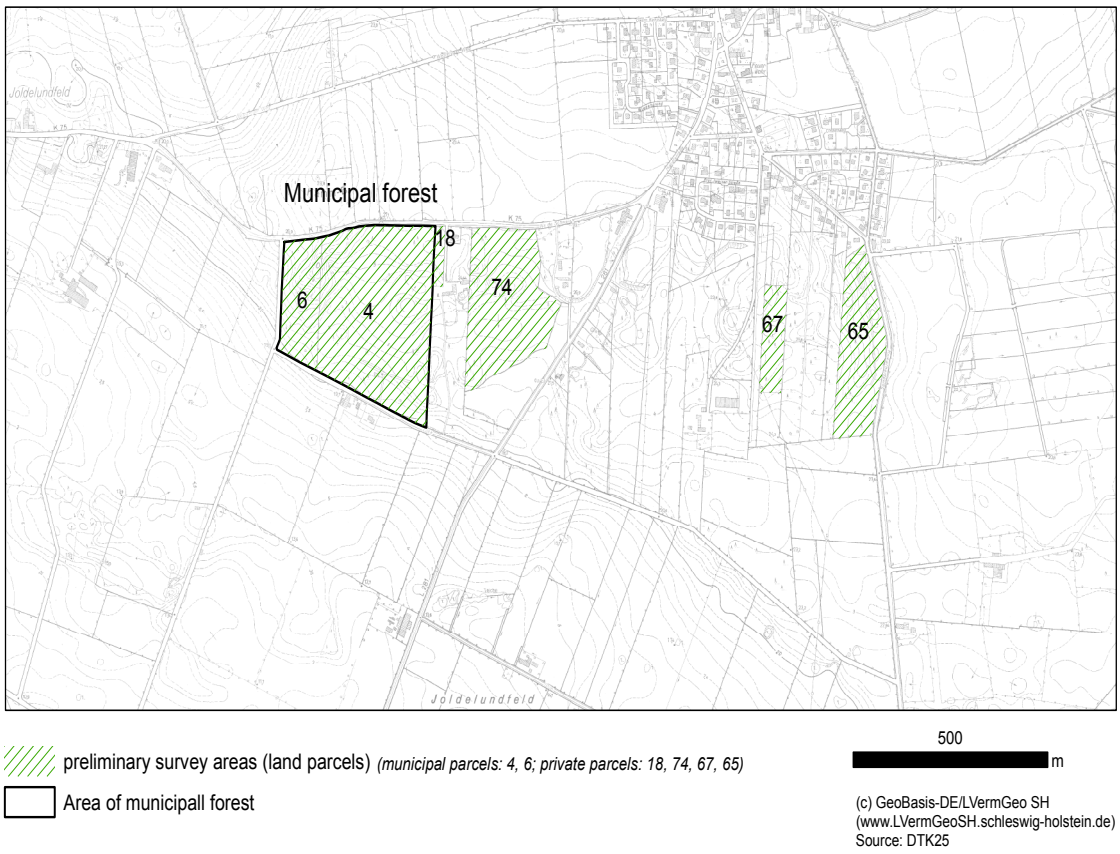

Figure 4.2: Areas of preliminary survey prior to site selection

dune complex twelve exposures up to ~ 25 m in length and ~ 2.5 m in depth were excavated with the help of an excavator. All excavation sites were created deep enough to reach the base of Holocene deposits. Where the distinct sediments of the underlying moraine deposits couldn't be reached by the excavator, an Edelman hand auger was used to determine the total depth of the dunes. Centered on the KHD (central area), eight profiles were opened within a maximum horizontal distance of ~ 50 m (profile 1–3, 6–8 and 12; Figure 4.3, Figure 4.4). Another four profiles were excavated towards the southern and north-western edge of the study area (Profile 4–5, 9–10; Figure 4.3, Figure 4.4). Two profiles (profile 1–2) are the cross-sections through the main dune body (KHD), with a total length of ~ 35 m and a maximum depth of ~ 2.3 m.

After cleaning and smoothening of the sidewalls of each profile, sand layers and (buried) soil horizons were identified and described using the following field methods:

i) all dune profiles were documented in scaled drawings and photographs;

ii) soil colour was determined using Munsell soil color chart;

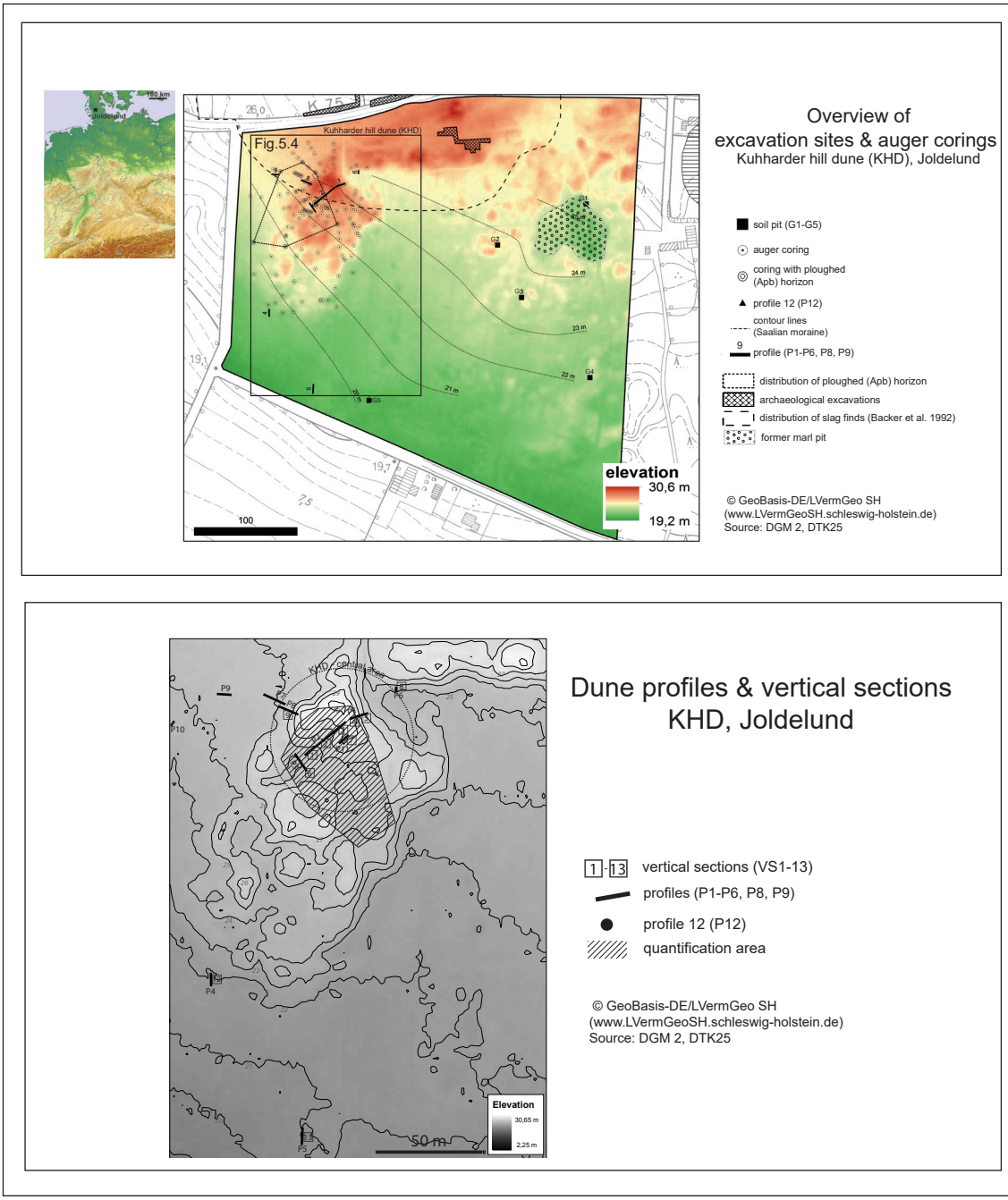

Figure 4.3: Overview of excavation sites (dune profiles and vertical sections) and location of auger corings

iii) texture, bulk density and soil formation processes were recorded according to the German Soil Mapping Guide KA5 (AG Boden 2005);

iv) soil types and (buried) soil horizons as well as aeolian deposits and their stratigraphy sequence were first described according to German soil classification and then translated into the international soil classification system WRB (IUSS Working Group WRB 2015);

v) archaeological finds and features such as iron slags, traces of slag pits or ditches were documented, sampled and interpreted together with specialists (e.g. archaeologists, geobotanists) of the University of Kiel (CAU).

To quantify sediment deposition at the KHD, the excavation sites were complemented with five shallow pits (G1–G5) in the central and southern part of the research area in November 2009 (Figure 4.3). Within all excavation sites the distinct glacial sediments (moraine, Pleistocene) underlying the dunes were reached, which ensured that the entire Holocene sedimentary record was analysed, and made the quantification of the total Holocene aeolian deposition possible.

In this thesis, nine of the twelve profiles were selected for sampling and further analysis (profile 1–6, 8, 9 and 12). Samples for sedimentological and pedological analyses such as grain size, organic matter, pH value, soil iron content and bulk density (undisturbed soil samples) were taken within 13 sampling sections (hereafter referred to as »vertical section« or »VS«) (Figure 4.3). Depending on topography, stratigraphy and length of the exposures, up to three vertical sections per profile were analysed. Samples were taken at the vertical sections from bottom to the top to avoid the mixing (and contamination) of the samples below. A rough stratigraphical sequence was developed along hte main soil horizons. Sampling for soil bulk density determination was limited to four vertical sections (profile 2, 3, 5 and 8), because sediment density is expected to be relatively homogeneous in sandy soils (~ 1.6 g cm^{-3}, Koorevaar et al. 1983).

For radiocarbon dating and charcoal analysis samples were taken from interbedded organic-rich horizons, charcoal/humic layers and a slag pit in profile 6 (Figure 4.4). Numerous charcoal pieces and samples of charcoal/humic layers (1000 g–2000 g) were collected according to the stratigraphic sequence. Samples for optical stimulated luminescence (OSL dating) were taken from sand deposits in three sections in profile 2. OSL sampling was performed during the day at regular depth intervals (~ 25 cm) using ~ 0.3 m long opaque tubes (diameter: 5 m), which were hammered into the outcrop. From each OSL sample a sample for the determination of the dose rate from a 30 cm region surrounding the sample tubes were collected (200–300 g).

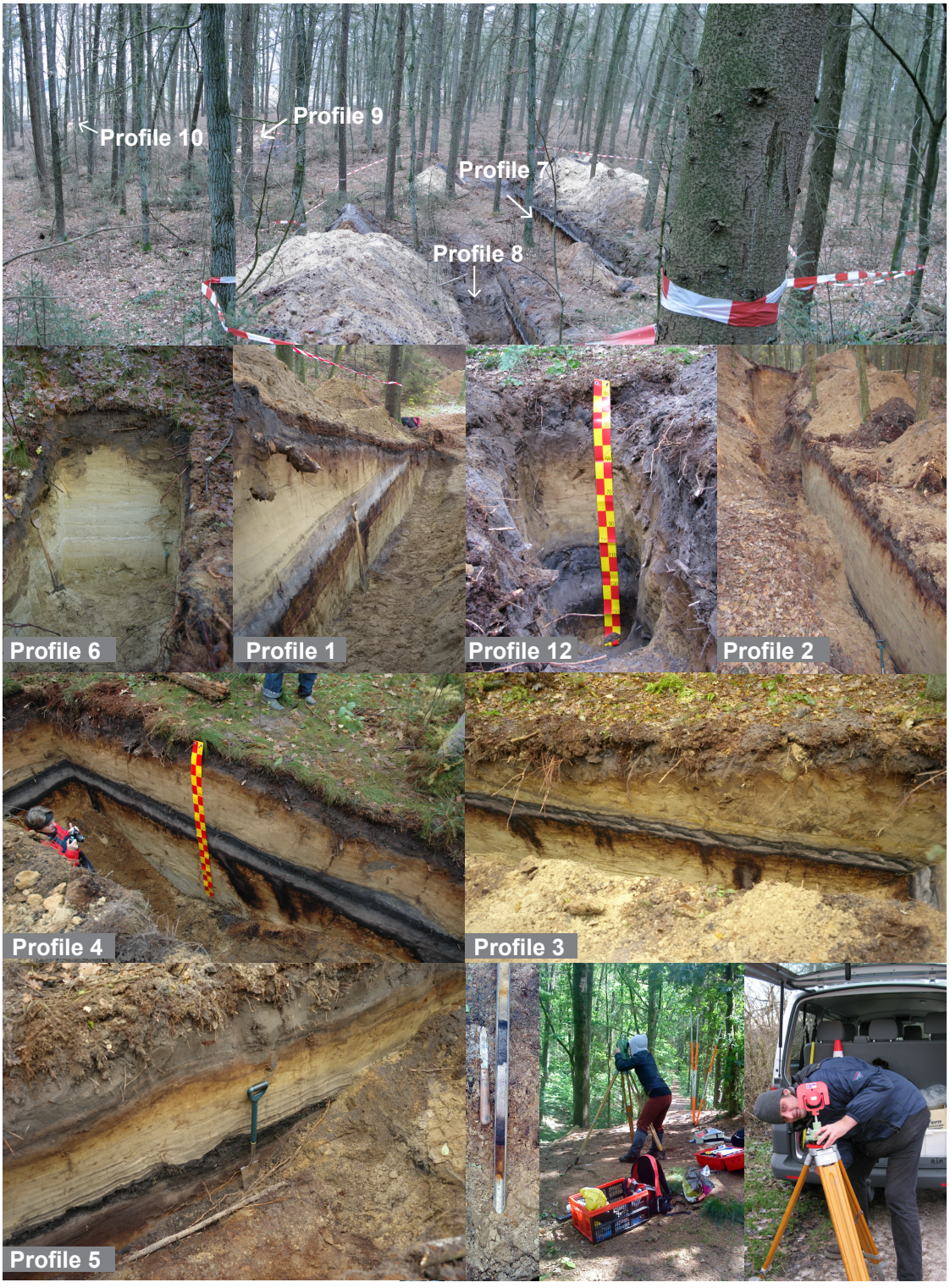

Figure 4.4: Field work: Excavation sites, auger coring and total station survey

4.2.3 Soil coring survey

A comprehensive coring campaign was carried out over six weeks from June until July 2010. The coring was done using Pürckhauer and Linnemann soil augers. The Pürckhauer corer was used for drillings up to a depth of 1 m, while the Linnemann auger with lengthening rod was used to reach 2 m drilling depth. In total, ~ 125 corings of up to 2 m were performed in order to log and model the height of marker horizons such as buried dune surfaces and soil horizons and to ensure a correct spatial interpolation of the sedimentary units (Figure 4.3). At all coring locations, the following pedological and geomorphological data were recorded: i) position and elevation, ii) upper and lower depths of soil horizons, iii) soil colour, iv) soil texture and v) stratigraphic context and thickness of sand deposits/soil horizon. Finally, all excavation sites and coring locations were surveyed with a laser-based Leica TCR-407 total station (Figure 4.4). All pedological and geomorphological data (position, elevation, chrono-stratigraphic correlation, and thickness of soil horizon/sediment layer, soil colour and estimated grain size) were imported into ESRI ArcGIS to allow further processing and quantification of sedimentary layers.

4.3 Laboratory analysis

4.3.1 Sediment analysis

All sedimentological and pedological analysis was conducted in the Department for Physical Geography, Landscape Ecology, and Geo-Information (GIS) laboratories within the Kiel Institute of Geography. For grain size analysis, sediment samples of 15 g (< 2 mm) were treated with H_2O_2 and subsequently sieved to 630 µm, 200 µm, 125 µm and 63 µm size fractions. All samples were dried at 105 °C and then weighted. Particles < 63 µm were analyzed applying standard procedure for grain size analysis (Köhn pipette).

In order to compare the different sedimentary deposits, the grain size data were processed using the grain size statistic program GRADISTAT (Blott and Pye 2001). Grain size parameters such as the mean (M) and median (Md) of each sample were calculated using the Folk and Ward (1957) method. In addition, Trask's sorting coefficient (So) and ratio of medium to fine sand (MS:FS) was calculated in order to compare the results with earlier studies (e.g. Alisch 1995, Müller 1999, Mauz et al. 2005)

Soil bulk density (SBD) was determined by taking at least three constant volume samples per sedimentary layer. The samples were dried at 105 °C, weighed, and the mean SBD with standard error was calculated (see chapter 6).

4.3.2 Soil analysis

The measurement of total organic carbon and nitrogen was performed applying the combustion method on a HekaTech Euro EA 3000 Elemental Analyser. Each sample was combusted at 1000 °C and elemental carbon was measured by a thermal conductivity detector. Organic matter con-

tent (OM) was then calculated using the conversion factor of 1.742, assuming that organic matter of soils amount to approximately 58 % organic carbon (Nelson and Sommers 1996).

The determination of pedogenic iron oxides (FeD) was processed using dithionite-citrate-bicarbonate (DCB) extraction method proposed by Mehra and Jackson (1960). A 1 g air-dried sample was first treated with 100 ml dithionite and heated up to 75–80 °C in water bath. It was then centrifuged and the supernatant was decanted. Iron was measured using a flame Atomic Absorption Spectroscopy (AAS) system (PerkinElmer). The amount of amorphous iron oxides (FeO) was determined using acid-ammonium oxalate (AAO) extraction technique introduced by Tamm (1932) and modified by Schwertmann (1964). For this, a 1 g air-dried sample was treated with a solution of 100 ml acid oxalate and then shaken for one hour in the dark.

Soil pH was determined for each sample. A 1:2 soil to deionized water mixture and a soil to 0.01M $CaCl_2$ mixture was prepared and stirred several times before left to settle into a supernatant solution. The pH of the solution was then measured with a pH meter.

4.4 Dating methods

4.4.1 Radiocarbon dating

Radiocarbon dating is an absolute dating technique which is based on the decay of naturally occurring radioactive elements. Radiocarbon (^{14}C) is one of three isotopes of carbon. The other two isotopes, ^{12}C and ^{13}C, are stable isotopes, while ^{14}C is unstable and weakly radioactive. ^{14}C is continually produced in the upper atmosphere (stratosphere) by the action of cosmic ray-induced radiation on ^{14}N atoms in the atmosphere (Libby 1955). It is then oxidized and mixed with the atmospheric CO_2 to form a particular form carbon dioxide ($^{14}CO_2$) (Geyh and Schleicher 1990). It then enters the global carbon cycle and is thus assimilated by plant through the photosynthetic process, and enters the food chain of animals. Once an organism dies, no further exchange of ^{14}C can take place and the radiocarbon concentration starts to decrease through radioactive decay with a half-life of a ^{14}C atom is 5730 ± 40 years (Godwin 1962). The radiocarbon dating is based on this rate of decay of the radioactive ^{14}C. It measures the age of the »carbonate phases in radiocarbon years by the level of nuclide ^{14}C remaining in the sample« (Jull and Burr 2015, p. 669). The common expression of how the remaining amount of ^{14}C atoms is related to time is

$$\frac{N}{N_0} = e^{-\lambda t} \qquad (1)$$

where N_0 is the number of ^{14}C atoms at the time $t=0$, N is the number at any time (t) and λ is the defined rate of decay (1/8.267 yrs). This implies an upper age limit of this dating technique of around 45000 years (Walter 2005).

The measured age is an uncalibrated result which is usually is given in years BP and called the »conventional radiocarbon age (CRA)« (Jull and Burr 2015). This age is not comparable to a historical age since

it includes i) the use of the incorrect half-life of 5568 years (»*Libby*« half-life) instead of 5730 years, ii) the assumption of a constant ^{14}C atmospheric concentrations during the past, and iii) the using year 1950 AD year zero (Stuiver and Polach 1977) and is therefore converted into calender age using calibration techniques. Calibration of the radiocarbon age is needed since it is well known that atmospheric ^{14}C concentrations vary over time due to fluctuation in the production rate of ^{14}C (de Vries 1958). Changes in ^{14}C production are known to be caused by »geomagnetic and solar modulation of the cosmic-ray flux, and the carbon cycle« (Reimer et al. 2013, p. 1870). Moreover, since industrial revolution (~ 1870 AD), variations in $^{14}C/^{12}C$ ratio triggered by the use of fossil fuel and resulted in a dilution of ^{14}C in the atmosphere by release of $^{12}CO_2$ (Suess 1955), which is known as »*Suess*-effect«. More recently, the testing of nuclear meapons lead to a constrasting effect (»*bomb*-effect«), namely a release of large quantities of ^{14}C into the atmosphere (Rethemeier 2014).

In our study, the abundance of numerous charcoal and organic-rich layers (humic layers and peat) in most of the sand layers permitted Accelerator Mass Spectrom-

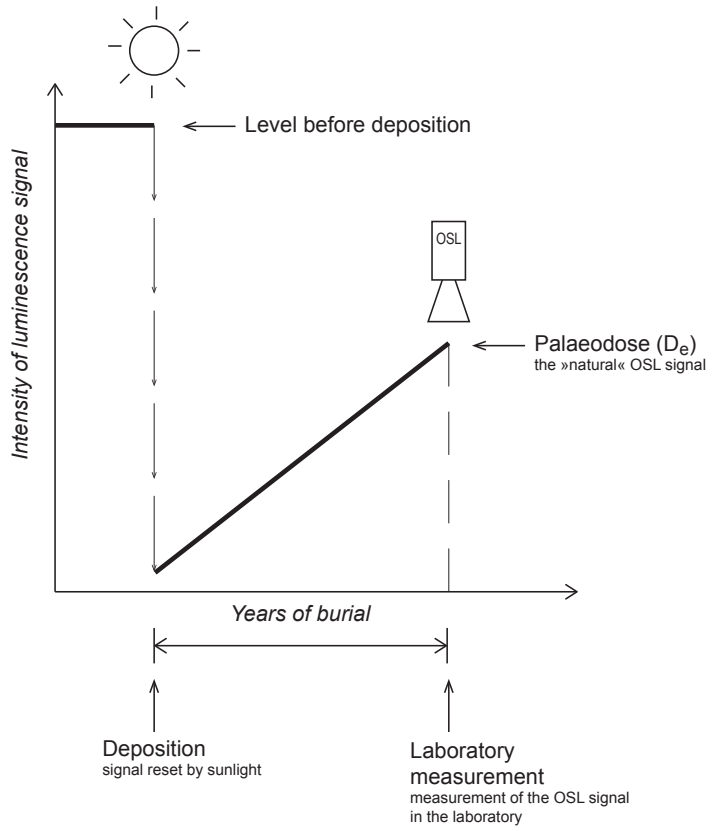

Figure 4.5: Basic principle of luminescence dating: the luminescence signal is set to zero or near to zero during daylight exposure and accumulates with time when buried and, thus, is sealed from daylight. For OSL dating the natural signal is obtained by exposure to a beam of light (graphic according to Aitken 1998)

etry (AMS) radiocarbon dating[1] to obtain the chronology of land-use change. Samples of charcoal and humic layers (1000 g–2000 g) were taken from the vertical sections and in the immediate periphery depending on the dune stratigraphy (chapter 6).

Prior to the radiocarbon dating, samples were dry-sieved through a 630 µm-mesh and taxonomic identification of wood charcoal was carried out to avoid the old wood effect and the dating of modern conifers such as *Picea*. Therefore, relatively short-lived woody taxa such as Ericaceae, *Populus/Salix*, and *Betula* were preferred to enhance the reliability of the ages (Gavin 2001, Gavin et al. 2003). According to Gavin et al. (2001) the age of the measured charcoal sampe relative to the time-since-fire is one crucial source of error in this dating approach and must be considered before interpreting fire ages. This so called »old-wood« effect appears when towards the end of a growing season tree rings are laid down and, accordingly, the carbon exchange with the biosphere ceases before death (Bowman 1990).

^{14}C dating were performed by the Leibniz-Laboratory for Radiometric Dating and Isotope Research at Kiel University, following standard methods (Nadeau et al. 1997, Nadeau et al. 1998, Grootes et al. 2004) and ages were calibrated according to Reimer et al. (2013) using OxCal v4.1.7.

In the following chapters, all ^{14}C results are reported in percent Modern Carbon (pMC)[2] with ± 2-σ measurement uncertainty. All dating results are documented in appendix 2.

4.4.2 Optical Stimulated Luminescence (OSL)

Optical luminescence dating, similar to thermoluminescence is based on the principle that energy (luminescence signal) is stored in the crystal lattice of minerals, such as quartz or feldspar, in response to the natural ionizing radiation (α, β and γ radiation) of the environment, and by cosmic rays (Duller 2015). This radiation causes the emission of free electrons from naturally occurring isotopes, mainly uranium (U), thorium (Th) and potassium (K), which are trapped in crystalline lattice defects (Aitken 1985). When a mineral grain (e.g. from aeolian sediment) is buried, electrons start to accumulate in the »electron traps« with time. As soon as the mineral is exposed to sunlight, for example during aeolian transport, the luminescence signal is bleached by releasing the electrons from the traps, known as »bleaching event« (Aitken 1998, Preusser et al. 2008, Cordier 2010, Liritzis et al. 2013). If the bleached sediment is buried again, the luminescence signal will start to build up again (Aitken 1998) (Figure 4.5).

The time elapsed since the last exposure to daylight can be calculated by dividing the total amount of radiation that the sample was exposed to (palaeodose or »natural« signal, Figure 5.5) by the amount of radi-

1 *In the following, the expression ^{14}C dating refers to AMS radiocarbon dating*

2 *According to Stuiver and Polach (1977) 100 pMC is defined as the ^{14}C-concentration of the atmosphere in 1950 AD.*

ation that the sample receives from the natural environment per year (dose rate):

$$Luminescence\ age\ (a) = \frac{palaeodose\ (Gy)}{dose\ rate\ (Gy\ a^{-1})}$$

In the laboratory, the luminescence signal can be measured through light stimulation (Huntley et al. 1985). The palaeodose can be estimated in the laboratory by the determination of the equivalent dose D_e, which is the amount of artificial simulated dose that would be required to produce the natural luminescence signal (Wintle 1997).

There are two approaches to evaluate the palaeodose: the additive method and the regeneration method. Both approaches include the calculation of a so-called dose response curve which reflects the increase of latent luminescence in the mineral grains with increasing dose (Preusser et al. 1998). Depending on the number of subsamples (aliquots) the estimation of De can be done using multiple aliquots protocols, single aliquots protocols or single grain techniques. Detailed informations on these approaches of luminescence dating technique are provided within many references by e.g. Wintle (1997), Aitken (1998), Stokes (1999), Duller (2001, 2008, 2015) and Preusser et al. (2008).

The annual dose rate comprises α, β and γ radiation from nuclear decay of U, Th and K and cosmic ray dose (Mejdahl and Christiansen 1994). It needs to be calculated i) from the internal radioactive content of a sample and ii) from the external radioactive contribution from the site of the deposition (Lowe and Walker 1997). It is usually assumed that the dose rate has remained unchanges since the sediment was deposited, although fluctuations in radiation levels over time may occur as a result of e.g. disequilibrium in the uranium decay series, changes of cosmic ray flux and gamma (γ) radiation with burial depth or changes in water content during burial period (Li et al. 2008).

Two parameter are particularly important when calculating the dose rate: i) the grain size of the minerals because of the different penetration power of the different kinds of radiation, and ii) the water content, since it is known that water absorbs radiation very differently than sediment and has the effect of »diluting« the dose-rate to the sample by almost the same proportion as its amount (Liritzis et al. 2013, p. 22).

As with every method, there are uncertainties in the luminescence method that needs to be considered when assessing OSL ages. A concise review of sources of errors of luminescence ages associated with uncertainties in both palaeodose and dose rate estimation are given by Wallinga and Cunningham (2015). One key concern lies in the degree of bleaching of any luminescence signal prior to deposition, which may not be sufficient for resetting (»zeroing«) the OSL signal and lead to an age overestimation. Sediments bearing a high potential for insufficient bleaching, such as in fluvial (Keen-Zebert 2015) glaciofluvial (Raukas 2004), deep-marine (Roberts 2015) and lacustrine sedimentary (Murray and Olley 2002) settings, are less likely to provide reliable ages. However, sediment exposure to daylight during ae-

olian transport is generally considered adequate to reset the OSL signal completely (Murray and Olley 2002, Kolstrup 2007). In addition, variations in the water content over the burial period are an important source of uncertainty for luminescence ages. The water content is important because attenuates the dose rate that reaches the mineral grains and therefore influences the age determination. An increase of 1 % in moisture content increases the age by roughly 1 % (Aitken 1985). To put it in a simplified way: the larger the water content increases over time, the larger the decrease in dose rate and, hence, the likelihood of overestimating the age increases.

Other sources of uncertainty, such as sediment mixing as a result of reworking or bioturbation, radioactive disequilibria (fluctuation in radiation level) can also influence the dose rate and, thus, the age result of the sediment. Despite all these sources of potential uncertainty, through the careful sampling design, preparation and analytical methods, the minimum relative errors for sample ages are typically 5–10 % at 1σ–range (68 % confidence interval) (Tooth 2015). With respect to the possible age range using OSL, many laboratories can nowadays produce age estimates from a few decades old to more than 500 ka (Murray and Olley 2002). »However, the use of quartz for OSL dating is typically limited to the last 100–150 ka because of saturation effects of the quartz luminescence signal with increasing dose« (Zander and Hilger 2013, p. 719).

Within the scope of this study, OSL dating was carried out at the University of Szeged, Hungary, and the following laboratory procedures were kindly provided by Dr. Sipos György (appendix 2).

In the laboratory, all sample preparation was carried out under subdued light of low pressure Na lamps, filtered by a Schott BG 18 glass in order to avoid any loss of luminescence. For sample preparation standard techniques were used as proposed by Aitken (1998) and (Mauz et al. 2002). Prior to luminescence measurment, quartz grains of 90–150 µm size were extracted and for each sample, 24 aliquots were prepared to determine the equivalent dose (D_e) and an additional 21 aliquots were used to perform a preheat plateau test. Then, preheat plateau test of dose was carried out on each sample. The quartz samples were stimulated by 470 nm blue light and the luminescence signal was detected using a Hoya U-340 filter set to 290–390 nm.

The equivalent dose was measured using the standard single-aliquot regenerative-dose protocol (SAR) described by Wintle and Murray (2006). The measurement of the natural luminescence signal was followed by three regenerative cycles with increasing doses, and a cycle with zero dose. Finally, the lowest regeneration dose was repeated for the calculation of the recycling ratio. The sensitivity change of aliquots during the procedure was monitored with identical test doses administered following the measurement of the natural signal and the regenerated signals. The value of test doses was set to be similar to the expected equivalent doses. At the end of the SAR cycle an infrared stimulated luminescence (IRSL) / OSL test

measurement was also inserted in order to determine the IRSL depletion ratio and check for possible feldspar contamination (Duller 2003, Mauz and Lang 2004), however no evidence for this was found.

Prior to the actual equivalent dose measurements, preheat plateau tests were made on each sample in order to define the preheat temperature at which reproducibility and precision are the highest (appendix 2). Adequate preheat temperature was found to be between 210 °C and 240 °C. Cut heat temperature was set to 160 °C (Wintle and Murray 2006). The received and corrected OSL data were evaluated using RISO Analyst 3.24 (2007). The integration of the first 0.6 s of the shine down curve was taken as the OSL signal, and the last 10 s as the background. During calculation of aliquot equivalent doses, a 2.0 % systematic error was added in order to reflect uncertainty in the intensity of the OSL stimulation source and the positioning of the aliquot relative to the beta source (Vandenberghe et al. 2004). Some aliquots were rejected from equivalent dose calculations for the following reasons: i) the recycling ratio was outside 1.00 ± 0.05 (referring to increased sensitivity change), ii) the error of the De was larger than 10 % (referring to deviation from linear fitting and error in sensitivity correction), or iii) the recuperation signal was over 5 % of the natural signal (referring to significant charge transfer).

Sensitivity corrected dose responses (Lx/Tx) were fitted with a saturating exponential function (y = a(1-exp(-x/b)) (appendix 2). Individual D_e values and errors determined for the aliquots of the same sample were then determined from the frequency histograms, with the mean value providing the sample D_e and the standard deviation taken as the sample D_e error. The errors for sample D_e were all in the range of 10–15 %.

Environmental dose rate calculations were based on the Th (ppm), U (ppm) and K (%) content of samples, as provided by high resolution, low-level gamma spectrometry. Radioactive disequilibrium in the uranium chain was not observed. Dry dose rates were determined after Adamiec and Aitken (1998). The dose rate of beta radiation was corrected using the attenuation factors given by Mejdahl (1979). Wet dose rates were assessed on the basis of in situ water contents and assuming a 5 % error in order to account for possible fluctuations (Table 6.3). The rate of cosmic radiation was determined on the basis of burial depth and following the method of Prescott and Hutton (1994).

4.4.3 Combining ^{14}C and OSL dating

In order to provide a detailed and comprehensive chronology for developing an appropriate interpretation from the dune record, two independent dating techniques were used. Where organic material such as charcoal was abundant ^{14}C dating was favoured for chronological reconstructions. However, the uncertainties associated with sedimentary charchaol results have to be considered, as older charcoal may have been reworked due to aeolian processes and mixed with younger deposits. Therefore, the ^{14}C age of charcoal is po-

tentially a maximum age of the aeolian deposit (see chapter 7), with the reliability of the dates therefore based on the assumption that the charcoal was incorporated into sand deposits soon after the burning event. This particular disadvantage of the dating technique can be reduced when OSL dating is applied in combination with ^{14}C dating (Cheetam et al. 2010). OSL is particularly useful to determine the moment of deposition and burial by measuring the time since the sediments were last exposed to sunlight, provided that the mineral grains have been fully bleached by the transport event. In contrast to ^{14}C dating the uncertainty surrounding OSL ages (at least 4–5 %) (Duller 2015) is relatively large.

4.5 Palaeoecological methods

Paleaeecology focuses on long-term vegetation pattern and dynamics and encompasses a number of palaeobotanical methods such as pollen analysis (palynology) and charcoal analysis (antracology) in order to study past changes in these terrestrial envrionments (Twiddle 2012). Both pollen and charcoal analysis are well-established methods to investigate past vegetation composition and to improve the interpretation and reconstruction of the history of human impact on the landscape (Mazier et al. 2006, Nelle et al. 2010). While pollen analysis is used to identify occurrences and relative changes at regional scales in tree and herb species and cryptogams (Faegri and Iversen 1989), charcoal analysis provides local site-related information on woody vegetation and is based on the extraction, quantification, and identification of wood charcoal from soils or sediments (Nelle et al. 2013).

However, both methods have many potential limitations: e.g. pollen identification suffers from limited taxonomic resolution (Birks and Birks 2000), implying that some ecologically important taxa can not be individually distiguished. Moreover, the composition of the background pollen influx »is exceedingly complex, comprising different proportions of taxa ranging from species that produce small amounts of locally dispersed pollen to other species that produce huge quantities of wind-dispersed pollen« (Birks and Birks 2000, p. 31) that may bias the record. The quality of the pollen archive and, thus, the preservation conditions also have to be considered when interpretion pollen data.

The main limitations of charcoal analysis are: only information on the woody vegetation are provided, depositional processes of charcoal rarely occur continuously, and that a bias towards specific wood species for different purposes, such as fire making or house building, cannot ruled out in the interpretation of the vegetation composition (Nelle et al. 2010). Hence, as suggested by Nelle et al. (2010, p. 2127) a combination of both approaches might compensate for their disadvantages and strengthen the interpretations of vegetation composition and dynamics on a local and regional scale.

4.5.1 Charcoal analysis

Pedoanthracological analysis, or the taxonomic analysis of wood charcoal from

soils and sediments was carried out in order to gain local, small-scale information of the occurrence of woody species in the study area over time. In combination with pollen studies, charcoal analysis can be a powerful tool to reconstruct the local fire and vegetation history. Moreover, charcoal taxa were identified prior to radiocarbon dating to avoid the previously discussed old wood effect, and to exclude modern species from dating, i.e. *Picea*. Therefore, short-lived species such as Ericaceae, *Populus*/*Salix*, and *Betula* were preferred. *Pinus* was not used since it is known to also occur in modern plantations.

During the field campaign, ~ 50 samples were taken from charcoal-enriched and humic layers of the profiles 1–6, 8 and 11. In the laboratory, the samples were dry-sieved using a mesh width of 630 µm. Charcoal analysis were then performed within the Department of Palaeoecology of the Institute for Ecosystem Research in Kiel by Dr. Doris Jansen, Dr. Vincent Robin and PD Dr. Oliver Nelle.

For each charcoal sample a minimum of 30 pieces were analysed, apart from a few samples which contained less than 30 pieces. Taxonomic identifications of the very small wood charcoal (1 to several millimeters, very rarely up to 1 cm) was carried out using a stereoscope with magnification up to x112 (Nikon SMZ 1500) and an incident-light microscope with magnification up to x500 (Nikon ME 600, light and dark field) following Schweingruber (1990a, b) and the reference collection of charred wood of the Palaeoecology Research Group of the Institute for Ecosystem Research, Kiel.

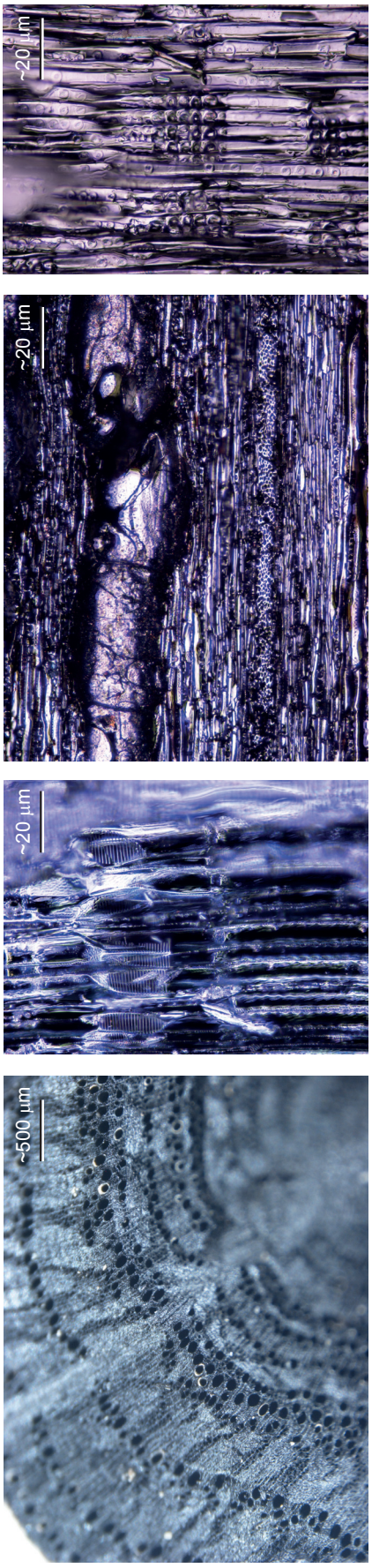

Figure 4.6: Microscopic features of *Quercus* (transversal and tangential section), *Alnus* (radial section and *Pinus* (radial section) (Source: D. Jansen)

As charcoal preserves the cellular structure of wood, its anatomy can be easily recognized (Pique and Pique 1993). For identification it is necessary to study charcoal from three standard anatomical sections: specifically the transveral, radial and tangential section (Figure 4.6). Therefore, the charcoal is manually broken under the stereoscope (x7.5–10) to obtain fractured surfaces that expose these three orientations. The identified fragments were subsequently weighed for each species to calculate percentages on the number and weight. If the charcoal pieces were large enough, wood diameter measurement were also performed on the basis of the visible growth ring curvatures in combination with the angles of wood rays (Nelle 2002, 2003, Ludemann et al. 2004).

4.5.2 Pollen analysis

Palaeobotanical sampling was carried out using special metal box (»Stechkasten«) of 30 x 15 x 10 cm to sample an undisturbed bloc of an organic rich infill from a settlement pit structure preserved in profile 5. From this bloc, eight samples of 1 cm^3 from the organic rich layers were taken for pollen analysis. The samples were treated according to standard procedure (Faegri and Iversen 1989), using potassium hydroxide to dissolve organic matter, fluoric acid to get rid of sand material, and acetolysis. Pollen and palynomorphs were counted with a Nikon Eclipse light microscope with x400 and x1000 magnification, up to 500 arboreal pollen grains per sample. Percentages are based on the total land pollen sum, including *Calluna*. *Alnus* which was categorized as a wetland plant, and excluded from the calculation sum. The pollen calculations and diagram were completed using the software Tilia 1.7.14 (Eric Grimm, 1999–2011).

4.6 Archaeological and historical data

4.6.1 Evaluation of maps

The evaluation of available topographic and historic maps of the study area may reveal important information on the more recent development and land-use changes to the landscape. The oldest historic map of the area (1793 AD) shows the land use in the municipality of Joldelund after the so called »Verkoppelung«, an agrarian reform in Germany initiating the partitioning of commons from rural communities (Prass 2000). Furthermore, topographic maps covering a period over of 130 years could be evaluated in order to reconstruct land-use history from the late 18th century to present (see chapter 5, Figure 5.8).

4.6.2 Archaeological and historical data

During the afforestation in the 1950s, several archaeological sites were discovered, and formed the basis for further archaeological investigations at the end of the 20th century (Jöns 1997). Special emphasis was placed on botanical and anthracological analysis of iron ore production sites (Dörfler 2000, Dörfler and Wiethold 2000). Results of these archaeological investigations have been included in the landscape

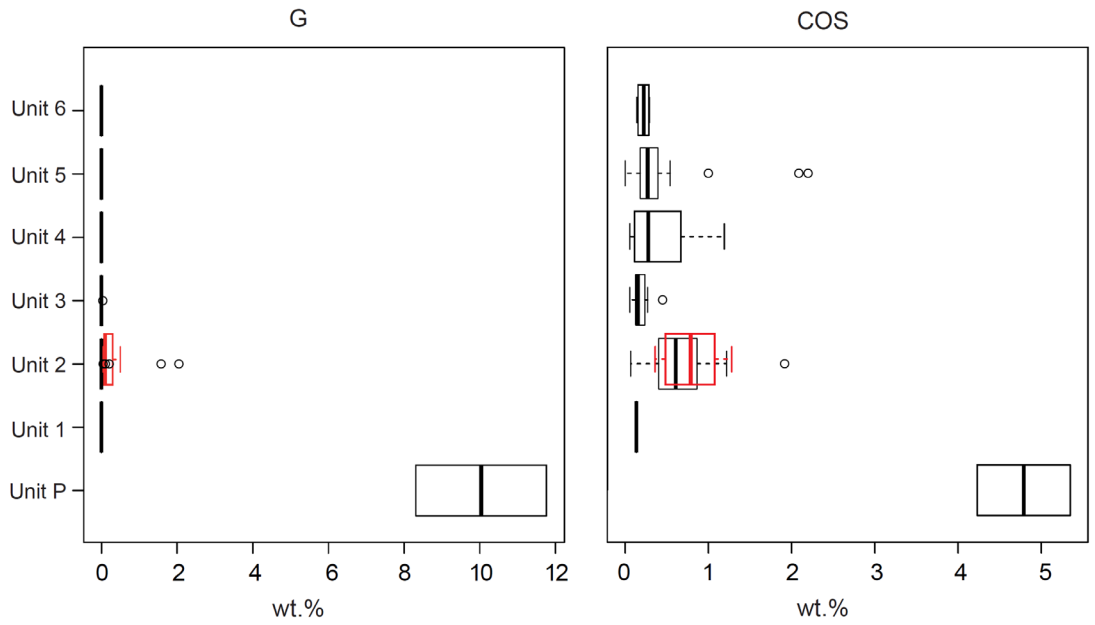

Figure 4.7: Examples of multiple box-whisker-plots plotted in stratigraphical order of the sedimentary units (unit P–unit 6) for the parameter gravel content and coarse sand fraction

reconstruction presented in this study. Historic sources might also give hints on the type of historic land-use, possessions and settlement history. Publications of hand-written copies of the church registry of Schleswig Minster by Hansen and Jessen (1904) were available in Latin; and were kindly partially translated into German by Uta and Georg Emunds.

4.7 Data processing and modeling

4.7.1 Descriptive statistics

Descriptive statistics analysis were used to evaluate and compare the sedimentological and pedological results (chapters 4.3.1 and 4.3.2).

Results of grain size analysis of ~ 130 samples were processed using the the grain size statistic program GRADISTAT provided by Blott and Pye (2001). Statistical grain size parameters such as the mean (M) and the median (Md) were calculated for each sample based on the Folk and Ward (1957) method. Then, the classic Trask sorting coefficient (So) is determined by dividing the 75^{th} percentile by the 25^{th} percentile. In addition, the ratio of the particle classes medium sand to fine sand (MS:FS) was calculated in order to assess conditions of sand accumulation within the profile. Descriptive statistics were also used to analyse and compare the main soil parameters such as soil organic matter (OM), soil bulk density (SBD), soil pH and pedogenic iron oxides (FeD, FeO).

Box-and-whisker-plots were then created in order to depict similarities and differences within sedimentary and soil pa-

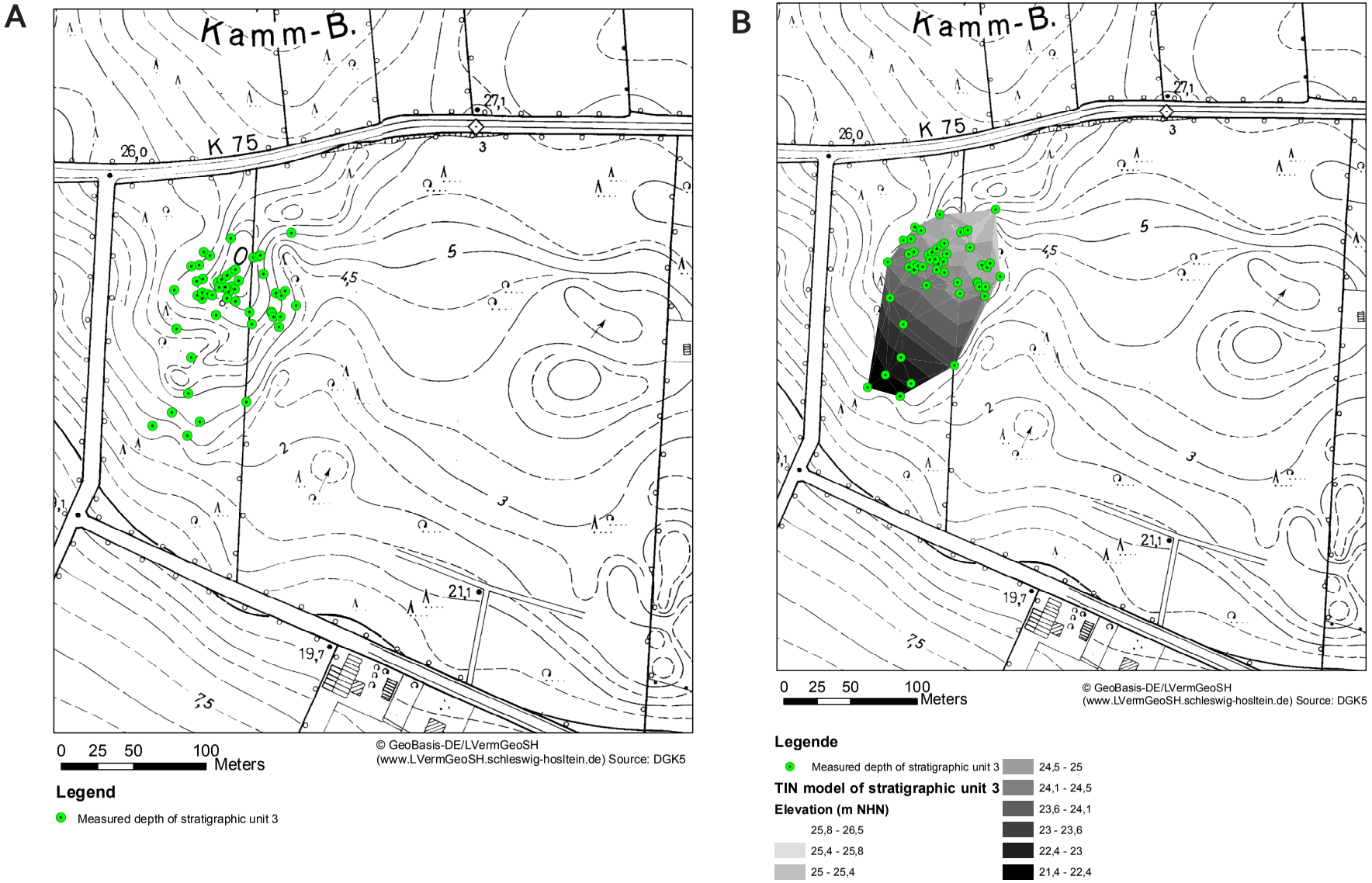

Figure 4.8: Reconstruction of buried dune surfaces on the basis of point sample measurements. A: Measured elevation data of stratigraphic unit 3 (marker horizon); B: Derived TIN model

rameter of the identified stratigraphical units and soil horizons using the statistical software R. Each box-and-whisker-plot provides a graphical view of the median, quartiles (75^{th} and 25^{th} percentile), maximum, and minimum as well as outliners of a data set. For each grain size fraction and soil parameter multiple box-and-whisker-plots were plotted in stratigraphic order of the identified sedimentary units (Figure 4.7).

4.7.2 Modelling past dune surfaces

In order to reconstruct past dune surfaces on a spatial scale the point-related (or profile-related) pedological and geomorphological data (e.g. position, depth, chrono-stratigraphic correlation and thickness of marker horizons, soil colour and estimated grain size) needed to be regionalized. This means that spatial features (e.g. buried dune surfaces) are derived from the spatial distribution of measured properties (e.g. depths of a dated marker horizon).

For the generation of digital elevation models of the past dune surfaces, the following steps were undertaken (see chapter 6):

i) Determination of exact location of 125 field measurements of the depth of the different identified marker horizons (buried soil horizon, sedimentary boundaries) using laser-based total station

ii) Determination of exact location of ~ 125 field measurements of the depth of the underlying Pleistocene moraine deposit using laser-based total station

iii) data preparation (Microsoft Excel) and import of all elevation (depth) information as (3D) point cloud (xyz-data set) into ESRI ArcGIS 10.1

iv) Generation of a TIN model (Triangulated Irregular Network) for each stratigraphic unit.

v) Conversion of all TIN models to separate surface raster models (DEMs) through natural neighbor interpolation using the 3D Analyst.

By way of example, Figure 4.8 shows the reconstruction of the surface of the stratigraphic unit 3 based of measured elevation data.

In order to quantify and evaluate the geomorphic changes of the KHD over time, the ArcGIS Add-In version of the Geomorphic Change Detection (GCD) software (www.gcd.joewheaton.org) was applied. The open-source GCD tool was used to derivate spatial error models and estimate geomorphic changes (changes in net volumes) in the dune topography while accounting for significance of uncertainties in DEMs (see chapter 6).

4.8 Visualization methods

Three different 3D visualization software products were applied to visualize geo-archaeological results and to spatially reconstruct landscape development within the study area. What follows are short descriptions of the 3D visualization software and its use in this study (chapter 8).

4.8.1 Autodesk® 3ds Max®

The 3D CAD animation software Autodesk® 3ds Max® 8 was used to visualize the dune building phases of KHD, local vegetation history and small-scale land-use changes. Autodesk® 3ds Max® 8 is a comprehensive visualization tool primarily applied in the fields of design and architecture, and also in computer games. The basic principle of Autodesk® 3ds Max® 8 is to model 3D objects and create materials representing their surfaces. Simple 3D objects such as spheres, cubes or planes serve as basic elements for complex shapes. Materials are termed a collection of textures, either from raster images or processed in a procedural manner, which are used to define the non-geometrical appearance of the surface characteristics of a 3D object such as colour, shade, opacity and others. Scene objects can be animated in many ways, e.g. the animation of spatial position, size or surface characteristics of any parameter.

To achieve a photorealistic appearance of the virtual landscape, maps and textures can be used, such as photographs of grazing animals and plants or designed bitmap files of soil profiles. Furthermore, dynamism of landscape processes can be created by animating different materials and maps, for example, by fading 3D objects and animating fire events by modelling flames and smoke.

4.8.2 Visual Nature Studio™2.86

Scenarios of the past and actual landscape surfaces were visualized using the GIS-based software Visual Nature Studio™2.86 (VNS) developed by 3D Nature. In contrast to 3D CAD software, VNS is specialized for modelling natural landscapes. By using different geospatial data, such as a digital elevation model (DEM) and vector datasets, raster images as well as modelled 3D objects as input, VNS enables the user to generate photorealistic landscape images and animations. VNS provides a number of pre-defined tools, so-called components, to generate a virtual landscape. Comparable to a modular construction system, landscape features such as vegetation, terrain surfaces and manipulations, illuminations and cloud types and water bodies can be defined and animated independently. Furthermore, texture mapping of terrain surfaces or 3D objects allow users to create a realistic appearance of surfaces, for example, by covering them with hatches, patterns or images using GIS data and their attributes (e.g. for density, positioning and orientating). By animating single parameters, the software provides representation of landscape feature dynamics, e.g. vegetation, surface movement and land use patterns. In order to represent plants and vegetation types, billboards are used. Billboards are center-view-oriented vertical

rectangle planes (Gabler-Mieck and Duttmann 2007), textured with an image representing geo-objects such as trees, flowers and animals. Hence, virtual ecosystems can be associated with vector objects to define spatial position and distribution. In addition, 3D objects (e.g. houses) can be integrated in the virtual landscape.

4.8.3 Real-time environment a3dc

The third tool applied is a web-based 3D real-time environment named a3dc. It provides interactive visualizations of the landscapes using Java3D libraries (Gabler-Mieck and Duttmann 2007). Thus, a3dc displays geospatial and thematic information as provided from common geographic information systems. The a3dc software also offers numerous other interaction options: Using DEM as basic input, it permits unrestricted navigation. A3dc also allows modifications to illumination, visibility conditions and positioning of 3D objects. Therefore, it empowers users to perform, for example, interactive 3D visibility analyses. Data is organized in a freely-definable layer structure, enabling the depiction of 3D text, billboards, thematic maps or 3D objects as layer objects. These could be associated with attribute data or with URLs to show websites or local HTML content. In addition, a3dc allows the assignment of one or more behaviours to any layer object, for example, the animation of layer objects for a predefined path (Gabler-Mieck and Duttmann 2007). Comparable to VNS and Autodesk® 3ds Max® 8, raster images are also used as billboards for displaying single plants or a specific vegetation cover.

Regional Setting

5

5.1 Reaseach area

The research area is the Kuhharder Hill dune (KHD, german: Kuhharder Berg), a small inland dune southwest of the village Joldelund (54° 38‘ 45“ N, 9° 7‘ 14“ E, Northern Frisia), ~ 25 km southwest of the town Flensburg and ~ 25 km northeast of the town Husum (Figure 5.1). It lies in the municipality of Joldelund (Joldelund region), which is located in the so called »Geest« of Schleswig-Holstein, a part of the Weichselian outwash plain of the Jutland Peninsula. The Geest is embedded in the so-called European Sand Belt (ESB); this sand belt constitues extensive aeolian deposits formed mainly during the last glacial period (Zeeberg 1998, Koster 2005). Figure 5.2 shows the position of Joldelund within the ESB and the distribution and location of dunes within Schleswig-Holstein. Inland dunes and cover sands are most prevalent in the Geest of Schleswig-Holstein (comprising the so called »Vorgeest», »Altmoräne« or »Hohe Geest«) which form a narrow, north-south stretching landscape unit between the marshland in the West and the younger-moraine landscape in the East of Schleswig-Holstein.
The Joldelund region includes parts of the so called Schleswiger Vorgeest (»Vorgeest«) and Bredstedt-Husumer Geest (»Altmoräne«) (Meynen and Schmithüsen 1953–1962). The prevailing depositional units within the area are i) glaciofluvial sands, ii) periglacial reworked moraines of the Late Saalian (Warthe II) glaciation (MIS 6 according to Litt et al. 2007, Stephan 2014) as well as iii) aeolian and organogenic sediments.

The area of the KHD constitutes ~ 2 ha and forms the westernmost part of an ~ 80 ha large inland dune field. These dunes cover an end moraine ridge which is orientated from northwest to southeast. The surrounding relief is mostly flat and inclines gently towards the west (Backer et al. 1992, Riedel 1997). The highest point of the inland dune field is at KHD (~ 30.3 m asl); the lowest elevations are in the valley bottoms of Neue Au Creek and Ostenau Creek (~ 7 m a.s.l.[3]) (Figure 5.1). The difference in height in relation to the research area is maximum ~ 23 m.

At present, the inland dune field and research area is mainly covered by coniferous forest. It was afforested in the 1950s due to a government-funded afforesta-

3 *The expression m.a.s.l refers to the standard reference level »Normalhöhennull« (NHN)*

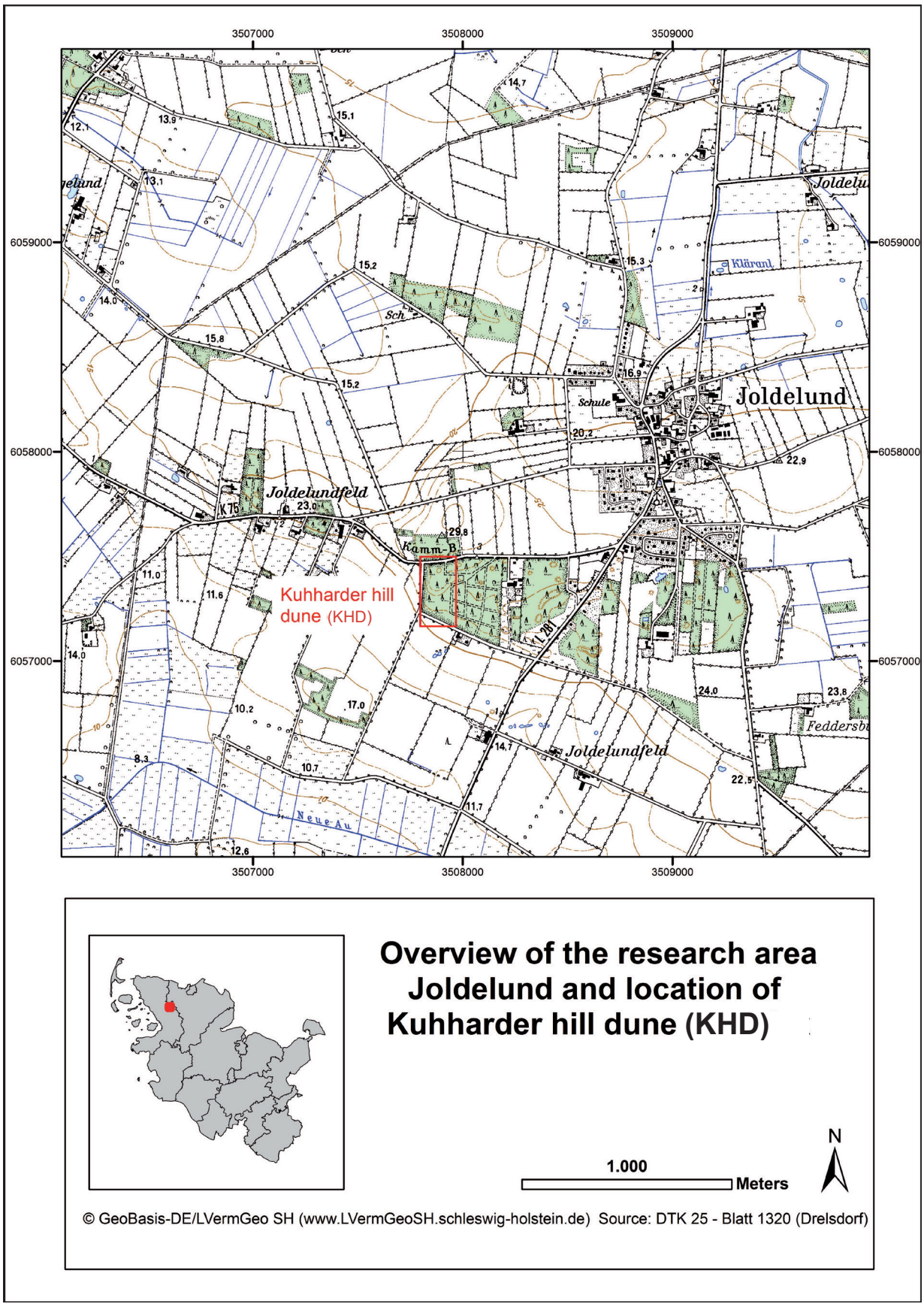

Figure 5.1: Overview of the research area: Joldelund region and location of Kuhharder Hill dune (KHD)

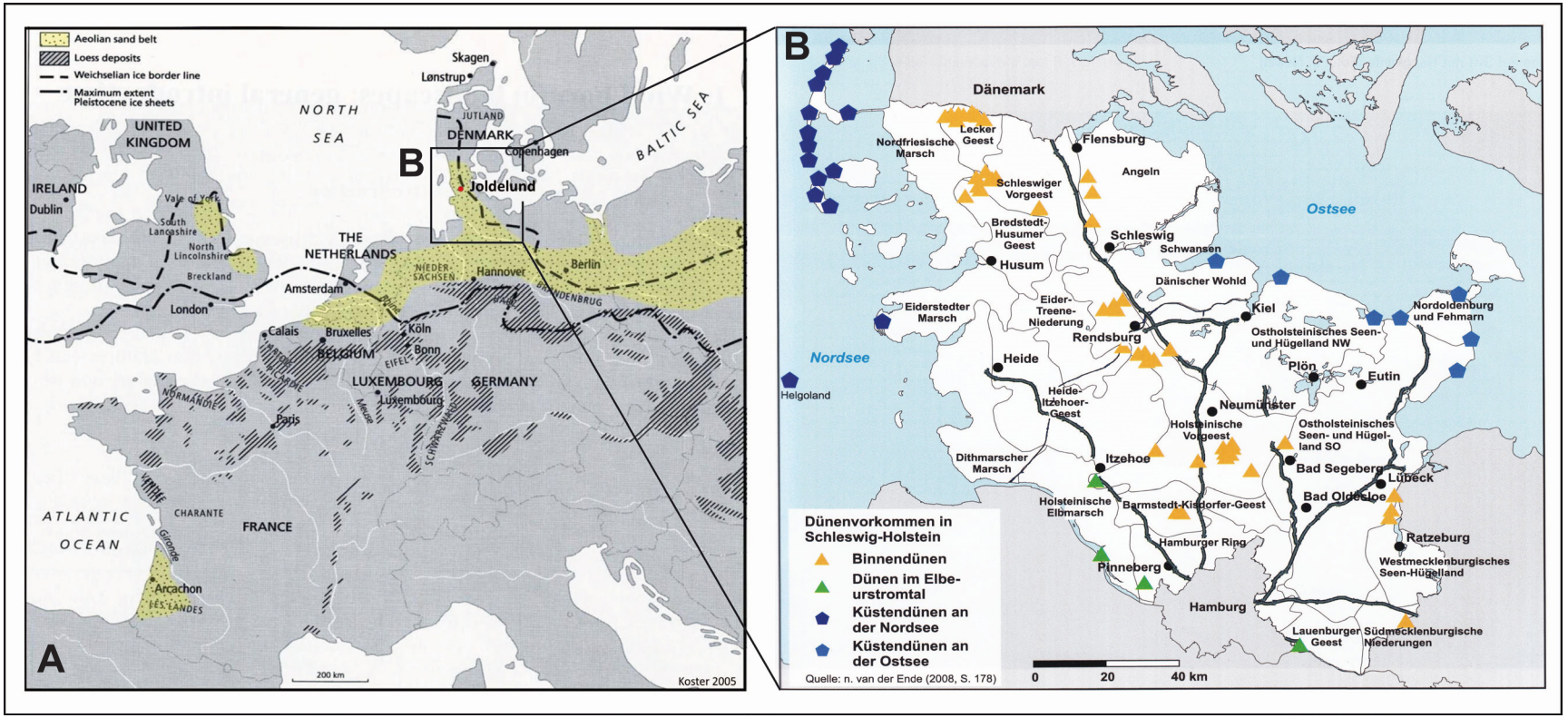

Figure 5.2: A: Location of Joldelund in the European Sand Belt (Koster 2005, modified). B: Location and distribution of inland dunes (»Binnendünen«), river dunes (»Dünen im Elbeurstromtal«) and coastal dunes (»Küstendünen an der Nordsee«, »Küstendünen an der Ostsee«) in Schleswig-Holstein (LLUR 2011 according to van der Ende 2008; modified)

tion program (Programm Nord 1979). The KHD is situated in the municipal forest of Joldelund which covers an area of ~ 13 ha (Figure 5.1).

After the field study presented here a severe European winter storm (Cyclone Christian) caused widespread damage in forests within Schleswig-Holstein in Oktober 2013 (DWD 2013, MELUR 2013, SHLF 2014a). This storm affected the forests of Joldelund. However, it was especially the falling trees (blowdowns) and the subsequent clearance of storm damage by heavy machinery (SHLF 2014b), which led to significant changes in the local dune topography.

5.2 Geologic setting and Geomorphology

The geology of the shallow subsurface of the Joldelund region is characterized by Pleistocene and Holocene sediments. Weichselian glaciofluvial deposits (glaciofluvial sands) of the Sandur plain dominate the Joldelund region. During the Weichselian Late Glacial Period glaciofluvial sediments were transported westwards from the glacial portals near Flensburg, Oeversee and Sieversted by melt water streams (Strehl 1999). Within these deposits, the grain size becomes progressively finer towards the west (Fränzle 1985). The research area is situated around 20 km from the Weichselian ice margin and relatively fine sediments like medium sands with varying proportions of fine sand, dominate the the glaciofluvial sediments, and serve as parent material for the local soils. Remains of an older end moraine (Kamm Hill; german: Kammberg) are exposed in the central and eastern part of the research area, and are associated with the younger Saalian (Warthe II) ice advance (Strehl 1999). These deposits were periglacially reworked and eroded during the Weichselian glaciation. At present, the Kamm Hill is ~ 29.8 m in height and rises above the surrounding relief of the Sandur plain which is mostly flat and inclines gently in the western direction (Figure 5.3).

In the northwest and southeast of the Saalian moraine aeolian cover sands and dunes superimpose the glacial and glaciofluvial deposits. The old aeolian relief in the wider region of Schleswig-Holstein, including the research area, was predominantly formed during the Weichselian Late Glacial (Older and Younger Dryas) (Gripp 1967, Jatho 1969, Müller 1999, Koster 2005, Mauz et al. 2005). In the Late Holocene several phases of aeolian activity and remobilization of aeolian sands are known to have occurred during the Roman Iron Age and from the Medieval Times until the recent past. Koster (2005) referred to aeolian deposits resulting from reactivation of sandy sediments by human impact since the Neolithic period as (aeolian) drift sands.

Peatlands (bogs, lowland fens) of the area formed during the Holocene. As a consequence of melioration measures and peat cutting the only remaining peatland areas are preserved along the Neue Au Creek and Ostenau Creek (Figure 5.3). At the end of the 18th century these organogenic sed-

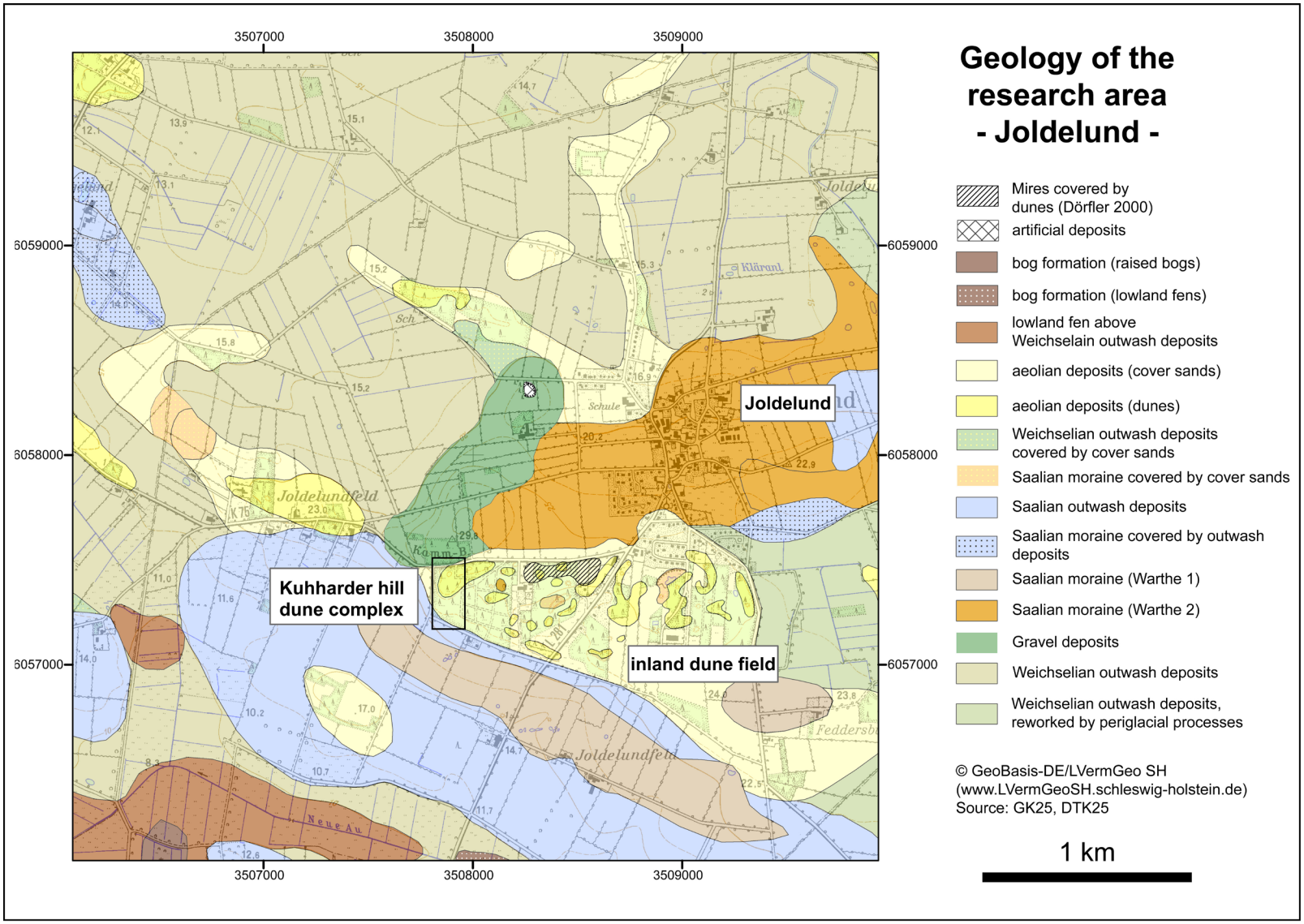

Figure 5.3: Geological units of the research area and Joldelund region

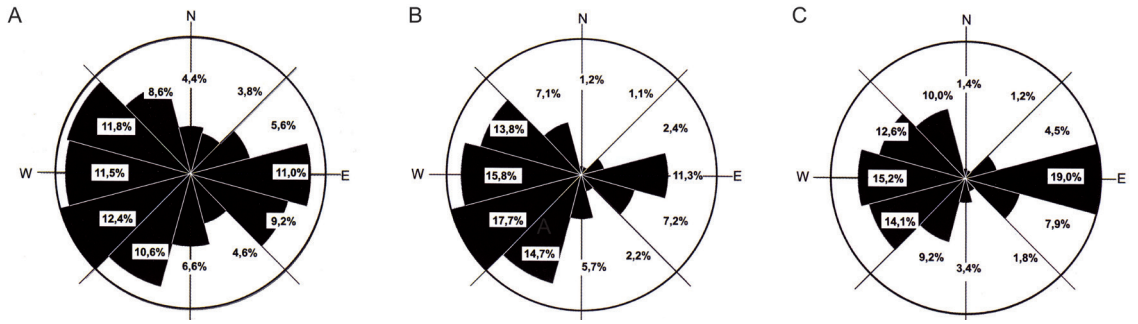

Figure 5.4: Wind direction distribution for the station Leck for the period of period 1973–2002 (Source: DWD, average hourly data of wind direction and wind velocity at standard height: 10 m). A: Frequency distribution of wind direction. B: Frequency distribution of wind direction for winds with velocities of more than 7 m/s. C: Frequency distribution of wind direction for winds with velocities of more than 7 m/s in March, April and May

iments still covered ~ 20 % of the area of Joldelund, while today the number is close to zero (Dörfler 2000).

5.3 The climate of the Joldelund region

The Joldelund region is located in the west wind zone and ~ 25 km distant from the North Sea, and is part of the temperate oceanic climate (Köppen climate classification: Cfb), with a 8.2 °C mean annual temperature and 820 mm mean annual precipitation (German Weather Service, DWD: climatological data for station Leck for the period 1975–2002). Westerly winds predominate the area during the year (Figure 5.4). The coldest month is January, with an average temperature of 0.3 °C and the warmest is July, when the average temperature is around 15.7 °C. The annual temperature amplitude is 15.2 °C. In terms of rainfall patterns, the area is determined by relatively high, year-round constant precipitations (Duttmann et al. 2004, source: DWD). On average, most rainfall occurs during September and November (> 85 mm), with maximum precipitation in October (~ 100 mm). Rainfall is relatively low during the spring months (February until May) with about 20 % of the mean annual rainfall (Bach 2008).

Figure 5.4 shows the average frequency of wind direction registered at station Leck in the period from 1973 until 2002. Westerly winds are prevailing with average annual wind velocities of 4.9 m/s at a standard height of 10 m (western wind quadrant: 35.7 %, eastern wind quadrant: 25.8 %, northern wind quadrant: 16.8 %, southern wind quadrant: 21.8 %) (Duttmann et al. 2004, Figure 5.4). Although winds with an average wind velocity of at least 7 m/s are most frequent from westerly directions, in the Schleswiger Geest (relatively dry) easterly winds instead of (relatively moist) westerly winds are associated with wind erosion and drift sands. From March to May, strong dry winds (> 7 m/s) occur from eastern directions (Hassenpflug 1998, Duttmann et al. 2004) and are mostly related to a circulation pattern with high pressure over Fennoscandia and Northern Russia (Gerstengarbe and Werner 2005) (Figure 5.4C).

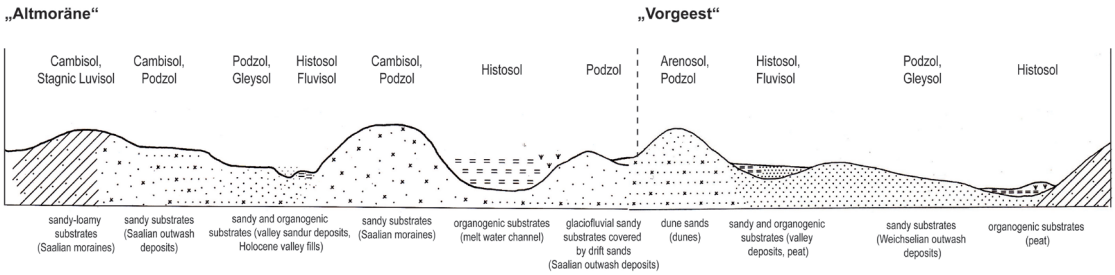

Figure 5.5: Simplified, schematic cross-section of the natural landscape units »Altmoräne« and »Vorgeest« of Schleswig-Holstein including typical parent material and soil types (LLUR 2012, modified)

5.4 Soils and soil formation

Soils of the research area strongly depend on the underlying geological units, and the soil parent material mainly consists of medium-to-fine glaciofluvial and aeolian sands, but also of (reworked, sandy loamy) glacial till and organogenic sediments (Figure 5.5). Glaciofluvial and aeolian deposits are silicate-poor, carbonate-free and deeply depleted (Fleige et al. 2006). The main soil formation processes typical for the natural landscape units of »Altmoräne« and »Vorgeest« are podzolization, gleyization, pseudogleyization and peat formation. Figure 5.6 shows the typical soils (according to IUSS Working Group WRB 2015) of the Joldelund area: i) Gleyic Podzols (~ 53 %), ii) Stagnosols and Stagnic Cambisol (~ 15 %), iii) Sapric Histosols and Ombric Histosols (~ 11 %), iv) Haplic Podzols and Dystric Arenosols (~ 8 %), Cambisols and (Cambi-) Haplic Podzols and v) Gleysols (~ 5 %).

At the KHD Haplic Podzols (~ 80 %) are widespread developed in aeolian sands, however, Spodi-Terric Anthrosol (~ 13 %) are to be found as a result of melioration measures in the 1950s as well as Dystric Arenosols (~ 6 %) and Arenic Regosols (~ 1 %). Podzols with a high proportion of fine to medium sand are dominant in aeolian sediments and are prone to wind erosion (Duttmann et al. 2004). Predominantly Gleyic Podzols and Gleysols have developed under the influence of groundwater in lower elevations. In the floodplains of Neue Au Creek and Ostenau Creek, Histosols formed under waterlogged condition.

5.5 Late Quaternary landscape change in the Joldelund region

5.5.1 Landscape development during Weichselian Late Glacial and Early Holocene

The aeolian relief of the Joldelund region mainly formed during the Weichselian Late Glacial Period under periglacial environmental conditons. A sparse vegetation cover, strong winds and abundant availability of sediments (Kolstrup 2005) have been the basis prerequisites for the widespread deflation and depositon aeolian deposits, such as cover sands and dunes in the research area and within northern-central Europe (Jatho 1969, Pyritz 1972, Koster 1988, Müller 1999,

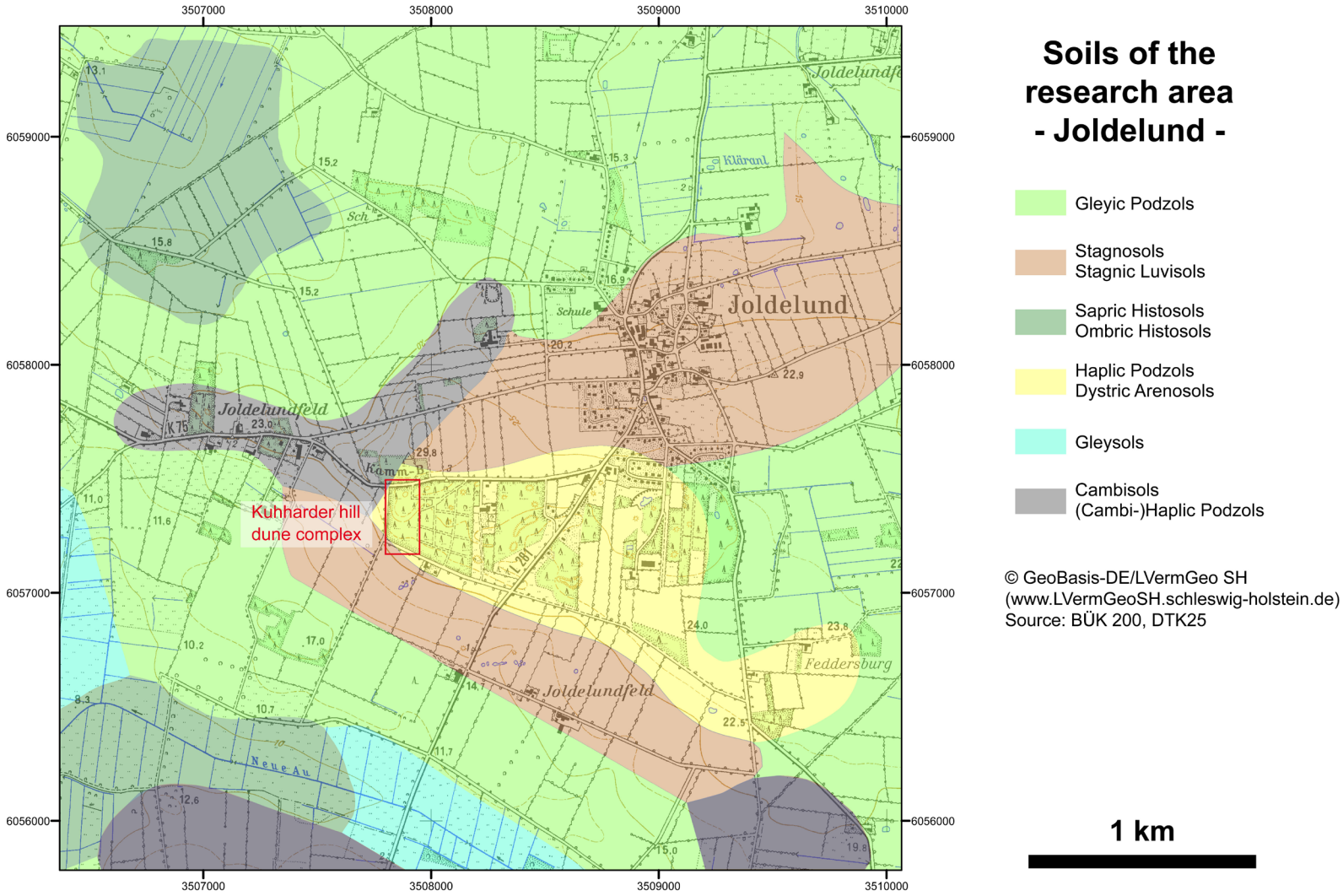

Figure 5.6: Soil map of the research area and Joldelund region

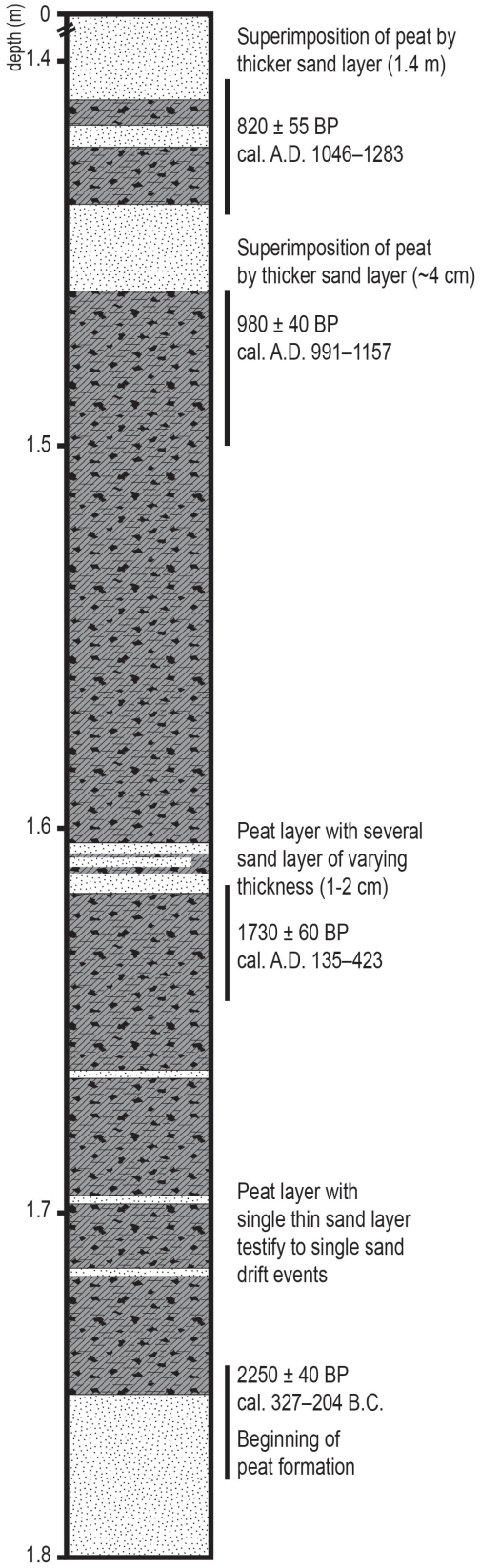

Figure 5.7: Simplified redrawn radiography of peat core 16 (mire covered by dunes, MUD; Dörfler 2000). Calibrated radiocarbon ages given in 2sigma and calibrated according to Reimer et al. (2013) using IntCal 13

Strehl 1999, Müller 2000, Koster 2005, Mauz et al. 2005). These »cold-climate aeolian deposits« (Koster 1988) formed during Older Dryas (13800–13670 v.y. BP) and Younger Dryas (12680–11590 v.y. BP) were interrupted by a period of »non-deposition« (Kasse 1999, p. 74) resulting in landscape stabilization due to woodland vegetation during the Allerød period (13.350–12.680 v.y. BP)[4]. In northern central Europe the start of the Younger Dryas period is often pedostratigraphically marked by the Usselo / Finow soil, a buried or fossil soil horizon that formed during Allerød to early Younger Dryas (Kaiser and Clausen 2005, Kaiser et al. 2009, Hoesel et al. 2012).

A similar palaeosol was also reported from Joldelund and the adjacent areas (Backer et al. 1992): a humic and charcoal enriched horizon formed at the surface of a ~ 0.4 m thick aeolian deposit and which was buried under dune sands of ~ 0.5 m thickness. Backer et al. (1992) identified and associated this humic layer with the Usselo (soil) horizon. Fleige et al. (2006) investigated a dune profile near Riebriek (municipality of Goldelund) ~ 8 km north of Joldelund, and identified a humus rich horizon (~ 5.9 % C_{org}) with features of cryoturbation, which was found near the bottom of the dune at a depth of 272–274 cm. It was dated using the radiocarbon dating method to an age of 10685 (+/-55) BP (KIA 25559, Leibniz-Laboratory for Radiometric Dating and Stable Isotope Research), indicating

4 *Datings of stratigraphic units of Weichselian Late Glacial are given by Litt et al. 2007 (v.y. BP. = varve years BP with reference year 1950)*

the last cold period of the Weichselian ice age (Younger Dryas, YD) as its formation period (Fleige et al. 2006, p. 15).

After the Late Glacial phase of aeolian activity warmer temperature in the Holocene (~ 11700 BP[5]) led to reforestation and stabilization of the surface in Northern Europe (Strehl 1999). Since the Early Holocene in the Joldelund region woodland was the dominant vegetation type. Dörfler (2000) showed that a mixed oak forest was typical for the region since at least 6000 BP, the start of the pollen record of the nearby mire Hörrmoos. The woodland was mainly composed of oak (*Quercus*), hazel (*Corylus*), birch (*Betula*) and alder (*Alnus*). In contrast to the occurrence of wind erosion towards the end of the last glacial period, remobilization of aeolian deposits during the Holocene are mainly triggered by human activities.

5.5.2 Landscape change under human influence

In the region of Joldelund the first traces of human occupation have been documented from the Mesolithic period (Hingst 1975, Jöns 1997). Early agricultural land-use date to the Neolithic period, in which »initially the exposed sites on the older moraines were cultivated« (Duttmann et al. 2006, p. 5). The first phase of major reactivation of aeolian deposits is known to have occurred during the Roman Iron Age (Riedel 1997, Dörfler 2000). Settlement activities associated iron ore production are proven for the research area, which dated to the Late Roman Iron Age (4th–5th century AD) (Erlenkeuser et al. 1997). At that time woodland was dominant, albeit woodland clearing for agricultural land-use and pasture took place close to the settlement (Jöns 1997). During that time, human activities caused mainly local changes in landscape and vegetation, which resulted in moderate sand drifts (Dörfler 2000).

Radiographic and palynological analysis of a small mire close to the KHD (mire covered by dunes, MUD) indicate that human impact during the Early Iron Age and Roman Iron Age had only a local effect on the (aeolian) landscape (Figure 5.7). Layers of aeolian sands deposited in the peat core reflect the local human impact of the area Joldelund since the onset of peat formation: During the Roman Iron Age soil erosion on probably farmed land led to deposition of several, smaller sand layers in the peat profile. However, thicker sand layers did not occur before ~ 1000 AD, which indicates that widespread cultivation of land dates back to Medieval Times (Dörfler 1992, Dörfler 2000). This findings was interpreted as patchy, mosaic-like land-use during the Roman Iron Age, including open areas (settlement sites), semi-open areas (forest grazing, selective cutting, spread of heathland) and closed areas (relatively dense woodland) (Dörfler 2000).

Human impact decreased during the Migration Period (»settlement gap«) which was accompanied by the regeneration of forest vegetation (Nelle and Dörfler 2008). Palynological results of the MUD

5 *The Holocene begins with the Preboreal ~ 11700 BP, according to ice core data from NorthGRIP with reference date 2000 AD); cal ~ 9650 cal. BC (Nelle and Dörfler 2008).*

shows that there was less anthropogenic interference during the period between ~ 550 AD and ~ 870 AD (Dörfler 2000): non-boreal pollen and proportions of cerealia drop significantly, while percentages of tree and shrub pollen increase up to ~ 90 % of the total.

The large increase in human impact occurred during Medieval Times (~ 1000–1500 AD) (Richter 1965, Müller 1999, Mauz et al. 2005). Intensive deforestation and the expansion of agricultural land-use led to considerable changes in the landscape and vegetation cover. Within the research area, former woodlands were either converted into coppice wood or degraded to heathland (Duttmann et al. 2006, Bach 2008). Intensifying agriculture, grazing, removal of plaggen and slash-and-burn cultivation led to the deterioration of heathland which resulted in the recurrence of sand drifts (Pott 1998, Behre 2000b). Heathland replaced almost all forest vegetation and became the dominant landscape element in the region (Nielsen 1972, Behre 2000a, Dörfler 2000).

As a consequence of medieval landscape transformation, due to overexploitation, disastrous wind erosion events occurred in the research area and in neighboring communities, leading to vast degradation of farmland and the formation of inland dunes (Andresen 1924, Müller 1999). According to historical sources of the church register in Schleswig, in 1414 AD the medieval settlement of Joldelund (spelled »Hyoldelunt«) had been abandoned for approximately 30 years (Hinz 1949, Richter 1965) and no tax payments are recorded. Also, the village church had been empty and unused for more than 40 years (Nielsen 1981). The number of farmsteads recorded in the chronicles of the village Joldelund was very low: ~ 1400 AD there were only four farmsteads. The period of increasing aeolian activity seemed to end during the Thirty Years War (1618–1648) when, according to Müller (1999), widespread devastation and population decrease resulted in a decline of agricultural land-use.
In 1680 AD, ten farmsteads which in total cultivated an area of approximately 50 ha (Schnepel 1981) are recorded and indicate a re-population of the area. In the following hundred years, and in the course of agrarian reforms (»Verkoppelung«) at the end of the 18th century, the number of farmsteads went up to 20. As part of the reforming process, the formerly collectively owned heathland which was extensively used as common sheep and bee pasture, was divided up amongst the farmers.

The oldest historic map of the area (1793 AD) shows the land-use of municipality of Joldelund after the »Verkoppelung«. Over ~ 50 % of the area was covered with heaths (wet heath and sand heath), followed by mires with a ~ 20 % of the current area. Grasslands (~ 13 %) were concentrated along the Neue Au creek and arable land (~ 12 %) was strongly centred around the settlement. Forest cover was reduced to zero and recognizable dunes covered ~ 5 % of the total area (Dörfler 2000). By analysing topographical maps for the years 1793, 1878, 1950 and 1985, Dörfler (2000) showed that Joldelund underwent considerable changes during the past 200 years. Particularly at the end of the 19th century and at the beginning of the 20th

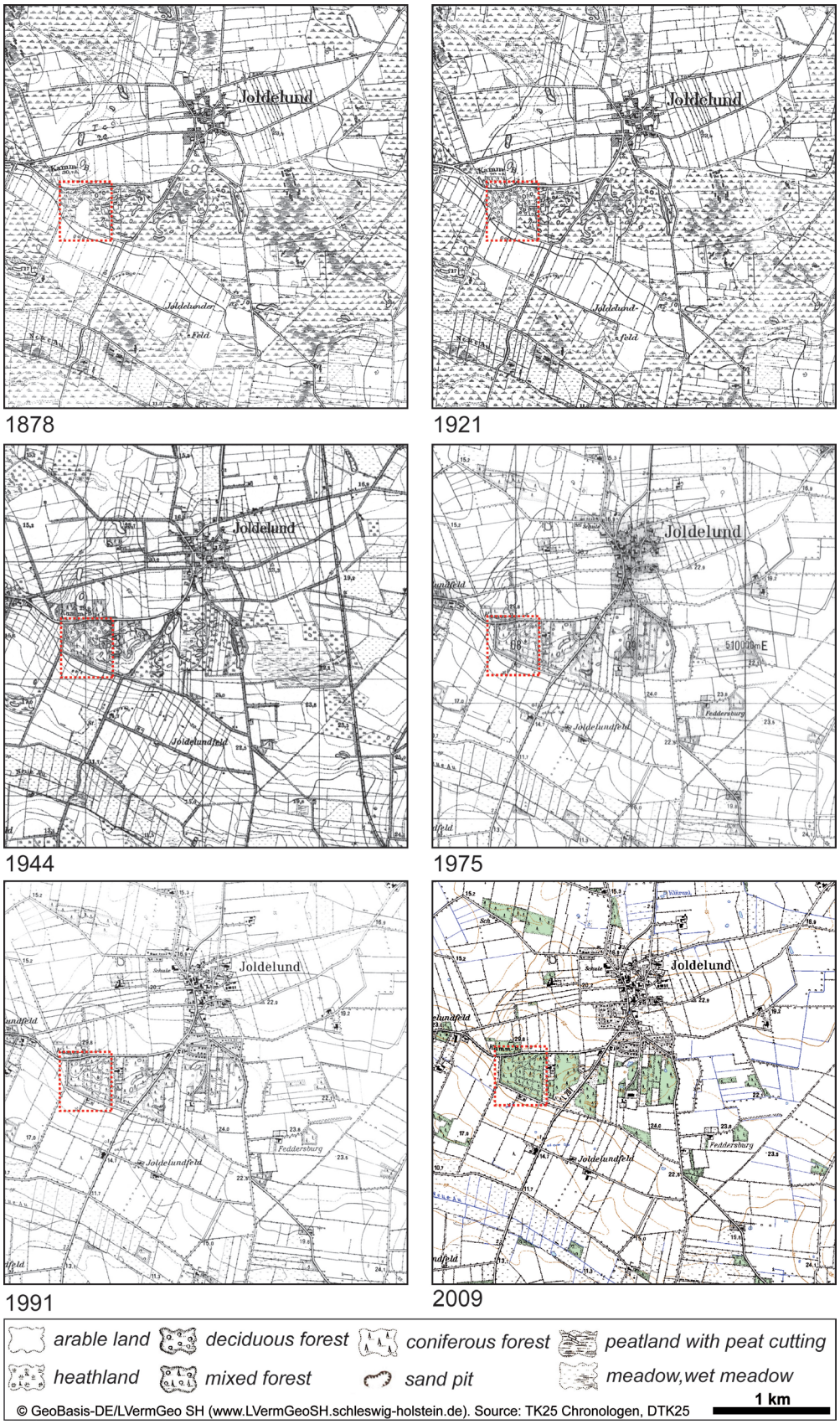

Figure 5.8: Historical topographic maps of the period 1878 until 2009 showing changes in land-use of the Joldelund region and the KHD area. Red dotted: the current boundary of municipal forest

century heathland was converted into arable land and peatland was drained and used as grassland (Dörfler 2000, Duttmann et al. 2004, Duttmann et al. 2006, Bach 2008). Modern machinery in farming (steam ploughs) and the use of mineral fertilizer finally enabled the intensive agricultural use of heathland. The intensification continued into the second half of the 20th century with the modification of almost all remaining heaths and mires into agriculture. In contrast, forest cover has increased due to an afforestation program against wind erosion in the 1950s (Programm Nord 1979). Figure 5.8 provides a synoptic presentation of local land-use changes for the area around Joldelund and the KHD research area for the period from 1878 to 2009. From 1878 until the beginning of the 1920s only minor chang-

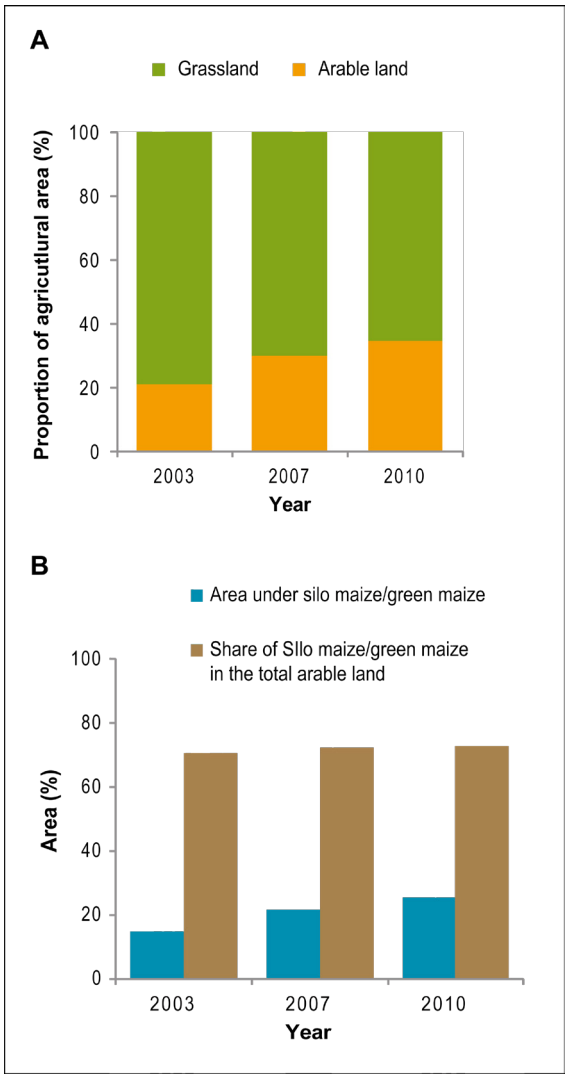

Figure 5.9: Recent changes in land-use within the Joldelund region. A: The ratio of grassland to arable land in the period from 2003 to 2010. B: Proportions of area cultivated with silo maize/green maize in relation to the total agricultural area and percentages of areas cultivated with silo maize/green maize of agrigultural areas of Joldelund from 2003 to 2010 (Statistikamt Nord 2005, 2009, 2013)

es in land-use can be found. Heaths are dominant on the inland dunes as well as in southern and northwestern parts of the area. Arable land is clustered around the village, and south of the inland dune field. The KHD was initially covered by heath, later by oak coppice wood. A single agricultural field is located directly adjacent to the dune complex. In 1944, heathland and mires have been significantly reduced to relatively small areas in northwestern and central part, while areas of agricultural use had increased accordingly. Parts of the inland dunes were covered with forest. In 1926, the municipality of Joldelund had begun to systematically afforest the area of today's municipal forest (~ 13 ha) including KHD (Schnepel 1981). The field was turned into coniferous forest.

During the increasing industrialization and mechanization of agriculture between 1944 and 1975, all of the remaining areas of heathlands and mires were either fully converted into arable land or grassland or afforested within the Programm Nord (Programm Nord 1979). Since then, the Joldelund ragion has been an intensively

Figure 5.10: Storm damages after Cyclone Christian on 27th and 28th of October 2013 in the municipal forest of Joldelund. A: View from highest point at Kuhharder Hill dunes onto eastern parts of forest. B: Central part of the forest with traces of forestry harvester and blowdowns (root plates)

used agricultural landscape. At the KHD the small agricultural field still present in 1921 was planted in conjunction with the program of the 1950s. At the same time, all coppiced wood has been removed and replaced by plantings of spruce (*Picea abies*, *Picea sitchensis*, *Picea glauca*), pine (*Pinus sylvestris*, *Pinus nigra*, *Pinus mugo*) and larch (*Larix kaempferi*) (Nielsen 1970). During the post-war years of the world wars, an increase in sand drifts was noticed in the Joldelund region (Richter 1965, Duttmann et al. 2004, Bach 2008). Reasons for this were i) an urgent need for wood as well as ii) a more intensive cultivation and the expansion of e.g. root crops as a contribution to the food security. The then ongoing structural change in agriculture was generally accompanied by a decline of the total area of productive agricultural land and the expansion of forage production. This resulted in a reduction of wind erosion processes (Bach 2008), albeit single sand drift events were documented continuously until present day (Hassenpflug 1971, 1981, 1998, 2011).

At present, the land-use of the area is dominated by pastures and meadows for dairy farming and cultivation of corn for the production of biogas. The ratio of arable land versus grassland is currently undergoing a change towards an increase of arable land. In the year 2003 the ratio of arable land to grassland was 20:80, in 2007 it changed into 30:80 and at present the ratio is about 35:65 (Figure 5.9A) (Statistikamt Nord 2005, 2009, 2013). This trend also becomes apparent within the neighboring communities where the proportion

Figure 5.11: Afforestation of the study area after storm damages in 2015 (Source: R. Duttmann)

of agricultural land that is used for arable land in relation to the total agricultural areas is higher than 50 % (Hassenpflug 2011). Recent changes in land-use relate to an increasing cultivation of energy crops, especially maize (Figure 5.9B). In the municipality of Joldelund, the proportions of the area cultivated with silo maize / green maize in relation to the total agricultural area comprised ~ 15 % in 2003. This proportion rose to ~ 25 % in only seven years (acreage of silo maize / green maize: 2003 = 221 ha, 2007 = 282 ha, 2010 = 318 ha) (Statistikamt Nord 2005, 2009, 2013). However, the share of silo maize / green maize in relation to the total area of arable land shows only a slight increase (2003: ~ 70 %, 2007: ~ 72 %, 2010: ~ 73 %). The effects of increasing maize / corn cultivation on wind erosion is still to be seen.

Recent changes at the KHD occurred in 2009 and 2013. In 2009, forest maintenance measures thinned out the southern part of the municipal forest was thinned out. Tree stumps were removed, and mixed forest was replanted. On 28th of October 2013 a winter storm (Cyclone Christian) caused severe damage to Joldelund municipal forest and adjacent forests (SHLF 2014a). Very strong winds (Beaufort Scale 12) resulted blowdowns of the whole forest sections all over Schleswig-Holstein (DWD 2013, MELUR 2013). Blowdowns and subsequent clearance of storm damage by heavy machines (SHLF 2014b) led to significant changes in the dune relief of the KHD (Figure 5.10). An afforestation with primarily mixed forest started in 2015 (Figure 5.11).

6

Anthropogenic initiation and acceleration of Aeolian dune activity in northern Germany over ~2500 yrs and feedbacks with socio-economic development

(To be submitted to: *Quaternary Science Reviews*)

6.1 Introduction

Since their arrival, humans have modified central European landscapes in many ways and to different degrees and intensities, most spatially extensive since the widespread implementation of agriculture from Neolithic time (~ 7.5 ka–5.5 ka, Delson et al. 2000). A large increase in population at ~ 1200 AD (Bork et al. 1998, Kaiser et al. 2002) in pre-industrial Europe lead to widespread settlement activity and deforestation in Medieval Times, which in turn lead to large human made landscape changes throughout central Europe (e.g. Bork et al. 1998, Dotterweich 2003, Larsen et al. 2013). This intensive phase of Medieval settlement activity ended in the abandonment of many villages and agricultural lands, for which the reason is heavily debated (e.g. Abel 1976, Beresford and Hurst 1989, Bork et al. 1998, Kaiser et al. 2002, Derese et al. 2010, Roesener 2010, Küster et al. 2014). One reason put forward is that the agricultural land-use had caused an unsustainable amount of erosion, which degraded soils to such a large degree that large areas were abandoned (Lang and Bork 2003). Medieval settlement abandonment possibly due to wind erosion and sand drifting within the European Sand Belt (ESB) has been suggested by several studies (Kaiser et al. 1992, Richter 1965, Derese et al. 2010), however precise analysis of cause and effect is lacking due to limited dating resolution and lack of quantification in the landscape response over time.

Aeolian processes, characterised by erosion, transport and deposition of sediment of the Earth's surface, occur widespread as natural land-forming processes in most arid and semi-arid region (Livingstone and Warren 1996), but are locally also a phenomenon of temperate climate areas such as northern Europe (Warren 2003, Gossens et al. 2001). Land's susceptibility to wind erosion mainly depends on four different factors and the feedbacks between them: i) climatic erosivity (e.g. wind velocity, turbulence, precipitation and evaporation), ii) soil erodibility (e.g. particle size, organic matter content, soil moisture), iii) landscape roughness including vegetation (Warren 2003, Pye and Tsoar 2009). Wind velocity near the soil surface is mainly controlled by the vegetation roughness, where advection can increase (decrease) with decreasing (increasing) vegetative cover along the fetch direction (Shao 2008, Borelli et al. 2016). Thus, by

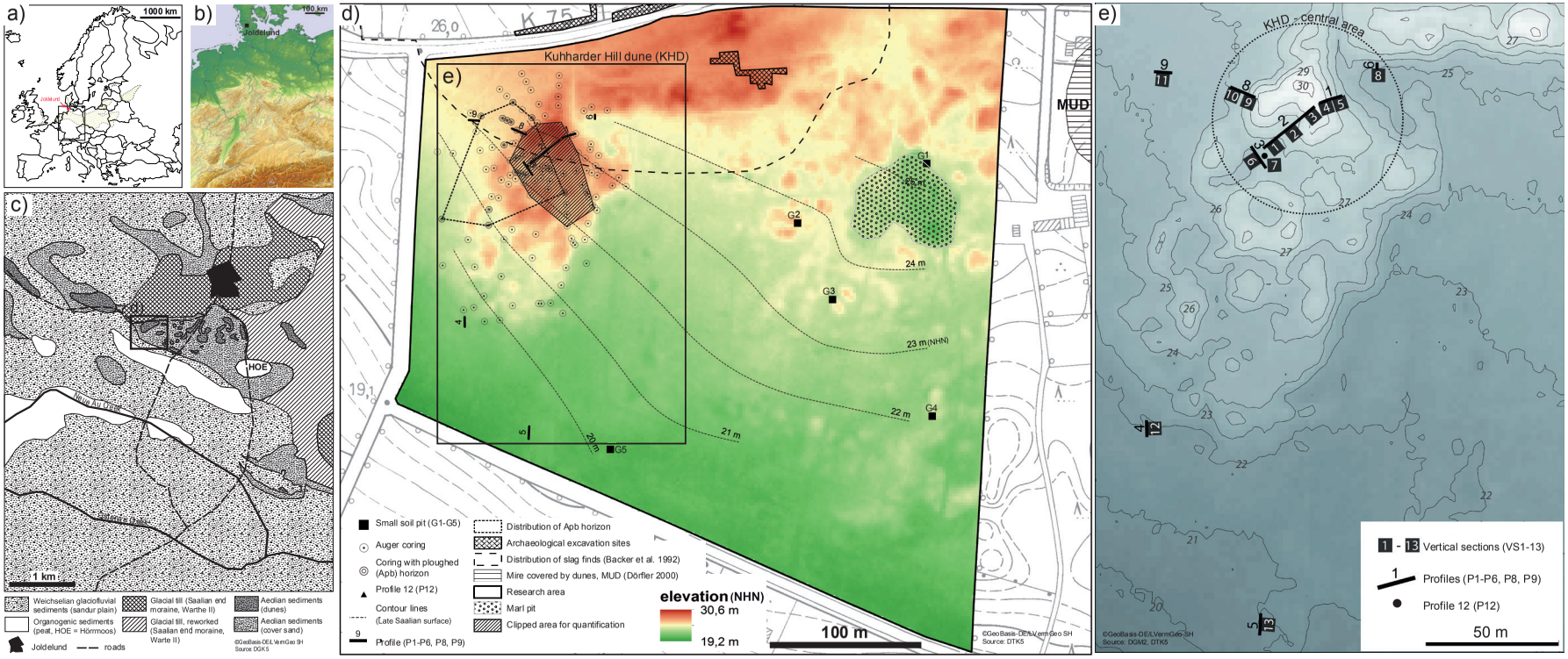

Figure 6.1: Study area. a) overview; b) location of the study area in central Europe; c) geology of the wider region; d) study area showing excavations and coring sites, quantification area and the location of mire covered by dunes (MUD, Dörfler 2000); e) central area of study area showing dune profiles and vertical sections. Base data for this map: geological map (1:5000, DGK5), topographic map (1:5000, DTK5) and digital elevation model (DEM); © by GeoBasis-DE/LVermGeo SH

reducing and removing vegetation cover (e.g. deforestation) for land-use purposes the exposed soil surface becomes prone to wind erosion processes (Leys 1999). During times of strong winds and without vegetation to reduce near surface advection, top soil may be detached, transported and deposited across open space over considerable distances. Human activities and land management practices exert considerable influence on these processes, as agricultural land-use can either increase soil erosion by practices that leaving the soil unprotected and vulnerable, or reduce this impact if the land is managed with suitable protection measures.

Within Northern-central Europe aeolian cover sands of Late Pleistocene origin are found widespread along the European Sand Belt (ESB, Figure 1a) (Kolstrup 1991, Koster 1988, Kozarski and Nowaczyk 1991, Manikowska 1991, Pyritz 1972 Koster 2005, Zeeberg 1998). Cover sands in the ESB are the product of widespread Aeolian processes throughout the Late Pleistocene (mainly between the Older and Younger Dryas) until widespread and ongoing stabilization took place with the onset of the Holocene climate amelioration and re-vegetation since the Holocene phase termed Preboreal ~ 10 ka–9 ka (Schirmer 1999, Koster 2005, Hilgers 2007). However, from the Neolithic Period until present several re-activation phases of these aeolian deposits characterized by relatively shallow drift sands occurred, which were mainly induced by anthropogenic land-use – land cover change (LUCC) such as forest clearing, cropping, and grazing. Archives of Holocene aeolian dynamics thus consist of alternating phases of aeolian activity and landscape stabilization, can therefore be attributed to changing patterns of human impact and used as sedimentary archives for past human-environmental interaction

This has been demonstrated by several studies, which have researched the formation of human-induced drift sand deposits in northern and north-central Europe, e.g. in Denmark (Boas 1997, Mikkelsen et al. 2007), The Netherlands (Castel 1991, Koster et al. 1993, Wallinga et al. 2007, van Mourik et al. 2010, Sevink et al. 2013), Belgium (Derese et al. 2010), the UK (Bateman and Godby 2004) and Poland (Kozarski and Nowaczyk 1991), and eastern Germany (e.g Pyritz 1972, Alisch 1995, De Boer 1995, Hilgers 2007, Tolksdorf and Kaiser 2012, Nicolay et al. 2014) However, no such study has been performed in north-central Germany, and we aim to fill this gap in this paper.

Additionally, with regards to the medieval settlement abandonment phase (MAP), only one study within the ESB was able to show a direct connection between aeolian activity and settlement abandonment. Derese et al. (2010) showed, that a village was abandoned due to early Medieval aeolian sediments covered the village area. In this study, we aim to test if Medieval aeolian activity was the main driver of settlement abandonment in the research area. We do this by incorporating many available sources of information, including Archaeology, Soil Science, Palynology, Anthracology, written historical sources and historical maps, and a high-resolution chrono-stratigraphy in combination with a geo-spatial model to quantify and com-

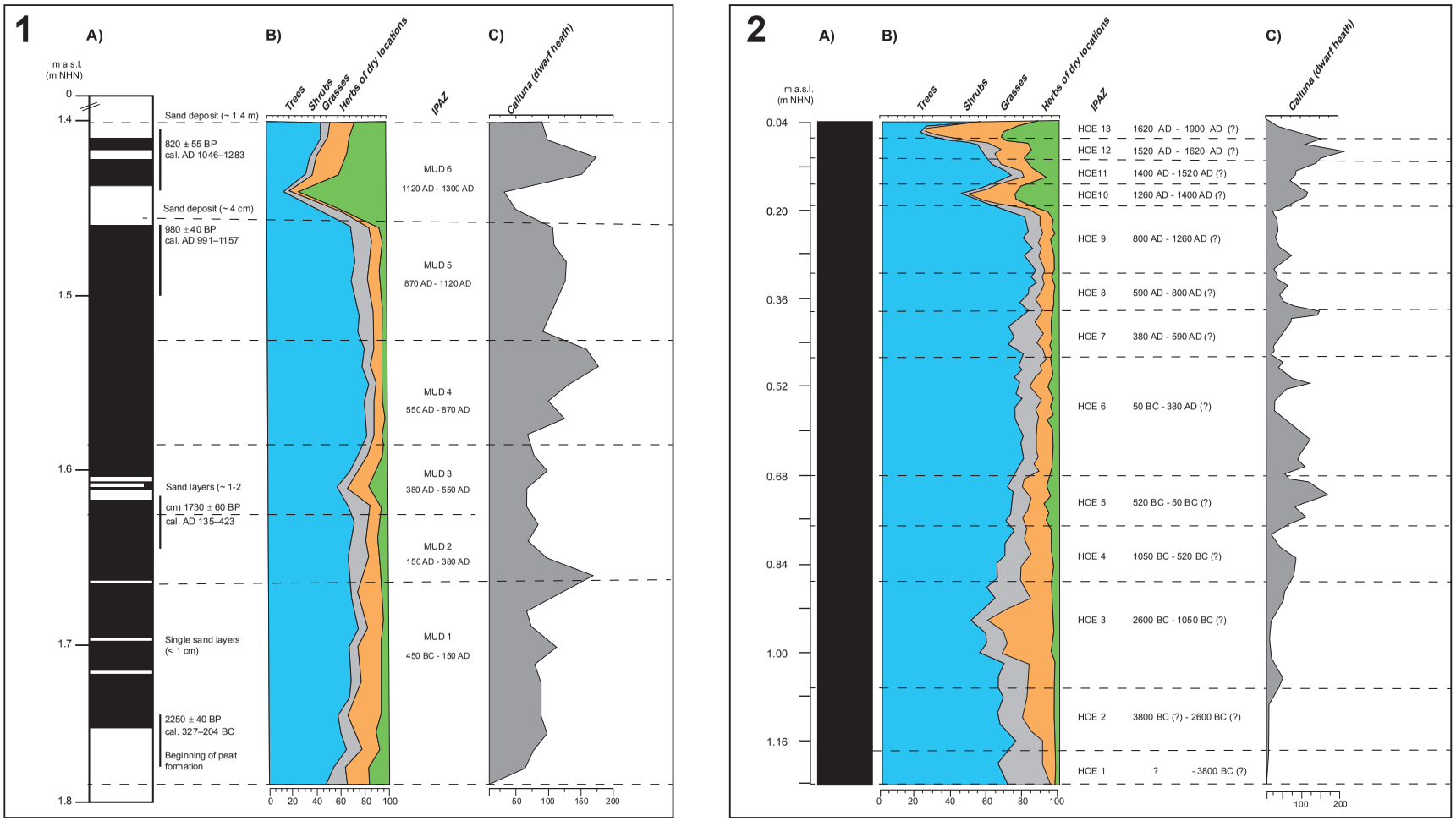

Figure 6.2: Redrawn and simplified pollen diagram of the 1) mire covered by dunes (MUD) and 2) Hörmoos mire (HOE), showing A) stratigraphy of peat core, B) the arboral, shrub and herbaceous pollen and C) percentages of Calluna (heath) pollen. MUD is located ~0.7 km distant to the study area and represents local vegetation record. HOE is located ~ 2.5 km distant to the KHD area and reflects the more regional vegetation history. 1A: Radiographic analysis showing layers of aeolian sand deposited in the peat core which resulted from soil erosion. 1-2B: A decrease in arboral pollen indicating a phase of human-induced deforestation during the Roman Iron Age (e.g. IPAZ MUD 3, HOE 7), Medieval Times (MUD 6, HOE 10) and Modern Times (HOE 12, HOE 13) and is interpreted as an increase in human impact and land-use intensity. Vice versa, an increase is interpreted as a phase of less human activities resulting in reforestation of the area (IPAZ = MUD 4, HOE 8, HOE 11). 1-2C: *Calluna* is considered as heathland indicator, typical secondary vegetation on sandy soils. An increase in Calluna indicates spreading of heathland areas and soil impoverishment. For details see Dörfler (2000)

pare phases of human induced aeolian activity. Through this interdisciplinary approach, we aim to i) establish a high-resolution reconstruction of aeolian landscape dynamics and palaeo-environmental conditions at the study site, ii) quantify spatiotemporal changes in the inland dune topography, iii) estimate intensities of aeolian sand deposition, and iv) causally link the role of landscape degradation to settlement abandonment in the area, and construct a detailed history of human-environmental interaction in the ESB.

6.2 Study area

This study focuses on the topographically highest point (Kuhharder Hill dune, KHD) of an inland dune system (»Joldelunder Schweiz«) in the vicinity of Joldelund, Northern Frisia, Schleswig-Holstein, Germany (54° 38' 45" N, 9° 7' 14" E). The area is located on the Jutland Peninsula (Schleswiger Geest), a glacial outwash plain formed mostly during the last glacial cycle. This outwash plain is dominated by i) Sandur plains, composed mainly by glaciofluvial sediments, ii) moraines related to Saalian glaciations (MIS 6) (Litt et al. 2007, Stephan 2014), which were reworked by periglacial processes during the Late Pleistocene, iii) aeolian sediments (cover sands and dunes), and iv) organic-rich sediments (Fränzle 1985, 1988, 2004; Strehl 1999) (Figure 6.1). The KHD is the highest dune (~ 30 m a.s.l.) of a larger, ~ 80 ha dune field that covers a Saalian end moraine ridge (~ 29.8 m a.s.l.) oriented from North-west to South-east (Backer et al. 1992, Riedel 1997) (Figure 6.1). The surrounding area dips gently westwards and is drained by the small streams Neue Au Creek and Ostenau Creek. Soil development reflects roughly the substrate and geomorphology, and can be differentiated into i) mostly acid and coarse-textured soils (podzols) on sandy substrates, which have only little cohesion and are therefore prone to erosion (Duttmann et al. 2006), or ii) gleys and histosols in water-logged and/or low-lying areas and depressions. The natural vegetation in the area can be divided into two types that are largely dependent on the groundwater level: on higher and therefore drier, mostly sandy surfaces, vegetation is likely to have been an oak-beech forest (*Fagus sylvatica, Quercus robur, Quercus petraea*). In areas where groundwater is nearer the surface atlantic-subatlantic birch-pedunculate oak forests (*Quercus robur, Betula pubescens*) prevailed together with alder-pedunculate oak forests on peatlands (Dierssen 2004).

Estimates of natural vegetation cover are however problematic as intensive land-use in the area has significantly altered the vegetation pattern in the region for thousands of years (Riedel 1997, Dörfler 2000). Vegetation and land-use history is therefore reconstructed using palynological investigations from two mires in the area (Mire covered by dunes, MUD; and Hörrmoos, HOE, Figure 6.1b-c and Figure 6.2) conducted by Dörfler (2000) from historic maps, dating back until the 18th century AD, and archaeological investigations. The earliest evidence from these investigations for clear human landscape activity is a prehistoric iron ore production site and settlement, dating to the late Roman Iron Age (4th–5th century AD) (Erlenkeuser et al. 1997). At that time forests

still dominated the area, albeit partially opened for agricultural land and pasture (Jöns 2000). Between this time and the creation of a detailed historic map in the 18th century, little is known about land-use in the area. By 1793 AD, the landscape is covered mainly with heath, pasture, meadows and mires. Until the late 19th century AD heathland is still dominant, although agricultural land and pastures increased in area (Nielsen 1972, Dörfler 2000). An intensification of agricultural land-use and utilization of heathland began at the end of 19th century AD with the implementation of deep ploughs and mineral fertilizers (Nielsen 1972, Duttmann et al., 2006). In 1926, the extant heathland with some oak coppiced trees (Nielsen, 1970) was afforested by the local council (Joldelund) (Schnepel 1981) (Figure 6.1). In the 1950s, a large afforestation program lead to the extensive planting of spruce (*Picea abies, Picea sitchensis and Picea glauca*), pine (*Pinus sylvestris, Pinus nigra and Pinus mugo*) and larch (*Larix kaempferi*) in the area (Nielsen 1970). From this time until the present, the KHD is mainly covered with larch and spruce (*Picea abies*). The land-use of the adjacent area is dominated by pasture for dairy farming, and cultivation of corn for the generation of biogas.

Aeolian erosion and deposition have a long recorded history in causing problems for agricultural land-use in the area (Mager 1930, Iwersen 1953, Hannensen 1959, Richter 1965, Duttmann et al. 2004), facilitated by near surface wind velocities of more than 7 ms^{-2} in March, April and May, when high pressure systems over Fennoscandia and Northern Russia influence the circulation pattern (Hassenpflug 1998, Gerstengarbe and Werner 2005, Duttmann et al. 2006, LLUR 2011). The general climate of the region is temperate oceanic, with 8.2 °C mean annual temperature and 820 mm mean annual precipitation (German Weather Service, DWD: climatological data for station Leck for the period 1975–2002).

6.3 Methods

6.3.1 Field methods and sampling

We employed a detailed chrono-stratigraphic approach in examining the dune record in order to examine the feedbacks between aeolian activity and past land-use change and past settlement activities within the study area. Nine profiles were analysed in the western part of the research area, their size ranging between 1 m to 25 m in length and ~ 1.7 to 2.6 m in depth (P1–P6, P8–9, P12, Figure 6.1e). Six profiles were excavated in the center of the KHD within a distance of ~ 50 m (P1–3, P6, P8 and P12) (Figure 6.1e). P1 and P2 constitute a cross-section of the KHD with 35 m in length and up to ~2.4 m in depth. Three profiles were excavated towards the southern (P9) and north-western edge of the research area (P4, P5). Five further shallow pits were excavated to the east of the KHD (G1–G5) in the central and southern parts of the research area (Figure 6.1d). Within all excavation sites the distinct glacial deposits (moraine, Pleistocene) underlying the aeolian dunes was reached, ensuring that the entire Holocene sedimentary record was analysed, and made the quantification of the Holo-

Table 6.1: Main physical and chemical features of soils and sedimentary units of KHD. Abbreviations: cm bgs = cm below ground surface; G = Gravel. > 2 mm; COS = coarse sand. < 2 mm; MS = medium sand. 2–0.63 mm; FS = fine sand. 0.63–0.2 mm; M = Mean; Md = Median; So = Sorting coefficient (TRASK 1932); OM = organic matter content; SBD = soil bulk density. Texture is given according to German Soil Systematics. Soil classification based on The World Reference Base for Soil Resources (IUSS WORKING GROUP WRB 2015).

Profile	Unit	Horizon	Depth	Colour	Texture (wt.%)						MS:FS	M	Md	So	pH	OM	FeD	FeO	FeO:FeD	SBD
Section		(WRB)	(cm)	(Munsell)	G	COS	MS	FS	Silt	Clay		mm	mm		$CaCl_2$	%	g/kg	g/kg		g/cm^3
P1	6	Ah	0-3	10YR 3/1	0.0	0.3	48.9	45.6	2.9	2.3	1.1	0.22	0.20	1.6	2.7	8.1	1.7	0.7	0.4	-
VC5	6	E	3-6	10YR 4/1	0.0	0.3	50.1	46.5	2.0	1.2	1.1	0.22	0.20	1.6	2.9	3.1	1.9	0.8	0.4	-
	5	2Ahb	6-11	10YR 3/1	0.0	0.4	44.5	46.6	3.2	5.3	1.0	0.19	0.19	1.6	2.8	7.2	1.5	0.6	0.4	-
	5	2Eb	11-17	7.5YR 6/2	0.0	0.1	50.7	46.0	0.3	2.8	1.1	0.19	0.20	1.6	3.1	1.2	1.2	0.4	0.3	-
	5	2Bwsb-C	17-35	7.5YR 5/4	0.0	0.5	57.1	40.3	0.3	1.7	1.4	0.24	0.23	1.6	3.4	0.7	1.7	0.8	0.5	-
	5	2C	35-50	10YR 6/4	0.0	2.1	52.9	41.7	0.6	2.7	1.3	0.23	0.22	1.6	3.8	0.3	1.2	0.4	0.3	-
	4	3C	50-87	7.5YR 5/4	0.0	0.4	54.9	42.3	0.6	1.7	1.3	0.23	0.22	1.6	4.3	0.2	0.8	0.3	0.4	-
	3	4Ahb	87-89	-	-	-	-	-	-	-	-	-	-	-	-	-	-	-	-	-
	3	4C	89-92	-	-	-	-	-	-	-	-	-	-	-	-	-	-	-	-	-
	1/2	5Ahub	92-108	7.5YR 5/2	0.1	0.8	50.8	43.6	3.0	1.9	1.2	0.22	0.21	1.6	4.2	0.7	2.5	0.5	0.2	-
	1/2	5Eb	108-119	10YR 6/2	0.2	1.0	48.9	46.1	2.0	1.9	1.1	0.22	0.20	1.6	4.1	0.3	0.4	0.3	0.9	-
	1/2	5Bhb	119-126	7.5YR 2/2	0.0	0.6	42.4	53.4	0.6	2.9	0.8	0.21	0.18	1.5	3.8	1.6	3.2	2.6	0.8	-
	1/2	5Bmsb	126-150	7.5YR 5/6	0.0	1.1	50.5	46.2	0.3	1.9	1.1	0.23	0.21	1.6	4.1	1.1	2.0	2.1	1.0	-
	1/2	5C	150-195	10YR 6/4	0.0	0.4	12.0	80.5	3.4	3.8	0.1	0.12	0.11	1.4	4.4	0.2	0.8	0.3	0.4	-
P1	5/6	Ah	0-6	10YR 4/1	0.0	0.1	39.7	55.3	2.9	2.0	0.7	0.20	0.18	1.5	2.8	6.6	1.5	0.5	0.4	-
VS4	5/6	E	6-17	7.5YR 5/2	0.0	0.0	48.3	45.7	0.5	5.5	1.1	0.22	0.20	1.6	3.1	1.6	1.2	0.4	0.4	-
	5/6	Bws-C	17-23	10YR 4/6	0.0	0.1	48.4	48.1	0.9	2.5	1.0	0.22	0.20	1.6	3.9	0.6	1.4	0.5	0.4	-
	5/6	C	23-93	10YR 6/5	0.0	0.2	45.0	50.3	0.8	3.6	0.9	0.22	0.19	1.5	4.3	0.4	0.9	0.4	0.5	-
	4	2C	93-130	10YR 6/5	0.0	1.2	50.8	44.2	0.3	3.6	1.1	0.23	0.21	1.6	4.4	0.2	1.0	0.3	0.4	-
	4	2C	130-165	10YR 6/5	0.0	0.8	57.0	37.7	0.6	3.8	1.5	0.24	0.23	1.6	4.5	0.1	0.8	0.3	0.4	-
	4	2C	165-201	10YR 6/4	0.0	0.2	51.7	44.1	0.3	3.7	1.2	0.23	0.21	1.6	4.3	0.2	0.9	0.4	0.4	-
P2	6	Eh	0-8	10YR 4/2	0.0	0.2	43.0	49.0	0.3	7.4	0.9	0.19	0.18	1.6	3.6	2.8	2.0	1.2	0.6	-
VS3	6	Bws-C	8-13	7.5YR 4/3	0.0	0.1	39.7	58.7	0.3	1.2	0.7	0.21	0.18	1.5	3.0	0.9	1.9	0.7	0.4	-
	5	2Ahb	13-19	7.5YR 4/1	0.0	0.2	51.3	43.0	3.3	2.2	1.2	0.23	0.21	1.6	3.3	8.3	1.8	0.8	0.4	-
	5	2Eb	19-29	7.5YR 4/3	0.0	0.3	46.7	50.5	1.8	0.7	0.9	0.21	0.19	1.6	3.0	1.8	1.3	0.6	0.5	-
	5	2Bwsb-C	29-40	7.5YR 5/2	0.0	0.3	42.0	54.0	0.8	3.0	0.8	0.21	0.18	1.5	3.5	1.0	1.0	0.3	0.3	-
	5	2C	40-89	10YR 6/5	0.0	0.2	65.4	31.9	0.2	2.3	2.0	0.26	0.26	1.6	4.5	0.1	0.9	0.3	0.4	-
	4	3C	89-160	10YR 6/5	0.0	0.1	45.9	50.8	0.4	2.7	0.9	0.21	0.19	1.6	4.4	0.2	1.0	0.4	0.4	-
	4	3C	89-204	10YR 6/4	0.0	0.1	50.1	47.1	0.8	1.9	1.1	0.23	0.20	1.6	4.4	0.2	0.8	0.3	0.4	-

P2	5/6	Ah	0-5	10YR 4/1	0.0	0.5	41.4	50.3	4.3	3.5	0.8	0.19	0.18	1.6	2.8	8.9	1.3	0.6	1.1	-
VS2	5/6	E	5-18	7.5YR 4/2	0.0	0.4	44.0	51.8	2.2	1.5	0.8	0.20	0.19	1.6	3.2	1.5	1.2	0.2	0.4	-
	5/6	Bws	18-38	7.5YR 4/3	0.0	0.3	38.2	58.4	2.0	1.2	0.7	0.19	0.17	1.5	3.3	1.1	2.2	1.4	0.1	-
	5/6	C	38-78	10YR 6/5	0.0	0.5	64.0	33.5	0.7	1.3	1.9	0.26	0.26	1.6	4.4	0.3	0.8	0.5	0.4	-
	5/6	C	78-123	10YR 6/5	0.0	0.4	65.1	32.3	0.3	1.9	2.0	0.26	0.26	1.4	4.4	0.2	1.0	0.3	0.4	-
	5/6	C	123-168	10YR 6/5	0.0	2.2	62.4	33.6	0.2	1.6	1.9	0.26	0.26	1.4	4.4	0.2	0.6	0.3	0.5	-
	4	2C	168-188	10YR 6/5	0.0	0.3	36.0	61.7	0.4	1.7	0.6	0.19	0.17	1.3	4.4	0.3	0.7	0.4	0.5	-
	3	3Ahb	188-193	-	-	-	-	-	-	-	-	-	-	-	-	-	-	-	-	-
	3	3C	193-213	10YR 6/5	0.0	0.1	40.5	57.8	0.3	1.3	0.7	0.20	0.18	1.5	4.3	0.2	0.6	0.4	0.6	-
P2	5/6	Ah	0-6	7.5YR 4/1	0.0	0.2	34.8	58.7	2.5	3.7	0.6	0.18	0.17	1.5	2.7	5.5	1.0	0.5	0.5	-
VS1	5/6	E	6-15	7.5YR 5/2	0.0	0.2	38.2	58.6	1.4	1.5	0.7	0.19	0.17	1.5	2.9	2.0	1.0	0.4	0.4	-
	5/6	Bws	15-35	7.5YR 3/4	0.0	0.1	37.0	60.5	0.6	1.8	0.6	0.19	0.17	1.5	3.2	1.3	1.6	1.2	0.8	1.56
	5/6	C	35-63	10YR 6/5	0.0	0.4	48.2	49.5	0.3	1.5	1.0	0.22	0.20	1.5	4.3	0.3	0.9	0.3	0.4	1.64
	4	2C	63-90	10YR 6/5	0.0	0.7	43.8	53.9	0.3	1.3	0.8	0.22	0.19	1.5	4.3	0.3	0.9	0.5	0.6	1.55
	4	2C	90-125	10YR 6/5	0.0	0.8	41.9	55.8	0.3	1.3	0.8	0.21	0.18	1.5	4.4	0.2	1.1	0.4	0.4	-
	4	2C	125-150	10YR 6/5	0.0	0.1	46.1	51.9	0.5	1.4	0.9	0.22	0.19	1.5	4.4	0.2	1.0	0.4	0.4	-
	4	2C	150-177	10YR 6/4	0.0	0.3	27.0	69.2	0.5	3.0	0.4	0.17	0.16	1.4	4.4	0.2	0.8	0.4	0.5	-
	3	3Ahb	177-187	-	-	-	-	-	-	-	-	-	-	-	-	-	-	-	-	-
	3	3C	187-189	10YR 5/3	0.0	0.4	58.5	38.6	0.6	1.9	1.5	0.24	0.24	1.6	4.3	0.2	0.2	0.1	0.4	-
	2-p	4Ab	189-190	-	-	-	-	-	-	-	-	-	-	-	-	-	-	-	-	-
	2-p	5Apb	190-195	10YR 4/1	0.1	0.9	40.7	48.2	8.2	2.0	0.8	0.18	0.18	1.6	3.8	4.0	0.4	0.3	0.9	1.35
	1/2	5Eb	195-209	10YR 5/2	0.0	1.2	43.5	51.9	0.7	2.7	0.8	0.20	0.19	1.6	3.9	1.3	0.1	0.1	0.9	1.47
	1/2	5Bhb	209-214	10YR 3/1	0.0	0.8	44.5	48.9	1.6	4.1	0.9	0.20	0.19	1.6	3.7	8.5	2.5	2.5	1.0	-
	1/2	5Bmsb	214-216	7.5YR 3/4	0.0	0.7	43.4	52.9	1.3	1.7	0.8	0.21	0.19	1.6	4.1	1.3	2.0	1.8	0.9	-
P3	4/5/6	Ah	0-8	7.5YR 2/1	0.0	0.2	34.2	58.1	3.3	4.2	0.6	0.17	0.17	1.5	2.7	5.5	0.8	0.4	0.5	-
VS6	4/5/6	E	8-16	7.5YR 3/2	0.0	0.3	30.2	66.2	1.1	2.3	0.5	0.18	0.16	1.4	3.3	1.4	1.1	0.4	0.4	1.43
	4/5/6	Bws-C	16-34	7.5YR 3/4	0.0	0.4	51.1	45.5	0.9	2.2	1.1	0.23	0.21	1.6	3.8	0.7	1.3	0.7	0.5	1.46
	4/5/6	C	34-52	10YR 4/6	0.0	0.1	13.5	83.5	0.7	2.2	0.2	0.14	0.15	1.2	4.2	0.7	1.4	0.6	0.5	1.54
	3	2Ahb	52-60	10YR 3/4	0.0	0.3	18.6	74.6	3.9	2.7	0.2	0.13	0.13	1.5	4.1	1.0	1.7	0.8	0.5	-
	3	2C	60-70	10YR 4/6	0.0	0.2	39.5	57.9	0.7	1.8	0.7	0.21	0.18	1.5	4.3	0.4	0.9	0.5	0.6	-
	3	2C	70-80	10YR 4/6	0.0	0.1	27.9	69.5	0.8	1.8	0.4	0.17	0.16	1.3	4.2	0.4	1.3	0.7	0.6	1.58
	2-p	3Ab	80-82	-	-	-	-	-	-	-	-	-	-	-	-	-	-	-	-	-
	2-p	4Apb	82-90	10YR 2/1	0.5	0.4	29.6	62.0	5.5	2.6	0.5	0.16	0.15	1.6	3.7	8.7	0.2	0.2	0.7	1.24
	1/2	4Eb	90-102	10YR 5/1	0.0	0.6	51.1	45.4	2.0	0.9	1.1	0.23	0.21	1.6	3.8	1.3	0.1	0.1	1.0	1.61
	1/2	4Bhb	102-110	7.5YR 2/1	0.0	1.1	48.3	41.6	2.4	6.5	1.2	0.21	0.20	1.6	3.7	7.8	4.1	4.5	1.1	-
	1/2	4Bmsb	110-134	7.5YR 3/3	0.0	0.4	42.8	53.4	1.7	1.6	0.8	0.20	0.18	1.6	4.2	1.0	1.4	0.9	0.6	1.39
	1/2	4C	134-212	10YR 6/4	0.0	0.1	70.1	28.2	1.0	0.7	2.5	0.27	0.28	1.5	4.3	0.1	0.6	0.1	0.2	1.53
P4	5/6	Ap1	0-8	10YR 4/1	0.0	0.3	23.0	66.8	2.7	7.1	0.3	0.15	0.15	1.4	2.8	16.1	1.9	0.9	0.5	-

VS12	5/6	Ap2	8-34	7.5YR 5/2	0.0	0.3	22.1	73.8	2.2	1.6	0.3	0.16	0.15	1.3	3.1	3.3	1.1	0.8	0.7	-
	5/6	Bws	34-43	7.5YR 4/3	0.0	0.2	21.7	75.7	0.9	1.5	0.3	0.16	0.16	1.2	3.8	1.6	1.2	0.8	0.7	-
	5/6	C	43-61	10YR 6/5	0.0	0.4	38.9	58.9	0.7	1.0	0.7	0.19	0.17	1.5	4.3	0.2	0.7	0.3	0.5	-
	5/6	C	61-79	10YR 6/5	0.0	0.1	16.7	80.0	1.3	2.0	0.2	0.13	0.14	1.4	4.3	0.0	1.2	0.7	0.6	-
	3/4	2Ab?	79-81	-	-	-	-	-	-	-	-	-	-	-	-	-	-	-	-	-
	3/4	2C	81-85	10YR 6/5	0.0	0.1	38.0	59.6	0.9	1.3	0.6	0.19	0.17	1.5	4.0	0.5	0.7	0.5	0.7	-
	1/2	3Ahb	85-99	10YR 3/1	0.0	0.6	55.8	40.6	1.1	2.0	1.4	0.24	0.23	1.6	3.7	5.1	0.4	0.5	1.0	-
	1/2	3Eb	99-113	7.5YR 6/2	0.0	0.7	50.9	46.8	0.9	0.8	1.1	0.23	0.21	1.6	3.8	0.5	0.1	0.0	0.7	-
	1/2	3Bhb	113-124	10YR 2/1	0.0	0.7	46.9	49.3	0.7	2.4	1.0	0.22	0.19	1.6	3.6	9.4	0.4	0.3	0.8	-
	1/2	3Bmsb	124-143	7.5YR 3/4	0.0	1.2	49.7	46.6	1.0	1.6	1.1	0.22	0.20	1.6	4.1	1.1	1.3	1.1	0.8	-
	1/2	3C	143-189	10YR 6/4	0.0	0.9	54.2	43.7	0.2	1.1	1.2	0.24	0.22	1.6	4.4	0.1	0.4	0.2	0.4	-
	1/2	3C	189-235	2.5Y 7/4	0.0	0.7	50.8	46.9	0.3	1.3	1.1	0.23	0.21	1.6	4.2	0.1	0.3	0.2	0.5	-
P5	6 ?	Ap1	0-7	10YR 3/2	0.5	0.3	35.4	60.4	2.2	1.7	0.6	0.18	0.17	1.5	3.2	3.2	1.1	0.9	0.8	-
VS13	6 ?	Ap2	7-15	10YR 4/2	0.6	0.4	31.7	63.4	2.6	1.9	0.5	0.17	0.16	1.5	3.7	2.7	1.1	0.8	0.7	1.51
	6 ?	Ap3	15-23	7.5YR 3/3	0.1	0.1	22.7	74.5	1.9	0.8	0.3	0.16	0.15	1.3	4.9	1.1	1.0	1.0	1.0	-
	5	2Ahb	23-28	10YR 3/2	0.0	0.4	23.2	70.3	3.6	2.6	0.3	0.15	0.14	1.5	5.0	5.6	2.8	2.7	0.9	-
	5	2Eb	28-34	7.5YR 5/2	0.0	0.2	29.0	67.3	2.5	1.0	0.4	0.16	0.16	1.5	4.3	1.6	0.5	0.3	0.7	-
	5	2Bwsb	34-42	7.5YR 4/4	0.0	0.3	28.7	67.4	2.6	1.0	0.4	0.17	0.16	1.5	5.0	1.5	1.2	1.0	0.8	-
	5	2C	42-56	10YR 6/4	0.0	0.2	36.9	61.0	0.8	1.1	0.6	0.19	0.17	1.5	4.6	0.6	0.4	0.4	0.9	1.56
	3/4	3C	56-90	10YR 6/5	0.0	0.3	27.9	68.5	1.9	1.4	0.4	0.16	0.15	1.5	4.5	0.3	0.3	0.1	0.4	1.66
	1/2	4Ahb	90-104	10YR 2/1	0.0	0.9	35.5	50.0	7.5	6.1	0.7	0.16	0.16	1.8	3.9	11.4	1.4	1.2	0.9	1.09
	1/2	4Eb	104-116	7.5YR 5/2	0.0	0.5	30.5	62.8	5.1	1.1	0.5	0.16	0.15	1.6	4.0	1.2	0.1	0.2	1.2	1.59
	1/2	4Bhb	116-126	7.5YR 2/1	0.0	0.6	30.9	62.6	4.8	1.1	0.5	0.16	0.15	1.6	4.0	3.1	0.1	0.1	1.1	-
	1/2	4Bsb	126-146	7.5YR 3/4	0.0	0.3	38.2	55.3	4.8	1.4	0.7	0.17	0.16	1.7	4.1	3.4	0.2	0.1	0.4	1.53
	1/2	4C	146-166	10YR 5/6	0.0	1.9	48.1	41.7	7.0	1.2	1.2	0.20	0.20	1.8	4.3	0.7	0.3	0.1	0.5	1.68
	P	5C	166-182	10YR 6/6	8.3	5.3	35.7	43.9	10.1	5.0	0.8	0.17	0.17	1.9	4.2	0.6	0.4	0.1	0.3	1.84
P6	2	SP1	0-5	7.5YR 4/2	2.0	0.5	37.6	50.1	9.1	2.7	0.8	0.17	0.17	1.6	2.9	3.8	3.1	1.1	0.4	-
VS8	2	SP2	5-60	7.5YR 4/4	1.6	0.4	45.4	51.3	1.7	1.2	0.9	0.21	0.19	1.6	3.9	1.8	2.7	1.3	0.5	-
	2	C	60-79	10YR 6/5	0.0	0.9	51.5	44.1	0.9	2.5	1.2	0.23	0.21	1.6	4.5	0.1	0.5	0.2	0.3	-
	2	C	79-99	10YR 6/5	0.0	0.4	30.8	66.6	1.1	1.1	0.5	0.18	0.16	1.4	4.6	0.1	0.6	0.2	0.4	-
	1	2C	99-158	2.5Y 7/4	0.0	0.1	30.1	68.1	0.3	1.3	0.4	0.18	0.17	1.4	4.5	0.1	0.4	0.2	0.4	-
	P	3C	158-176	2.5Y 6/6	11.8	4.2	36.7	40.8	11.7	6.6	0.9	0.15	0.17	2.0	3.8	0.1	1.2	0.3	0.2	-
P8	5/6	Eh	0-24	10YR 3/2	0.0	1.0	36.8	58.7	2.8	1.5	0.6	0.20	0.17	1.5	2.8	4.9	1.0	0.5	0.5	1.35
VS9	5/6	Bws	24-47	7.5YR 5/4	0.0	0.1	35.0	62.6	0.9	1.3	0.6	0.19	0.17	1.4	3.4	1.0	1.5	1.0	0.7	1.48
	5/6	C	47-66	10YR 6/5	0.0	0.2	36.1	62.2	0.7	0.9	0.6	0.20	0.17	1.5	4.2	0.7	0.8	0.4	0.5	1.54
	4	2C	66-101	10YR 6/5	0.0	0.1	70.5	27.8	1.0	0.8	2.5	0.27	0.28	1.5	4.5	0.2	0.7	0.3	0.4	1.62
	4	2C	101-136	10YR 6/5	0.0	0.3	40.0	58.6	0.5	0.6	0.7	0.20	0.18	1.5	4.4	0.4	0.4	0.4	1.0	-
	4	2C	136-173	10YR 6/5	0.0	0.2	32.3	66.1	0.5	0.8	0.5	0.18	0.17	1.4	4.4	0.3	0.8	0.4	0.5	-

	3	3Ahb	173-176	10YR 5/4	0.0	0.2	12.1	84.4	2.0	1.3	0.1	0.13	0.14	1.3	4.3	0.6	1.2	0.6	0.5	-
	3	3C	176-180	-	-	-	-	-	-	-	-	-	-	-	-	-	-	-	-	-
	2-p	4Apb	180-197	10YR 3/1	0.1	0.7	39.8	54.7	3.7	1.1	0.7	0.19	0.18	1.6	4.1	2.5	0.8	0.5	0.6	1.3
	1/2	4Eb	197-200	10YR 5/2	0.0	0.6	40.5	55.1	2.4	1.5	0.7	0.20	0.18	1.5	4.1	1.1	0.2	0.2	1.0	1.4
	1/2	4Bhb	200-204	7.5YR 2/1	0.0	0.4	49.2	45.9	1.5	3.0	1.1	0.22	0.20	1.6	3.8	4.0	4.0	4.5	1.1	1.4
	1/2	4Bmsb	204-219	7.5YR 4/3	0.0	0.2	53.3	43.9	0.7	1.9	1.2	0.23	0.22	1.6	4.1	0.8	1.4	1.2	0.8	
P8	4/5/6	Ap	0-14	10YR 4/2	0.0	0.1	27.5	68.0	2.5	1.9	0.4	0.17	0.16	1.3	3.0	3.0	1.1	0.7	0.6	-
VS10	4/5/6	Bws	14-26	7.5YR 4/3	0.0	0.2	30.1	66.5	1.0	2.3	0.5	0.17	0.16	1.4	3.4	1.3	1.5	1.3	0.8	-
	4/5/6	C	26-52	10YR 6/4	0.0	0.2	37.0	60.4	0.8	1.6	0.6	0.19	0.17	1.5	4.1	0.9	0.9	0.5	0.5	-
	3	2Ahb	52-59	10YR 4/3	0.0	0.1	23.1	71.7	2.8	2.2	0.3	0.15	0.15	1.4	4.1	1.5	1.1	0.7	0.7	-
	2-p	3Apb	59-72	10YR 4/1	0.1	0.5	43.8	51.6	3.1	1.1	0.8	0.20	0.19	1.6	4.1	2.2	1.2	0.5	0.4	-
	1/2	3Eb	72-80	10YR 6/2	0.0	0.4	47.4	49.4	2.3	0.4	1.0	0.22	0.19	1.6	4.2	0.6	0.1	0.2	1.0	-
	1/2	3Bhb	80-85	7.5YR 2/1	0.0	0.3	54.2	43.8	0.6	1.1	1.2	0.23	0.22	1.6	4.0	4.5	6.0	5.5	0.9	-
	1/2	3Bmsb	85-112	7.5YR 4/3	0.0	0.3	49.5	48.3	0.7	1.1	1.0	0.22	0.20	1.6	4.4	0.6	0.9	0.6	0.7	-
	1/2	3C	112-168	10YR 5/6	0.0	0.1	42.1	55.7	1.0	1.2	0.8	0.20	0.18	1.5	4.4	0.2	0.6	0.2	0.3	-
P9	3/4/5/6	Ap1	0-4	10YR 4/1	0.0	0.5	17.6	68.9	7.5	5.5	0.3	0.12	0.13	1.5	2.6	13.5	1.4	0.9	0.7	-
VS11	3/4/5/6	Ap2	4-13	7.5YR 4/3	0.0	0.4	28.3	66.6	3.8	0.9	0.4	0.16	0.15	1.5	3.0	3.3	1.8	1.7	0.9	-
	3/4/5/6	Ap3	13-19	7.5YR 5/3	0.0	0.5	28.7	66.6	3.2	1.1	0.4	0.16	0.15	1.5	3.3	2.1	1.7	1.4	0.8	-
	1/2	2Ahb	19-25	10YR 2/1	0.0	0.6	42.2	52.7	3.5	1.0	0.8	0.19	0.18	1.6	3.3	5.1	0.5	0.1	0.3	-
	1/2	2Eb	25-38	7.5YR 5/2	0.0	0.5	43.9	52.8	2.5	0.3	0.8	0.20	0.19	1.6	3.7	0.9	0.8	0.7	0.9	-
	1/2	2Bhb	38-46	10YR 3/1	0.0	0.4	43.5	52.5	1.1	2.5	0.8	0.21	0.19	1.6	3.6	8.3	0.1	0.1	1.0	-
	1/2	2Bmsb	46-81	7.5YR 3/4	0.0	0.3	43.3	54.4	0.7	1.2	0.8	0.21	0.19	1.5	4.2	1.0	0.7	0.5	0.6	-
	1/2	2C	81-172	10YR 5/3	0.0	1.0	58.7	38.5	0.5	1.4	1.5	0.25	0.24	1.6	4.4	0.1	1.2	0.9	0.8	-
P12	4/5/6	Ah	0-10	10YR 3/1	-	0.5	38.2	55.2	4.6	1.5	0.7	0.18	0.17	1.6	2.7	8.3	1.0	0.6	0.6	-
VS7	4/5/6	E	10-15	7.5YR 5/1	-	0.4	41.5	53.6	2.2	2.3	0.8	0.19	0.18	1.6	2.9	2.7	0.6	0.2	0.4	-
	4/5/6	Bws	15-35	7.5YR 3/4	-	0.4	41.4	50.6	3.9	3.6	0.8	0.18	0.18	1.7	3.2	1.6	1.8	1.3	0.7	-
	4/5/6	C	35-76	10YR 6/6	-	1.2	49.8	47.1	0.8	1.1	1.1	0.23	0.20	1.6	4.1	0.7	0.8	0.4	0.5	-
	3	2Ahb	76-86	10YR 5/3	-	0.1	11.4	72.1	4.6	11.8	0.2	0.10	0.11	1.5	4.3	0.8	0.5	0.2	0.4	-
	2-p	3Ab	86-88	10YR 2/1	-	1.3	46.1	43.8	6.7	1.9	1.1	0.19	0.19	1.8	3.8	8.1	0.2	0.2	0.9	-
	2-p	4Apb	88-102	10YR 3/1	-	1.1	38.4	44.9	8.4	7.0	0.9	0.16	0.17	1.8	3.9	4.5	0.7	0.5	0.7	-
	1/2	4Eb	102-122	2.5YR 4/1	-	1.0	49.5	45.4	2.1	2.0	1.1	0.21	0.20	1.6	4.0	1.0	0.1	0.1	0.9	-
	1/2	4Bhb	122-133	7.5YR 5/2	-	1.2	52.9	43.1	0.9	1.9	1.2	0.23	0.22	1.6	4.2	1.9	8.8	7.6	0.9	-
	1/2	4Bmsb	133-143	10YR 5/6	-	0.4	23.2	70.5	1.8	4.1	0.3	0.15	0.15	1.4	4.4	0.9	1.1	0.5	0.5	-
	1/2	4BC	143-165	10YR 6/6	-	0.3	12.8	71.6	2.5	12.8	0.2	0.11	0.11	1.5	4.1	0.7	1.0	0.4	0.4	-

cene aeolian deposition possible. For the remainder of the paper, the underlying Pleistocene deposits are addressed as »unit P«, whereas Holocene sediments are continuously numbered from bottom to top (unit 1–6). Where the Pleistocene moraine deposit was not accessible within the excavation sites, hand augers were used to determine its depth. Each profile was documented with scaled drawings and photographs. Samples for sedimentological and pedological analyses such as grain size, organic matter (OM), pH, iron content and soil bulk density (SBD) were taken using 13 vertical sections (VS) of the exposures. Soil types and horizons were first described and classified using German soil taxonomy (AG Boden 2005) and then translated into the international Word Reference Base of Soil Resources (IUSS Working Group 2015) (Table 6.1). To ensure an accurate spatial interpolation of the sedimentary units, ~ 125 further auger corings of up to 2 m in depth and with a diameter of 1.2–1.8 cm were created in which marker horizons such as buried soils, former dune surfaces and the absolute thicknesses of dune deposits were logged. Finally, all the excavation sites and coring locations were surveyed with a total station. All pedological and geomorphological data (position, elevation, chrono-stratigraphic correlation, and thickness of soil horizon/sediment layer, soil colour and estimated grain size) were subsequently imported into ESRI ArcGIS to allow further processing and quantification of sedimentary layers.

6.3.2 Sediment and soil analysis

In order to create coherent stratigraphic units throughout the research area, the soil and sediment characteristics of sedimentary layers were analysed using grain size analysis. For grain size analysis sediment samples of 15 g (< 2 mm) were treated with H_2O_2 and subsequently sieved (mesh width 630 µm, 200 µm, 125 µm and 63 µm), dried at 105 °C and weighted. Particles < 63 µm were analyzed applying standard procedure for sedimentation (Köhn pipette). The grain size data were subsequently processed using the program GRADISTAT (Blott and Pye 2001), where grain size parameter such as mean (M) and median (Md) of each sample were calculated using the Folk and Ward (1957) method. To ensure compatibility with earlier studies, the Trask's sorting coefficient (So) was calculated. In order to calculate the mass of the sediment, soil bulk density (SBD) was determined by taking at least three constant volume samples per layer. The samples were dried at 105 °C, weighed, and the mean SBD with standard error was calculated.

Vertical sections with enhanced soil formation within the stratigraphic record are likely to give evidence about phases of landscape stability (Warkentin 2006), and are therefore an important source of information about past landscape change within this study. In addition, buried soil horizons serve as stratigraphic markers and may provide information on the intensity and duration of soil forming processes. In this study, we characterize soil horizons using grain size analysis (GS), soil color (SC), pH, organic matter content

Table 6.2: Radiocarbon dates calibrated with OxCal v.4.1.7. (Bronk Ramsey 2010) using IntCal13 calibration data (Reimer et al. 2013). Abbreviations: Exp.: exposure; M: matter type; C: charcoal; P: peat; SOM: soil organic matter; cf.: lat. confer (engl. compare)

No.[a]	Exp./VS	Lab. ref.	M	Taxon	Context[b]	Depth (m)	Radiocarbon age (BP)	cal. BC/AD (2sigma) Int.Cal.13	Reference
1	P5 VS13	KIA40624	C	*Populus/Salix*	Unit 3/4, ditch	0.90	510 ± 90	1283–1631 cal. AD	Jansen et al. 2013
2	P5 VS13	KIA45530	P	-	Ditch (filling)	1.10	1305 ± 25	660–768 cal. AD	this study
3	P5 VS13	KIA45529	P	-	Ditch (filling)	1.20	1905 ± 30	25–211 cal. AD	this study
4	P2 VS2	KIA39157	C	*Quercus*	Unit 5/6	0.40	365 ± 20	1453–1631 cal. AD	Jansen et al. 2013
5	P2 VS3	KIA40623	C	*Quercus*	Unit 5/6	0.80	1780 ± 20	142–332 cal. AD	Jansen et al. 2013
6	P2 VS2	KIA40620	C	Ericaceae	Unit 5/6	0.80	1620 ± 20	387–535 cal. AD	Jansen et al. 2013
7	P2 VS3	KIA45182	C	*Fagus*	Unit 5/6	1.00	965 ± 25	1018–1155 cal. AD	Jansen et al. 2013
8	P1 VS5	KIA39154	C	*Fagus*	Unit 4	0.70	980 ± 25	996–1154 cal. AD	Jansen et al. 2013
9	P2 VS1	KIA39155	C	*Populus/Salix*	Unit 4	0.70	1595 ± 35	394–545 cal. AD	Jansen et al. 2013
10	P8 VS9	KIA45183	C	*Fagus*	Unit 4	0.80	925 ± 25	1032–1162 cal. AD	Jansen et al. 2013
11	P8 VS9	KIA45184	C	*Fagus*	Unit 4	1.40	900 ± 25	1040–1209 cal. AD	Jansen et al. 2013
12	P2 VS1	KIA40621	C	*Populus/Salix*	Unit 4	1.30	930 ± 20	1036–1157 cal. AD	Jansen et al. 2013
13	P2 VS2	KIA41023	C	*Betula*	Unit 3	2.00	1265 ± 25	667–800 cal. AD	Jansen et al. 2013
14	P3 VS6	KIA39156	C	Ericaceae	Unit 2-p	1.10	1610 ± 25	395–536 cal. AD	Jansen et al. 2013
15	P8 VS10	KIA38361	C	Ericaceae	Unit 2-p	0.70–0.90	1140 ± 25	777–979 cal. AD	Jansen et al. 2013
16	P3 VS6	KIA38360	C	Ericaceae	Unit 2-p	1.10–1.20	1135 ± 35	777–986 cal. AD	Jansen et al. 2013
17	P6 VS8	KIA40619	C	c.f. *Alnus*	Unit 1	1.10	10600 ± 500	11600–8945 cal. BC	Jansen et al. 2013
18	P12 VS7	KIA37875	SOM	-	Unit 3	0.90–1.00	1485 ± 30	474–646 cal. AD	this study
19	P12 VS7	KIA37876	SOM	-	Unit 2-p	1.00–1.01	1160 ± 25	775–964 cal. AD	this study
20	P12 VS7	KIA37877	SOM	-	Unit 2-p	1.16–1.17	2030 ± 25	111 cal. BC–51 cal. AD	this study
-	Jol 1	H 1906-1346	SOM	-	Unit 2-p?	1.00	2400 ± 70	766–385 cal. BC	Richter 1965
-	Jol 2	H 1907-1334	SOM	-	Unit 2-p?	1.10	2080 ± 80	358 cal. BC–70 cal. AD	Richter 1965
-	Jol 3	H 1908-1329	C	-	Slag pit, Unit 2?	-	1725 ± 55	141–420 cal. AD	Richter 1965
-	-	KIA25559	SOM	-	Unit 1?	2.72–2.74	10685 ± 55	10771–10611 cal. BC	Fleige et al. 2006

(OM), and pedogenic oxides (PO). Measurements of total carbon and nitrogen were performed on a HekaTech Euro EA 3000 Elemental Analyzer. Inorganic carbon is generally not present in the Late Glacial and Holocene sediments of the study area (Fleige et al. 2006). Therefore, it is assumed that the measured content of total carbon is equivalent to the content of soil organic carbon (SOC). Organic matter content (OM) was calculated using conversion factor of 1.742, assuming that organic matter of soils approximately 58 % organic carbon (Nelson and Sommers 1996). Determination of pedogenic iron oxides (FeD) was done using dithionite-citrate-bicarbonate (DCB) extraction method proposed by Mehra and Jackson (1960). A 1 g air-dried sample was treated with 100 ml dithionite, heated up to 75–80 °C in water bath and then centrifuged to remove the supernatant. Then, Fe was measured using a flame Atomic Absorption Spectroscopy (AAS) system. The amount of amorphous iron oxides (FeO) was determined using the acid-ammonium oxalate (AAO) extraction technique (Tamm 1932, Schwertmann 1964).

6.3.3 Radiocarbon dating

The abundance of charcoal and humic layers in most of the sand layer permitted AMS radiocarbon dating to obtain the chronology of land-use change. In addition, samples for AMS radiocarbon dating were taken from organic matter-enriched A horizons and peat. Samples of charcoal and humic layers (1000–2000 g) were taken in the vertical section and in the immediate periphery according to the given dune stratigraphy. Prior to the radiocarbon dating, samples were dry-sieved through a 630 µm-mesh and taxonomic identification of wood charcoal was carried out to reduce the risk of the old wood effect and the dating of modern conifers such as *Picea*. Therefore, relatively short-lived woody taxa such as Ericaceae, *Populus*/*Salix*, and *Betula* were preferred in order to make the radiocarbon data more reliable by reducing the potential »inbuilt age« (Gavin et al. 2003). In total, radiocarbon dating of 15 charcoal samples, three bulk soil samples and two peat samples were performed by the Leibniz-Laboratory for Radiometric Dating and Isotope Research at Kiel University, following standard methods (Nadeau et al. 1997, Nadeau et al. 1998, Grootes et al. 2004) and ages were calibrated according to Reimer et al. (2013) using OxCal v4.1.7 (Table 6.2). Before radiocarbon dating of soil samples, humus extraction was done using standard acid-alkali-acid (AAA) method. Samples were extracted with 1 % HCl and 1 % NaOH, both at 60 °C (humic acid fraction), then again with 1 % HCl, leaving the humin fraction as residue.

6.3.4 Optical Stimulated Luminescence (OSL)

OSL dating was carried out where clearly separated charcoal layer were lacking and/or in order to cross-check with radiocarbon dating. In total, six OSL samples were dated by the Luminescence Dating Laboratory at University of Szeged, Hungary (Table 6.3). Samples were taken during the day at regular depth intervals (~ 15 cm) using opaque tubes that were

Table 6.3: Optical stimulated luminescence (OSL) dating results.

No.[a]	Exp.	Lab. ref.	Context[b]	Depth (m)	Water content (%)	U (ppm)	Th (ppm)	K (%)	D_{cosmic} (Gy/ka)	D_{total} (Gy/ka)	D_e (Gy)	OSL age (yr)
1	P2	OSZ488	5/6	1.60	0.12	0.43 ± 0.02	1.49 ± 0.07	0.82 ± 0.04	0.19 ± 0.01	1.14 ± 0.10	0.79 ± 0.05	705 ± 75
2	P2	OSZ489	5/6	1.40	0.10	0.37 ± 0.02	0.98 ± 0.05	0.61 ± 0.03	0.19 ± 0.01	0.90 ± 0.08	0.60 ± 0.08	670 ± 105
3	P2	OSZ490	5/6	1.15	0.06	0.29 ± 0.01	1.46 ± 0.07	0.69 ± 0.03	0.19 ± 0.01	1.02 ± 0.09	0.63 ± 0.05	620 ± 75
4	P2	OSZ491	5/6	0.40	0.07	0.52 ± 0.03	1.27 ± 0.06	0.76 ± 0.04	0.20 ± 0.01	1.12 ± 0.10	0.68 ± 0.07	605 ± 85
5	P2	OSZ627	5/6	0.45	0.10	0.39 ± 0.02	1.03 ± 0.05	0.71 ± 0.04	0.19 ± 0.01	1.00 ± 0.09	0.51 ± 0.05	510 ± 70
6	P2	OSZ628	4	1.40	0.10	0.35 ± 0.02	1.00 ± 0.05	0.62 ± 0.03	0.19 ± 0.01	0.90 ± 0.08	0.69 ± 0.04	765 ± 80

[a] refers to figure 2; [b] refers to units 1–6. Abbreviations: Exp.: Exposure; D_{cosmic}: Cosmic dose rate; D_{total}: Total dose rate; D_e: laboratory equivalent dose

Table 6.4: Results of quantification

Unit	*Area* (m^2)	*Volume*(m^3)	*SBD* (g cm^{-3})	*Sediment mass* (kt)	*Deposition rate* (t/ha/a)
Unit 5/6	2453.9	3221.24 ± 355.60	1.52 ± 0.03	4.88 ± 0.54	5.02 ± 0.55
Unit 4	2453.9	1831.69 ± 363.62	1.56 ± 0.05	2.87 ± 0.57	3.05 ± 0.61
Unit 3	2453.9	149.28 ± 69.02	1.62 ± 0.02	0.24 ± 0.11	0.32 ± 0.15
Unit 2-p	1003.2	124.40 ± 12.44	1.41 ± 0.04	0.18 ± 0.02	0.12 ± 0.02
Unit 1–2	2453.9	6803.23 ± 368.08	1.46 ± 0.05	9.96 ± 0.54	1.48 ± 0.05
aggregated results					
Unit 3–6	2453.9	5212.87 ± 368.08	1.57 ± 0.03	8.16 ± 0.38	2.69 ± 0.13
Unit 1–2	2453.9	6803.23 ± 368.08	1.46 ± 0.05	9.96 ± 0.54	1.48 ± 0.05
Unit 1–6	2453.9	12016.1 ± 368.08	1.54 ± 0.04	18.51 ± 0.38	-

forced into the profiles. Preparation of samples was made using standard techniques (Aitken 1998, Mauz et al. 2002) and for dating quartz grains of 90–150 µm size were extracted. For each sample, 24 aliquots were prepared to determine the equivalent dose (D_e) and an additional 21 aliquots were used to perform a preheat plateau test. Preheat plateau test of dose was carried out on each sample. All OSL measurements were made on a Risø DA-15 automated TL/OSL system using the standard single-aliquot regenerative-dose (SAR) protocol (Wintle and Murray 2006). Quartz samples were stimulated by 470 nm blue light and the detection of the OSL signal was made with Hoya U-340 filter (290–390 nm). The preheat temperature was between 210 °C and 240 °C for each sample. Cut heat temperature was set to 160 °C (Wintle and Murray 2006). The received and corrected OSL data were evaluated by Software RISO Analyst 3.24 (2007). Environmental dose rate calculations were based on the 232Th (ppm), U (ppm) and K (%) content of samples, provided by high resolution, low-level gamma spectrometry. Radioactive disequilibrium in the uranium chain was not observed. The rate of cosmic radiation was determined on the basis of burial depth and following the method of Prescott and Hutton (1994).

6.3.5 Quantification of sediment mass

In order to analyse spatiotemporal changes in the inland dune topography, we performed a detailed analysis of the spatial extension of each Holocene sedimentary layer (units 1–6) and the Pleistocene surface within the central area of KHD (Figure 1). With the exception of unit 1, all upper boundaries of the chrono-stratigraphic units could be clearly identified and surveyed.

A 3D model of the surface terrain was then constructed using spatial data generated with a laser-based Leica TCR-407 total station with ~ 3 cm accuracy. The same total station was used to determine the exact locations of ~ 125 field measurements of the depth of the analysed Holocene (top) sedimentary layers (units 1–6), and 16 field measurements of the depth of the underlying Pleistocene deposits (unit P). Depth measurements were performed to the nearest cm, however in order to account for measurement inaccuracies, e.g. surveying on soft forest floor or layer compression within corings, we attributed a vertical and horizontal accuracy of ~ 0.15 m to all measurements. Within sedimentary unit 3, we have explicitly cross-checked the depths of the coring points and exposures, and therefore assume a slightly higher accuracy of ~ 0.05 m. All elevation data was imported as point clouds into ESRI ArcGIS 10.1 and for each stratigraphic unit a TIN model was created. All TIN layers were clipped with a polygon of the central area of KHD in order to have the same spatial extension (~ 0.24 ha in size) of all TIN layers in order to set up the quantification on the same storage area (clipped area for quantification, Figure 6.1e). All TIN layers were then converted to separate surface raster models (DEMs) through natural neighbor interpolation using 3D Analyst. To quantify the net volumes and their uncertainties between sur-

faces, we used the Geomorphic Change Detection (GCD) add-in (www.gcd.joe-wheaton.org/). The minimum level of detection threshold was set to 0.15 m and for unit 3 to 0.05 m in order to distinguish actual change from inherent noise (Wheaton 2008). Spatially uniform errors were created and propagated for the volume of each sedimentary layer (Table 6.4).
We quantified the sediment mass (*M*, in metric tons) of all Holocene sedimentary units, using

$$M = V\rho \quad (1)$$

where *V* is the sediment volume derived from the calculation above, and ρ the soil bulk density (in g cm^{-3}) (Section 6.3.2) (Table 6.4). Standard errors were propagated.

In order to compare the differences in sediment masses over time, we determined the deposition rate by dividing the sediment masses by the time length of each unit (stratigraphic units 1–2, 2-p, 3, 4 and 5/6), based on the defined area for quantification which is ~ 0.24 ha (Figure 6.1). We estimated the time length of each deposit using the outer error margins of ages from the upper and lower layers of the stratigraphical units (Figure 6.2). Although this will most likely lead to an overestimation of the length period and subsequently an underestimation of deposition rates, it nonetheless provides a conservative estimate of the long-term evolution of KHD and the speed of dune accumulation. Based on the detailed stratigraphic analysis and high resolution age control through variable dating techniques (OSL, Radiocarbon, and Archaeological dating), we were able to exclude dates from the settlement period of Roman Iron Age / Migration period from unit 4 and unit 5/6 (Figure 6.4). These erroneous ages most likely originate from the re-deposition of older charcoal fragments during periods of wind erosion at the KHD.

6.3.6 Visual analysis of historic maps

We established the history of land-use change within the study area for the past 225 years through the geo-spatial analysis of historic and present maps. The oldest historic map of the area (1793 AD) shows land-use types of the Joldelund region after the agrarian land reform which took place in the German states at the end of the 18th century, however the exact areal extent of land-use areas could not be quantified. Topographic maps to scale (1:25000) are available for the time period between 1878 AD and 2009 AD (130 years), and provide a coherent dataset of land-use change. Here, we build upon research done by Dörfler (2000), who quantified land-use changes within the wider region using similar methods.

6.4 Results

6.4.1 Geomorphology of the research area

The heterogeneous surface morphology of the research area is mostly caused by aeolian sand deposition of variable thickness, ranging between ~ 0.4 m to 6.5 m.

The characteristics of these sediments are typical for dune sands which consist of moderately to well-sorted sands with grains mainly in the size range 0.07–0.25 mm (Pye and Tsoar 2009) (Figure 6.3). The KHD is a »Kuppen-/Kupstendüne« (hummock dune), which are characterized by a mostly rounded plan profile, and a hummocky shape (Pyritz 1972, Pye and Tsoar 2009). A drop in elevation in the western part of the research area at the south-eastern part of the KHD stretches around ~ 120 m from north-east to south-west (Figure 6.1c), and represents an erosional boundary. Greater aspect and gradient of dune slopes occur in the western part of the research area, and are more likely to be exposed north-east to south-east, while slopes in the central and eastern part show no clear pattern.

6.4.2 Soils and sedimentary units

The subsurface of the KHD is broadly dominated by Holocene dune sands, in which one thick, buried soil and several humic layers are developed. These soils were used to separate the otherwise homogenous sedimentary sequence into six sedimentary units (unit 1–6), which are described below. These sand-soil sedimentary complexes are clearly distinct from the underlying Pleistocene moraine deposits (unit P) which forms the boundary for the accumulation rate analyses (Figure 6.3). The moraine deposits are characterized by a wide range of particle sizes, poor sorting and the abundance of angular clasts (Figure 6.3), and are always capped by a distinct gravel layer showing signs for wind erosion (ventifacts). This gravel layer inclines towards the south-west (~ 1.5 m / 100 m) along with the main drainage lines of the glacial melt water flow (Riedel 1997, Duttmann et al. 2006) (Figure 6.1b).

6.4.2.1 Unit 1

The lowermost sandy sedimentary unit (unit 1) is deposited on top of a gravel layer which separates the glacial and aeolian deposits, and is capped by a thin charcoal layer. Dating of charcoal fragments yield a radiocarbon age of 10600 ± 500 BP (11600–8945 cal. BC; KIA40619) (P6 VS8 in Figure 6.5), indicating that unit 1 represents an aeolian depositional episode during the Late Glacial/Early Holocene. All sediments of unit 1 are characterized by horizontally laminated, medium-sandy fine sands with median (Md) and mean (M) diameter of 0.17 mm and 0.18 mm (Figure 6.3).

Grain size analysis shows a dominance of fine sand (~ 68 wt.%), a smaller amount of medium sand (~ 30 wt.%) and minor amounts of coarse sand (Figure 6.2). Typical for aeolian sands, the amounts of silt and clay are small (< 1 wt.%). The aeolian cover sands have a light yellow (2.5Y 7/4) colour and are typically well sorted (Pye and Tsoar 2009) with a sorting coefficient (So) of 1.4 (Figure 6.3). Unit 1 has a limited maximum thickness of ~ 0.5 m and could only be confidently distinguished from the superimposed unit 2 within profile 6 (Figure 6.3).

6.4.2.2 Unit 2 (-p)

Unit 2 is characterized by horizontally bedded, fine-grained and gravel-free sands with a yellowish brown colour (Table 6.1). Within the top of this depositional unit a ~ 0.6 m thick podzol soil (Figure 6.4) has developed, with an upper bleached E horizon and a lower strongly colored illuvial B horizon with accumulation of organic matter and sesquioxides (Sauer et al. 2007, Figure 6.4). Maximum thickness of ~ 3.8 m is reached for this unit at the highest point of the KHD, but decreases to around 0.8 m towards south the of the research area (exposure P4 VS13) (Figure 6.5). Clear differences between unit 1 and 2 can be seen within grain size distribution, statistical parameter (Md, M, S0) and the colour of the sediments (Table 6.1), which indicates this is likely a distinct phase of aeolian sedimentation. All sediments of unit 2 show lower proportions of fine sands (mean: ~ 51 %) and higher proportions of medium sands (mean: ~ 44 %). Generally, silt and clay are only slightly higher (0–5 wt.%), however the proportions are significantly higher in A horizons and illuvial B horizons of the podzol described below (Figure 6.3). Soil bulk densities (SBD) reach their lowest values measured in this study between ~ 1.1 g cm^{-3} and 1.7 g m^{-3}, with an average of 1.46 ± 0.05 g cm^{-3} (n=14). Sediments are well to moderately sorted and the ratio of medium to fine sand (MS:FS-ratio) suggests a relatively homogenous depositional regime.

Sediments within unit 2 tend to fine upwards, which can be attributed to soil processes within the horizons overlying unit 2. This ~ 0.6 m thick native soil is an Ortsteinic Podzol (IUSS Working Group WRB 2015). From top to bottom, this soil consists of a humous topsoil (A horizon, Ab) (Figure 6.4) that ranges in colour from black to brown (Table 6.1), with organic matter content that varies between ~ 0.7 % and 11.5 % (mean: 4.5 %), and which contains numerous charcoal fragments. The underlying bleached, eluvial E horizon (Eb) has a reddish grey (2.5Y 4.5/1) to brownish grey colour (10YR 5/1) and shows well-developed tongues up to a depth of ~ 1 m, which can presumably be linked to old root channels Figure 6.6). The strongly cemented, spodic B horizons (Bhb, Bsb/Bmsb) underlie the E horizons and are characterized by brownish black to reddish brown colors (Table 6.1, Figure 6.4). Thin dark-coloured humic bands (< 2 mm) in B and C horizons up to a depth of ~ 1.5 m are the result of deep humus illuviation (Wiechmann 1981, van Breemen and Buurman 2002). The pH values vary between 3.3 and 4.4, but show no vertical trend. The podzol soil has a typical strongly expressed Fe profile with the highest amount of oxalate- and dithionite-extractable Fe in B horizons (van Breemen and Buurman 2002), while activity ratios (FeO:FeD) higher than 1.0 occur in B as well as in E horizons (Figure 4). Charcoal fragments of the topsoil (A horizon: Ahb/Apb) provide the following ages: 777–979 cal. AD (KIA38361), 777–986 cal. AD (KIA38360). A sample of soil organic matter (SOM) was dated to 775–964 cal. AD (KIA37876).

In a ~ 0.4 ha wide area that extends from Kuhharder Hill to the western edge of the study area we observed parallel plough marks in the topsoil of the podzol (unit 2-p) (Figure 6.1), indicating an old agricultural

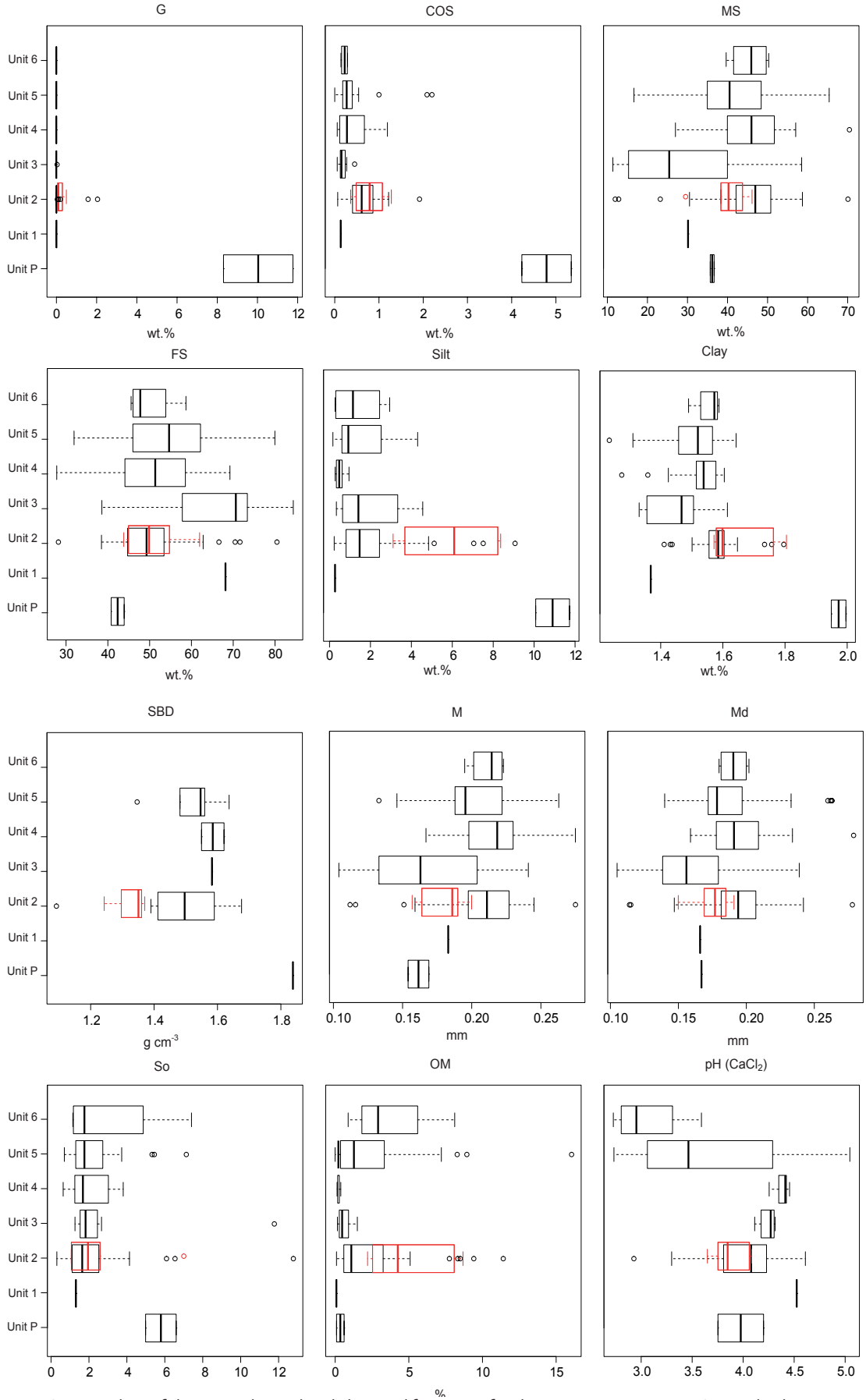

Figure 6.3: Boxplots of the main physical and chemical features of sedimentary unit P to unit 6, in red colour: unit 2-p

cropping technique, a turning plough, was employed at this time (Figure 6.1d, Figure 6.6). The ploughed and turned horizon (unit 2-p) is characterized by clearly distinguishable brownish black color (Figure 6.4, Table 6.1).This makes the furrow-slices clearly visible within the lighter Eb horizon, in which the furrow-slices were incorporated by the turning plough (Figure 6.6). The clear visibility of the turned soil is supported by strong differences between the analysed soil variables within the furrow-slices and the surrounding E horizon (Figure 6.3). The ploughed horizon is shallow, and ranges in thickness only between ~ 0.06 m to 0.17 m. Repeated ploughing would have mixed surface and subsoil material, which was not found in unit 2, which indicates that the field was only ploughed once. Throughout the ploughed horizon (unit 2-p), charcoal fragments and very fine gravel are evenly distributed (Table 6.1). These charcoal pieces were most likely incorporated into the soil by the ploughing process, and their age provides evidence for earlier settlement activities in the study area (395–536 cal. AD, KIA39156), and similar ages were obtained by dating of the soil organic matter (111 cal. BC–51 cal. AD, KIA37877).

In areas of unit 2 without signs for ploughing, slag pieces of up to 15 cm in size, burnt clay fragments, stone fragments (> 5 cm) and larger charcoal pieces (> 1 cm) are distributed within the top ~ 15 cm of unit 2 (e.g. exposure P1 VS5, Table 6.1). In combination with an iron-melting furnace and slag pit which was found dug into unit 2 (exposure P6 VS8, Figure 6.5), these findings testify to the presence of iron smelting and related activities in the area. Similar archaeological findings are well studied in the study area, and date to the Roman Iron Age (~0–400 AD) (Backer et al. 1992, Jöns 1997). A man-made pit (~ 1.2 m in length, ~ 0.3 m in depth) dug into unit 2 for unknown purposes was found within exposure P5 (Figure 8). The OM within the bottom sediments of this pit yield an age of 25–211 cal. AD (KIA45529), the upper part show an age of 660–768 cal. AD (KIA45530). These ages indicate the creation of the pit during Roman Times, and then a slow infilling process until Medieval Times.

6.4.2.3 Unit 3

A horizontally laminated sand layer (unit 3) overlies unit 2. The extension of this layer is limited to the central area of KHD (Figure 6.1e). Unit 3 is characterized by a yellowish brown colour with a thickness of maximum ~ 0.3 m. This layer is dominated by fine sands with the lowest values of middle sand found in this study (~ 28 %), and the highest values in SBD (mean: 1.62 ± 0.02 g cm^{-3}, n=4) (Table 6.1, Figure 6.3). Layer 3 is characterized by a series of three undulating humic sublayers of less than 2 cm thickness, which were intercalated with sand dominated layers of 3–8 cm thickness. Charcoal particles are generally finely dispersed throughout but also concentrated within the humic layer. Unit 3 is capped by a weakly developed; partially diffuse A horizon (2Ahb, Figure 6.4) with organic matter content varying between 0.6 % and 1.5 % (Table 6.1). The A horizon is only slightly higher in extractable Fe than the underlying parent material (C horizon) (Table 6.1, Figure 6.4), which

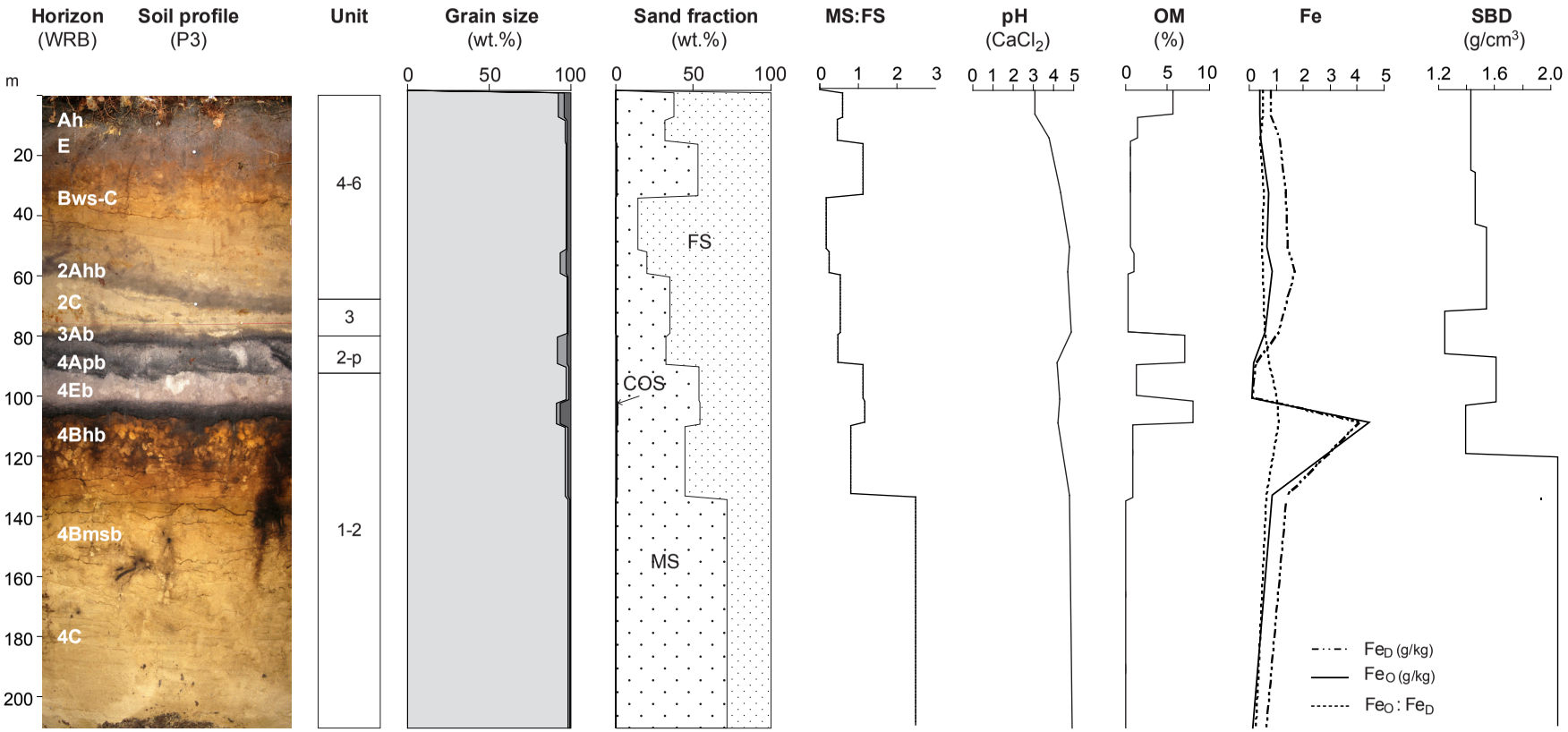

Figure 6.4: Typical soil morphology of the study area. Abbreviations: COS = coarse grained sand, MS = medium sand, FS = fine sand; OM = organic matter content, Fe = soil iron content, SBD = soil bulk density. Depth given in m above the base level height (NHN, Normalhöhennull)

can be interpreted as representing a relatively short period of soil formation. Charcoal pieces sampled and dated from the A horizon (667–800 cal. AD, KIA41023) are not coherent with radiocarbon dates derived from dating SOM (474–646 cal. AD, KIA37875), but overall suggest soil development occurred between ~ 474–800 AD.

6.4.2.4 Unit 4

Unit 4 consists of horizontally laminated, partially cross-bedded sands of reddish brown to light yellowish brown color. The layer has a minimum thickness of ~ 0.4 m at NE-slope and a maximum thickness of ~ 2.4 m at the dune crest of KHD (unit 4) (Table 6.1), and therefore accounts for the bulk of the dune crest thickness. Unit 4 shows sediment characteristics similar to those of unit 2 (Figure 6.3), especially in the alternation of charcoal and sandy sublayers: Eleven thin charcoal layers (< 1 cm) alternate with sand dominated layers (Figure 6.7). Three charcoal pieces extracted from the uppermost charcoal sublayer were dated to 394–545 cal. AD (KIA39155), 996–1154 cal. AD (KIA39154) and 1032–1162 cal. AD (KIA45183). A charcoal piece from a more central sublayer was radiocarbon dated to 1040–1209 cal. AD (KIA45184), and the lowest sublayer to 1036–1157 cal. AD (KIA40621). An OSL ages of 765 ± 80 yrs (1164–1324 AD, OSZ628) was obtained from a lower sandy layer.

The upper boundary of unit 4 is sharp, which cuts through sedimentary layers and is therefore likely to be erosional. This erosional boundary forms a 1 m deep and 8 m long depression at the western slope of the KHD (P2 VS2 in Figure 6.3). An age obtained from the layer underneath this depression gives a maximum age for this erosional event of 705 ± 75 yrs (1229–1379 AD; OSZ488), and also provides the oldest age of layer 4. Man-made, ~ 0.9 m deep ditches of unknown purpose and 0.3–0.5 m in diameter were dug from the surface of unit 4 into unit 2 (Figure 6.8). In exposure P4, the strongly leached sediments of the E horizon (unit 2) were found next to the ditch feature indicating that spoils were deposited nearby, and the ditches were later refilled with sands of unit 4.

6.4.2.5 Unit 5 and 6

A confident distinction between unit 5 and unit 6 was only possible within two vertical sections (P1 VS5, P2 VS3, dune crest of KHD) (Figure 6.5). Hence, in most analysis unit 5 and 6 are grouped together as unit 5/6. Unit 5 consists of laminated sands with sediment characteristics (grain size distribution, Md, M, So) similar to those of unit 2 and 4 (Section 6.4.2.2 and 6.4.2.4) with a maximum thickness of 1.7 m (Figure 6.5). Several diffuse and discontinuous sublayers of increased organic matter content, indicated by the much darker color (10YR 5/4) are randomly distributed throughout the sediments. Charcoal fragments collected from these layers yield variable dates spanning a period from 142 up to 1631 cal. AD (1018–1155 (KIA45182), 1453–1631 cal. AD (KIA39157), 142–332 cal. AD (KIA40623) and 387–535 cal. AD (KIA40620). This is likely to be caused by the reworking of older charcoal fragments. OSL dating of this unit shows rapid

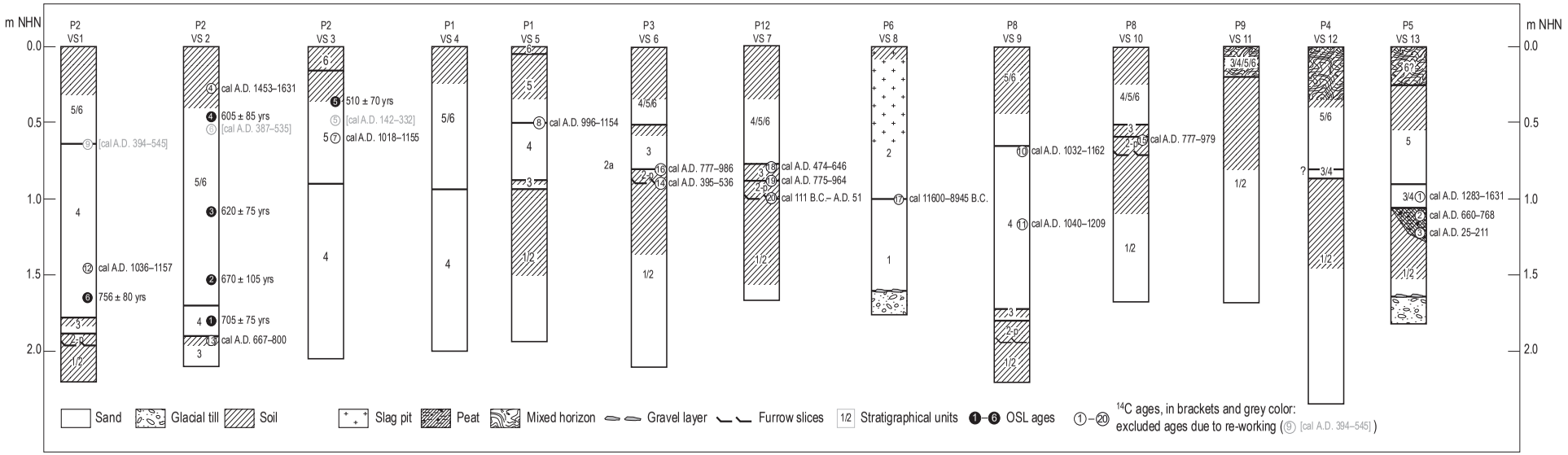

Figure 6.5: Simplified composite stratigraphy of all vertical sections (VS1-13) of the study area

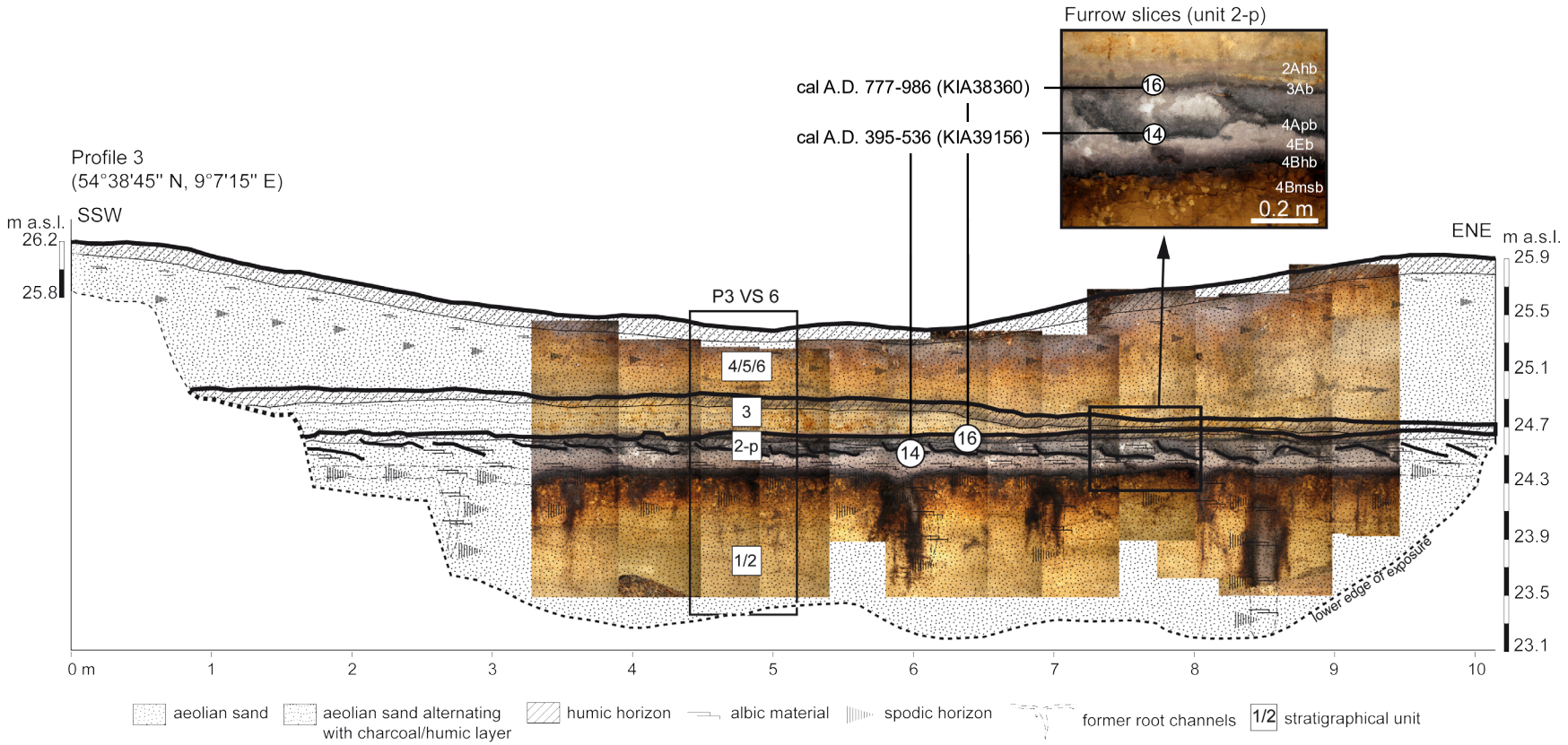

Figure 6.6: Profile 3 showing plough marks

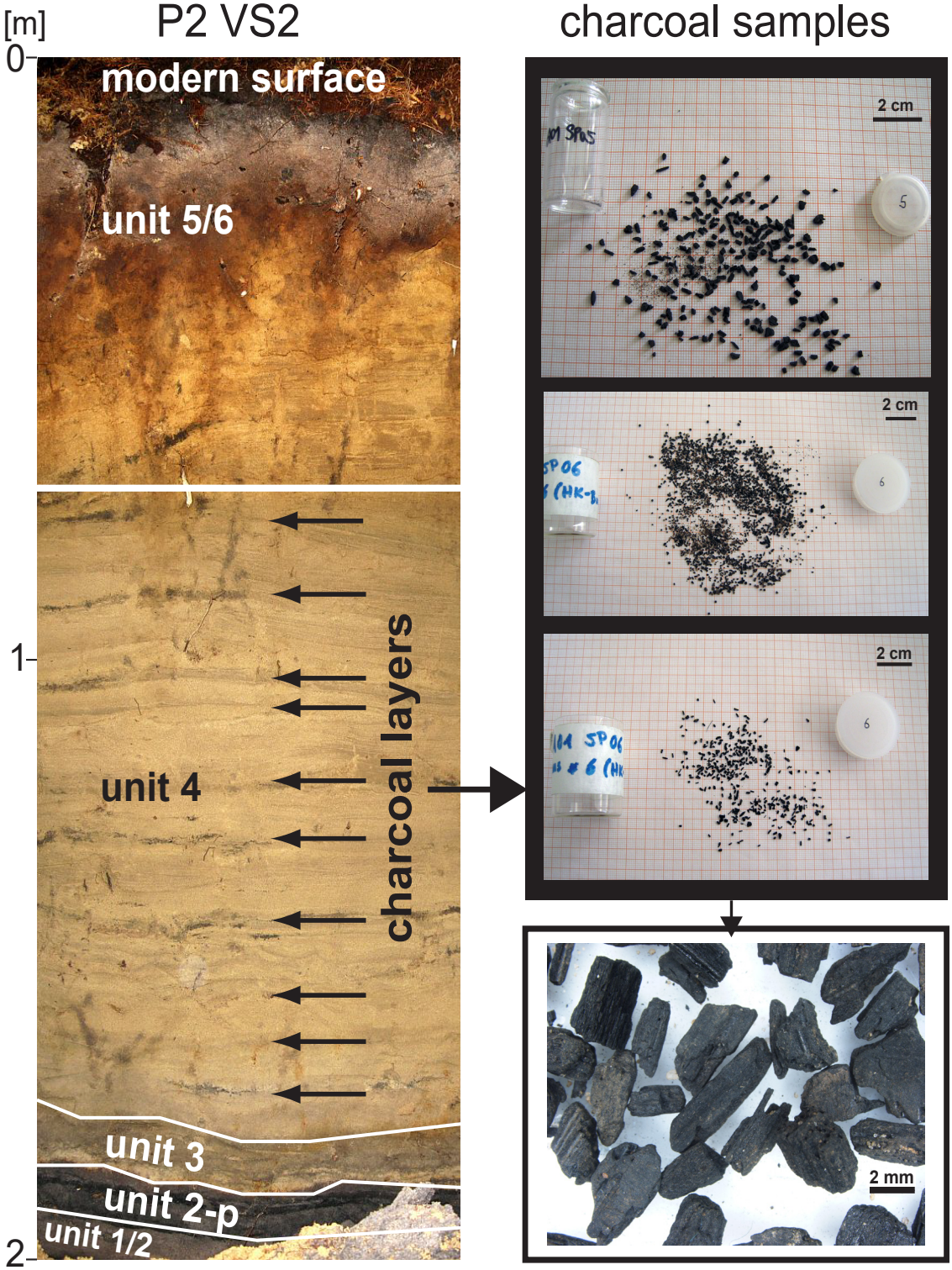

Figure 6.7: Charcoal layer embedded in unit 4 (Profile 2, Vertical Section 2)

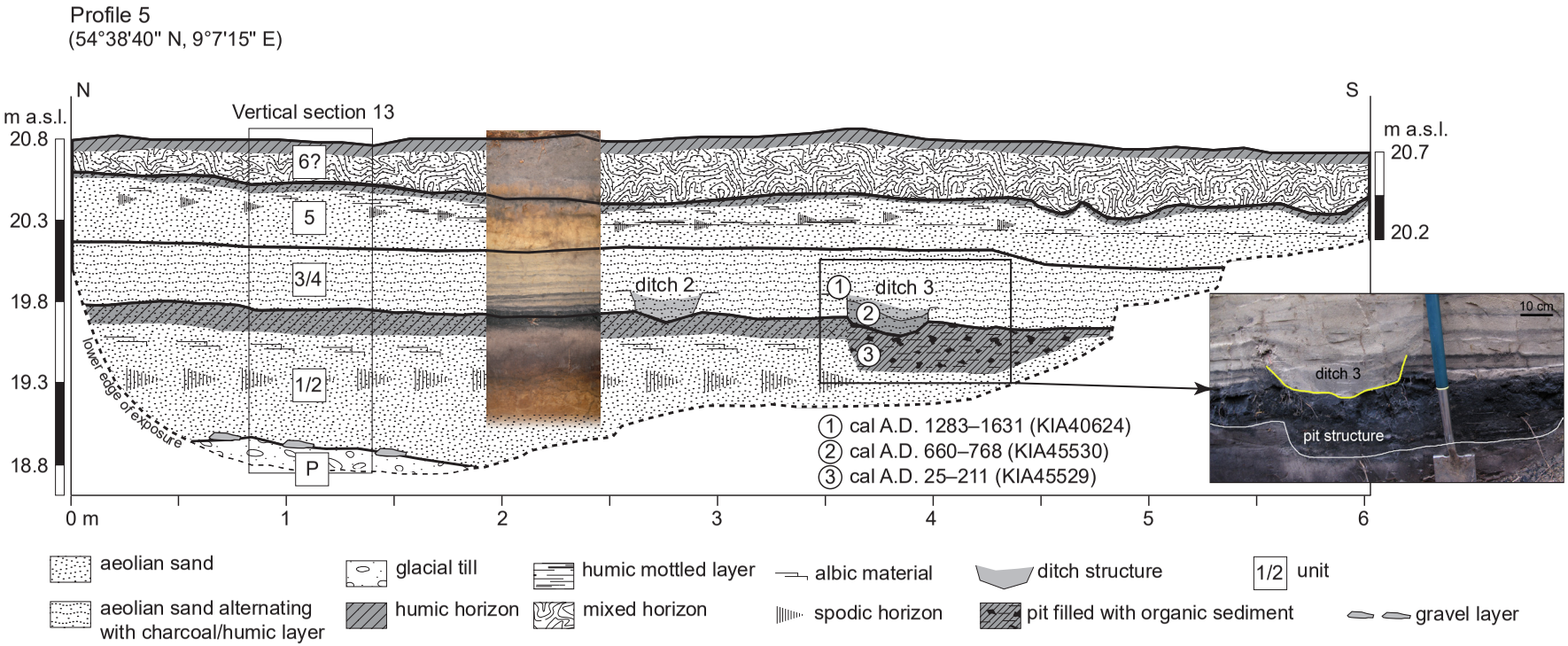

Figure 6.8: Profile 5 showing a settlement pit and two ditch structures

sand accumulation around ~ 1400 AD, as all ages are within error ranges. The bottom layer yields an age of 670 ± 105 yrs (1234–1444 AD, OSZ489); the central sediments an age of 620 ± 75 yrs (1314–1464 AD, OSZ490), and the upper part of this unit was dated to 605 ± 85 yrs (1319–1489 AD, OSZ491), and 510 ± 70 yrs (1429–1569 AD, OSZ627) respectively.

At the top of unit 5 the sequence forms a ~ 0.4 m thick, weakly developed soil with podzolic features (podzolised Arenosol) (IUSS Working Group WRB 2015) (Table 6.1). In profiles in which we were able to distinguish between unit 5 and 6, unit 6 is a thin sand layer between 0.06 m and 0.13 m in thickness, which is slightly podzolised and subsequently shows a 3–8 cm-thin A horizon (Ah) and a humous E horizon (Eh). Where they lay close to the present surface, soil horizons of units 5 and 6 show a layer of ~ 0.35 m that is clearly disturbed likely as a consequence of melioration measures prior to afforestation, and thus represents a typical mixing layer (exposures: P4, P5 and P9) (Figure 6.5, Figure 6.8). This mixing could also explain the extreme ranges of values found in organic matter content and pH values (Figure 6.3).

6.4.3 Quantification of deposition rates

We estimated the total sediment mass within the research area (KHD, ~ 0.24 ha in size), and for each sedimentary unit (unit 1–2, 2-p, 3, 4 and 5/6) respectively. (Table 6.4, Figure 6.1) using equation 1. The total Late Quaternary net sediment mass deposited within the research area was calculated to be 18.51 ± 0.38 kt. Sediments very likely to have been deposited during the Late Glacial/Early Holocene, but prior the Preboreal (11600–8945 cal. BC) amount to 9.96 ± 0.54 kt (units 1–2), which is ~ 55 % of the total Late Quaternary net sediment mass. Sediments stored in ploughed part of unit 2 (unit 2-p) (395–986 cal. AD) were calculated to be 0.18 ± 0.02 kt, which is less than 1 % of the total net deposition. Only 0.24 ± 0.11 kt (~ 1 % of the total mass) was deposited in unit 3 during the time period of 667–979 AD. The second largest sediment mass is stored in the high-late Medieval deposits, unit 4 (996–1379 cal. AD) and unit 5/6 (1235–1631 cal. AD) respectively (~ 42 % of the total mass). Unit 4 was calculated to hold 2.87 ± 0.57 kt (~ 15 %), and unit 5 4.88 ± 0.54 kt (~ 26 %). This means, that Medieval Times (700–1500 AD) accounts for a deposition of 8.16 ± 0.38 kt, which is ~ 45 % of the total Late Quaternary sediment mass. Converting these masses to accumulation rates using the available chronological controls, we calculated the highest deposition rates during Medieval Times, and within this time period the rate increased towards the surface (Table 6.4).

6.5 Discussion

6.5.1 Causes of alternating phases of aeolian sand deposition and geomorphic stability

6.5.1.1 Phase 1: Late-Pleistocene to Mid-Holocene (~ 11700–3800 cal. BC)

After a phase of till formation (unit P) at around ~191–130 ka BP (Cohan and Gibbard 2012), this study finds evidence of the onset of cover sands in the area at between 11600 and 8945 cal. BC (P6 VS 8, Figure 6.5). Northern European cover sands are reported to be initiated mainly in the Older Dryas (OD: 11850–11750 cal. BC), and Younger Dryas (YD: 10730–9640 cal. BC) (Müller 1999, Mauz et al. 2005, Fleige et al. 2006) (Figure 6.9A). These late glacial, phases of widespread aeolian activity were interrupted by a phase of relative surface stability (Allerød warm period, ~ 11700–10700 cal. BC) in which woodland covered the study region (Nelle and Dörfler 2008), and the entire NW Europe (van der Hammen 1951, Iversen 1954, Kasse 1999, Hoek 2001, Mortensen et al. 2011), which caused a characteristic soil to develop (Usselo / Finow soil) (van der Hammen 1957, van Geel et al. 1989, de Boer 1995, Manikowska 1991, Kowalkowski et al. 1999, Schirmer 1999, Schlaak 1999, Kaiser et al. 2009). An earlier study on wood charcoal fragments of unit 1 has found evidence for the presence of boreal pine and birch woodland during this time period (Jansen et al. 2013), and supports the existence of an Allerød birch-pine woodland. This woodland potentially accumulated sufficient dead and dry biomass to burn regularly (van der Hammen 1951, Hoek and Bohnke 2002, van der Hammen and van Geel 2008), which would explain the presence of the large amount of charcoal particles within unit 1 sediments (11600–8945 cal. BC, KIA40619, Table 6.2, Figure 6.5). However, the analysed charcoal fragments are small, exhibit signs of transportation (Jansen et al. 2013), and are distributed throughout the sedimentary layer. In combination with the deposition age of 11600–8945 cal. BC, we interpret the sediments of unit 1 to be very likely the result of large aeolian activity during the YD, which has largely eroded the original Allerød soil in the research area and re-deposited these as aeolian sediments, including the charcoal fragments (Figure 6.9A). With the beginning of the Holocene at ~ 11650 cal. BP (Cohan and Gibbard 2012), the land surface in Northern Europe (Castel 1991, Schirmer 1999, Koster 2005), and the region (Müller 1999, Mauz et al. 2005) is generally considered to have stabilized. This was due to an increase of temperature and vegetation cover (Nelle and Dörfler 2008). This is likely to be also true for the KHD, as we do not find any evidence for aeolian activity during the entire early-mid Holocene period (~ 9650–3800 cal. BC) (Figure 6.9B). The existence of a thick Podzol, developed within the late glacial cover sands supports this time period as a phase of relative geomorphic stability. Our results are consistent with earlier studies from the region, in which well-developed, similar podzols have been reported, and their time of formation was

Phase 1: Late-Pleistocene to early-mid Holocene (~ 11700–3800 BC)

~ 11700–9600 BC

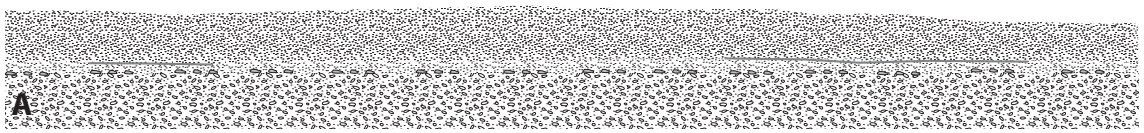

~ 9600–3800 BC

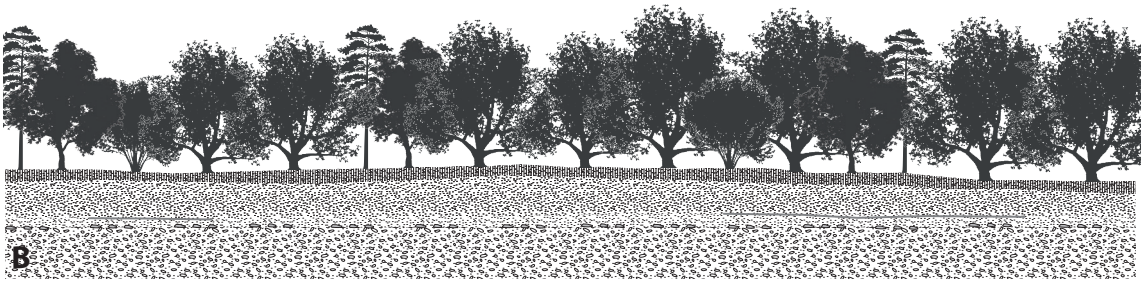

Phase 2: Roman Iron Age to Migration period (~ 0–700 AD)

~ 0–500 AD

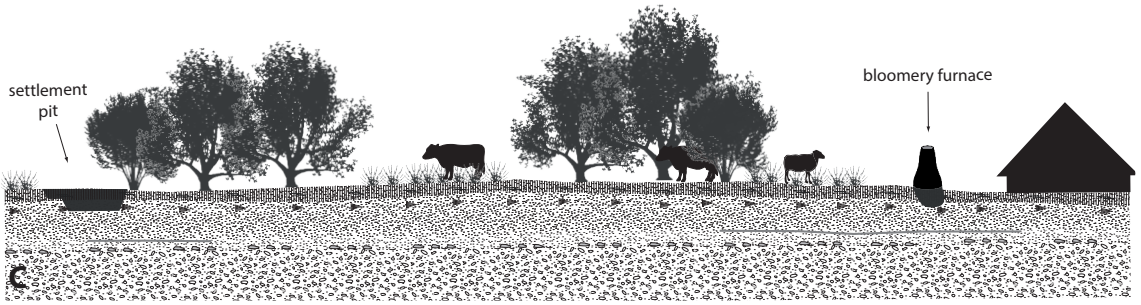

~ 500–700 AD

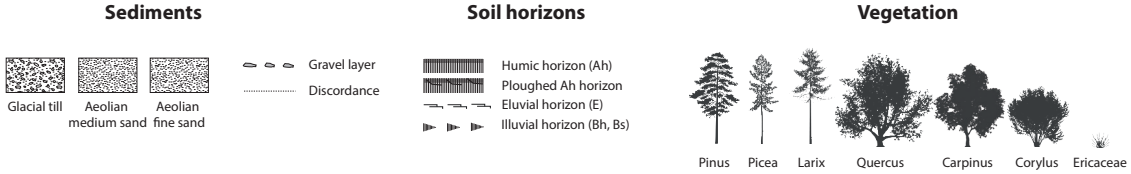

Figure 6.9: Idealized landscape evolution model for KHD area

Phase 3: Early Medieval Times (~ 700–1000 AD)

~ 700–800 AD

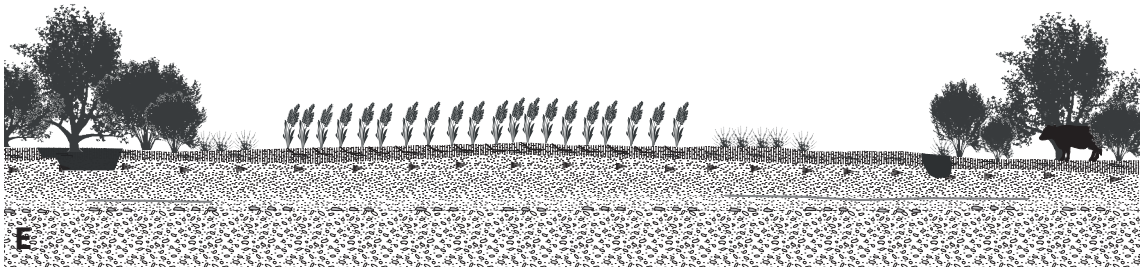

~ 800–1000 AD

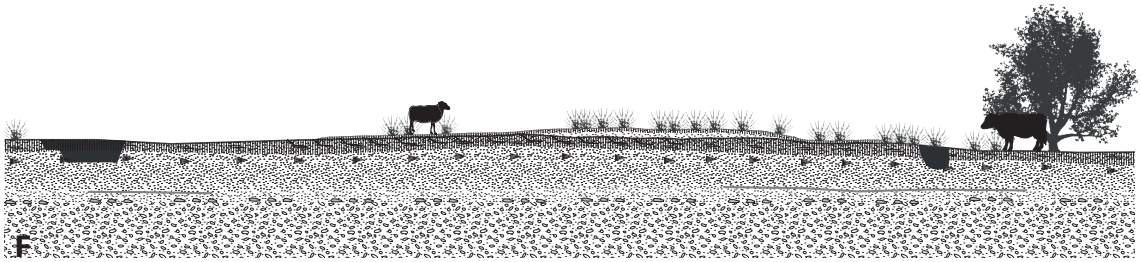

Phase 4: High- to Late Medieval Times (~1000–1500 AD)

~ 1000–1300 AD

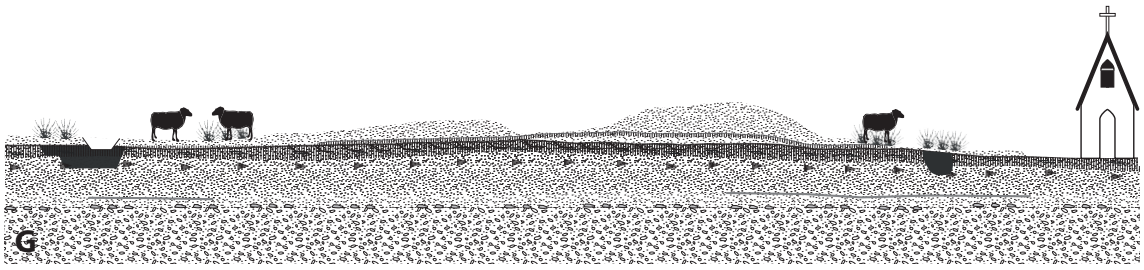

~ 1300–1500 AD

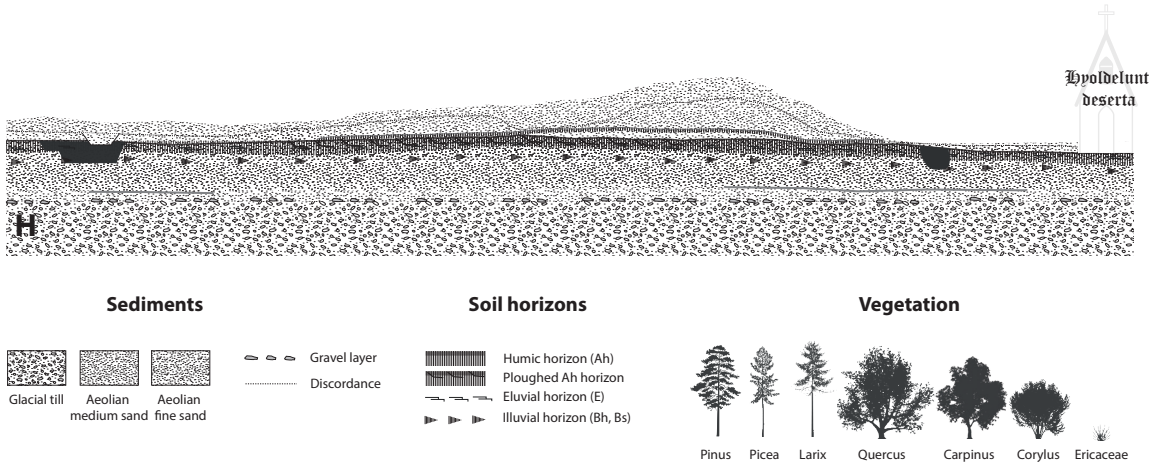

Figure 6.9 - continuation: Idealized landscape evolution model for KHD area

Phase 5: Modern Times (~ 1500 AD–present)

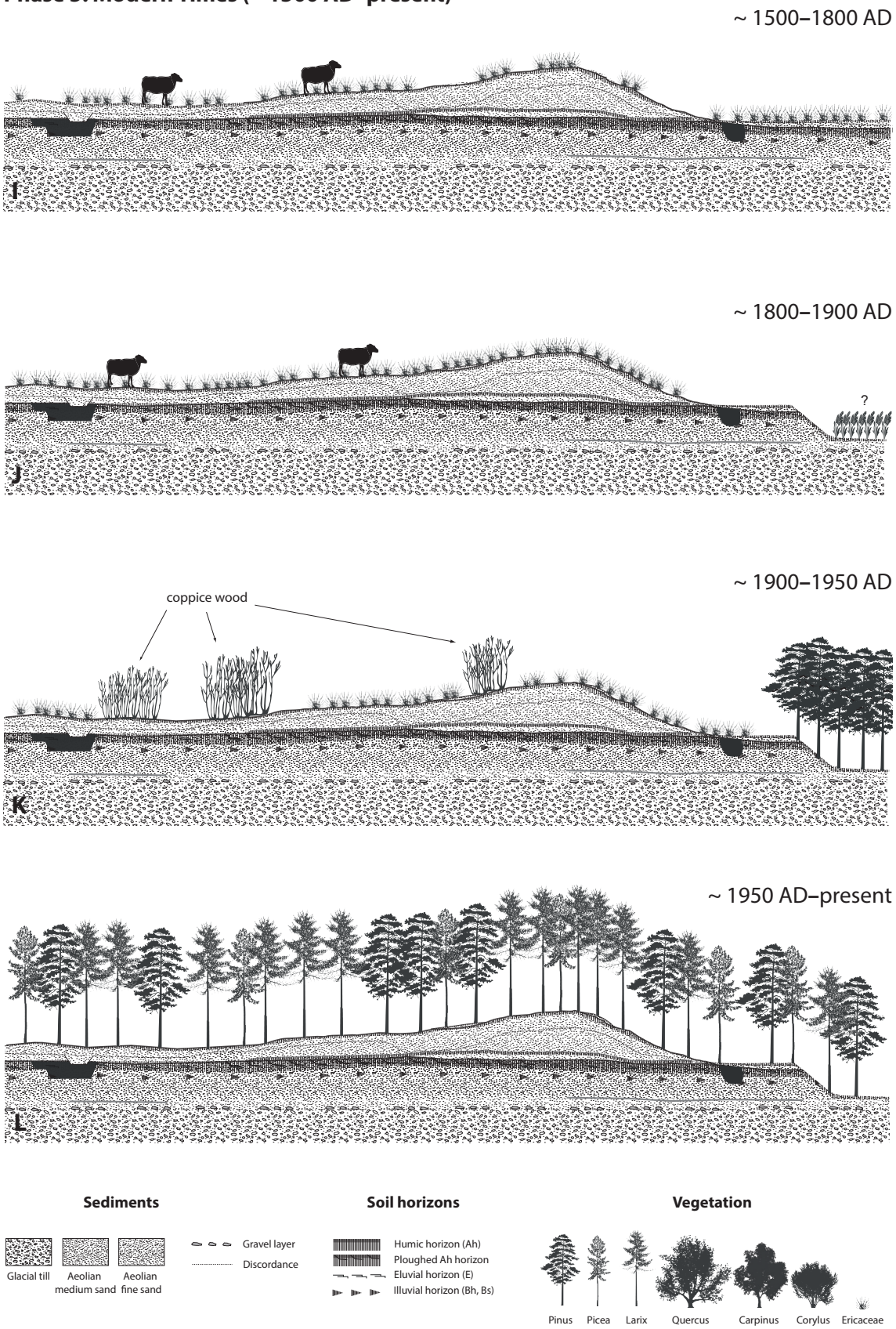

Figure 6.9 - continuation: Idealized landscape evolution model for KHD area

estimated to be several thousand years (Jatho 1969, Backer et al. 1992, Müller 1999, 2000, Mauz et al. 2005). The high values of pedogenic iron content and activity ratio in the buried illuvial horizons (Bhb/Bmsb) found in the KHD Podzols result from the inhibition of sesquioxide crystallization by OM (Blume and Schwertmann 1969, Cornell and Schwertmann 2003), which can be attributed to a comparably long time of formation (Sauer et al. 2007). Although settlement traces date back to Bronze Age in the Joldelund region (Jöns 1997), there is no evidence for Bronze Age aeolian activities in our record. This is consistent with a study by Richter (1965) who dated charcoal from the surface of the buried Podzol closed to KHD to 358 cal. BC–70 cal. AD (Jol 2, Table 6.2), which indicates a phase of surface stability to at least the Early Iron Age.

6.5.1.2 Roman Iron Age to Migration period (~ 0–700 AD)

We found several signs for Roman Iron Age (~ 0–500 AD) settlement activity and iron ore production within our excavations at KHD. An old slag pit (profile 6), very likely belonging to an iron smelting furnace (bloomery furnace), typical for Iron Ages iron production (Jöns 1992), was dug into the Podzol and underlying sands (Figure 6.9C). This finding supports our interpretation of a surface stability phase from the early Holocene to the Roman Iron Age. Additional evidence for a Roman Iron Age occupation of the surface of unit 2 deposits (Section 6.4.2.2) comes from numerous slag pieces distributed over this surface (P1VS5, Figure 6.5). Our finding of settlement activity during the Roman Iron Ages in the area is supported by earlier archaeological studies, which had already found remains of iron ore production and human settlement activity during the Roman Iron Age Period in the wider area (Jöns 1997) (Figure 6.9C). A more detailed archaeological excavation (~ 300 m from KHD) has established a main Roman Iron Age settlement phase at Joldelund, associated iron smelting and processing, charcoal production, and crop and livestock farming from ~ 300–450 AD (Erlenkeuser et al. 1997).

Even though there is clear evidence for direct human impact in the research area, there is only evidence for minor aeolian activity at the KHD during the Roman Iron age. However, disturbance of the Podzol in Medieval Times could have had the potential to destroy records of small drift sand layers. In combination with evidence indicating aeolian deposition of several, thin sand layers intercalated with peat in a small mire ~ 0.7 km away (Dörfler 2000, Figure 1d), we interpret the land-use to be patchy during Roman Iron Age, which prevented larger scale aeolian activity. This is also supported by palynological evidence and analysis of wood species from charcoal fragments (from the archaeological site), which shows changes in woodland composition at this time and evidence for agricultural land-use in the direct vicinity of the settlement, but not to the extent expected from large scale deforestation (Dörfler 2000, Dörfler and Wiethold 2000). We find no evidence for aeolian activity between ~ 450 AD until the Early Medieval Times (~ 700–1000 AD), which in combination with an increase in aboreal pollen and a decrease in plantation pollen

(Erlenkeuser et al. 1997, Dörfler 2000, Nelle and Dörfler 2008), we interpret as reflecting human abandonment and reforestation of the area (Figure 9F). This finding is in accordance with a general decrease in settlement activities throughout NW Germany at this time, which lasted from the 5th to the 7th century AD (Hamerow 2002, Dörfler 2003, Nelle and Dörfler 2008).

6.5.1.3 Phase 3: Early Medieval Times (~ 700–1000 AD)

Within the early Medieval Period, human impact becomes more evident within our record in several ways (Figure 6.9E–F). First, a horizon of clear plough marks (unit 2-p), which turns over the mature Holocene Podzol, indicates a single attempt to use the KHD area for cropping agriculture (Figure 6.9E), after which this effort was abandoned and heath covered the area again (Jansen et al. 2013) which helped develop a thin humic horizon (3Ab horizon, Figure 6.4). Earlier studies have interpreted the plough marks to be of Iron Age, as Radiocarbon Ages from the overturned soil yielded ages from this period (358 cal. BC–70 cal. AD (Jol 2, H 1907-1334, and Table 6.2) (Richter 1965). In this study, we also dated the same overturned black soil and obtained a similar result (395–536 cal. AD, KIA39156; 111 cal. BC–51 cal. AD, KIA37877, and Table 6.2). However, we argue these ages do not give evidence for the time of ploughing, but rather of the Roman Iron Age occupation of the soil surface, that is itself being ploughed. Instead, we suggest that the thin sedimentary layer (unit 3) on top of the initially formed A horizon is likely to be the result of a local sand drift caused, firstly, by ploughing activity in the vicinity of KHD and secondly by burning of heathland, which is evident by the presence of the large amount of charcoal particles the initial A horizon (777–979 cal. AD, KIA3836; 777–986 cal. AD, KIA38360; 775–964 cal. AD, KIA37876). Therefore the ploughing would have occurred much later at around ~ 800 AD (Figure 6.9F). This thin sand layer is the first evidence for human destabilisation of the KHD, which was then again stabilised by the regrowth of heathland vegetation, as suggested by the wood charcoal analysis (Jansen et al. 2013), and a subsequent humic A horizon (2Ahb horizon in figure 4) which was dated to the very beginning of the Early Medieval (667–800 cal. AD, KIA41023; 474–646 cal. AD, KIA37875).

When combined with a the pollen and radiographic analysis of mire only 0.7 km away (Dörfler 2000) which does not show any evidence for drift sands before ~ 1100 AD, we are confident in suggesting that there was no major phase of aeolian activity prior to High Medieval Times. This is also supported by another regional pollen record which indicates some deforestation and agricultural activity in early Medieval Times in the area, and which progressively increased into High Medieval Times (Dörfler 1992, Dörfler 2000). This relative stability of the land surface and minor aeolian activity in Early Medieval Times can also be found throughout Northern Europe, and stresses the potential of KHD as important sedimentary archive (Pyritz 1972, Castel 1991, Koster et al. 1993, Alisch 1995, *Müller* 1999, Mauz et al. 2005, Hilgers 2007).

6.5.1.4 Phase 4: High- to Late Medieval Period (~ 1000–1500 AD)

The largest sediment accumulation and re-activation at the KHD took place between ~ 1000 AD and 1500 AD (High to Late Medieval Times), and represents the most significant phase of aeolian activity within the Holocene deposits. We observe two main depositional layers, which we interpret as two distinct depositional phases: firstly a High Medieval sand layer deposited ~ 1200 AD (996–1154 cal. AD, KIA39154; 1032–1162 cal. AD, KIA45183; 1040–1209 cal. AD, KIA45184; 1036–1157 cal. AD, KIA40621; 1164–1324 AD; OSZ628) (Figure 6.9G), and secondly a Late Medieval sand layer formed ~ 1400 AD (1234–1444 AD, OSZ489; 1314–1464 AD, OSZ490; 1319–1489 AD, OSZ491; 1429–1569 AD, OSZ627) (Figure 6.9H). Both of which were likely deposited relatively rapidly (< 800 years for ~ 45 % of the total sediment; Section 6.4.3). We interpret this aeolian activity to be the result of widespread deforestation, melioration processes, land-use change, and general soil degradation in the area. Human occupation is also testified to by three hand-dug ditches of unknown use found in the Medieval deposits (1283–1631 cal. AD, KIA40624), and the existence of many (at least 10) charcoal layers alternating with sand layers within the High Medieval deposits (~ 1200 AD, Figure 6.7). These charcoal layers suggest burning as a part of cultivation techniques in the area surrounding the KHD, and their very low inclination (~ 0–2°) also suggests relatively constant wind conditions, which would exclude changing climatic conditions with an associated increase in wind velocities as a cause for the observed dune re-activation. A vast and rapid expansion of land-use in the area is also observed within the pollen record of MUD at this time (~ 800 years ago), and supports our interpretation that settlement and land-use expansion caused the largest re-activation and sediment accumulation of the KHD dune complex in the Holocene. The observed magnitude and timing of dune-reactivation has also been found within chrono-stratigraphical studies in other regions in the northern European Sand Belt (ESB), and where the cause is also attributed to land-use change, including grazing, removal of heath sods (»plaggen« and burning cultivation (Schirmer 1999, Koster 2005, Mauz et al. 2005, Hilgers 2007, Tolksdorf and Kaiser 2012). A phase of High–Late Medieval land degradation is also observed in many other areas of central Europe, where deforestation lead to a reduction of woodlands from ~ 94 % to ~ 15 % within the period between 650 AD and 1310 AD (Bork et al. 1998), and has been attributed to the enhancement of hillslope erosion, gully incision and floodplain accumulation (Dotterweich 2008, Larsen et al. 2013, Larsen et al. in press).

6.5.1.5 Phase 5: Modern Times (~ 1500 AD–present)

From ~ 1500 AD until ~ 1630 AD, only very minor and spatially discontinuous deposition in the center of the research area is observed in the KHD sedimentary record (unit 6 in exposure P1 VS 5 and P2 VS 4 only) (Figure 6.5, Figure 6.9I). Dune stability until present time is evident from the development of an Arenosol (with the

tendency to podzolization) within the uppermost layer of the dune sediments that were deposited mostly in late Medieval Times (unit 5, Figure 6.5). We interpret this comparably small aeolian activity in the past 500 years at the KHD, which is also found in the nearby pollen record of HOE (Figure 6.2b), to be the result of extensive implementation of new land management practices, dominated by the widespread regrowth of heathland, as documented in the KHD dune itself, the wider area (Dörfler 2000), throughout the region (Hase 1961), and the entire ESB (Schnepel 1981). Historical sources from the area report that the heathland supported sheep pasture, including the production of honey (bee farming) (Schnepel 1981, Figure 6.9J). Other studies investigating the origin of the expansion of early modern heathland in Northern Europe have also argued for a disturbance-induced heathland formation (Webb 1998), but the processes involved in this remain under debate. It is clear from the ubiquitous finding of charcoal fragments that fire must have been a factor, but forest clear-cutting, followed by cattle and sheep grazing, and additional use of the remaining woody vegetation for fuel (charcoal production), and for winter fodder (Pape 1970, Nielsen 1970, Behre 1995, Mallik 1995, Pott 1998, Behre 2000b) would have all played a role. Other studies have argued for widespread slash-and-burn agriculture, and cutting of sod from the heath (plaggen), which also promoted wind erosion (Behre 2000b, Bach 2008). In the study area, the HOE record shows a recovery in the remaining woodland patches within the period ~ 1400–1520 AD and an increase in Calluna-heathland from ~ 1250 AD (Figure 6.2). These findings seem to support the relative geomorphic stability of the KHD area in the transition of Late Medieval to Modern Times. However, the degree of surface stability in the research area remains surprising especially because i) spatial analysis of historic maps from A.D. 1878 (Figure 6.9J) shows the location of an agricultural field in the south-west of the research area, whose boundaries correlate with a sharp erosional hiatus found along south-eastern part of the KHD (Figure 9J), and could promote wind erosion, and ii) many studies on Holocene aeolian deposits in the Northern ESB shows a final surface destabilization attributed to increased cropping cultivation during 18th and 19th century (Pyritz 1972, Koster et al. 1993, Mauz et al. 2005, Hilgers 2007, Tolksdorf and Kaiser 2012), which continued into the early 20th century because of a high demand for food production related to the World Wars (Nielsen 1970, Richter 1965, Duttmann et al. 2004). At this time, increasing areas of former heathlands were modified into agricultural fields with the introduction of modern machinery in farming (steam ploughs) and the use of mineral fertilizer (Dierssen 2004). This is also true for the research area and surroundings, where analysis of topographic maps from 1921 and 1944 shows that heathland was converted into arable land and the peatland was drained for use as grassland (Dörfler 2000, Duttmann et al. 2004, Bach 2008). As a consequence severe wind erosion is repeatedly recorded in nearby settlements and villages at the end of the 1930s (Schultz 1978), and again at the end of the 1940s (Nielsen 1970). As a result, the first modern land-management measures to prevent aeolian activity were taken in the 1930s,

with re-forestation targeted within areas especially vulnerable to wind erosion. This re-forestation program included the KHD area, which explains the absence of new sediment deposition from this time period of otherwise widespread dune re-activation (Figure 6.9K). Aeolian activity ceased in the region from the 1940s with increasingly comprehensive land management strategies, including systematic afforestation of heathland and inland dunes, and the planting of hedge rows (»knicks«) to increase surface roughness between fields (Figure 6.9L).

6.5.2 The quantification of Holocene aeolian activity and past landscape change

The first phase of sediment deposition recorded in the KHD complex, spanning a time period between the Older Dryas up to the Preboreal (Section 6.5.1.1), represents ~ 4800 years of vegetation retardation in the region (Nelle and Dörfler 2008). This phase accounts for the largest sediment mass in the record (9.96 ± 0.54 kt) of the total Late Quaternary sediment deposition (~ 55 %), and yet was deposited at a relatively slow rate of 1.48 ± 0.05 $tha^{-1}a^{-1}$ (Figure 6.10). The ~ 5000–6000 years' time period up until the Roman Iron Age, which constitutes much of the Holocene, is characterized by a relatively stable surface, with no aeolian activity recorded in the research area, and only very minor (< 1 cm) sand drift recorded in the adjacent MUD site (MUD 1 and MUD 2 in Figure 2a). The observed surface stability during this time is due to a dense vegetation cover, and if human land-use did exist, it was likely only patchy throughout the Holocene until ~ 380 AD (MUD 1–MUD 2 in Figure 6.2a, and HOE 1–8, in Figure 6.2b). This long period surface stability has also been found throughout the ESB (Müller 1999, Schirmer 1999, Koster 2005).

Settlement and iron smelting activities during Roman Iron Age caused some disturbance of the vegetation (MUD 3 in Figure 2a, HOE 7 in Figure 6.2b), which resulted in local, and small scale re-activation of cover sands reflected in a patchy deposition of thin sand layers in the vicinity of KHD area (MUD 3 in Figure 6.2a). Although evidence of this small scale surface instability in the sediments of the KHD has likely been destroyed through subsequent human activity, in order to accommodate the potential surface instability during this time period within our calculations, we quantified the sediment mass of the ploughed soil horizon as a rough (and likely overestimated) measure. The significance of such an overestimate is negligible given the sediment deposited in this phase amounts to only 0.18 ± 0.02 kt, or < 1 % of the total net sediment mass, which translates into the lowest deposition rate (0.12 ± 0.02 t ha^{-1} a^{-1}) (Figure 6.10) found in this study. This very limited geomorphic activity during the Roman Iron Age which is quickly stabilized by settlement abandonment during the Migration Period as indicated by a complete recovery of the vegetation to pre-Roman Iron Age levels (MUD 4 in Figure 2a, HOE 8 in Figure 2b) and re-stabilization of the dune surface.

In early Medieval Times minor aeolian activity is recorded at around ~ 800 AD, which lies with 0.24 ± 0.11 kt within the error range of the Roman Iron Age aeolian activity, and also constitutes less than

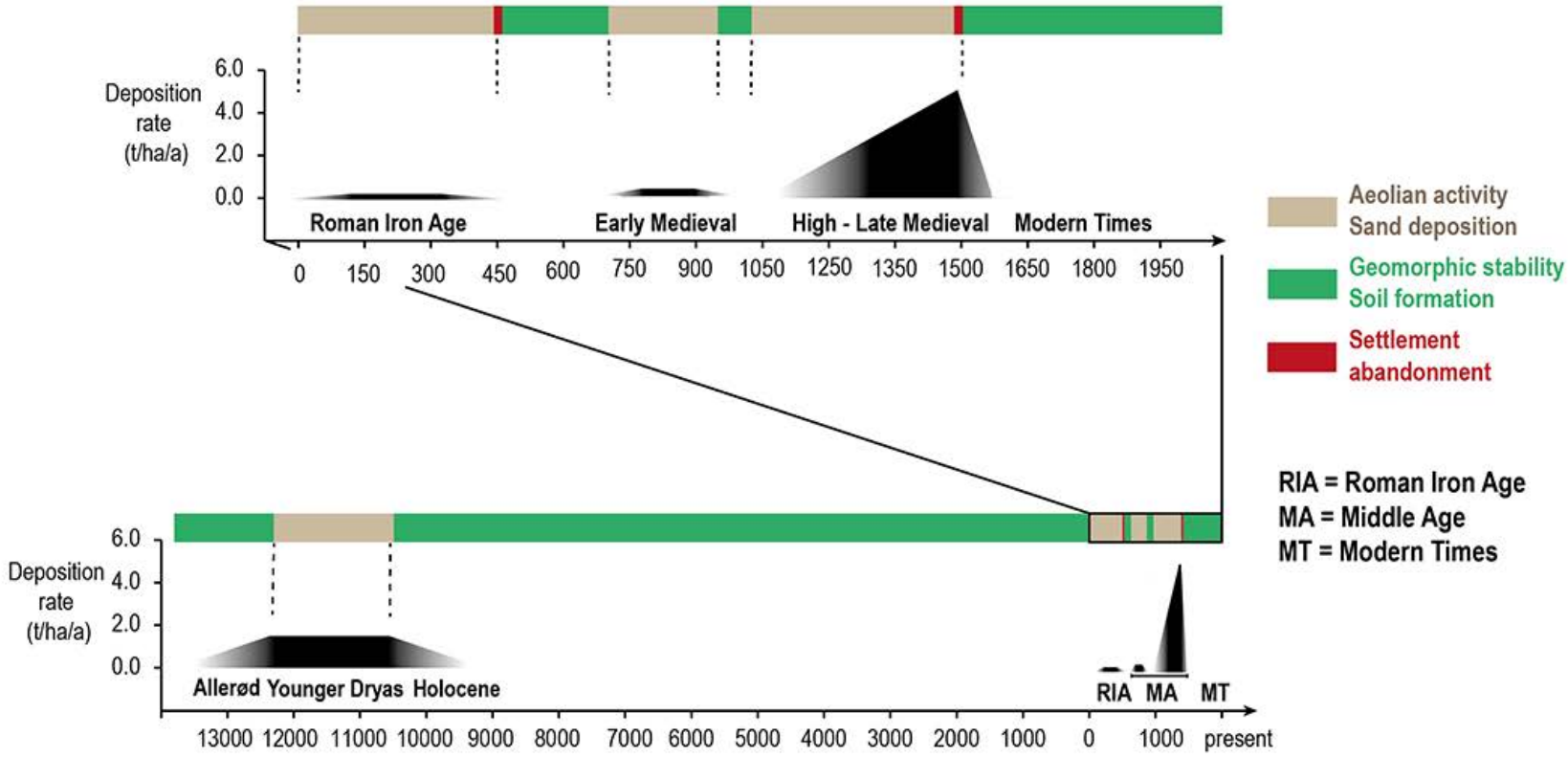

Figure 6.10: Phases of Aeolian activity, geomorphic stability (soil formation) as well as settlement abandonment in the study area. For quantified deposition rates also see Table 6.4.

1 % of the total net mass. During this time period, the KHD was influenced by minor human impact through a single ploughing event, and is immediately followed by minor deposition with a rate of 0.32 ± 0.15 t $ha^{-1}a^{-1}$, which is twice as fast as during the Roman Iron Age (Figure 6.10).

High Medieval Times are characterized by significant deforestation and settlement activity (Section 6.5.1.4). The response of the dune systems is reflected in a one order of magnitude increase in deposition rate (3.05 ± 0.61 t $ha^{-1}a^{-1}$, Figure 6.10), which is the largest change in deposition rate found in this study. In combination with the pollen record showing the largest deforestation activity recorded before the 19th century (MUD 6 in Figure 6.2a, HOE 10 in Figure 6.2b), we interpret this to be the phase of most rapid landscape change, and it accounts for ~ 35 % (2.87 ± 0.57 kt) of the net Medieval deposition. Deposition rates continue to rise with increasing land-use change up to 5.02 ± 0.55 t $ha^{-1}a^{-1}$ in Late Medieval Times and sediments in this phase account for 4.88 ± 0.54 kt deposited during this period, which is ~ 60 % of the medieval mass and nearly one third of the total. This constitutes the largest depositional phase and the highest geomorphic activity found in this study. At the same time, the adjacent mire MUD is covered by a thick layer or drift sand (Figure 6.2a), which supports our interpretation of widespread aeolian activity during this time period. With the onset of the modern time period, the surface of the KHD is stabilized, and no net deposition is recorded.

6.5.3 Medieval land degradation leads to settlement abandonment

Aeolian dune accumulation rates first rise slowly in early Medieval Times (from 0 to 0.32 ± 0.15 t $ha^{-1}a^{-1}$), and then continue to rise until Late Medieval Times (up to 5.02 ± 0.55 t $ha^{-1}a^{-1}$), with the fastest increase in the transition between Early and High Medieval Times (from 0.32 ± 0.15 t $ha^{-1}a^{-1}$ to 3.05 ± 0.61 t $ha^{-1}a^{-1}$). It is interesting to note however, that the end of the medieval deposition phase is surprisingly abrupt. In combination with a sudden phase of vegetation recovery after ~ 1400 AD (HOE 11 in Figure 6.2b) and onset of soil formation in the deposits of the KHD, we interpret this as evidence of a sudden, Late Medieval abandonment of the area, which coincides with the simultaneous abandonment of the nearby village Hyoldelunt (Hinz 1949, Richter 1965) (Figure 6.9H), and large economic losses in the area (Mager 1930). An increase in the amount of arable land through deforestation also reduced surface roughness thus accelerating soil erosion and deposition of widespread drift sand deposits. Our results indicate that this abrupt abandonment of the village and its surrounding area was caused by the initial Medieval intensification of farming and overgrazing which resulting in widespread landscape degradation. Similar responses to medieval land-use changes and wind erosion processes are reported for other areas in Schleswig-Holstein, e.g. from the Medieval settlement Süderlügum, ~ 30 km northwest to the study area, which was destroyed by drift sands around ~ 1550 AD (Andresen 1924, Mager 1930). We therefore argue, that Medieval landscape degradation is – at least in landscapes easily

destabilized by deforestation – an important, if not the dominant factor leading to a widespread settlement abandonment in Late Medieval Times. This is in accordance with findings from Northern Belgium and Northern Germany, indicating Medieval settlement abandonment due to extensive sand-drifting (Andresen 1924, Nielsen 1970, Derese et al. 2010). These findings reduce the need to invoke socio-economic changes favored in the prevailing hypothesis, that in some cases in combination with environmental and climate change (Kaiser et al. 2002, Küster et al. 2014) has led to a phase of settlement abandonment in the late 14th century. Given the timescale over which the settlements expanded following initial landscape changes, it is also likely that any recorded socio-economic changes were themselves in large part a response to increasingly dire wind erosion and soil degradation conditions.

6.6 Conclusion

In this study, we have quantified the large influence of Medieval settlement expansion on an inland dune complex in the ESB. The combination of detailed chrono-stratigraphy, a geospatial model, and pollen records showed that deforestation and intensification of agriculture lead to destabilization of the soil surface, increasing local wind speeds and aeolian activity. We can clearly identify four phases of aeolian sedimentation, and each with increasing magnitude, to historical settlement and land-use. Human activities during Roman Iron Age Period (0–500 AD) had only low impacts on the landscape, and provided the lowest deposition rate (0.12 ± 0.02 t ha^{-1} a^{-1}). Since the ~ 700 AD Medieval deforestation and overexploitation of the land resulted in rapid dune-building and the highest aeolian accumulation rates in the KHD record since the deposition of aeolian sands began during the Late Pleistocene. We demonstrate that phases of aeolian deposition and their rate of deposition match closely the results of pollen records in the area. This highlights that, in addition to pollen records, inland dunes may provide important, complementary archives for identifying landscape system thresholds and quantifying the effects of land degradation. We also show that late Medieval settlement abandonment is coincident with an abrupt cessation of dune sedimentation, following the largest phase of dune re-activation found in the record. Hence, we argue that unsustainable land-use in Medieval Times has led to increased aeolian activity, which caused soil degradation and finally the abandonment of the village and adjacent farmland. The observed feedback structures of human-environmental interactions appear cyclical: Due to poor land-use management in historic and recent times severe drifting of sand and the accumulation of dunes occurred, forcing field and settlement abandonment, and finally, after a phase of recovery, adaptation through the use of suitable land management practices (extensive grazing, afforestation). Our results have implications for other studies on aeolian sedimentation throughout the ESB, suggesting a larger importance for Medieval land degradation for the widely observed phase of Medieval settlement abandonment than previously thought.

7

Wood charcoal from an inland dune complex at Joldelund (Northern Germany). Information on Holocene vegetation and landscape changes

(published in: *Quaternary International*)

7.1 Introduction

Pedoanthracology, i.e. the analysis of wood charcoal from soils and sediments of Holocene and Pleistocene formation is a powerful tool for the reconstruction of the occurrence of woody species in time and space (Carcaillet and Thinon 1996, Carcaillet et al. 2006, Haesaerts et al. 2010). While the analysis of archaeological charcoal, also called archaeo-anthracology (Vernet 2002) has a long history, the investigation of charred wood remains in soils and sediments became increasingly important in the last 30 years with the development of pedoanthracology or geoanthracology (Vernet 2002). To date, many studies have used charcoal from soil profiles to reconstruct fire and vegetation history (e.g. Talon 2010, Poschlod and Baumann 2010, Robin et al. 2011). However, there is relatively little scientific literature where charcoal from sand sediments were analysed taxonomically, especially from dunes (Keit and Mothes 1942). Thus, the application of charcoal analysis as part of dune investigations is not yet developed, although charcoal layers were mentioned in publications on dune development (Seppälä 1995, Schlaak 1999), and charcoals are routinely used for radiocarbon dating of layers within profiles (Seppälä 1995, Kowalkowski et al. 1999, Schirmer 1999, Loope and Arbogast 2000, Ivester and Leigh 2003). The usages of bulk samples from dunes are even more difficult because further factors as incorrect calculation due to the hard water effect have to be considered. These may cause large dating errors up to several thousand years (Yang and Scuderi 2010, Yang et al. 2011), which means that charcoals are essential to date the dune history if their origins can be identified. Occasionally, microscopic charcoal is quantified in combination with pollen studies in the framework of dune research (De la Vaga Leinert et al. 2000, Franco-Mugica et al. 2005).

As a part of a project which addresses the Late Holocene aeolian activity triggered by human and their impact on the landscape and dune development in Northern Germany (PhD project of U. Lungershausen), large profiles in an inland dune complex near to Joldelund were examined. An exceptional number of black, charcoal-rich layers were observed in these dune profiles and lead to further examination. Thus, samples were taken in order to quantify the content of charred plant material, as well as for performing taxo-

nomic analysis of wood charcoal. The goal of this work is to gain a better understanding of the processes of dune development, and to test the potential of aeolian sediments as archives of former occurrences of woody species.

This paper presents the first study that uses taxonomic information of dune charcoal, to (1) support geomorphological interpretation by anthracological correlation of the dune profiles, and (2) gain local, small-scale information of past vegetation composition, which is previously only known from pollen analysis on a less detailed spatial resolution in the area (Dörfler 2000). Given the widespread distribution of coastal and inland dune systems within the European Sand Belt (Koster 2005), not to speak globally (e.g. Yang et al. 2012), it is necessary to figure out the possibilities of using charcoal research in this geological context. Which species can be found in the dune sediments? Is it possible to locate the origins of charcoal, and thus the potential provenance of the dune sand? Did the vegetation cover change during the course of dune accumulation? Can taxonomic charcoal assemblages support the sedimentological / geomorphological interpretation and interconnection of several neighboring profiles?

7.2 Study area

7.2.1 Present situation

The Kuhharder Hill is a small inland dune complex covering an area of approximately 2 ha southwest of Joldelund, North Frisia, Germany (54° 38‘ 45“ N, 9° 7‘ 14“ E). The area is located in the Weichselian outwash plain of northern Europe and consists mainly of glaciofluvial sands, periglacial reworked Saalian moraines, and aeolian and organogenic sediments (Figure 7.1). The Kuhharder Hill dunes form the westernmost part of an 80 ha large inland dune field which in turn covers an old Saalian moraine. The research area has a height of approximately 30 m asl. The region´s cover sand and inland dunes were formed predominantly during the Older and Younger Dryas (Müller 1999, Müller 2000, Koster 2005, Mauz et al. 2005). Remobilization of these aeolian sediments was triggered during the Holocene by human activities, such as intensive deforestation, agricultural land-use and timber production.

The climate is temperate oceanic, with about 8 °C mean annual temperature and around 800 mm mean annual precipitation (climatological data of the station Leck for the period 1975–2002, obtained from the German Weather Service, DWD). The soils are particularly prone to erosion. Sandy light soils (podzols) with a high proportion of fine to medium sand are dominant in aeolian sediments (Duttmann et al. 2004). In lower elevations predominantly gleys have developed under the influence of groundwater.

The natural vegetation of the area on minerogenic sites would be composed of oak-beech forests (*Fagus sylvatica, Quercus robur*, *Q. petraea*) with *Lonicera periclymenum, Deschampsia flexuosa, Vaccinium myrtillus* and *Ilex aquifolium*. On sites close to the groundwater table, atlantic-subatlantic birch-pedunculate oak

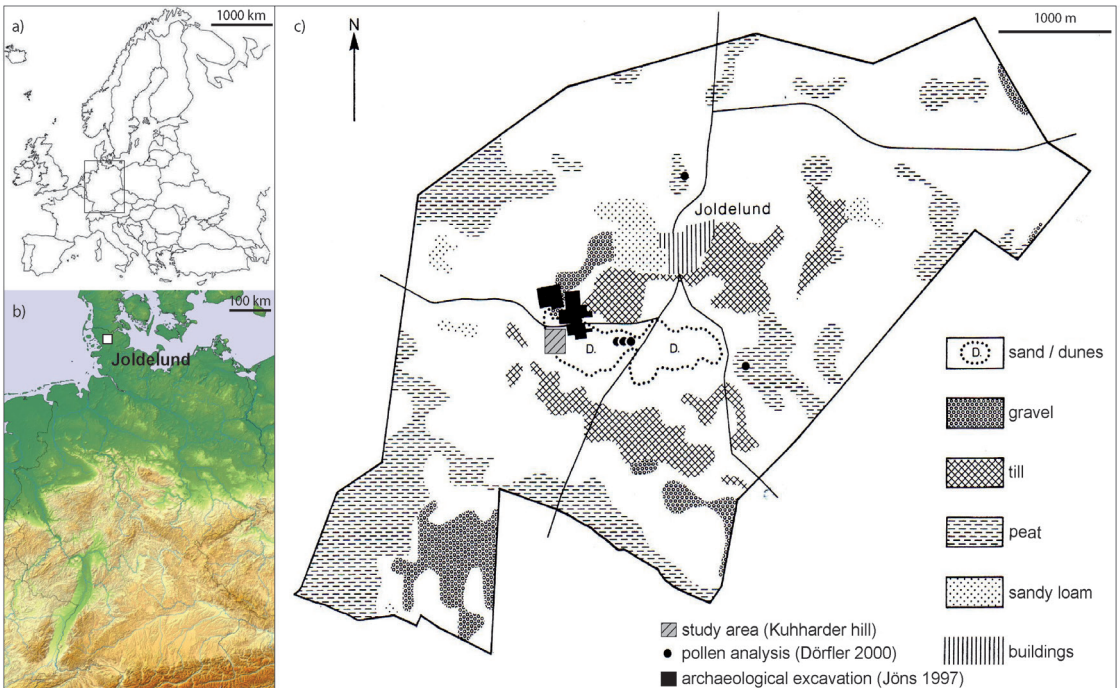

Figure 7.1: Study area. (a) overview; (b) localisation of the study area in Central Europe; (c) geological situation within municipal boundaries of Joldelund (Schleswig-Holstein), 1: Hörrmoos, 2: »Mire covered by dunes« (from Dörfler 2000, modified).

forests (*Quercus robur*, *Betula pubescens*) with *Frangula alnus*, *Molinia caerulea*, and partly *Myrica gale* and *Carex nigra* (Bundesamt für Naturschutz 2000) would prevail in a mosaic with alder-pedunculate oak forests on minerotrophic peatlands (Dierssen 2004).

In the 1950s, the inland dune field was afforested mainly with spruce (*Picea abies*, *Picea sitchensis*, *Picea glauca*), pine (*Pinus sylvestris*, *Pinus nigra*, *Pinus mugo)* and larch (*Larix kaempferi*) (Nielsen 1970). The adjacent areas are nowadays used as pastures and meadows for dairy farming and corn production for the extraction of biogas.

7.2.2 Previous studies

During the afforestation in the 1950s, several archaeological sites were discovered, the basis for further archaeological investigations at the end of the 20th century (Figure 7.1). Special emphasis was placed on botanical and anthracological analysis of iron ore production sites (Dörfler 2000, Dörfler and Wiethold 2000). Settlement activities and iron ore production are dated to the 4th and 5th century AD. At that time, changes in landscape and vegetation are considered to be remarkable, albeit the local effect solely resulted in moderate sand drifts.

Intensive deforestation and agricultural land-use during Medieval Times led to

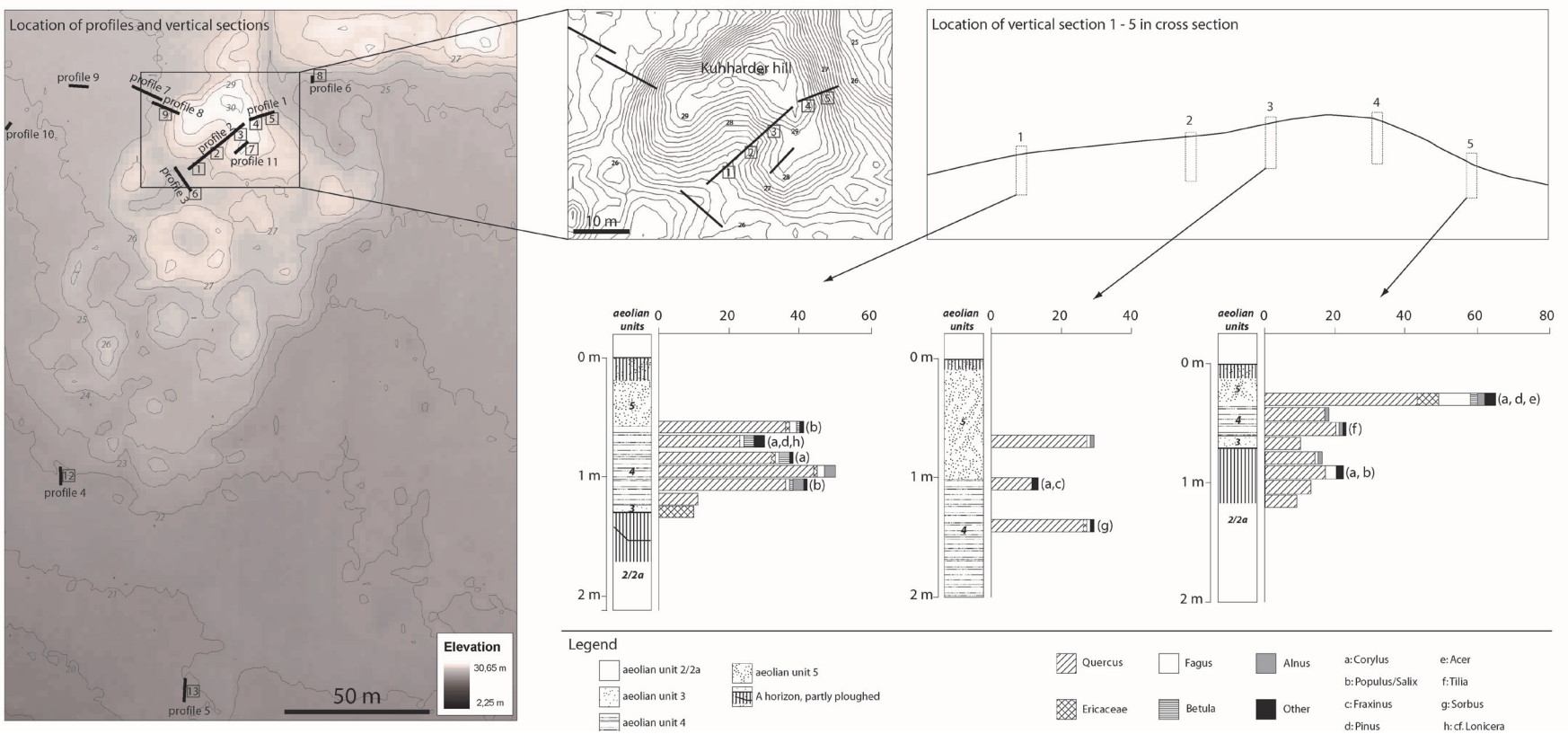

Figure 7.2: Left side: localisation of the profiles and vertical section on the dune complex with detail of the Kuhharder Hill; right side: Simplified cross-section of Kuhharder Hill dune (profiles 1 and 2) with vertical sections (1-5). Assemblages of charcoal samples of section 1, 3 and 5 is exemplarily depicted. Numbers of taxa-identified charcoal per sample are given

at least three phases of dune development, and considerable changes in the morphology of the dunes. The Medieval dune development was interrupted by at least two periods of stability and soil development, which are preserved as humic horizons. Pollen analyses of an adjacent buried peat bog (Dörfler 2000, »mire covered by dunes«, Figure 7.1) coincide with the Kuhharder Hill dune record. Historical sources of the church register of Schleswig point out that in the 15th century AD, since more than 30 years, no tax payments were received from the Medieval village Joldelund (Richter 1965). Dramatic degradation of agricultural land due to wind erosion processes were recorded in the neighboring communities. Despite some local activities for prevention of wind erosion damages since the 16th century (Duttmann et al. 2004), a comprehensive protection program was not established before the end of the 19th century. Since 1950, the governmental-initiated »Programm Nord« promoted a systematic afforestation of wastelands and planting of hedge rows in the area. The wind erosion protection measures resulted in a relative morphological stability of the Kuhharder Hill for a period of 60 years. -Although the main periods of aeolian activity are known, estimations about the frequency of wind erosion events during these periods remain elusive. Thus, an interdisciplinary PhD-research project carried out by U. Lungershausen aims to reconstruct historical wind erosion and the development of the Kuhharder Hill dune complex in a high spatial and temporal resolution.

7.3 Methods

7.3.1 Field methods

Eleven profiles with up to 25 m in length and up to 2.5 m in depth were excavated at the study site on the area of ~2 ha. In the central part, seven profiles (Figure 7.2) were opened within a maximum distance of 50 m apart. Profile 1 and 2 constitute a cross-section of the Kuhharder Hill dune with 35 m in length and up to 2.3 m in depth. Four profiles are situated in a greater distance to Kuhharder Hill dune, the profiles 4 and 5 being the furthest away (~ 200 m). Each profile was documented with scaled drawings and photographs. Samples for pedological analyses such as grain size, bulk density, organic matter, pH-value and iron content were taken within vertical sections in eight profiles (Lungershausen et al. 2016, submitted). The basal Saalian moraine was reached in nine profiles by using a hollow auger, in order to determine the thickness of aeolian sedimentary record. Samples for charcoal analysis and radiocarbon dating were taken according to the given dune stratigraphy. Within the dune profiles numerous thin charcoal and humic layers were observed, intercalating with the aeolian deposits (Figure 7.3). These charcoal and humic layers were sampled for charcoal analysis in the vertical sections and in the immediate periphery. Samples were taken by filling material of 1000 g to 2000 g into plastic bags. In addition, approximately 150 auger corings were carried out to gather spatial data from the fossil dune surfaces, which allow the subsequent quantification of deposit volumes (Lungershausen et. al 2016, unpublished).

7.3.2 Dating methods

Radiocarbon dating of 15 charcoal samples were carried out by the Leibniz-Laboratory for Radiometric Dating and Isotope Research at Kiel University and ages were calibrated according to Reimer et al. (2009) using IntCal09. Aeolian sediments, with their embedded charcoal layer, provided the possibility of radiocarbon dating. However, the ^{14}C age of the charcoal indicates just the maximum age of the dated aeolian deposit. It is assumed that the fire event was closely related to the erosion event or took place in the immediate vicinity of the study site. At least two charcoal samples were dated in the respective aeolian sediment in order to ensure the reliability of the chronology. If ^{14}C ages differ widely within a single dune phase we suppose that the charcoal was reworked as a consequence of wind erosion. Prior to

Figure 7.3: (a) Profile 2 with at least eight charcoal-rich layers; (b) sieved charcoal sample; (c) detailed photo of sample, abrasion of charcoal pieces visible

the radiocarbon dating, the charcoal taxon was determined to avoid the old wood effect and the dating of modern conifers, i.e. *Picea*. Therefore, short-lived species such as Ericaceae, *Populus* / *Salix*, and *Betula* were preferred. *Fagus* was chosen to check the history of its immigration and dispersal which starts, according to the available pollen profiles, after ~400 AD (Dörfler 2000). *Pinus* was not used since it also occurs in modern plantations.

7.3.3 Charcoal analysis

For charcoal analysis 49 samples were taken from the charcoal and humic layers of the profiles 1–6, 8 and 11. The samples were dry-sieved (mesh 630 mm) in the laboratory. The taxonomic identification of the very small wood charcoal (1 to several millimetres, very rarely up to 1 cm) was carried out using a stereoscope with magnification up to x112 (Nikon SMZ 1500) and an incident-light microscope with magnification up to x500 (Nikon ME 600, light and dark field) following Schweingruber (1990a, b) and the reference collection of charred wood of the Palaeoecology Research Group of the Institute for Ecosystem Research, Kiel. The differentiation between *Quercus* and *Castanea* is often not possible due to the small size of fragments. *Castanea* is highly improbable since the study area is well away from the natural range of chestnut trees, and the climate is not suitable even for introduced individuals. Hence we added these charcoals to the *Quercus* values. Charcoal fragments were manually broken under the stereoscope (x7.5-10) to attain fractured surfaces of transversal, tangential

Table 7.1: Radiocarbon datings calibrated according to Reimer et al. (2009) using IntCal09. Abbreviations of matter type: C, Charcoal

Sampling site/ Profile	Lab. ref.	Matter	Taxon	Context	Depth (cm)	$\delta^{13}C$	Radiocarbon age (BP)	cal. BC/AD (2sigma)
Profile 5	KIA40624	C	Populus/ Salix	Ditch, aeolian unit 5	90	-31.41 ± 0.51	510 ± 90	1283–1631 cal. AD
Profile 2	KIA39157	C	Quercus	Aeolian unit 5	40	25.70 ± 0.15	365 ± 20	1452–1631 cal. AD
Profile 2	KIA40623	C	Quercus	Aeolian unit 5	80	-25.16 ± 0.15	1780 ± 20	140–332 cal. AD
Profile 2	KIA40620	C	Ericaceae	Aeolian unit 5	80	-26.32 ± 0.33	1620 ± 20	391–534 cal. AD
Profile 2	KIA45182	C	Fagus	Aeolian unit 5	100	-29.08 ± 0,08	965 ± 25	1018–1155 cal. AD
Profile 1	KIA39154	C	Fagus	Aeolian unit 4	70	-27.41 ± 0.20	980 ± 25	995–1154 cal. AD
Profile 2	KIA39155	C	Populus/ Salix	Aeolian unit 4	70	-28.54 ± 0.26	1595 ± 35	396–547 cal. AD
Profile 8	KIA45183	C	Fagus	Aeolian unit 4	80	-25.06 ± 0,17	925 ± 25	1029–1165 cal. AD

Profile 8	KIA45184	C	Fagus	Aeolian unit 4	140	-28.26 ± 0,12	900 ± 25	1041–1211 cal. AD
Profile 2	KIA40621	C	Populus/ Salix	Basis of aeolian unit 4	135	-26.00 ± 0.18	930 ± 20	1035–1158 cal. AD
Profile 2	KIA41023	C	Betula	Aeolian unit 3	200	-28.35 ± 0.12	1265 ± 25	668–809 cal. AD
Profile 3	KIA39156	C	Ericaceae	Aeolian unit 2a (ploughing mark	115	-22.59 ± 0.17	1610 ± 25	403–536 cal. AD
Profile 8	KIA38361	C	Ericaceae	Aeolian unit 2a	70-90	-25.83 ± 0.11	1140 ± 25	782–981 cal. AD
Profile 3	KIA38360	C	Ericaceae	Aeolian unit 2a	110-120	-26.83 ± 0.22	1135 ± 35	781–988 cal. AD
Profile 6	KIA40619	C	c.f. Alnus	Aeolian unit 1/2	110	-	10600± 500	11628–8946 cal. BC

and radial orientation. The identified fragments were weighed for each species to calculate percentage on the number and weight. A wood diameter measurement, which is possible when analysing larger charcoal fragments, on the basis of the visible growth ring curvatures in combination with the angles of wood rays (Nelle 2002, 2003, Ludemann et al. 2004), was not possible due to the small size of the charcoal. For each charcoal sample a minimum of 30 pieces were analysed, apart from a few samples which contained less than 30 pieces.

7.3.4 Pollen analysis

From an organic rich infill of a ditch / pit structure in profile 5 a vertical section with a special sample box (»Stechkasten«) was taken, which allows to cut out an undisturbed sediment bloc of 30 x 15 x 10 cm. From that, eight samples of 1 cm³ from the organic rich layers were taken for pollen analysis. The samples were treated according to standard procedure (Faegri and Iversen 1989), using potassium hydroxide to dissolve organic matter, fluoric acid to get rid of sand material, and acetolysis. Pollen and palynomorphs were counted with a Nikon Eclipse light microscope with x400 and x1000 magnification, up to 500 arboreal pollen grains per sample. Percentages are based on the total land pollen sum, including *Calluna*. *Alnus* was categorized as a wetland plant, and excluded from the calculation sum. Calculations and diagram was done with the software Tilia 1.7.14 (Eric Grimm 1999–2011).

7.4 Results

7.4.1 Summary of the geomorphological dune development

The stratigraphic sequence of the Kuhharder Hill dune complex reveals at least six phases of sand deposition, which are

Table 7.2: Results of charcoal analysis from dune context of Joldelund. n: number of charcoal; W: weight [g]; dec.: decidiuous wood; conif.: coniferous wood; id.: not determinable. In the column »other«, taxa with only one fragment per sample are mentioned. Analysis: Y. Dannath, D. Jansen, O. Nelle, V. Robin

	Vertical section	Aeolian unit	Quercus		Ericaceae		Fagus		Betula		Alnus		Corylus		Populus / Salix		Salix		Fraxinus		Pinus		other	indeterminata			sums		No. of taxa/
																								dec.	conif.	id.			
			n	W [g]	n	W [g]	n	W [g]	n	W [g]	n	W [g]	n	W [g]	n	W [g]	n	W [g]	n	W [g]	n	W [g]	Taxon: n=1 (W [g])	n	n	n	n	W [g]	sample
Profile 1	1	4/5	32	0.15	3	0.01	5	0.016	2	0.012	.	.	1	<0.001	.	.	.	.	.	.	.	.	.	2	.	.	45	0.198	5
	1	4/5	11	0.016	3	0.002	4	0.004	.	.	1	0.001	.	.	.	.	.	.	.	.	1	<0.001	Acer (0.003)	.	.	4	25	0.026	6
	1	4	20	0.033	.	.	1	<0.001	.	.	1	<0.001	.	.	.	.	.	.	.	.	.	.	Tilia (<0.001)	2	.	5	30	0.033	4
	1	4	10	--	.	.	.	.	.	.	.	.	.	.	.	.	.	.	.	.	.	.	.	1	.	4	15	0.006	1
	1	2	17	0.048		.	3	0.003	.	.	.	.	1	0.006	.	.	1	<0.001	.	.	.	.	.	.	.	3	25	0.068	4
	1	2	14	0.044	.	.	1	<0.001	.	.	1	0.005	.	.	.	.	.	.	.	.	.	.	.	2	.	.	18	0.054	3
	1	2	13	0.05	.	.	.	.	.	.	.	.	.	.	.	.	.	.	.	.	.	.	.	1	.	1	15	0.059	1
	1	2	9	0.009	.	.	.	.	.	.	.	.	.	.	.	.	.	.	.	.	.	.	.	3	.	.	12	0.010	1
	1; single finds	2, 3	12	0.098	.	.	.	.	.	.	.	.	.	.	.	.	.	.	.	.	.	.	.	.	.	.	12	0.098	1
	2	4	17	0.06	.	.	.	.	.	.	1	0.001	.	.	.	.	.	.	.	.	.	.	.	1	.	1	20	0.061	2
Profile 2	3	5	27	0.073	.	.	1	0.009	.	.	1	0.001	.	.	.	.	.	.	.	.	.	.	.	1	.	1	31	0.083	3
	3	4/5	13	0.044	.	.	.	.	.	.	.	.	1	<0.001	.	.	.	.	1	<0.001	.	.	.	2	.	3	20	0.044	3
	3	4	26	0.077	1	0.001	1	<0.001	.	.	.	.	.	.	.	.	.	.	.	.	.	.	Maloideae (0.004)	1	.	.	30	0.082	4
	3	5	2	--	.	.	.	.	.	.	.	.	.	.	.	.	.	.	.	.	.	.	.	.	.	.	2	--	1
	4	5	18	0.031	.	.	.	.	.	.	1	0.002	.	.	.	.	.	.	.	.	.	.	.	1	.	.	20	0.034	2
	4	5	28	0.228	2	0.001	.	.	.	.	.	.	.	.	.	.	.	.	.	.	.	.	.	.	.	.	30	0.229	2
	4	5	20	0.082	2	0.006	.	.	.	.	.	.	.	.	.	.	.	.	.	.	.	.	.	.	.	.	22	0.088	2
	4	5	31	0.124	.	.	.	.	.	.	.	.	.	.	.	.	.	.	.	.	.	.	.	.	.	.	31	0.124	1
	4	4	26	0.043	.	.	4	0.003	1	0.002	.	.	.	.	.	.	.	.	.	.	.	.	.	.	.	.	31	0.048	3
	4	3	16	0.029	1	--	.	.	4	0.005	.	.	.	.	.	.	.	.	2	0.003	.	.	.	.	.	2	25	0.038	4
	4	3	18	0.02	1	0.001	1	0.001	1	0.003	.	.	1	0.002	.	.	.	.	.	.	.	.	Tilia (0.001)	.	.	2	25	0.030	6
	5	4/5	36	0.21	1	0.009	2	0.015	1	0.01	.	.	.	.	1	0.013	.	.	.	.	.	.	.	.	.	.	41	0.257	5
	5	4	35	0.132	.	.	1	0.001	1	0.009	3	0.001	.	.	1	--	.	.	.	.	.	.	.	.	.	.	41	0.143	5
	5	4	44	0.217	1	<0.001	2	0.005	.	.	3	0.013	.	.	.	.	.	.	.	.	.	.	.	.	.	.	50	0.235	4
	5	4	32	0.077	1	--	1	0.001	3	0.009	.	.	1	0.001	.	.	.	.	.	.	.	.	.	.	.	2	40	0.092	5
	5	4	23	0.103	.	.	1	0.006	3	0.027	.	.	1	0.004	.	.	.	.	.	.	1	0.003	Lonicera (0.001)	.	.	.	30	0.144	6
	5	3/4	11	0.009	.	.	.	.	.	.	.	.	.	.	.	.	.	.	.	.	.	.	.	.	.	4	15	0.010	1
	5	3	.	.	10	0.009	.	.	.	.	.	.	.	.	.	.	.	.	.	.	.	.	.	.	.	.	10	0.009	1
Profile 3	6	4/5	24	0.054	1	0.003	2	0.001	1	<0.001	.	.	1	0.001	.	.	.	.	1	<0.001	.	.	.	.	.	.	30	0.059	6
	6	3	2	<0.001	.	.	1	<0.001	.	.	.	.	.	.	.	.	.	.	.	.	.	.	.	1	.	1	5	<0.001	2
	6	3	2	0.005	2	0.003	1	0.002	.	.	.	.	.	.	.	.	.	.	.	.	.	.	.	1	.	1	7	0.010	3
	6	2a	.	.	1	--	.	.	.	.	.	.	.	.	.	.	.	.	.	.	.	.	.	.	.	.	1	--	1
	6	2a	.	.	.	.	.	.	.	.	.	.	.	.	.	.	.	.	.	.	.	.	.	3	.	.	3	--	.
	6	2a	3	<0.001	114	0.362	.	.	.	.	.	.	.	.	.	.	.	.	.	.	.	.	.	2	.	1	120	0.365	2
	6	2a	.	.	78	0.371	.	.	.	.	.	.	.	.	.	.	.	.	.	.	.	.	.	.	.	.	78	0.371	1
P 4	12	3	8	0.013	5	0.01	.	.	.	.	.	.	.	.	.	.	.	.	.	.	.	.	.	3	.	4	20	0.023	2
	12	4/5	24	0.098	2	0.005	2	0.004	2	.	1	0.005	1	<0.001	.	.	.	.	.	.	.	.	.	1	.	2	35	0.112	6
Profile 5	13	ditch	1	<0.001	2	0.003	.	.	.	.	.	.	.	.	.	.	.	.	.	.	.	.	.	3	.	.	6	0.003	2
	13	ditch	24	0.065	2	0.001	.	.	1	0.003	.	.	.	.	.	.	.	.	.	.	.	.	.	2	.	1	30	0.069	3
	13	4/5	22	0.02	1	<0.001	.	.	.	.	.	.	.	.	1	--	.	.	.	.	1	<0.001	.	.	.	3	28	0.020	4
P 6	8	1	.	.	.	.	.	.	5	--	cf.	--	.	.	.	.	1	--	.	.	1	--	.	5	3	1	17	--	4
	8; pit	2	5	0.064	.	.	.	.	.	.	.	.	.	.	.	.	.	.	.	.	.	.	.	.	.	.	5	0.064	5
Profile 8	9	4/5	12	0.025	.	.	2	0.008	.	.	1	0.001	.	.	.	.	.	.	.	.	.	.	.	.	.	2	17	0.034	3
	9	4	16	0.066	3	0.016	1	0.004	1	0.003	.	.	.	.	.	.	1	0.002	.	.	.	.	Acer (0.006)	3	.	2	28	0.097	6
	9	4	25	0.119	.	.	5	0.021	1	0.002	.	.	.	.	.	.	.	.	.	.	.	.	Maloideae (0.002)	3	.	.	35	0.144	4
	9	4	21	0.131	3	0.012	4	0.03	.	.	.	.	.	.	1	0.007	.	.	.	.	.	.	.	.	.	1	30	0.180	4
	9	4	16	0.057	1	<0.001	3	0.015	.	.	.	.	1	0.001	.	.	.	.	2	0.003	.	.	Acer (0.003), Maloideae (<0.001)	3	.	2	30	0.079	7
	9	3	.	.	5	0.011	.	.	.	.	.	.	.	.	.	.	.	.	.	.	.	.	.	5	.	.	10	0.011	1
	9	2a	38	0.121	84	0.442	.	.	.	.	.	.	.	.	.	.	.	.	.	.	.	.	.	.	.	.	122	0.563	2
Profile 11	7	5	2	<0.001	.	.	2	0.002	.	.	.	.	.	.	6	0.004	1	<0.001	.	.	.	.	bark (0.001)	3	.	2	17	0.008	4
	7	4/5	23	0.055	2	0.001	1	0.001	1	<0.001	.	.	2	<0.001	.	.	.	.	.	.	.	.	.	1	.	.	30	0.057	5
	7	4	16	0.052	.	.	.	.	.	.	.	.	1	0.003	.	.	.	.	.	.	.	.	Maloideae (0.001)	1	.	.	19	0.056	3
	7	4	12	0.009	1	<0.001	.	.	.	.	1	<0.001	.	.	.	.	.	.	.	.	.	.	Tilia (<0.001)	5	.	.	20	0.009	4
Total sum:			857	2.965	333	1.279	52	0.152	28	0.085	16	0.03	12	0.018	10	0.024	4	0.002	6	0.006	4	0.003	11; 0.021	62	3	55	1454	4.637	15
% of taxa-identified:			64.2	64.7	25.0	27.9	3.9	3.3	2.1	1.9	1.2	0.7	0.9	0.4	0.8	0.5	0.3	<0.1	0.5	0.1	0.3	0.1	0.9; 0.40				1333	4.585	

described by the following aeolian units. The basal aeolian unit is characterized by brownish yellow, medium-to-fine grained sands with a thickness of about 0.6 m (aeolian unit 1). It is covered by a pale yellow, medium-to-fine sand layer, on which a fossil podzol developed (aeolian unit 2). The thickness of this unit ranges from c. 1.0 to 2.5 m. A charcoal remain from two thin charcoal-rich layers from the uppermost part of aeolian unit 1 yield a ^{14}C age of 11628–8946 cal. BC (Table 7.1). Accordingly, the age in connection with the results of Müller (1999) indicates that early dune formation probably occurred during the Older Dryas (aeolian unit 1) and Younger Dryas (aeolian unit 2). The fossil aeolian surface on top of unit 2 shows a relatively flat terrain. Traces of iron ore production and ore processing such as cinder pits with slag fragments were found in the northern profiles close to the archaeological excavation sites showing the use of this area during the Roman Iron Age. Clearly con-

served ploughing structures on the surface of the unit indicate that the Kuhharder Hill area was used for agriculture (aeolian unit 2a[6]). Dating of Ericaceae charcoal points out that this usage took place during Early Medieval Times. Three distinct phases of sand deposition overlay the fossil aeolian surface. The lowest layer is characterized by dark, yellowish-brown and mainly fine grained sands with a maximum thickness of 0.2 m (aeolian unit 3). One ^{14}C-measured charcoal of this unit yielded an Early Medieval date. The overlaying unit 4 consists of medium-to-fine grained sand which alternate with charcoal enriched layers. A maximum thickness of ~2.5 m was recorded for this deposit. Radiocarbon dating of embedded charcoal provides evidence for a dune formation during High Medieval Times, although one ^{14}C sample dated to the Late Iron Age (369–547 cal. AD). The uppermost sediments consist of similar grain size distribution and a brownish-yellow color (aeolian unit 5) forming a layer of up to ~ 1.5 m in thickness. Charcoal pieces are present but appeared speckled, sometimes ribbon-shaped. Despite two Iron

6 *Notice: The used naming of this unit changed in the course of this thesis. The initial name was »unit 2a« and was then changed in »unit 2-p« to point out that this unit was ploughed.*

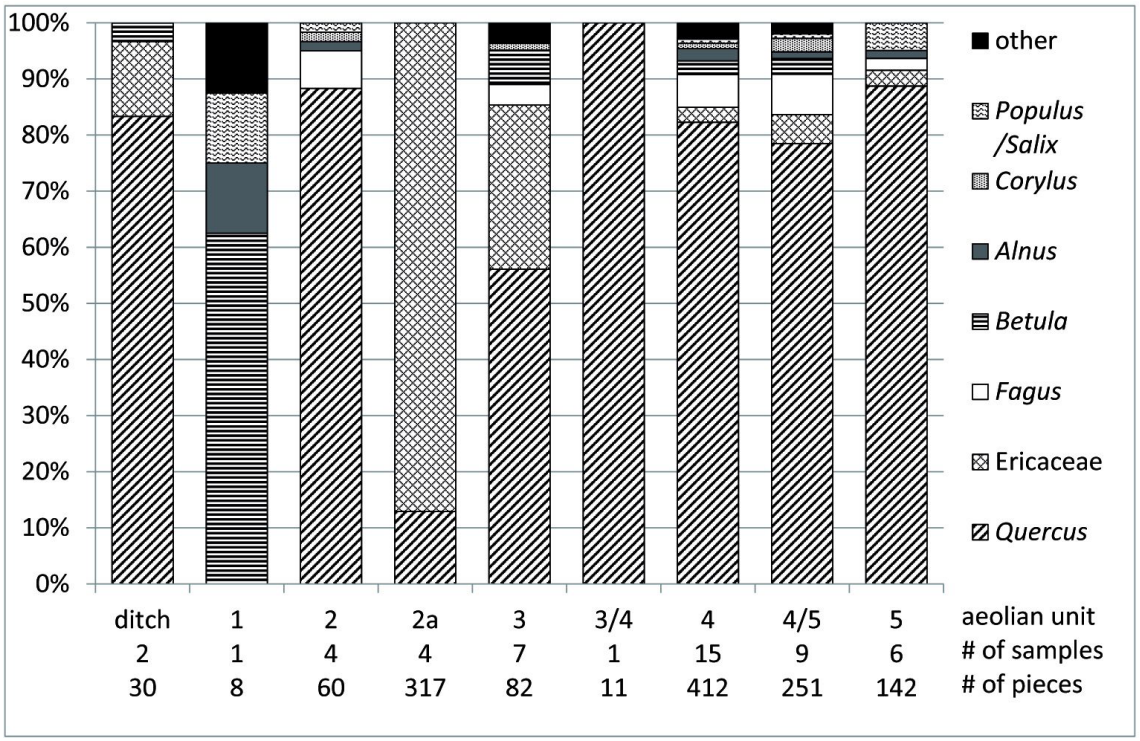

Figure 7.4: Charcoal assemblages of aeolian units and ditch/pit structure. Samples summarized as 4/5 derive from the unit boundary of 4 and 5. Single charcoal finds and aeolian units with just one sample (1 and 3/4) are not reproduced. Others include *Fraxinus*, *Pinus*, *Acer*, *Tilia, Maloideae* and *Lonicera*

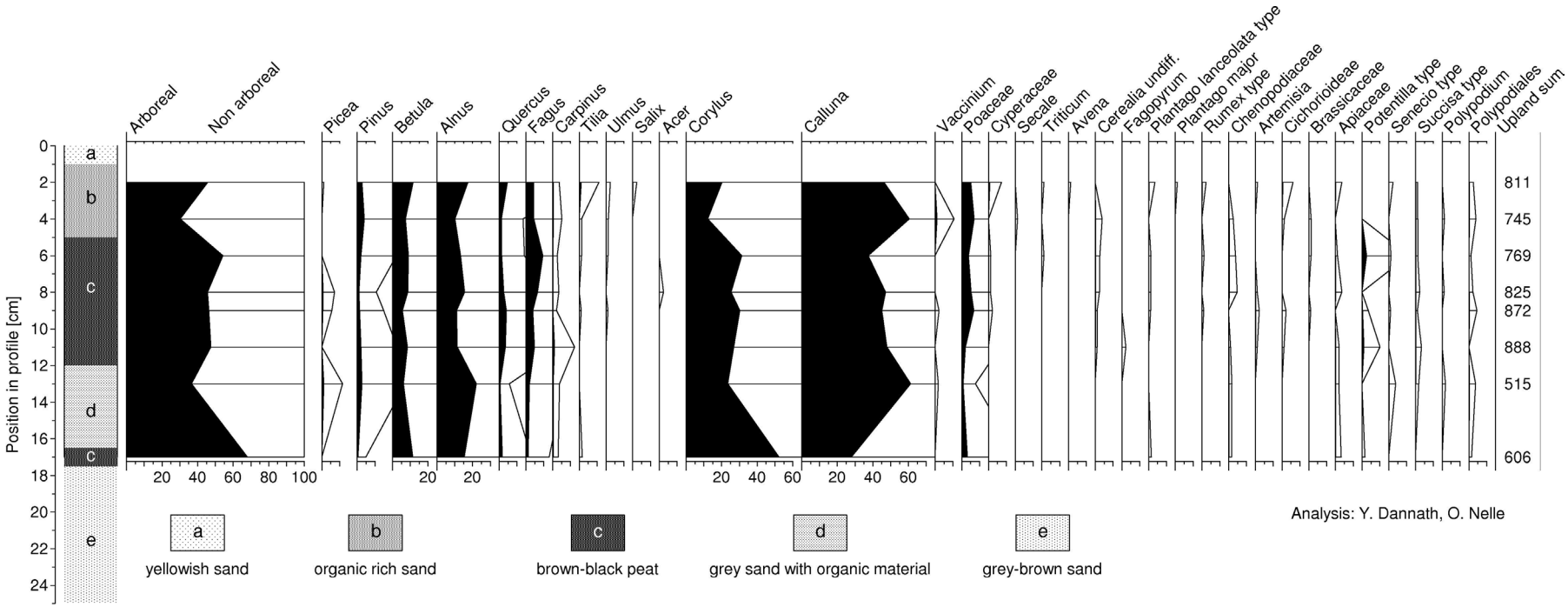

Figure 7.5: Simplified pollen diagram of the vertical section from an organic rich ditch/pit infill at profile 5. Percentage values of selected pollen and spore types (black curves). White curves with depth bars show 10-times exaggeration. Calculation base: upland sum including *Calluna*

Age dated charcoals, the datings show that this unit was formed during Late Medieval / Early Modern Times. A sedimentation discontinuity separates the High Medieval layer from the younger deposits. In most profiles a podzol has developed on the youngest sediment.

In profiles 4 and 5, three nearly parallel ditch structures were observed, which cut the A-horizon of the fossil podzol. One ^{14}C sample of the youngest charcoal layer which was cut by the ditch structure yielded an age corresponding to Late Medieval / Early Modern Times (1284–1631 cal. AD). Underneath a ditch in profile 5 a pit structure was found, approximately 120 cm in length and 20 cm in depth.

7.4.2 Overall charcoal data

The amount of charcoal differed significantly in the sampled charcoal-enriched layers. In some samples only single or few charcoals were found, while most of the samples contained 15 to 40 pieces, and occasionally more than 40. A total 1333 pieces (4.59 g) were taxonomically identified and 121 remained undetermined (indet) mainly because they were too small for identification and / or the woods' anatomical characteristics were poorly visible. The total charcoal spectrum is composed of 14 taxa (Table 7.2). It is dominated by *Quercus* (oak; 64 %). Ericaceae (heather; 25 %) are present in many samples, albeit usually with low values, but three samples from aeolian unit 2a show exceptionally high values of Ericaceae. However, we assume that *Calluna vulgaris* is an important species, as it is one of the characteristic plants of the north-western European heathland. *Fagus* (beech; 4 %) has a relatively high frequency, and is present in most samples. Further woody taxa are *Betula* (birch; 2 %), *Alnus* (alder; 1 %), *Populus/Salix*-type (poplar / willow; *Salix* was determined in some cases; 1 %) and species with less than 1 %: *Corylus* (hazel), *Fraxinus* (ash), *Pinus* (pine), *Acer* (maple), *Tilia* (lime), *Maloideae* (the apple subfamily, including *Pirus*, *Malus*, *Crataegus* and *Sorbus*), and *Lonicera* (honeysuckle). Most samples are dominated by *Quercus*, some by Ericaceae, other species occur in low numbers per sample (Table 7.2, Figure 7.2). In several samples, we additionally observe a considerable number of charcoal pieces having a rounded shape (see Figure 7.3c).

7.4.3 Charcoal assemblages of aeolian units

In total five different aeolian units were identified. The aeolian unit 1 was exposed only in profile 6, and one charcoal sample was taken. It contains a few small charcoal pieces identifiable as *Betula*, *Alnus*, *Salix* and *Pinus*. Charcoal samples of the fossil podzol (aeolian unit 2) corresponding to the Roman Iron Age show high values of Quercus and just a few pieces of other taxa (*Fagus, Alnus, Corylus* and *Populus/Salix*, Figure 7.4). Aeolian unit 2a which is related to the Early Medieval Times (ploughing horizon) is dominated by Ericaceae; only one other taxa was identified (*Quercus*). In the aeolian units 3–5 Ericaceae are still present, but they never reach again such a high level as in the aeolian unit 2a. Nevertheless, Ericaceae are still numerous in

aeolian unit 3 and occur together with the dominant *Quercus* and some pieces of *Fagus* and *Betula*. The charcoal assemblages of the aeolian units 4 and 5 are dominated by Quercus, but species such as *Fagus*, *Betula*, *Alnus* and *Corylus* are commonly found in the samples. Comparable results are given by samples from the ditch structure of profile 5.

7.4.4 Pollen analysis

The ditch which was sampled for pollen analysis was dug down from the Medieval soil surface, according to radiocarbon dating and stratigraphy. The ditch with its organic sediment was later, probably in the 15th or 16th century, refilled and covered by drift sand. Thus, the uppermost sediment of the »Stechkasten« profile formed during Late Medieval Times, and the pollen assemblages date to this period. The following part of the pollen section reflects the filling of the pit structure. The pit with its organic sediments is estimated to be Medieval, based on the stratigraphy. The eight samples from the small profile show high values of *Calluna* and *Corylus*, with significant amounts of *Betula*, *Alnus* and *Fagus* (Figure 7.5). *Quercus* is less abundant than Fagus, which shows an increase along the profile. All samples contained high quantities of microscopic charcoal, indicating fire activities at the site. Arboreal to non-arboreal pollen (AP/NAP) ratio is between 6:4 and 3:7.

7.5 Discussion

7.5.1 Formation and provenance of charcoal

The origin of charcoal plays an important role for the interpretation of anthracological assemblages. In soils and sediments, charcoal fragments might have several origins, which are usually difficult to assess. Charcoal might be formed by natural forest fires, as well as anthropogenic fires such as campfires or intentional burning of wood- and heathland for agricultural and pastoral purposes. At Joldelund, iron ore production and early human settlement are known in the vicinity of the dune complex, which have occurred during the Roman Iron Age (Jöns 1997). As different processes of transport of charcoal after their formation are possible, we distinguish between primary distribution at the time of the fire event, and secondary dispersal, i.e. reworking of charcoal by wind erosion processes. The dispersal during fire events depend on various factors such as particle size, wind speed and openness (wind fetch) of the landscape. A survey with charcoal traps in an experimentally burnt boreal forest showed that almost no charcoal > 0.5 mm was found outside the burnt area (Ohlson and Tryterud 2000). Trapping of charcoal in Switzerland, after a fire caused by an arsonist, showed a dispersal of charred remains (> 1.4 mm) of more than 5 km (Tinner et al. 2006). Primary dispersal might have occurred due to burning of wood- or heathlands on the dunes; nevertheless in our case the secondary dispersal of charcoal probably plays an important role. Human triggered

remobilization of dune sediments – due to deforestation and intensification of agriculture – resulted in the reworking of charcoal with the drift of sand. In contrast to soil erosion by water, wind erosion is not a slope-dependent, spatially oriented process, but occurs omnidirectional. Thus, the localization of the catchment area is more difficult to characterize, and depends on wind direction, wind speed and landscape properties (Strehl 1999; Duttmann et al. 2004). Scott et al. (2000) stated that small charcoal (<4 mm) can be transported by strong wind similar to the transport of sand. Many of the Joldelund charcoal showed signs of abrasion (rounding) which were probably caused by longer transport. Single charcoal could have been displaced several times before they were finally deposited, potentially by moving together with sand material.

Due to the ecological characteristics of the woody species that occur, we assume different origins. *Quercus*, Ericaceae and *Pinus* probably grow well on sandy soils and are naturally dominant on the dune complex. If the site conditions become more favorable in the course of soil formation and increasing nutrient and water availability, *Quercus* will then outcompete *Pinus* and *Betula*. Though *Fagus* proves its superiority only on sites with a medium water supply and an at least moderate nutrient availability, it can grow on nutrient-poor sandy sites, thus Fagus charcoal might have been blown in from the immediate vicinity as well as from further away. Other species found in the assemblages, like *Corylus* and especially *Alnus*, need soils with at least a larger water storage capacity and especially in the case of *Corylus* also a reasonable nutrient availability. *Alnus* possibly grew on sites with a high ground-water table nearby the dunes. Hence we assume that some woody species have been transported as charcoal from locations with different growing conditions around the dunes. Additionally, some of the *Quercus* pieces were rounded in shape and seem to be transported over a longer distance. *Quercus* charcoal might also originate in part from richer and wetter soils near the dunes. In conclusion, we have to consider two source areas: 1) a local origin, where fire events took place on the dune complex, with subsequent local charcoal deposition; and 2) an extra local source of unknown distance, charcoal rolled along the surface with wind as the transport agent. In the single charcoal layers within the dune complex both sources can be mixed – hence it is difficult to distinguish between local or extralocal/regional sources. However, we assume that Ericaceae mostly derive from local sources (Scott et al. 2000), whereas, for example *Alnus* and *Populus/Salix*-type do not grow on the dune itself and must be transported together with the sand.

Another taphonomic aspect to consider is a potential bias in the assemblages due to different charcoalification processes. Scott et al. (2000) found no evidence of such a difference; their charred remains well represent the vegetation of a contemporary heathland fire.

7.5.2 Vegetation history

The charcoal assemblages represent the wood spectra from different burning

events. Charcoal is mainly formed during woodland/heathland fires, which are possibly caused by human activity (apart from aeolian unit 1, where natural fire is probable during the Late Glacial; however, human presence cannot be ruled out, because there is evidence for it in the wider region, e.g. Clausen 1997). Charcoal produced in these fires represent the current vegetation at the burning time and place. The first two aeolian units were formed before the Preboreal. Natural dune-forming processes seem to end with the establishment of the first forest systems. Only a few charcoals were found which reflect the presence of woody species within the lowest aeolian unit (*Betula*, *Pinus*, *Salix* and *Alnus*). The cover of vegetation was re-opened again with the intensification of land-use by humans, which reactivated the aeolian sediments. The surface of aeolian unit 2 is dated back to the Late Roman Iron Age (~ 400–550 AD), when *Quercus* was the dominant species. Perhaps there was a first opening of the Kuhharder Hill and its surrounding, and it was used as semi-open woodland pasture. Aeolian unit 2a is a ploughing horizon and dates to the Early Medieval Times (~ 800–1000 AD). During the following period, *Calluna* increased as a result of opening the forest for pastoral use. Only charcoal from the local heather vegetation (Ericaceae and *Quercus*) is present in the samples and it seems that no aeolian process was involved. This indicates that ploughing took place after the burning of heathland. In aeolian unit 3, higher values of *Betula* occur, which grows as a pioneer species well after the decline of human usage. Furthermore, we found no *Alnus* and *Populus/Salix*-type in this unit, indicating lower regional impact to this charcoal assemblage. The aeolian units 4 and 5 and the ditch in the profile 5 seem to represent a mixture of local (Ericaceae) and regional vegetation (e.g. *Alnus*, *Populus/Salix*-type). The decrease of *Calluna* in High to Late Medieval Times may be amplified due to higher values of regional charcoal. *Quercus* is the dominant tree species in the Roman Iron Age and during Medieval Times. *Fagus* is present during these periods as well, but the appearance of *Fagus* in the Iron Age could not be confirmed by dating due to the very small size of these fragments. Thus a later rearrangement of *Fagus* cannot be ruled out. The dated *Fagus* fragments so far support the assumption that *Fagus* is present in the local woodlands after ~400 AD, as seen in pollen diagrams (Dörfler 2000). Whether *Fagus* immigrated earlier, possibly around 500 BC, remains to be tested by dating of macroremains. Pollen values during this time are low and cannot be interpreted as a clear local presence of the species.

Charcoal, analysed by Dörfler and Wiethold (2000) from the nearby investigated iron ore production sites, was dominated by *Quercus* with high values of *Alnus* and single records of *Corylus*, *Betula*, *Fraxinus*, *Populus/Salix*-type, *Acer*, *Carpinus* and *Hedera*. However, no *Fagus* occurred. The charcoal assemblages of Dörfler and Wiethold (2000) represent mixed oak forests on wetter soils. In our dune samples species such as *Alnus* are very rare. If reworking of Roman charcoal from the settlement took place in higher quantity, then we should find more *Alnus*. Further Dörfler (1995) presented a model for calculation of the wood consumption of the

iron ore production in Joldelund. He points out that a high amount of wood was required, but compared to other wood consuming activities like the construction of houses or tools, the wood demand for iron ore production was moderate, and did not cause deforestation.

The charcoal data can be compared to palynological evidence from the nearby mire Hörrmoos, which is situated one kilometre east of the Kuhharder Hill (Figure 7.1). Dörfler (2000) showed that a mixed oak forest was typical for the region since at least 6000 BP, the start of the pollen record. The woodland was mainly composed of *Quercus*, *Corylus*, *Betula* and *Alnus*. *Tilia*, *Ulmus*, *Fraxinus* and *Salix* seem to be continuously present, while *Acer* and *Populus* occur with very low values. *Acer* is insect-pollinated, and *Populus* pollen grains are very sensitive to degradation. The curves of *Fagus* and *Carpinus* rise after ~400 AD, giving much discussion about whether this is an indication of the first occurrences of the late immigrating trees at the local scale, or whether single trees, that were already present, spread on a larger scale. Human indicators such as *Rumex* and *Plantago* appear around 2600 BC together with the first cereal grains. Since 1300 AD a change to more intensified agriculture is visible in the diagram, resulting in lower values of tree pollen and higher values of cereals. Hereafter sand layers are visible in the core. Before ~1300 AD, deforestation took place only at a locally restricted dimension. During Medieval Times intensive land-use connected with a broad woodland cutting and an increase of heathland happened (Dörfler 2000). A second mire analysed by Dörfler (2000) is situated approximately 500 m east of the Kuhharder Hill dune (»Mire covered by dunes«, Figure 7.1). The pollen record stretches from 400 BC until 1200 AD, when the mire was overlaid by sand. While the overall vegetation recording is comparable to the Hörrmoos, a higher local pollen input is visible due to the small size of the mire, as can be seen in very high values for *Calluna*. Further, a change due to the Roman Iron Age settlement is visible, resulting in very low values of trees and shrubs.

In this broader palynological context, the newly analysed small ditch pollen profile provides a very local, on-site impression of the vegetation composition. The finding of a *Fagopyrum* (buckwheat) pollen grain in the lower part of the profile supports the geomorphological dating of the sediment formation. Buckwheat was introduced to Northern Germany in the 14th century AD (Wiethold 1998). With high proportions of non arboreal pollen and considerable values of *Calluna*, the assemblages indicate the openness of the site during High Medieval / Late Medieval Times. However, the increase of *Fagus* in the upper part of the diagram might be connected to a period of less intense land-use in the 15th century AD, which is also reported by Dörfler (2000). Surprisingly high values of *Corylus* contradict its general scarceness in the charcoal record.

7.5.3 Linking geomorphology and anthracology

For this study, scientists from botany as well as geomorphology worked closely together, initiated by the geomorphological work. One important aspect was the taxonomic identification of wood charcoal prior to radiocarbon dating. The unexpectedly large number of charcoal rich layers provided an abundant amount of datable material. It turned out that the taxonomical selection of datable charcoal was indispensable for the development of the dune stratigraphy. In this respect we excluded charcoal from dating which could be assumed to result in erroneous ages, like coniferous species which were introduced in recent times. The use of relatively short-living woody taxa such as Ericaceae and *Populus/Salix* makes the date more reliable by reducing the potential »inbuilt age« (Gavin et al. 2003), which is for *Quercus* possibly up to 30–400 years. For this reason, *Quercus* was chosen only exceptionally for dating (see Table 7.1). Charcoal analysis thus helps to establish a more precise chronostratigraphy of dune formation.

The comparison of charcoal assemblages from correlated aeolian units in different neighboring profiles can support or contradict the stratigraphic assumptions. In this respect, the dating of aeolian unit 1 was supported by the woody species assemblage. The layers in profile 3 and 8 which are related as aeolian unit 2a showed similarly high values of *Quercus* and Ericaceae, which support the geomorphologic interpretation as well. The correlation of the aeolian units 4 and 5 is neither really supported nor contradicted by taxa spectra, but is supported by the number of taxa per sample, which is higher in these aeolian units compared to the underlying ones. Another aspect of synergy concerns the interpretation of charcoal assemblages for the reconstruction of past vegetation. Without the stratigraphic context, taxonomic data are impossible to interpret. This is particularly the case if charcoal pieces are rearranged over time. Of the total of dated charcoal samples, we identified four measurements that cannot be connected with the dune activity itself and are from relocated charcoals. With the exception of one sample, the relocated charcoal dated to the Roman Iron Age.

Vegetation cover is the main factor which controls aeolian sediment transport. Thus, charcoal analysis contributes to the reconstruction of local vegetation of the different past dune surfaces and gives an insight into the wood species composition prior erosional events. Additionally, our assumption of potential wood provenances can assess plausibility of the potential source areas for the aeolian sediment. For example, local charcoal sources of *Alnus* as well as *Salix* and *Populus* are most likely suspected to the north-northeast as well as west-southwest of Kuhharder Hill, where these species possibly grew in respective stands in the low lying wetlands, which are influenced by groundwater. During the Roman Iron Age, the areas of Saalian moraine were favored for agricultural land-use, and thus constitute potential areas for sand and charcoal origin. As both the minerogenic as well as peatland sites are suitable for *Calluna*, potential catchment areas of heathland are in the

surrounding lowlands and at the dunes itself. *Quercus* was intensively used during the Roman Iron Age. It is assumed that local charcoal transport occurred from settlement and iron production sites, but this was only slight. Due to the broad site conditions under which *Quercus* can possibly grow, ranging from dry sandy soils to wet soils with higher nutrient availability, *Quercus* can grow almost everywhere on and around the dunes.

7.6 Conclusion

Sandy deposits forming dunes serve as palaeoarchives and contain taxonomically identifiable wood charcoal. These can be used to obtain information on the occurrences of woody taxa, for the reconstruction of vegetation and dune dynamics. Due to various factors influencing the charcoal spectra, including particularly the reworking processes during the dune accumulation, the interpretation of the results is complicated. Therefore, an interdisciplinary collaboration is an essential basis, in this respect: geomorphological work on dune formation makes these archives accessible through profiles, and provides stratigraphic hypotheses which can be cross-checked by the charcoal assemblages. This is supported by physical dating to establish a chronostratigraphy, which is then used to interpret the woody taxa occurrences through time. As a counterpart, vegetation and human activity trigger the dune development. For this reason, the knowledge about the causing processes is essential to comprehend former sedimentation events.

In the case of the Joldelund dune complex previous archaeological and especially palaeobotanical analysis complete the picture. The two types of botanical records – pollen and charcoal – show some minor differences, which can be explained by the varying catchment areas, and the proportion of species in the records is linked to botanical factors like pollen production of single species. A further factor that should not be ignored is that charcoals in the dune context are mostly originating from fires caused by human. Even if no selection of wood for any purpose is reflected in our samples, actions to lighting a fire on special areas may affect our results. Despite this methodological subject, our results demonstrate the development of the dune area near to Joldelund. In contrast to the vegetation today (coniferous afforestation) the dune was formerly forested with a mixed deciduous oak forest. In times of human influences a heathland with Ericaceae developed. In summary, a more precise landscape history scenario can be formulated based on this integrated approach compared to a single discipline approach.

Turning human-nature interaction into 3D landscape scenes: An approach to communicate geoarchaeological research

8

(published in: *Kartographische Nachrichten*)

8.1 Introduction

Today, 3D landscape visualizations are commonly used in spatial science and urban as well as landscape planning. In addition, they play an increasing role in geoarchaeology and support the three-dimensional reconstruction of historic and prehistoric landscape changes and processes (Sheppard 2001, Lewis and Sheppard 2006, Ghilardi and Desruelles 2009, Siart et al. 2011). Geoarchaeological research aims to obtain information on palaeoenvironmental changes and to unravel the impact of human activities on the development of landscapes (Bork et al. 1998, Rapp and Hill 2006). Based on chronologically ordered data from geo-bio-archives, such as slope deposits, soils, lacustrine and aeolian sediments and on the expert's knowledge from various scientific disciplines as well, landscape visualizations support an improved understanding of landscape change processes over time (Duttmann et al. 2012). Moreover, they are well-suited to communicate the results of geoarchaeological research outcomes to a broader public. In this respect, a major challenge is to create 3D landscape visualizations that meet various expectations of different target groups such as the scientific and public communities. How can we communicate geoarchaeological results via photorealistic 3D landscape visualization techniques to researchers and to the broad public alike? How can we create reliable 3D scenarios of past landscape surfaces on different geographical scales, thus implementing different temporal and spatial resolutions? This paper presents a visualization model which aims to (1) create reliable 3D visualizations based on verified data from field studies and lab analyses, (2) to integrate knowledge from multiple disciplines to support an interdisciplinary dialogue and (3) to link scientific knowledge transfer and public outreach to improve communication between scientists and non-scientists. In this study, 3D visualization software products were applied to visually reconstruct landscape and dune development in an inland dune formation. Based on the following case study in Northern Germany, we present the implementation of a visualization model and the corresponding results.

8.2 Study area and geoarchaeological context

In a PhD project funded by the Graduate School *Human Development in Landscapes* (GSHDL) at Kiel University, human-induced wind erosion and its consequences for landscape and dune development have been investigated. A small inland dune complex in the vicinity of Joldelund (Northern Frisia, Germany) was used as a case study to investigate timing, intensity and frequency of aeolian reactivation reflected in sandy deposits of the so-called Kuhharder Hill. Bearing in mind that vegetation cover is the main factor that controls aeolian sediment transport, focus of the project was also to reconstruct vegetation history and past land-use change. The Kuhharder Hill dune complex covers an area of approximately 2 ha and reaches a maximum height of ~30.3 m above sea level. It forms the westernmost edge of a larger approximately 80-hectare inland dune field. The study area is located in the Weichselian outwash plain of Schleswig-Holstein and is embedded in the so-called European Sand Belt; a sand belt of extensive aeolian deposits formed predominantly during the last glacial (Koster 2005). Wind erosion and the occurrence of drift sand have been typical phenomena related to the outwash plain of Schleswig-Holstein since the very beginning of deforestation and agricultural land-use (Richter 1995, Duttmann et al. 2004). In the region of Joldelund, the first mayor reactivation of aeolian deposits is known to have occurred during the Roman Iron Age (Dörfler 2000). At that time, human activities such as settlement and iron ore production caused predominantly local changes in landscape and vegetation, which resulted in moderate sand drifts (Dörfler 2000, Jansen et al. 2013). As a consequence of intense deforestation and agricultural land-use during the Middle Ages, disastrous wind erosion events occurred, leading to vast degradation of farmland and the formation of inland dunes such as the Kuhharder Hill. Wind erosion processes and remobilisation of sandy deposits during Modern and recent times were also recorded in neighboring communities (Duttmann et al. 2004). Although there have been local activities to prevent erosion damage since the 16th century, it took until the 1950s for a comprehensive program against wind erosion, the Programm Nord, to be successfully implemented. Within this government-funded program, badlands were afforested systematically and hedge rows were planted to protect wind erosion-prone areas. Since then, the aeolian sediments have been stabilized under a dense coniferous forest, which nowadays serves as woodland and is also used for recreational purposes by local residents (Nielsen 1970). In 1975, a ~1.1 km long natural trail was inaugurated in the municipality forest of Joldelund providing basic information on tree species, native animals and archaeological finds (Nielsen 1978).

8.3 Turning human-environmental interaction into 3D landscape scenes

8.3.1 Reconstructing human-nature interactions and past environmental change

A reconstruction of human-driven landscape changes and the development of Kuhharder Hill were achieved by a multi-disciplinary approach interlinking geomorphological and pedological analysis of soil-sediment-sequences, chronology, palaeo-botanical analysis as well as archaeological and historical records. In total, eleven profiles were excavated 5–25 m in length and up to ~2.8 m in depth. With a focus on the largest dune body, seven profiles were constructed at the Kuhharder Hill, two dune profiles form a cross-section. Past soil surfaces and aeolian deposits were documented via scaled drawings, identified, and stratigraphically sampled for pedological analysis, e.g. grain size, organic matter and bulk density. In addition, sampling for radiocarbon dating (Jansen et al. 2013) and OSL dating were carried out according to dune stratigraphy. The dune profiles display numerous charcoal layers intercalated with sandy deposits. Therefore they were sampled in order to get information on age and species. Around 150 drilling cores have been obtained to gather information on the spatial distribution of past dune surfaces and the thickness of aeolian deposits. Based on dated stratigraphy, several phases of dune formation have been identified. The dune record revealed three main phases of dune formation during the Middle Ages as a response to a strongly growing population and intensified agricultural land-use. The youngest deposits were probably deposited during Modern Times.

8.3.2 From field results to 3D landscape scenarios

Different 3D visualization software products (Autodesk® 3ds Max®, Visual Nature Studio and the Division-owned product a3Dc) were applied to visualize geoarchaeological results and to reconstruct landscape development within the study area. In the following, short descriptions of 3D visualization software and their approaches are provided.

Autodesk® 3ds Max® – A 3D CAD animation software

Dune formation, local vegetation and landscape changes at Kuhharder Hill were visualized using Autodesk® 3ds Max® 8, a comprehensive visualization tool primarily applied in the fields of design and architecture – and also in computer games. The basic principle of Autodesk® 3ds Max® 8 is to model 3D objects and create materials representing their surfaces. Simple 3D objects such as spheres, cubes or planes serve as basic elements for complex shapes. Materials are a collection of textures, either from raster images or processed in a procedural manner, which are used to define the non-geometrical appearance of the surface characteristics of a 3D object such as color, shade, opacity and others. Scene objects can be animated in many ways, e.g. animation of spatial position, size or surface characteristics of any pa-

Table 8.1: Selection criteria for offline rendering visualization software concerning landscape scenarios

Visual Nature Studio™2.86	Autodesk® 3ds Max® 8
Visualization of larger, rural landscapes including many vegetation objects	Visualization of urbanized landscapes (e.g. cities) including less "natural" areas
Variety of vegetation: visualization of many different vegetation objects parametrized by attribute data	Variety of vegetation: visualization of less diversity of vegetation - without attribute data (e.g. density, heights)
Visualization of terrain-based modifications (e.g. ditches) using 2D vector- and corresponding attribute data	Visualization of many dynamic effects (e.g. fire, rain) using particle systems
Camera position: if a higher camera position is desired (e.g. bird's eye-view)*	Camera position: if a lower camera position is desired (e.g. human eye-level)
Desired result: rather natural or for 3D cartographic applications	Desired result: rather schematic or a photorealistic design rendering
Import of data with different map projections	Import of data with one map projection which has to be defined in the CAD environment
3D modelling: any other 3D modeller for generating 3D objects is needed	3D modelling: any imaginable and geometrical describable object can be modelled
If import of vector and corresponding attribute data is needed	If no import attribute data is needed

** If the camera position is higher the billboards (e.g. trees) are calculated with an algorithm, which result in a more realistic overhead view. In contrast, Autodesk® 3ds Max® 8 will just project the billboards to the ground that they appear like fallen trees.*

rameter. According to chronostratigraphy of the dune under study, 3D objects have been modelled representing changes of former surfaces and morphology. Thus, the modeling of dune formation is based on scaled drawings and graphically rectified photographs of profiles as well as on additional drilling. The dune development has been visually reconstructed as a dynamic process over time by visualizing not only changes in dune morphology but also soil formation processes, changes in vegetation and land-use patterns as well as human activities such as burning, ploughing and smelting iron ore. To achieve a photorealistic appearance of the virtual landscape, maps and textures were used such as photographs of grazing animals and plants as well as designed bitmap files of soil profiles and aeolian deposits. Dynamism of landscape processes was created by animating different materials and maps, for example, by fading 3D objects and animating fire events by modeling flames and smoke.

Visual Nature Studio™2.86 – A GIS-based landscape visualization software

Scenarios of the past and actual landscape surfaces were visualized using the GIS-based software Visual Nature Studio™2.86 (VNS) developed by 3D Nature. In contrast to 3D CAD software, VNS is specialized in modeling natural landscapes. By using different geospatial data, such as a

digital elevation model (DEM) and vector datasets, raster images as well as modelled 3D objects as input, VNS enables the user to generate photorealistic landscape images and animations. VNS provides a number of pre-defined tools, so-called components, to generate a virtual landscape. Comparable to a modular construction system, landscape features such as vegetation, terrain surfaces and manipulations, illumination and cloud types and water bodies can be defined and animated independently. Furthermore, texture mapping of terrain surfaces or 3D objects allow users to create a realistic appearance of surfaces, for example, by covering them with hatches, patterns or images using GIS data and their attributes (e.g. for density, positioning and orientating). By animating single parameters, the software provides representation of landscape feature dynamics, e.g. vegetation, surface movement and land-use patterns. Within the project, VNS was used to visualize 3D landscape scenarios as well as virtual tours for three different time periods, specifically for a time travel through the Kuhharder Hill dune complex during the Roman Iron Age, the Middle Ages and modern times. The landscape scenarios are based on a DEM12.5 and a DEM2 of the area´s recent topography. A major task was to generate a vegetation cover, including plant composition and density for each time period. According to literature reviews, archaeological evidence and pollen records from the Joldelund region, different ecosystem components were designed, e.g. a mixed-oak forest for the Roman Iron Age and heathland for the Middle Ages. In order to represent plants and vegetation types, billboards were used. Billboards are center-view-oriented vertical rectangle planes textured with an image representing geo-objects such as trees, flowers and animals. Subsequently, ecosystems were associated with vector objects to define spatial position and distribution. In addition, 3D objects representing houses of an ancient settlement and bloomery furnaces were integrated in the virtual landscape. One animation uses a static camera position to observe the gradual succession of vegetation development under different anthropogenic influences. Along today´s natural trail for visitors, explanations are given at various points of interest, hence creating a virtual tour through our three time periods. This virtual path was created via a moving camera attached to a predefined route along Joldelund natural trail.

a3dc – A web-based 3D real-time environment

The third tool we used is a web-based 3D real-time environment named a3dc. It provides interactive visualizations of landscapes using Java3D libraries (Gabler-Mieck and Duttmann 2007). Thus, a3dc displays geospatial and thematic information as known from common geographic information systems. But, the a3dc software offers numerous other interaction options: Using DEM as basic input, it permits unrestricted navigation. a3dc also allows modifications of illumination, visibility conditions and positioning of 3D objects. Therefore, it empowers users to perform, for example, interactive 3D visibility analyses. Data is organized in a freely-definable layer structure, enabling the depiction of 3D text, billboards, thematic

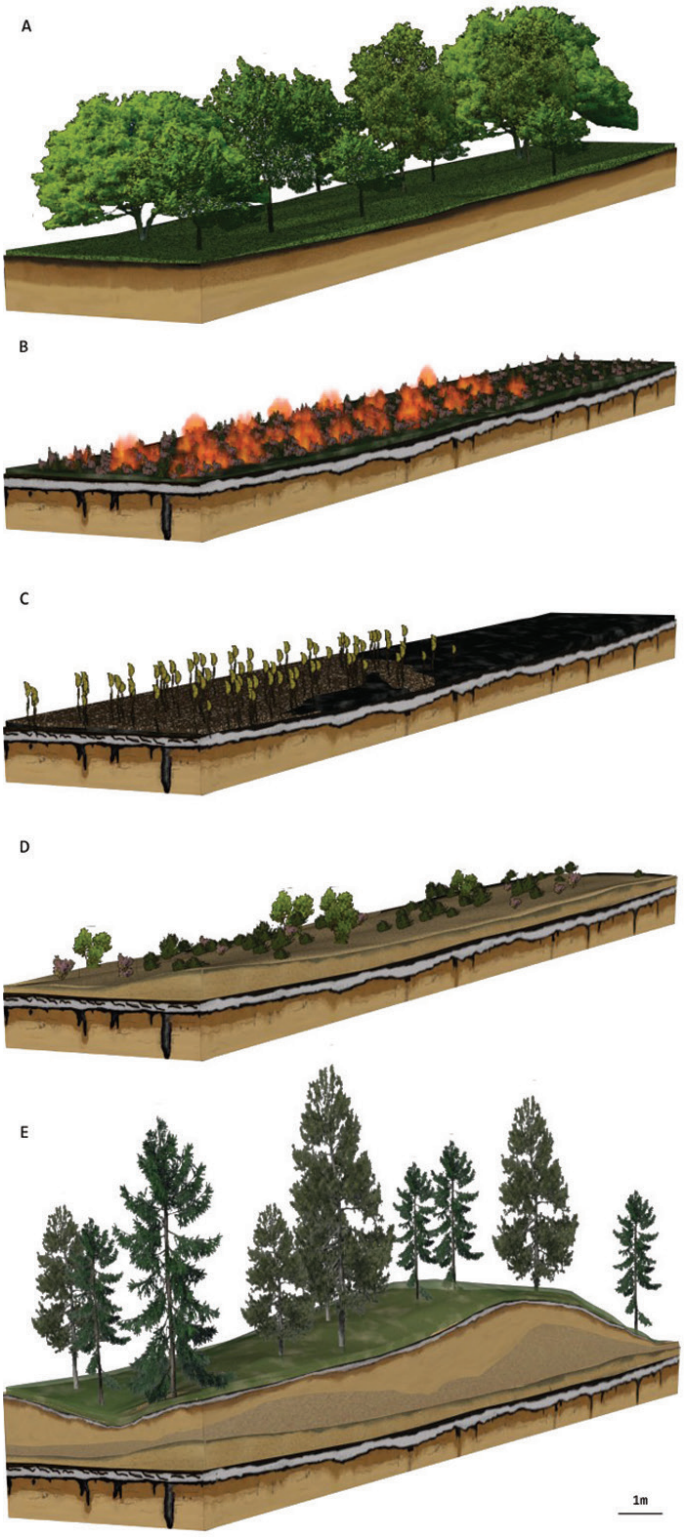

Figure 8.1: Visualization of dune formation using Autodesk® 3ds Max® 8. A: Silvopastoral woodland dominated by oaks; B: Burning of heathland; C: Agricultural land-use during the Early Middle Ages; D: First phase of dune formation during the Early Middle Ages; E: Present situation

maps or 3D objects as layer objects. These could be associated with attribute data or with URLs to show websites or local HTML content. In addition, a3dc allows the assignment of one or more behavior to any layer object, for example, the animation of layer objects for a predefined path (Gabler-Mieck and Duttmann 2007). Comparable to VNS and Autodesk® 3ds Max® 8, raster images are used as billboards for displaying single plants or a specific vegetation cover. As a result, by translation in height, two historical DEMs can be displayed in a 3D real-time environment – in addition to the recent surface. Each DEM is organized with its associated recorded data in a different layer. Using the results of local landscape visualization done before via Autodesk® 3ds Max® 8, the excavation hot spot, a cross-section of Kuhharder Hill was positioned as POI and associated to an autonomous HTML file showing our results.

8.4 3D visualization of landscape history – local, regional and interactive

Scientifically valuable 3D visualizations of landscape evolution scenarios and past landscape surfaces require geoarchaeological data of particular high spatiotemporal resolution. Such data can often be obtained on a relatively large scale only. Geoarchaeological data within our project are available in varying quality concerning temporal and spatial resolution. It was possible to develop, on the one hand, a detailed chronostratigraphy of the dune complex and to reconstruct local vegetation changes. On the other hand, existing palynological, archaeological and historic data were used to reconstruct landscape changes up to regional scale. Hence, a visual reconstruction of past landscape surfaces pose a particular challenge. In order to obtain reliable and valid visualization re-

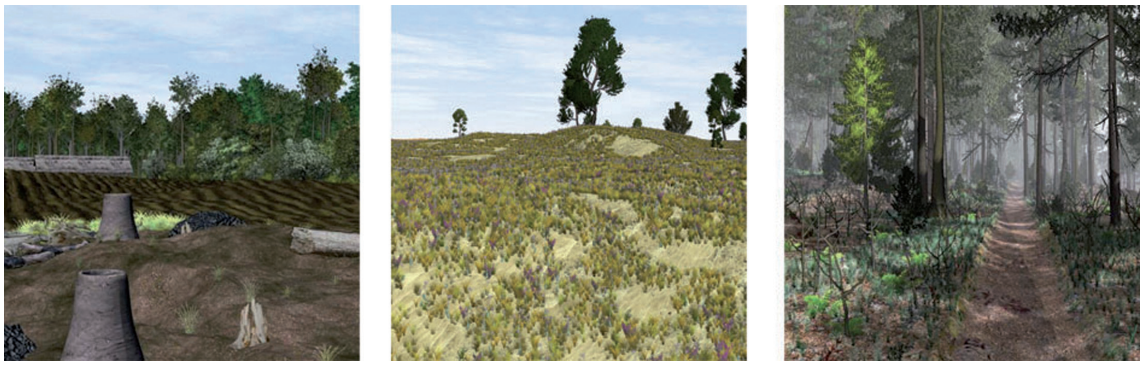

Figure 8.2: 3D visualization of landscape scenarios (from left to right): (A) Roman Iron Age; (B) Middle Ages (Köllner 2009); and (C) the present situation of the study area

sults, it is essential to create 3D landscape visualizations adapted to the spatiotemporal resolution of the data. Accordingly, visualizations of local and regional scale landscape reconstruction were developed using Autodesk® 3ds Max® 8 and Visual Nature Studio™2.86, respectively. Considering the scale of the modelled scenes, each visualization software has its advantages and disadvantages (see Table 8.1). Not only the scale, but also the amount of objects and the desired appearance of the scene are important selections. Table 8.1 summarizes some selection criteria for choosing the adequate software.

Figure 8.1 exemplarily shows the 3D reconstruction of development of the Kuhharder Hill dune and its vegetation and land-use alterations following anthropogenic activity. It starts when the natural forest was supposed to have been increasingly cleared by grazing and iron ore production during the Roman Iron Age. Hence, forest clearing, changes in vegetation patterns, probable grazing of goats, sheep and cattle are displayed as well as the smelting of iron ore. In the course of this 3D visualization, the different phases of aeolian sand deposition (dune-building) during the Middle Ages in conjunction with soil development, burning events, ploughing activities and spread of heathland were reconstructed. Reconstruction of the local vegetation was particularly based on charcoal analysis of charred wood found embedded in dune sediment. Radiocarbon and OSL dating were used for a chronology of dune development.

Based on palynological records, ancient settlement patterns and smelting traces, scenarios of the Joldelund region have been visually reconstructed for the Roman Iron Age and the Middle Ages (Figure 8.2A-B). In addition, historical maps, a map of potential natural vegetation and expert knowledge was taken into account

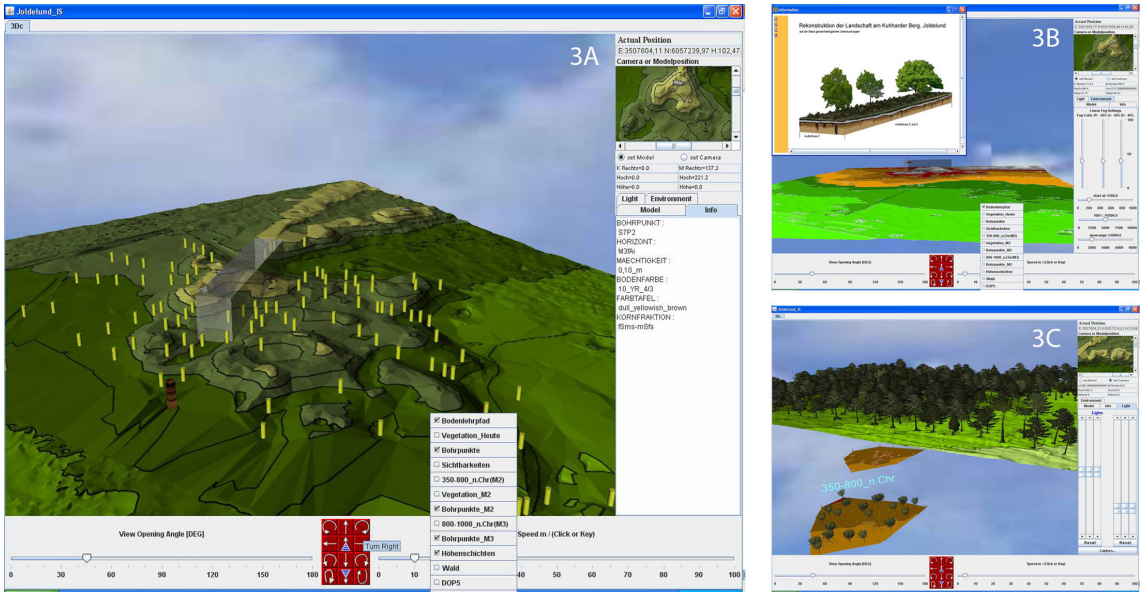

Figure 8.3: Interactive visualization of Joldelund applying 3D real-time environment a3dc (screenshots).

to provide further information on ancient landscape conditions and to enhance the validity of regional scale visualizations. All scenarios are based on the recent digital elevation model, thus, changes in aeolian morphology could not be displayed on this scale. The present situation of the study area was visualized using botanical records, investigator observations and photographs of the dune profiles (Figure 8.2C). The excavated trenches at the dune complex were incorporated in the DEM and were displayed using photographs as texture. In this way, a presentation of geoarchaeological field work is included. By using the same virtual camera path as mentioned before, landscapes scenarios can be compared with respect to the particular changes in vegetation and land-use patterns over time. However, visualizations which serve as pure visual presentations are only of limited value if they do not provide additional information and analytical and/or interactive functionalities (Duttmann et al. 2012). This also holds particular true for the 3D visualization and reconstruction of palaeo-environmental conditions. Photorealistic landscape visualizations easily involve the impression that the past landscape might have exactly appeared like the virtual landscape scenario (Winterbottom and Long 2006).

In this respect, data transparency and traceability of geoarchaeological results are indispensable for the legitimacy and reliability of a 3D landscape reconstruction. It should therefore be assumed that visualizations of past development of landscapes – no matter if they are 2D or 3D – are derived from an incomplete data record. They are visual outcomes of comprehensive interdisciplinary research efforts. However, to achieve the objective of appropriate visualization and, thus, communicating our results to the scientific community and the public alike, interactive visualization techniques provide opportunities to meet different requirements of »user-orientated« visualization.

By integrating an interactive real-time environment into our visualization model, we intended to support scientific discussion on the acquired field data, palaeo-botanical analyses, laboratory and dating results as well as to improve geoarchaeological interpretation on landscape changes. The 3D real-time software a3dc we introduced here uses online rendering that calculates at least 15 images per second. Therefore, generating results as photorealistic as those that result in offline rendering is not possible.

Using a3Dc, an interactive exploration of virtual landscapes, analysis of different dune surfaces and the query of data were combined with visualization results of local and regional landscape reconstructions (Figure 8.3A–C). In addition to DEM of the recent landscape surface, two further elevation models representing past dune surfaces of the Roman Iron Age and the Early Middle Ages have been integrated. The corresponding elevation data of former dune surfaces derived from excavated dune profiles and from drilling records were subsequently interpolated within ArcGIS 9.3 (ESRI).

As a result, the past relief becomes evident: Users can navigate freely and explore the reconstructed former aeolian relief.

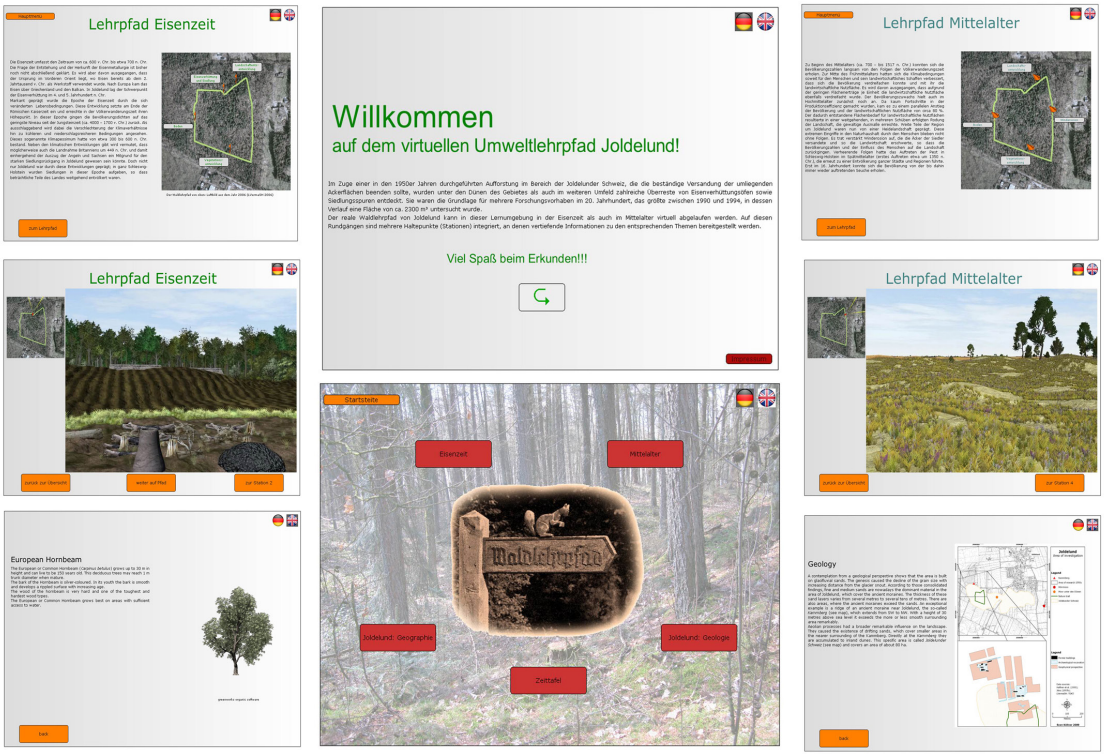

Figure 8.4: Interactive learning environment designed as a virtual circular trail for a wider general public (Köllner 2009)

Scientists and the public alike can choose a user-defined walk in the virtual environment of past-to-present Kuhharder Hill dune (Figure 8.3C). The respective data set of each drilling core can be queried by selecting a layer containing positions as well as pedological and geomorphological field records. Figure 8.3A shows the acquired data record of one drilling core, including core identification, stratigraphical correlation and thickness of soil horizon/sediment layer, determination of soil color and results of grain size analysis. Further information, such as dating results, palynological/charcoal analysis etc., can be included and queried. The 3D real-time environment thus serves as an information system for the underlying geoarchaeological record. By defining options for different layer objects, the actual coniferous forest as well as results of local vegetation reconstruction (charcoal analysis) is presented by using billboard (Figure 8.3C). Figure 8.3B shows how visualization results of local and regional landscape reconstructions are integrated in the real-time environment. A cuboid-shaped layer object representing the cross section of Kuhharder Hill dune was configured as POI. The results of local landscape visualization appear in the HTML-Viewer as a new window (Figure 8.3A–B). Analysis functionalities are provided: To process visibility analyses, the user can choose viewpoints himself and can configure illumination and visibility conditions (Figure 8.3C).

To evaluate landscape scenarios, profound knowledge of the data basis is essential. Given this prerequisite, 3D visualization

techniques enable an enhanced understanding of past landscape development. Thus, former change processes became clear, and can be interpreted in geoarchaeological contexts. For the widespread communication of our results there is a need to adapt presentation and visualization of the data according to demands of the users. The information given should be easy to understand – without scientific background knowledge. For environmental education, interactive features help to promote a better understanding of space and time scales (Boldt et al. 2005).

This proved true in the project worked out by Köllner (2009), who created an interactive multimedia learning environment using Macromedia Shockwave Director® 8.5. This bilingual learning environment represents 3D landscape scenarios of two cultural periods: the Roman Iron Age and the Middle Ages. It integrates additional information on human-environmental interaction such as metallurgy, settlement, vegetation, soil development and wind erosion (Figure 8.4). When users select a time frame, they are guided through the reconstructed virtual landscape: Along the trail, four learning stations (POI) provide additional information on demand.

The learning station of the Roman Iron Age, for example, provides facts on 1) metallurgy and settlement 2) soil types and their development 3) former tree species and vegetation development as well as 4) agricultural land-use with influences on landscape dynamics. Compared to the above mentioned 3D real-time environment, the learning environment implemented by Köllner (2009) offers

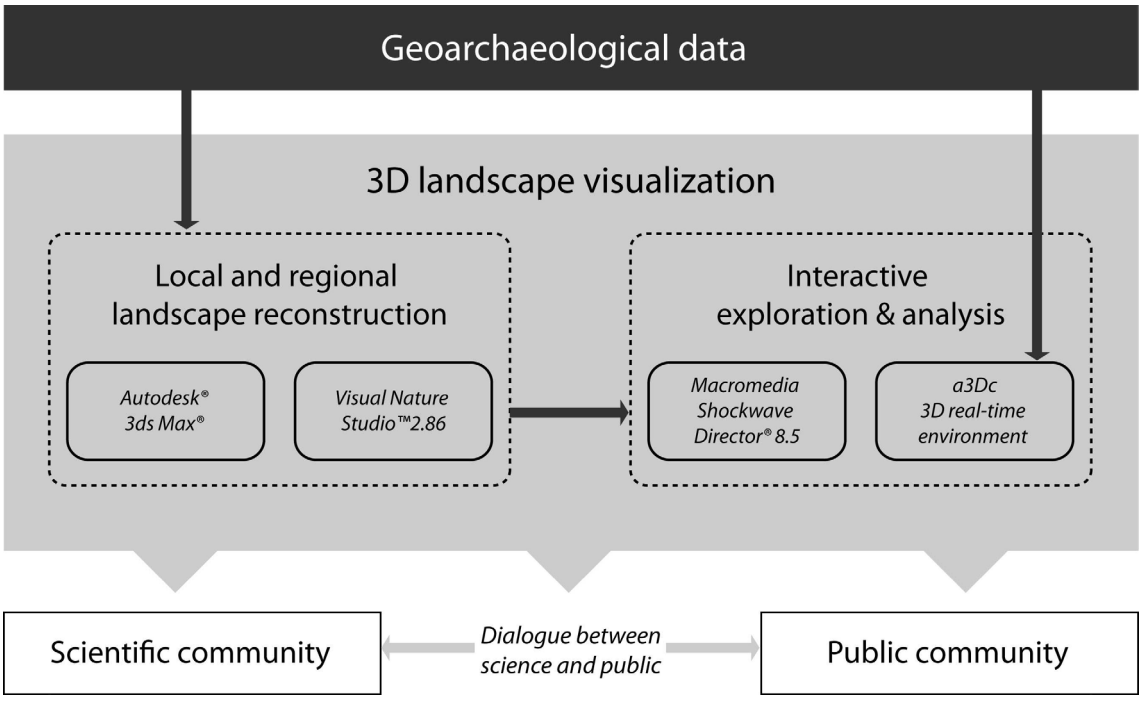

Figure 8.5: Visualization model

less interactivity in favour of a guided knowledge transfer. Therefore, the interactive learning environment developed in our project for public knowledge transfer enables the user to select topics according to his or her own interests.

Figure 8.5 summarizes the visualization model described above: Based on geoarchaeological data from field studies and lab analyses 3D landscape scenarios of different geographical scales – thus, different spatial and temporal resolution of the data – are created. Photorealistic 3D visualizations of past landscape changes and dune development are integrated in an interactive multimedia learning environment as well as in a3Dc, a web-based 3D real-time environment. The latter provides analysis functionalities and query of additional information on the original field and lab data and, thus, can improve scientific interpretation on landscape changes of the past. A communication of our research results to the general public is achieved via a learning environment that is aiming to support environmental education.

8.5 Summary

Within a PhD project on geoarchaeological reconstruction of aeolian landscapes, three 3D visualization software products were applied in order to visualize and, thus, communicate scientific results to the scientific community and the general public alike. Landscape visualizations for geoarchaeological purposes should overcome different geographical scales and levels of detail. For that reason, highly detailed, local 3D landscape reconstructions and also general scenarios of past landscape surface changes were realised. To enhance and support geoarchaeological interpretation and to facilitate the generation of knowledge on landscapes changes, a 3D real-time environment was implemented. In the visualization model, interactive data analysis, query, exploration and transparency represent the main advantages of real-time environment a3dc.

The combination of both offline and online rendering techniques allows a comprehensive visualization of geoarchaeological results and thus allows us to bridge different scientific requirements and the expectations of public users. Not only interdisciplinary critique on data records is promoted this way, but also a discourse on different 3D visualization results is supported. 3D visualization tools serve as communication instruments which are useful for the scientific community and informative for the general public alike. By integrating a multimedia learning platform, our visualization model contributes to science and public outreach as well as to environmental history education and may revive a constructive dialogue between researchers and the general public.

9 Conclusion

Landscape development and human-environmental interactions over the past ~ 2500 years have been in focus of the geoarchaeological research presented in this thesis. Using an inland dune landscape in Northern Germany as a case study, aspects of timing, causes and effects of human-initiated landscape changes were investigated in the context of wind-induced soil erosion and re-activation of sandy sediments. In the following paragraphs, the main conclusions and possible implications of this study are summarized.

In chapter 6 a chronology for the Holocene aeolian sedimentation of a northern-German inland dune sequence was established with high temporal and spatial resolution that is based on a multidisciplinary approach linking both ^{14}C and OSL dating techniques. In this study the effects of land degradation caused by medieval settlement and land-use expansion on the formation drift sand deposits could be quantified for the first time. The combination of a detailed chrono-stratigraphic approach, geospatial models and pollen records was able to show that widespread deforestation and intensification of agriculture in the research area led to an instant destabilization of the before stable surface, and to a subsequent onset of large Aeolian activity. Four phases of aeolian sedimentation of increasing magnitude have been identified and related to past regional settlement and land-use history. Human activities during the Roman Iron Age Period (~ 0–500 AD) had only low impact on the landscape, which resulted in the lowest sediment values and deposition rates (0.12 ± 0.02 t ha^{-1} a^{-1}). Since the Early Medieval period (~ 700 AD), intensification of land-use caused overexploitation of the land which, in turn resulted in rapid dune formation and the highest deposition rates (< 800 years for ~ 45 % of the total net sediment mass) found in the KHD record since the Late Pleistocene. The study demonstrates that the identified phases of increased Aeolian activity and results of quantification are in very good correlation with pollen records of the area. It could be highlighted that, in contrast to pollen records which may reflect indirectly degrading of environmental conditions, inland dunes may provide important, complementary archives for identifying landscape system thresholds and quantifying the effects of land overexploitation. Additionally, this study shows that medieval sediment reactivation is coincident with settlement abandonment and likely

to be its cause. The observed feedback structures of human-environmental interactions found to be cyclical: Due to poor land-use management in historic and recent times severe drifting of sand and the accumulation of dunes occurred, forcing the local farmers to abandon their field and even their settlement, and adapting more extensive land management practices (extensive grazing, afforestation). Our results may have implications on studies on aeolian sedimentation throughout the ESB that previously argued medieval settlement abandonment to be usually multicausal.

In chapter 7, past local vegetation and dune dynamics are reconstructed on the basis of an integrated approach that combines pollen analysis with wood analysis from soil charcoal and the geomorphological context of the deposits in which they are incorporated. The study shows that sandy deposits forming dunes serve as palaeoarchives and contain taxonomically identifiable wood charcoal. These can be used to obtain information on the occurrences of woody taxa, for the reconstruction of vegetation and dune dynamics. Due to various factors influencing the charcoal spectra, including particularly the reworking processes during the dune accumulation, the interpretation of the results is complicated. Therefore, an interdisciplinary collaboration is an essential basis, in this respect: Geomorphological work on dune formation makes these archives accessible through profiles, and provides stratigraphic hypotheses which can be cross-checked by the charcoal assemblages. This is supported by physical dating to establish a chronostratigraphy, which is then used to interpret the woody taxa occurrences through time. As a counterpart, vegetation and human activity trigger the dune development. For this reason, the knowledge about the causing processes is essential to comprehend former sedimentation events. In the case of the Joldelund dune complex previous archaeological and especially palaeobotanical analysis complete the picture. The two types of botanical records – pollen and charcoal – show some minor differences, which can be explained by the varying catchment areas, and the proportion of species in the records is linked to botanical factors like pollen production of single species. A further factor that should not be ignored is that charcoals in the dune context are mostly originating from fires caused by human beings. Even if no selection of wood for any purpose is reflected in our samples, actions to lighting a fire on special areas may affect our results. Despite this methodological subject, our results demonstrate the development of the dune area near to Joldelund. In contrast to the vegetation today (coniferous afforestation) the dune was formerly forested with a mixed deciduous oak forest. In times of human influences a heathland with Ericaceae developed. This implies, that a more precise landscape history scenario can be formulated based on this integrated approach compared to a single discipline approach.

On the basis of comprehensive geoarchaeological research, in chapter 8, a visualization model is established and is found to be suitable to meet the various expectations of different target groups such as the scientific and public communities. This

study finds that the combination of offline and online rendering techniques allows the creation of reliable scientific visualizations of palaeoenvironmental reconstructions that meet the challenge of different spatiotemporal resolutions inherent in the multiple data sets. Using the software Autodesk® 3ds Max® 8 and Visual Nature Studio™2.86, photo-realistic 3D visualizations of i) local vegetation history and dune development and ii) regional-scale scenarios of past environmental conditions were established. As pure visual presentations are lacking analytical and / or interactive functionalities, the visualization model was expanded to also include online rendering techniques, such as the 3D real-time environment a3Dc and a multimedia learning environment using Macromedia Shockwave Director® 8.5. Importantly, the a3Dc is found to permit the user to interactively analyse, query and explore the reconstructed virtual 3D landscape and to provide additional information on the geoarchaeological records on which landscape reconstruction is based. Not only interdisciplinary critique on data records is promoted this way, but also a discourse on different 3D visualization results is supported. The study concludes that 3D visualization tools serve as powerful communication instruments which are useful for the scientific community and informative for the general public alike. By integrating a multimedia learning platform, our visualization model contributes to science and public outreach as well as to environmental history education and may revive a constructive dialogue between researchers and the general public.

References 10

Abel, W. (1976): Die Wüstungen des ausgehenden Mittelalters. Stuttgart (Quellen und Forschungen zur Agrargeschichte 1). 3rd ed.

Adamiec, G. und Aitken, M. (1998): Dose-rate conversion factors: update. In: Ancient TL 16 (2), pp. 37–49.

AG Boden (2005): Bodenkundliche Kartieranleitung. Ad-Hoc-Arbeitsgruppe Boden der Staatlichen Geologischen Dienste und der Bundesanstalt für Geowissenschaften und Rohstoffe. Hannover. 5th ed.

Aitken, M. J. (1998): An introduction to optical dating: the dating of Quaternary sediments by the use of photon-stimulated luminescence. Oxford.

Aitken M. J. (1985): Thermoluminescence dating. Orlando.

Alisch, M. (1995): Das äolische Relief der mittleren Oberen Allerniederung (Ostniedersachsen): spät- und postglaziale Morphogenese, Ausdehnung und Festlegung historischer Wehsande, Sandabgrabungen und Schutzaspekte. Diss. Univ. Köln (Kölner Geographische Arbeiten 62).

Andresen, L. (1925): Bekämpfung des Flugsandes im 16. Jahrhundert. In: Die Heimat 35 (9), p. 213.

Andresen, L. (1924): Aus Nordschleswig. In: Die Heimat 34 (3), p. 76.

Appleton, K., A. Lovett, G. Sünnenberg and T. Dockerty (2002): Rural landscape visualisation from GIS databases: a comparison of approaches, options and problems. In: Computers Environment and Urban Systems 26 (2–3), pp. 141–162.

Bach, M. (2008): Äolische Stofftransporte in Agrarlandschaften: experimentelle Untersuchungen und räumliche Modellierung von Bodenerosionsprozessen durch Wind. Diss. Univ. Kiel.

Backer, S., W. Dörfler, M. Ganzelewski, A. Haffner, A. Hauptmann, H. Jöns, H. Kroll and R. Kruse (1992): Frühgeschichtliche Eisengewinnung und -verarbeitung am Kammberg bei Joldelund. Frühe Industrie oder bäuerliche Selbstversorgung? In: Müller-Wille, M. and D. Hoffmann, eds.: Der Vergangenheit auf der Spur: Archäologische Siedlungsforschung in Schleswig-Holstein. Neumünster, pp. 83–110.

Bateman, M. D. and S. P. Godby (2004): Late-Holocene inland dune activity in the UK: a case study from Breckland, East Anglia. In: The Holocene 14 (4), pp. 579–588.

Bateman, M. D. (1998): The origin and age of coversand in North Lincolnshire, United Kingdom. In: Permafrost and Periglacial Processes 9 (4), pp. 313–325.

Behre, K.-E. (2000a): Frühe Ackersysteme, Düngemethoden und die Entstehung der nordwestdeutschen Heiden. In: Archäologisches Korrespondenzblatt 30, pp. 135–151.

Behre, K.-E. (2000b): Der Mensch öffnet die Wälder: zur Entstehung der Heiden und anderer Offenlandschaften. In: Rundge-

spräche der Kommission für Ökologie der Bayrischen Akademie der Wissenschaften 18, pp. 103–116.

Behre, K.-E. (1995): Vom Naturraum zur Kulturlandschaft: 10.000 Jahre Umweltveränderungen durch den Menschen. Amsterdam.

Bender, O., H. J. Boehmer, D. Jens and K. P. Schumacher (2005): Using GIS to analyse long-term cultural landscape change in Southern Germany. In: Landscape and Urban Planning 70, pp. 111–125.

Beresford, M. and J. Hurst (1990): Wharram Percy. Deserted medieval village. New Haven.

Birks, H.H. and H. B. J. Birks (2000): Future uses of pollen analysis must include plant macrofossils. In: Journal of Biogeography 27 (1), pp. 31–35.

Blaser, A. D., M. Sester, M. and M. J. Egenhofer (2000): Visualization in an early stage of the problem-solving process in GIS. In: Computers & Geosciences, 26, pp. 57–66.

Blott, S. J. and Pye, K. (2001): GRADISTAT: a grain size distribution and statistics package for the analysis of unconsolidated sediments. In: Earth Sufaces, Processes and Landforms 26, pp. 1237–1248.

Boas, N. A. (1997): Settlements and fields covered by sand drift in the Bronze Age, Djursland, East Jutland. In: Internationale Archäologie 38, pp. 16–28.

Böse, M. (1991): A palaeoclimatic interpretation of frost-wedge casts and aeolian sand deposits in the lowlands between Rhine and Vistula in the Upper Pleniglacial and Late Glacial. In: Kozarski, S., ed.: Late Vistulian (=Weichselian) and Holocene aeolian phenomena in Central and Northern Europe. In: Zeitschrift für Geomorphologie, Supplement 90, pp. 15–28.

Boldt, K.-W., M. Lechner, M. Zeh and R. Glaser (2005): Virtuelle Realität in den Geowissenschaften: Interaktives E-Learning auf der Basis von Geodaten und photorealer 3D-Visualisierung. In: Kartographische Nachrichten 2, pp. 70–75.

Bork, H.-R. (2006): Landschaften der Erde unter dem Einfluss des Menschen. Darmstadt.

Bork, H.-R. (1983): Soil erosion, holocene and pleistocene soil development In: Bork, H.-R. and W. Ricken, eds.: Bodenerosion, holozäne und pleistozäne Bodenentwicklung: Soil Erosion, Holocene and Pleistocene Soil Development. Cremlingen (Catena Supplement 3).

Bork, H.-R., H. Bork, C. Dalchow, B. Faust, H.-P. Piorr and Th. Schatz (1998): Landschaftsentwicklung in Mitteleuropa: Wirkungen des Menschen auf Landschaften. Gotha.

Bork, H.-R., G. Schmidtchen and M. Dotterweich (2001): Die Wechselwirkungen zwischen Landnutzung und Bodenzerstörung in Mitteleuropa. In: Beiträge zur Siedlungsarchäologie und zum Landschaftswandel. Ergebnisse zweier Kolloquien in Regensburg, 9.-10. Oktober 2000, 2.-3. November 2000. DFG-Graduiertenkolleg 462 »Paläoökosystemforschung und Geschichte«. Regensburg (Regensburger Beiträge zur Prähistorischen Archäologie), pp. 43–55.

Borelli, P., P. Panagos, C. Ballabio, E. Lugato, M. Weynants and L. Montanarella (2016): Towards a pan-European assessment of land susceptibility to wind erosion. In: Land degradation and development 27, pp. 1093–1105.

Bowman, S. (1990): Radiocarbon dating. London (Interpreting the past 1).

Brande, A., M. Böse, M. Müller, M. Facklam and S. Wolters (1991): The Bliesendorf soil and aeolian sand transport in the Potsdam area. In: Schirmer, W., ed.: Dunes and fossil soils. Münster (GeoArchaeoRhein 3), pp. 147–161.

Bronk Ramsey, C., M. Dee, S. Lee, T. Nakagawa and R. A. Staff (2010): Developments

in the calibration and modeling of radiocarbon dates. In: Radiocarbon 52 (1–2), pp. 953–961.

Buhmann E. (2002): Using GIS for visualization of changing landscape of the brown coal mining areas at the building exhibition (IBA) Fuerst Pueckler Land. In: Buhmann E., U. Nothhelfer and M. Pietsch, eds.: Trends in GIS and virtualization in environmental planning and design: proceedings at Anhalt University of Applied Sciences. Heidelberg, pp. 48–54.

Bundesamt für Naturschutz (BfN) (2000): Karte der natürlichen Vegetation Europas. Bd. 3: Karten. Münster.

Butzer, K. W. (2008): Challenges for a cross-disciplinary geoarchaeology: the intersection between environmental history and geomorphology. In: Geomorphology 101 (1–2), pp. 402–411.

Buurman, P., P. Vidal-Torrado and V. M. Martins (2013): The podzol hydrosequence of Itaguaré (São Paulo, Brazil). 1. Geomorphology and Interpretation of Profile Morphology. In: Soil Science Society of America 77 (4), pp. 1294–1306.

Carcaillet, C. and M. Thinon (1996): Pedoanthracological contribution to the study of the evolution of the upper treeline in the Maurienne Valley (North French Alps): methodology and preliminary data. In: Review of Palaeobotany and Palynology 91 (1–4), pp. 399–416.

Carcaillet, C., P. J. H. Richard, H. Asnong, L. Capece and Y. Bergeron (2006): Fire and soil erosion history in East Canadian boreal and temperate forests. In: Quaternary Science Reviews 25, pp. 1489–1500.

Castel, I. Y. (1991): Late holocene eolian drift sands in Drenthe (the Netherlands). Amsterdem (Nederlandse Geografische Studies 133).

Castel, I. Y., E. Koster and R. Slotboom (1989): Morphogenetic aspects and age of late Holocene eolian drift sands in Northwest Europe. In: Zeitschrift für Geomorphologie 33, pp. 1–26.

Cheetam, M. D., A. F. Keene, W. D. Erskine, R. T. Bush, K. Fitzsimmons, G. E. Jakobsen and S. J. Fallon (2010): Resolving the holocene alluvial record in southeastern Australia using luminescence and radiocarbon techniques. In: Journal of Quaternary Science 25 (7), pp. 1160–1168.

Clausen, I. (1997): Neue Untersuchungen an späteiszeitlichen Fundplätzen der Hamburger Kultur bei Ahrenshöft, Kr. Nordfriesland (ein Vorbericht). In: Archäologische Nachrichten aus Schleswig-Holstein 8, pp. 8–49.

Cohan, K. M. and P. L. Gibbard (2012): Regional chronostratigraphical correlation table for the last 270,000 years. North Atlantic – Greenland – West, North, Central, Eastern Europe, Russia – Siberia (poster section, GSA 2012). URL: http://www.stratigraphy.org/upload/Quaternary_last270ka.pdf (Stand: 03.07.2016).

Cordier, S. (2010): Optically stimulated luminescence dating: procedures and applications to geomorphological research in France. In: Géomorphologie: relief, processus, environnement 16 (1), pp. 21–40.

Cornell, R. M. and U. Schwertmann (2003): The iron oxides: structure, properties, reactions, occurrences and uses. Weinheim. 2nd ed.

Dearing, J. A. (2006): Climate-human-environment interactions: resolving our past. In: Climate of the Past Discussions, European 2 (4), pp. 563–604.

Dearing, J. A. (1994): Reconstructing the history of soil erosion. In: Roberts, N., ed.: The changing global environment. Oxford, pp. 61–242.

De Boer, A. (2009): Creating realistic 3D GeoVEs of cultural landscapes using historical maps and drawings. In: De Maeyer, P., T. Neutens and M. De Ryck, eds.: Proceedings of the 4th international workshop on 3D geo-information. Ghent, pp. 63–68.

De Boer, W. M. (1995): Äolische Prozesse und Landschaftsformen im mittleren Baruther Urstromtal seit dem Hochglazial der Weichselkaltzeit. Berlin (Berliner Geographische Arbeiten 84)

De la Vega Leinert, A. C., D. H. Keen, R. L. Jones, J. M. Wells and D. E. Smith (2000): Mid-Holocene environmental changes in the Bay of Skaill, Mainland Orkney, Scotland: an integrated geomorphological, sedimentological and stratigraphical study. In: Journal of Quaternary Science 15 (5), pp. 509–528.

Delson, E.,I. Tattersall, J. A. van Couvering and A. S. Brooks, eds.(2000): Encyclopedia of Human Evolution and Prehistory. New York. 2nd ed.

Derese, C., D. Vandenberghe, N. Eggermont, J. Bastiaens,R. Annaert and P. van den haute (2010): A medieval settlement caught in the sand: Optical dating of sand-drifting at Pulle (N Belgium). In: Quaternary Geochronology 5, pp. 336–341.

Deutscher Wetterdienst (DWD) (2013): Orkantief CHRISTIAN am 28. Oktober 2013. Hintergrundberichte des Deutschen Wetterdienstes. URL: http://www.dwd.de/bvbw/generator/DWDWWW/Content/Oeffentlichkeit/KU/KU2/KU24/besondere__ereignisse__global/stuerme/20131028__CHRISTIAN__europa,templateId=raw,property=publicationFile.pdf/20131028_CHRISTIAN_europa.pdf (Stand: 8.10.2014).

de Vries, H. (1958): Variations in concentration of radiocarbon with time and location on earth (Proceedings of the Nederlandsche Akademie van Wetenschappen B61). Amsterdam, pp. 267–281.

Dierssen, K. (2004): Vegetation Schleswig-Holsteins. In: EcoSys Supplement 41, pp. 36–60.

Dörfler, W. (2003): Rural economy of the continental saxons from the Migration period to the tenth century. In: Green, D. H. and F. Siegmund, eds.: The continental Saxons from the Migration period to the tenth century: An ethnographic perspective. Woodbridge.

Dörfler, W. (2000): Palynologische Untersuchungen zur Vegetations- und Landschaftsentwicklung von Joldelund, Kr. Nordfriesland. In: Haffner, A., H. Jöns and J. Reichstein, eds.: Frühe Eisengewinnung in Joldelund, Kr. Nordfriesland. Ein Beitrag zur Siedlungs- und Technikgeschichte Schleswig-Holsteins. Teil 2: Naturwissenschaftliche Untersuchungen zur Metallurgie- und Vegetationsgeschichte. Universitätsforschungen zur prähistorischen Archäologie 59, pp. 147–208.

Dörfler, W. (1995): Versuch einer Modellierung des Energieflusses und des Rohstoffverbrauchs während der römisch-kaiserzeitlichen Eisenverhüttung in Joldelund, Ldkr. Nordfriesland. In: Probleme der Küstenforschung im südlichen Nordseegebiet 23, pp. 175–185.

Dörfler, W. and J. Wiethold (2000): Holzkohlen aus den Herdgruben von Rennfeueröfen und Siedlungsbefunden des spätkaiserzeitlichen Eisengewinnungs- und Siedlungsplatzes am Kammberg bei Joldelund, Kr. Nordfriesland. In: Haffner, A.,H. Jöns and J. Reichstein, eds.: Frühe Eisengewinnung in Joldelund, Kr. Nordfriesland. Ein Beitrag zur Siedlungs- und Technikgeschichte Schleswig-Holsteins. Teil 2: Naturwissenschaftliche Untersuchungen zur Metallurgie- und Vegetationsgeschichte. Universitätsforschungen zur prähistorischen Archäologie 59, pp. 217–262.

Dotterweich, M. (2008): The history of soil erosion and fluvial deposits in small catchments of central Europe: Deciphering the long-term interaction between humans and the environment: a review. In: Geomorphology, 101 (1–2), pp. 192–208.

Dotterweich, M. (2004): Vierdimensionale Landschaftsanalyse als Hilfsmittel zur Rekonstruktion früherer Umweltbedingungen in Franken: Auswirkungen und Rückkopplungsmechanismen historischer Landnutzung auf die Landschaft. In: Becker, H. and J. Ericsson, eds.: Mittelalterliche

Wüstungen im Steigerwald: Bericht über ein Symposium des Zentrums für Mittelalterstudien der Otto-Friedrich-Universität Bamberg am 3. Februar 2001. Bamberg (Bamberger Geographische Schriften, Sonderfolge 7), pp. 47–79.

Dotterweich, M. (2003a): Land use and soil erosion in northern Bavaria during the last 5000 years. In: Lang, A., K. Hennrich and R. Dikau, eds.: Long-term hillslope and fluvial system modelling. Concepts and Case studies from Rhine river catchment. Berlin, pp. 201–229.

Dotterweich, M. and S. Dreibrodt (2010): Past land use and soil erosion processes in central Europe. In: PAGES news 19 (2), pp. 49–51.

Dotterweich, M., A. Schmitt, H.-R. Bork, G. Schmidtchen (2003b): Jungholozäne Bodenerosion und Kerbenentwicklung im Wolfsgraben bei Bamberg. In: Bork, H.-R., G. Schmidtchen, M. Dotterweich, eds.: Bodenbildung, Bodenerosion und Reliefentwicklung im Mittel- und Jungholozän Deutschlands. Flensburg (Forschungen zur deutschen Landeskunde 253), pp. 129–164.

Dreibrodt, S., C. Lubos, B. Terhorst, B. Damm and H.-R. Bork (2010): Historical soil erosion by water in Germany: Scales and archives, chronology, research perspectives. In: Quaternary International 222, pp. 80–95.

Dreibrodt, S. and J. Wiethold (2015): Lake Belau and its catchment (northern Germany): A key archive of environmental history in northern central Europe since the onset of agriculture. In: The Holocene 25 (2), pp. 296–322.

Duller, G. A. T. (2015): Luminescence dating. In: Rink, W. J. and J. W. Thompson, eds.: Encyclopedia of scientific dating methods. Dordrecht.

Duller, G. A. T. (2008): Single-grain optical dating of Quarternary sediments: why aliquot size matters in luminescence dating. In: Boreas 37, pp. 589–612.

Duller, G.A.T. (2003): Distinguishing quartz and feldspar in single grain luminescence measurements. In:Radiation Measurements 37, pp. 161–165.

Duller, G. A. T. (2001): Equivalent dose determination using single aliquots. In: Nuclear Tracks and Radiation Measurements 18, pp. 371–378.

Duttmann, R., H. Fleige, R. Horn and M. Bach (2004): Landschafts- und Bodenentwicklung im Raum Goldelund (Schleswiger Geest) unter Berücksichtigung der Winderosion. In: EcoSys Supplement 41, pp. 131–151.

Duttmann, R., M. Bach, R. Fleige (2006): Landscape development and land management practises on light soils in the Northwest of Schleswig-Holstein / Germany: the region of »Goldelund« as an example. In: Horn, R., H. Fleige and S. Peth: Soil and landuse management systems in Schleswig-Holstein (Germany): Guide of ISTRO Excursion 2006. Kiel (Schriftenreihe des Instituts für Pflanzenernährung und Bodenkunde, 72), pp.2–11.

Duttmann, R., M. Bach, K. Krüger, H. Fleige, S. Gebhardt, P. Hartmann and R. Horn (2006): Soil forming processes and land management practices on light soils in the Northwest of Schleswig-Holstein. In: Horn, R., H. Fleige and S. Peth, eds.: Soils and Landuse Mangement Systems in Schleswig-Holstein (Germany): Guide of ISTRO Excursion 2006. Kiel (Schriftenreihe des Instituts für Pflanzenernährung und Bodenkunde Universität Kiel 72), pp. 1–32.

Duttmann, R., R. Gabler-Mieck and U. Lungershausen (2012): Landscape visualisation – Approaches and applications. In: Farsang, A., L. Musci and I. Keveiné Bárány, eds.: Táj – Érték, lépték, változás. Szeged, pp. 85–96.

Erlenkeuser, H., H. Willkomm, I. B. Wagner and G. A. Wagner (1997): Naturwissenschaftliche Datierungsmethoden. In: Jöns, H., ed.: Frühe Eisengewinnung in Joldelund, Kr. Nordfriesland: Ein Beitrag zur Sied-

lungs- und Technikgeschichte Schleswig-Holsteins. Teil 1: Einführung, Naturraum, Prospektionsmethoden und archäologische Untersuchungen. Bonn (Universitätsforschungen zur prähistorischen Archäologie 40), pp. 197–221.

Faegri, K. and J. Iversen (1989): Textbook of Pollen Analysis. Chichester. 4th ed.

Fleige, H., P. Hartmann, R. Duttmann, M. Bach, S. Gebhardt, R. Horn and K. Krüger (2006): Soils of the sandur plain (»Lower Geest« in the Northwest of Schleswig-Holstein / Germany: the region of »Goldelund« as an example. In: Horn, R., H. Fleige and S. Peth, eds.: Soils and Landuse Mangement Systems in Schleswig-Holstein (Germany): Guide of ISTRO Excursion 2006. Kiel (Schriftenreihe des Instituts für Pflanzenernährung und Bodenkunde Universität Kiel 72), pp. 12–19.

Folk, R. L. and W. C. Ward (1957): Brazos River bar: a study in the significance of grain size parameter. In: Journal of Sedimentary Petrology 27, pp. 3–26.

Foster, I. D. L., T. M. Mighall, C. Wotton, P. N. Owens, D. E. Walling (2000): Evidence for medieval soil erosion in the South Hams region of Devon, UK. In: Holocene 10, pp. 261–271.

Fouache, E. (2013): The Geoarchaeological Approach. In: Corsi, C., B. Slapšak and F. Vermeulen, eds.: Good Practice in Archaeological Diagnostics. Cham, pp. 245–252.

Fränzle, O. (2004): Reliefentwicklung und Bodenbildung in Schleswig-Holstein. In: EcoSys Supplement – Beiträge zur Ökosystemforschung 41, pp. 11–35.

Fränzle, O. (1988): Glaziäre, periglaziäre und marine Reliefentwicklung im nördlichen Schleswig-Holstein. In: Schriften des Naturwissenschaftlichen Vereins für Schleswig-Holstein 58, pp. 1-30.

Fränzle, O. (1985): Erläuterungen zur geomorphologischen Karte 1: 100 000 der Bundesrepublik Deutschland. GMK 100, Blatt 7, C 1518 Husum. Berlin.

Franco-Múgica, F., M. García-Antón, J. Maldonado-Ruiz, C. Morla-Juaristi, H. Sainz-Ollero (2005): Ancient pine forest on inland dunes in the Spanish northern meseta. In: Quaternary Research 63, pp. 1–14.

Fuest R. and M. Schnirch (2003): Visualization of vegetation Dynamics During the Holocene Period for Educational Purposes. In: Buhmann, E. and S. Erwin, ed.: Trends in landscape modeling: proceedings of the Anhalt University of Applied Sciences. Heidelberg, pp. 56–65.

Gabler-Mieck, R. and R. Duttmann (2007): Application of geovisualisation techniques in coastal zone management. In: Wachowicz, M. and L. Bodum, eds.: The European Information Society: leading the way with geoinformation: proceedings 10th AGILE International Conference on Geographic Information Science. Aalborg, pp. 1–13.

García-Hidalgo, J. F., J. Temiño and M. Segura (2007): Holocene aeolian development in Central Spain: chronology, regional correlations and causal processes. In: Quaternary Science Reviews 26, pp. 2661–2673.

Gavin, D. G., L. B. Brubaker, K. P. Lertzman (2003): An 1800-year record of the spatial and temporal distribution of fire from the west coast of Vancouver Island, Canada. In: Canadian Journal of Forest Research 33, pp. 573–586.

Gavin, D. G. (2001): Estimation of inbuilt age in radiocarbon ages of soil charcoal for fire history studies. In: Radiocarbon 43 (1), pp. 22–44.

Gerstengarbe, F.-W. and P. C. Werner (2005): Katalog der Großwetterlagen Europas (1881–2004) nach Paul Hess und Helmut Brezowsky. Potsdam. 6th ed.

Geyh, M. A. and H. Schleicher (1990): Absolute age determination: physical and chemical dating methods and their applications. Heidelberg.

Ghilardi, M. and S. Desruelles (2009): Geoarchaeologoy: where human, social

and earth sciences meet with technology. In: Surveys And Perspectives Integrating Environment & Society 2 (2). URL: http://sapiens.revues.org/422 (Stand: 03.07.2016).

Godwin, H. (1962): Half-life of radiocarbon. In: Nature 195, p. 984.

Goldberg, P. and R. I. Macphail (2006): Practical and theoretical geoarchaeology. Oxford.

Goossens, D., J. Gross and W. Spaan (2001): Aeolian dust dynamics in agricultural land areas in lower Saxony, Germany. In: Earth Surface Processes and Landforms 26 (7), pp. 701–720.

Gripp, K. (1967): Flugsand, Dünen, Vorgeschichte. In: Fundamenta 2, pp. 228–243.

Grootes, P. M., M.-J. Nadeau and A. Rieck (2004): 14C-AMS at the Leibniz-Labor: radiometric dating and isotope research. In: Nuclear Instruments and Methods in Physics Research B 223–224, pp. 55–61.

Grube, A. (2016): Das Binnendünengebiet Halloh-Latendorf (südlich Boostedt, mittleres Schleswig-Holstein): interglaziale und -stadiale Ablagerungen sowie oberholozäne Dünendynamik. In: Zeitschrift der deutschen Gesellschaft für Geowissenschaften 167 (1), pp. 33–47.

Haesaerts, P., I. Borziac, V. P. Chekha, V. Chirica, N. M. Drozdov, L. Koulakovska, L. A. Orlova, J. van der Plicht and F. Damblon (2010): Charcoal and wood remains for radiocarbon dating Upper Pleistocene loess sequences in Eastern Europe and Central Siberia. In: Palaeogeography, Palaeoclimatology, Palaeoecology 291 (1-2), pp. 106–127.

Hamerow, H. (2003): Early Medieval settlements: the archaeology of rural communities in Northwest Europe 400–900. Oxford.

Hannesen, H. (1959): Die Agrarlandschaft der Schleswig-Holsteinischen Geest und ihre neuzeitliche Entwicklung. Kiel (Schriften des Geographischen Instituts der Universität Kiel 17,3).

Hansen, R. and W. Jessen, eds. (1904): Quellen zur Geschichte des Bistums Schleswigs. Kiel (Quellensammlung der Gesellschaft für Schleswig-Holsteinische Geschichte 6).

Hase, W. (1981): Beiträge zur Geschichte der Forstverwaltung in Schleswig-Holstein. Kiel.

Hassenpflug, W. (2011): Maisanbau und Bodenverwehung in Schleswig-Holstein im Frühjahr 2011. In: Natur- und Landeskunde. Zeitschrift für Schleswig-Holstein, Hambung und Mecklenburg 10–12, pp. 137–148.

Hassenpflug, W. (1998): Bodenerosion durch Wind. In: Richter, G., ed.: Bodenerosion. Analyse und Bilanz eines Umweltproblems. Darmstadt, pp. 69–682.

Hassenpflug, W. (1981): Die Flächen- und Mengenbilanz eines Sandsturmes auf der Schleswiger Geest: eine Abschätzung aus Luftbildern. In: Mitteilungen der Deutschen Bodenkundlichen Gesellschaft 30, pp. 335–340.

Hassenpflug, W. (1971): Sandverwehung und Windschutzwirkung im Luftbild. In: Jahrbuch für die Schleswigsche Geest 19, pp. 19–30.

Hilgers, A. (2007): The chronology of Late Glacial and Holocene dune development in the northern Central European lowland reconstructed by optically stimulated luminescence (OSL) dating. Diss. Univ. Köln.

Hingst, H. (1975): Ein Faustkeil aus Joldelund, Kr. Nordfriesland. In: Archäologisches Korrespondenzblatt 5 (1), pp. 5–9.

Hinz, H. (1949): Hyoldelunt deserta. Über das Schicksal einer mittelalterlichen Siedlung. In: Die Heimat 56, pp. 177–179.

Hoek, W.Z. (2001): Vegetation response to the w14.7 and w11.5 ka cal. BP climate transitions: is vegetation lagging climate? In: Global and Planetary Change 30 (1), pp. 103–115.

Hoek, W. Z. and S. J. P. Bohncke (2002): Climatic and environmental events over the Last Termination, as recorded in the

Netherlands. In: Netherlands Journal of Geosciences 81 (1), pp. 123–138.

Hoesel, A. van, W. Z. Hoek, F. Braadbaart, J. van der Plicht, G. M. Pennock and M. R. Drury (2012): Nanodiamonds and wildfire evidence in the Usselo horizon postdate the Allerød-Younger Dryas boundary. In: Proceedings of the National Academy of Sciences of the United States of America 109 (20), pp. 7648–7653.

Hooke, R. L. (2000): On the history of humans as geomorphic agents. In: Geology 28 (9), pp. 843–846.

Huntley, D. J., D. I. Godfrey-Smith and M. L. W. Thewalt (1985): Optical dating of sediments. In: Nature 313, pp. 105–107.

IUSS Working Group WRB (2015): World Reference Base for Soil Resources 2014. Update 2015. International soil classification system for naming soils and creating legends for soil maps. Rom (World Soil Resources Reports 106).

Ivester, A. H. and D. S. Leigh (2003): Riverine dunes on the Coastal Plain of Georgia, USA. In: Geomorphology 51, pp. 289–311.

Iversen, J. (1954): The late-glacial flora of Denmark and its relation to climate and soil. In: Danmarks Geologiske Undersøgelser 2 (80), pp. 87–119.

Iwersen, J. (1953): Windschutz in Schleswig-Holstein. Aufgezeigt am Beispiel der schleswigschen Geest. Schleswig (Gottorfer Schriften zur Landeskunde Schleswig-Holsteins 2).

James, A. (2013): Legacy sediment: definitions and processes of episodically produced anthropogenic sediment. In: Anthropocene 2, pp. 16–26.

Janetzko, P. and B. Burbaum (2000): Bodenentwicklung auf quartären Substraten: mit Beiträgen zu Bodenkartierung und Bodenschutz in Schleswig-Holstein. In: Brandenburgische Geowissenschaftliche Beiträge 7 (1/2), pp. 73–81.

Jansen, D., U. Lungershausen, V. Robin, Y. Dannath and O. Nelle (2013): Wood charcoal from an inland dune complex at Joldelund (Northern Germany): information on Holocene vegetation and landscape changes. In: Quaternary International 289, pp. 24–35.

Jatho, G. (1969): Flugsandbildungen im Bereich der Soholmer Au. Diss. Univ. Kiel.

Jöns, H. (1997): Frühe Eisengewinnung in Joldelund, Kr. Nordfriesland: ein Beitrag zur Siedlungs- und Technikgeschichte Schleswig-Holsteins. Teil 1: Einführung, Naturraum, Prospektionsmethoden und archäologische Untersuchungen. Bonn (Universitätsforschungen zur prähistorischen Archäologie 40).

Jöns, H. (1992): Archäologische Forschungen am Kammberg. In: Müller-Wille, M. and D. Hoffmann, eds.: Der Vergangenheit auf der Spur: archäologische Siedlungsforschung in Schleswig-Holstein. Neumünster, pp. 93–100.

Kääb, A., Y. Isakowski, F. Paul and A. Neumann (2003): Glaziale und periglaziale Prozesse: von der statischen zur dynamischen Visualisierung. In: Kartographische Nachrichten 53, pp. 206–212.

Kaiser, K., A. Hilgers, N. Schlaak, M. Jankowski, P. Kühn, S. Bussemer and K. Przegietka (2009): Palaeopedological marker horizons in northern central Europe: characteristics of Lateglacial Usselo and Finow soils. In: Boreas 38, pp. 591–609.

Kaiser, K. and I. Clausen (2005): Palaeopedology and stratigraphy of the Late Palaeolithic Alt Duvenstedt site, Schleswig-Holstein (Northwest Germany). In: Archäologisches Korrespondenzblatt 35, pp. 1–20.

Kaiser, K., T. Schoknecht, W. Janke, K. Kloss and B. Prehn (2002): Geomorphologische, palynologische und archäologische Beiträge zur holozänen Landschaftsgeschichte im Müritzgebiet (Mecklenburg-Vorpommern). In: Eiszeitalter und Gegenwart 51, pp. 15–32.

Kaiser, K., H.-P. Mühmel-Horn and M. Walther (1989): Spätglaziale und holozäne Dünen im Rendsburger Staatsforst beiderseits des mittleren Sorgetales zwischen Tetenhusen/Föhrden und Krummenort (Schleswig-Holstein). In: Meyniana 41, pp. 97–152.

Kasse, C. (2002): Sandy aeolian deposits and environment and their relationship to climate during the Last Glacial Maximum in northwest and central Europe. In: Progress in Physical Geography 26 (4), pp. 507–532.

Kasse, C. (1999): Late pleniglacial and late glacial aeolian phases in the Netherlands. In: Schirmer, W., ed.: Dunes and fossil soils. Münster (GeoArchaeoRhein 3), pp. 61–82.

Kasse, C. (1997): Cold-climate aeolian sand-sheet formation in North-Western Europe (c. 14±12.4 ka):a response to permafrost degradation and increased aridity. In: Permafrost and Periglacial Processes 8, 295–311.

Keen-Zebert, A. (2015): Luminescence, fluvial sediments. In: Rink, W. J. and J. W. Thompson, eds.: Encyclopedia of scientific dating methods. Dordrecht, pp. 465–469.

Keit, E., K. Mothes (1942): Pollen- und Holzkohlenanalysen alter Waldhorizonte der Kurischen Nehrung. In: Botanisches Archiv 44 (2), pp. 155–171.

Köllner, S. (2009): Application of 3D-geovisualisation-techniques for environmental education at the example of a nature trail (Joldelund, Northern Germany). Diploma thesis (unpublished), Univ. Kiel (Department of Geography).

Kolstrup, E. (2007): OSL dating in palaeoenvironmental reconstructions: a discussion from a user's perspective. In: Estonian Journal of Earth Sciences 56 (3), pp. 157–166.

Kolstrup, E. (2005): Periglacial geomorphology. In: Koster, E. A., ed.: The physical geography of Western Europe. Oxford, pp. 75–92.

Kolstrup, E. (1991): Danish Weichselian and Holocene aeolian deposits and their environment: a preliminary account. In: Kozarski, S., ed.: Late Vistulian (=Weichselian) and Holocene aeolian phenomena in Central and Northern Europe (Zeitschrift für Geomorphologie, Suppl. 90), pp. 89–97.

Koorevaar, P., G. Menelik and C. Dirksen (1983): Elements of Soil Physics. Development in Soil Science 13, Amsterdam. 3rd ed.

Koster, E. A. (2005): The physical geography of Western Europe. Oxford.

Koster, E. A. (1988): Ancient and modern cold-climate aeolian sand deposition: review. In: Journal of Quaternary Science 3 (1), pp. 69–83.

Koster, E. A. (1982): Terminology and lithostratigraphic division of (surficial) sandy eolian deposits in the Netherlands: an evaluation. In: Geologie en Mijnbouw 61, pp. 121–129.

Koster, E.A., I. I.Y. Castel, R. L. Nap (1993): Genesis and sedimentary structures of late Holocene aeolian drift sands in northwest Europe. In: Pye, K., ed.: The dynamics and environmental context of aeolian sedimentary systems. London (Geological Society Special Publication 72), pp. 247–267.

Koster, E. A. (2005): The Physical Geography of Western Europe. Oxford.

Koster, E. A. (2010): Origin and development of Late Holocene drift sands: geomorphology and sediment attributes. In: Fanta, J. and H. Siepel, eds.: Inland drift sand landscapes. Zeist, pp. 25–48.

Kowalkowski, A., B. Nowaczyk and I. Okuniewska-Nowaczyk (1991): Chronosequence of biogenic deposits and fossil soils in the dune near Jasien, Western Poland. In: Schirmer, W., ed.: Dunes and fossil soils. Münster (GeoArchaeoRhein 3), pp. 107–125.

Kozarski, S. and B. Nowaczyk (1991): Lithofacies variation and chronostratigraphy of Late Vistulian and Holocene aeolian phenomena in north-western Poland. In: Kozarski, S., ed.: Late Vistulian (=Weich-

selian) and Holocene aeolian phenomena in Central and Northern Europe (Zeitschrift für Geomorphologie, Suppl. 90), pp. 107–22.

Kramer, W. (2007): 3D-Terrainmodelle in der Anwendung am archäologischen Großdenkmal Danewerk. In: Berichte zur deutschen Landeskunde 81 (1), pp. 79–85.

Küster, M., A. Fülling, K. Kaiser and J. Ulrich (2014): Aeolian sands and buried soils in the Mecklenburg Lake District, NE Germany: Holocene land-use history and pedo-geomorphic response. In: Geomorphology 211, pp. 64–76.

Kuntze, H. (1988): Bodenkunde. Stuttgart. 4th ed.

Landesamt für Landwirtschaft, Umwelt und ländliche Räume des Landes Schleswig-Holstein (LLUR) (ed.) (2011): Winderosion in Schleswig-Holstein: Kenntnisse und Erfahrungen über Bodenverwehungen und Windschutz. Flintbek (LLUR SH. Geologie u. Boden 15).

Landesamt für Landwirtschaft, Umwelt und ländliche Räume des Landes Schleswig-Holstein (LLUR), ed. (2012): Winderosion in Schleswig-Holstein: Kenntnisse und Erfahrungen über Bodenverwehungen und Windschutz. Flintbek (LLUR SH. Geologie u. Boden 11).

Landesvermessungsamt Schleswig-Holstein and J. Newig (1982): Karte des Herzogtums Schleswig: topographische Aufnahme, vorwiegend aus dem letzten Viertel des 18. Jahrhunderts: zusammengetragen und gezeichnet in den Jahren 1804 und 1805 von H. du Plat mit Hilfe der Lieutnants Ferd. Bauditz. Teil 4: Bredstedt, Wyk auf Föhr. Maßstab: 1:100.000. Kiel.

Lang, A. (2003): Phases of soil erosion-caused colluviation in the loess hills of South Germany. In: Catena 51, pp. 209–221.

Lang, A. and H.-R. Bork (2006): Past Soil erosion in Europe. In: Boardman, J. and J. Poesen, eds.: Soil erosion in Europe. Chichester, pp. 465–478.

Lange, E. (2002): Visualization in Landscape Architecture and Planning – Where we have been, where we are now and where we might go from here. In: Buhmann, E., U. Nothhelfer and M. Pietsch, eds.: Trends in GIS and Virtualization in Environmental Planning and Design. Proceedings at Anhalt University of Applied Science. Heidelberg, pp. 8–18.

Lange, E. (2001): Prospektive 3D-Visualisierung der Landschaftsentwicklung als Grundlage für einen haushälterischen Umgang mit der Ressource Landschaft. In: Natur und Landschaft 76, pp. 513–519.

Larsen, A., H.-R.Bork, A. Fuelling, M. Fuchs, J. R.Larsen (2013): The processes and timing of sediment delivery from headwaters to the trunk stream of a Central European mountain gully catchment. In: Geomorphology 201, pp. 215–226.

Leopold, M. and J. Völkel (2006): Colluvium: definition, differentiation, and possible suitability for reconstructing Holocene climate data. In: Quaternary International 162–163, pp. 133–140.

Leshner, A. (2003): Public engagement with science. In:Science 299, p. 977.

Lewis, J. L. and S. R. J. Sheppard (2006): Culture and communication: can landscape visualization improve forest management consultation with indigenous communities? In: Landscape and Urban Planning 77, pp. 291–313.

Leys, J. F. (1999): Wind erosion on agricultural land. In: Goudie, A. S., I. Livingstone, S. Stokes, eds.: Aeolian environments, sediments and landforms. Chichester, pp. 143–166.

Li, B., S.-H. Li and A. G. Wintle (2008): Overcoming environmental dose rate changes in luminescence dating of waterlain deposits. In: Geochronometria 30, pp. 33–40.

Libby, W. F. (1955): Radiocarbon dating. Chicago. 2nd ed.

Liritzis, I., A. K. Singhvi, J. K. Feathers, G. A. Wagner, A. Kadereit, N. Zacharias and

S.-H. Li (2013): Luminescence dating in archaeology, anthropology, and geoarchaeology. An overview. Cham.

Litt, T., K.-E. Behre, K.-D. Meyer, H.-J. Stephan and S. Wansa (2007): Stratigraphische Begriffe für das Quartär des norddeutschen Vereisungsgebietes. In: E&G. Eiszeitalter und Gegenwart. Quaternary Science Journal 56 (1–2), pp. 7–65.

Livingstone, I. and A. Warren (1996): Aeolian geomorphology: an introduction. Boston.

Loope, W. L. and A. F. Arbogast (2000): Dominance of an ~150-Year Cycle of Sand-Supply Change in Late Holocene Dune-Building along the Eastern Shore of Lake Michigan. In: Quaternary Research 54, pp. 414–422.

Lowe, J. J. and M. J. C. Walker (1997): Quaternary environments. London. 2nd ed.

Ludemann, T., H.-G. Michiels and W. Nölken (2004): Spatial patterns of past wood exploitation, natural wood supply and growth conditions: indications of natural tree species distribution by anthracological studies of charcoal-burning remains. In: European Journal of Forest Research 123, pp. 283–292.

Lüning, J. (1996): Anfänge und frühe Entwicklung der Landwirtschaft im Neolithikum (5500–2200 v. Chr.). In: Lüning, J., A. Jockenhövel, H. Bender and T. Capelle, eds.: Deutsche Agrargeschichte: Vor- und Frühgeschichte. Stuttgart, pp. 15–139.

Lungershausen, U., C. Heinrich, R. Duttmann and R. Gabler-Mieck (2013): Turning human-nature interactions into 3D landscape scences: An approach to communicate geoarchaeological reseach. In: Kartographische Nachrichten. Journal of Cartography and Geographic Information 63 (5), pp. 269–275.

Mager, F. (1930): Die Entwicklungsgeschichte der Kulturlandschaft des Herzogtums Schleswig in historischer Zeit. Bd. 1: Entwicklungsgeschichte der Kulturlandschaft auf der Geest und im östlichen Hügelland des Herzogtums Schleswig bis zur Verkoppelungszeit. Breslau (Veröffentlichungen der Schleswig-Holsteinischen Universitätsgesellschaft 25; Schriften der Baltischen Kommission zu Kiel 17).

Mallik, A. U. (1995): Conversion of temperate forests into heaths: role of ecosystem disturbance and ericaceous plants. In: Environmental Management 19 (5), 675–684.

Manikowska, B. (1991): Vistulian and Holocene aeolian activity, pedostratigraphy and relief evolution in Central Poland. In: Kozarski, S., ed.: Late Vistulian (=Weichselian) and Holocene aeolian phenomena in Central and Northern Europe (Zeitschrift für Geomorphologie, Supplement 90), pp. 131–142.

Marcucci, D. J. (2000): Landscape history as a planning tool. Landscape and Urban Planning 49, pp. 67–81.

Mauz, B., T. Bode, E. Mainz, H. Blanchard, W. Hilger, R. Dikau and L. Zöller (2002): The luminescence dating laboratory at the University of Bonn: equipment and procedures. In: Ancient TL 20 (2), pp. 53–61.

Mauz, B. and A. Lang (2004): Removal of the feldspar-derived luminescence component from poloymineral fine silt samples for optical dating applications: evaluation of chemical treatment protocols and quality control procedures. In: Ancient TL 22, pp. 1–8.

Mauz, B., W. Hilger, M. J. Müller, L. Zöller and R. Dikau (2005): Aeolian activity in Schleswig-Holstein (Germany): landscape response to Late Glacial climate change and Holocene human impact. In: Zeitschrift für Geomorphologie 49 (4), pp. 417–431.

Mazier, F., G. Galop, C. Brun and A. Buttler (2006): Modern pollen assemblages from grazed vegetation in the western Pyrenees, France: a numerical tool for ore precise reconstruction of past cultural landscapes. The Holocene 16 (1), pp. 91–103.

McLure, J. T. and G. H. Griffiths (2002): Historic landscape reconstruction and vi-

sualisation, West Oxfordshire, England. In: Transaction in GIS 61 (1), pp. 69–78.

Mehra, O. P. and M. L. Jackson (1960): Iron oxide removal from soils and clays by a dithionite-citrate system buffered with sodium bicarbonate. In: Clays and Clay Minerals 7, pp. 317–327.

Mejdahl, V. (1979): Thermoluminescence dating: beta-dose attenuation in quartz grains. In: Archaeometry 21, pp. 61–72.

Mejdahl, V. and H. H. Christiansen (1994): Procedures used for luminescence dating of sediments. In: Quaternary Science Reviews 13, pp. 403–406.

Meynen, E. and J. Schmithüsen (1953–1962): Handbuch der Naturräumlichen Gliederung Deutschlands. Bad Godesberg.

Mikkelsen, J. H., R. Langohr and R. I. Macphail (2007): Soilscape and land-use evolution related to drift sand movements since the Bronze Age in Eastern Jutland, Denmark. In: Geoarchaeology: An International Journal 22 (2), pp. 155–179.

Ministerium für Energiewende, Landwirtschaft, Umwelt und ländliche Räume (MLUR) (2013): Bilanz der Sturmschäden in den Wäldern: Es gilt weiter ein Betretungsverbot im Norden Schleswig-Holsteins. Pressetext vom 01.11.2013, 13:25 Uhr. URL: http://www.schleswig-holstein.de/MELUR/DE/Service/Presse/PI/2013/1113/MELUR_131101_Waldschaeden.html (Stand: 8.10.2014).

Mortensen, M.F., H. H. Birks, C. Christensen, J. Holm, N. Noe-Nygaard, B. Vad Odgaard, J. Olsen and K. L. Rasmussen (2011): Late Glacial vegetation development in Denmark: new evidence based on macrofossils and pollen from Slotseng, a small-scale site in souther Jutland. In: Quaternary Science Review 30 (19–20), pp. 2534–2550.

Müller, M. J. (2000): Altersbestimmung an schleswig-holsteinischen Binnendünen mit Hilfe von Paläoböden. In: Trierer Bodenkundliche Schriften 1, pp. 23–31.

Müller, M. J . (1999): Genese und Entwicklung schleswig-holsteinischer Binnendünen. In: Berichte zur deutschen Landeskunde 73, pp. 129–150.

Murray, A. S. and J. M. Olley (2002): Precision and accuracy in the optically stimulated luminescence dating of sedimentary quartz: a status review. In: Geochronometria 21, pp. 1–16.

Nadeau, M.-J. , P. M. Grootes, M. Schleicher, P. Hasselberg, A. Rieck and M. Bitterling (1998): Sample throughput and data stability at the Leibniz-Labor AMS facility. In: Radiocarbon 40, pp. 239–245.

Nadeau, M.-J., M. Schleicher, P. M. Grootes, H. Erlenkeuser, A. Gottdang, D. J. W. Mous, J. M. Sarnthein and H. Willkomm (1997): The Leibniz-Labor AMS facility at the Christian-Albrechts-University, Kiel, Germany. In: Nuclear Instruments and Methods in Physics Research Section B 123 (1–4), pp. 22–30.

Nelle, O. (2003): Woodland history of the last 500 years revealed by anthracological studies of charcoal kiln sites in the Bavarian Forest, Germany. In: Phytocoenologia 33 (4), pp. 667–682.

Nelle, O. (2002): Charcoal burning remains and forest stand structure: examples from the Black Forest (south-west Germany) and the Bavarian Forest (south-east Germany). In: Thiébault, S., ed.: Charcoal analysis. Methodological approaches, palaeoecological results and wood uses. Proceedings 2nd International Meeting of Anthracology, Paris, Sept. 2000. Oxford (BAR International 1063), pp. 201–207.

Nelle, O. and W. Dörfler (2008): A summary of the Late- and Post-glacial vegetation history of Schleswig-Holstein. In: Dengler, J., C. Dolnik and M. Trepel, eds.: Flora, vegetation, and nature conservation from Schleswig-Holstein to South America – Festschrift for Klaus Dierßen on occasion of his 60th birthday. Kiel (Mitteilungen der Arbeitsgemeinschaft Geobotanik in Schleswig-Holstein und Hamburg 65), pp. 45–68.

Nelle, O., S. Dreibroth and Y. Dannath (2010): Combining pollen and charcoal: evaluating Holocene vegetation composition and dynamics. In: Journal of Archaeological Science 37, pp. 2126–2135.

Nelle, O., V. Robin and B. Talón (2013): Pedoanthracology: analysing soil charcoal to study Holocene palaeoenvironments. In: Quaternary International 289, pp. 1–4.

Nelson, D.W. and L. E. Sommers (1996): Total carbon, organic carbon and organic matter. In: Sparks, D. L., A. L. Page, P. A. Helmke and R. H. Loeppert, eds.: Methods of soil analysis Part 3: Chemical methods. Madison (Soil Sciences Society of America Book Series 5.3), pp. 961–1010.

Nicolay, A., A. Raab, Th. Raab, E. Bönisch, and A. S. Murray (2014): Evidence of (pre)historic to modern landscape and land use history near Jänschwalde (Brandenburg, Germany). In: Zeitschrift für Geomorphologie 58 (2), pp. 7–32.

Nielsen, M. (1981): Die vollständige Begrünung von Joldelund und der Schleswigschen Geest. Unveröffentlichtes Manuskript, Joldelund.

Nielsen, M. (1978): Der Waldlehrpfad in der »Joldelunder Schweiz«. In: Jahrbuch für die Schleswigsche Geest 26, pp. 39–46.

Nielsen, M. (1972): Joldelund einst und jetzt. In: Jahrbuch für die Schleswigsche Geest 20, pp. 103–109.

Nielsen, M. (1970): Der Gemeindewald von Joldelund. In: Jahrbuch für die Schleswigsche Geest 18, pp. 66–72.

Niller, H.-P. (1998): Prähistorische Landschaften im Lößgebiet bei Regensburg-Kolluvien, Auenlehme und Böden als Archive der Paläoumwel. Regensburg (Regensburger Geographische Schriften 31).

Ohlson, M. and E. Tryterud (2000): Interpretation of the charcoal record in forest soils: forest fires and their production and deposition of macroscopic charcoal. In:The Holocene 10, pp. 519–525.

Orland, B., K. Budthimedhee and J. Uusitalo (2001): Considering virtual worlds as representations of land-scape realities and as tools for landscape planning. In: Landscape and Urban Planning 54, pp. 139–148.

Paar, P. (2006): Landscape visualizations: applications and requirements of 3D visualization software for environmental planning. In: Computers, Environment and Urban Systems 30, pp. 815–839.

Pape, J. C. (1970): Plaggen soils in The Netherlands. In: Geoderma 4 (3), pp. 229–255.

Pedersen, S. A. S. and K. S. Petersen (1995): Geological map of Djursland. 1:50.000. Kopenhagen (DGU Kortserie 51).

Pettit, C. J., C. M. Raymond, B. A. Bryan and L. Hayden (2011): Identifying strengths and weaknesses of landscape visualisation for effective communication of future alternatives. In: Landscape and Urban Planning 100, pp. 231–241.

Pimentel, D. (2006): Soil erosion: a food and environmental threat. In: Environment, Development and Sustainability 8, pp. 119–137.

Pimentel, D., C. Harvey, P. Resosudarmo, K. Sinclair, D. Kurz, M. McNair, S. Christ, L. Shpritz, L. Fitton, R. Saffouri and R. Blair (1995): Environmental and economic costs of soil erosion and conservation benefits. In: Science, New Series 267, pp. 1117–1123.

Pique i Huerta, R. and J. M. Pique i Huerta (1993): Automatic Recognition and Classification of Archaeological Charcoals. In: Andresen, J., T. Madsen and I. Scollar, eds.: Computing the Past. Computer Applications and Quantitative Methods in Archaeology. CAA92. Aarhus, pp. 85–90.

Poschlod, P., A. Baumann (2010): The historical dynamics of calcareous grasslands in the central and southern Franconian Jurassic mountains: a comparative pedoanthracological and pollen analytical study. In: The Holocene 20, pp. 13–23.

Pott, R. (1998): Effects of human interference on the landscape with special reference to the role of grazing livestock. In: WallisDe Vries, M. F., J. P. Bakker and S. E. Van Wieren, eds.: Grazing and conservation management. Dordrecht (Conservation Biology 11), pp. 107–134.

Prass, R. (2000): Die Reformen im Dorf: Gemeinheitsteilungen im Beziehungsgeflecht dörflicher Gesellschaften. In: Jahrbuch für Wirtschaftsgeschichte 2, pp. 71–84.

Prescott, J. R. and J. M. Hutton (1994): Cosmic ray contributions to dose rates for luminescence and ESR dating: large depths and long-term time variations. In: Radiation Measurements 23 (2–3), pp. 497–500.

Preusser, F., D. Degerin, M. Fuchs, A. Hilgers, A., Kadereit, N. Klasen, M. Krbetschek, D. Richter and J. O. G. Spencer (2008): Luminescence dating: basics, methods and applications. In: E & G. Eiszeitalter und Gegenwart. Quarternary Science Journal 57 (1–2), pp. 95–149.

Priestnall, G. and D. Hampson (2008): Landscape visualizations: science and art. In: Dodge, M., M. McDerby and M. Turner, eds.: Geographic visualization: concepts, tools and applications. Chichester, pp. 241–258.

Programm Nord (= Programm-Nord-GmbH), ed. (1979): 25 Jahre Programm Nord. Gezielte Landentwicklung. Kiel.

Pye, K. and H. Tsoar (2009): Aeolian sand and sand dunes. Berlin.

Pyritz, E. (1972): Binnendünen und Flugsandebenen im Niedersächsischen Tiefland (Göttinger Geographische Abhandlungen 61). Göttingen.

Radtke, U., ed. (1998): Lumineszenzdatierung äolischer Sedimente. Beiträge zur Genese und Altersstellung jungquartärer Dünen und Lösse in Deutschland (Kölner Geographische Arbeiten 70). Köln.

Rapp, G. R. and C. L. Hill (2006): Geoarchaeology: the earth-science approach to archaeological interpretation. New Haven.

Raukas, A. (2004): Application of OSL and 10Be techniques to the establishment of deglaciation chronology in Estonia. In: Proceedings of the Estonian Academy of Science Geology 53, pp. 267–287.

Reimer, P. J., E. E. Bard, A. Bayliss, J. W. Beck, P. G. Blackwell, C. Bronk Ramsey, C. E. Buck, H. Cheng, R. L. Edwards, M. Friedrich, P. M. Grootes, T. P. Guilderson, H. Haflidason, I. Hajdas, C. Hatté, T. J. Heaton, D. L. Hoffmann, A. G. Hogg, K. A. Hughen, K. F. Kaiser, B. Kromer, S. W. Manning, M. Niu, R. W. Reimer, D. A. Richards, E. M. Scott, J. R. Southon, R. A. Staff, C. S. M. Turney and J. van der Plicht (2013): IntCal13 and Marine13 radiocarbon age calibration curves, 0–50,000 years cal BC. In: Radiocarbon 55 (4), pp. 1869–1887.

Reimer, P. J., M. G. L. Baillie, E. Bard, A. Bayliss, J. W. Beck, P. G. Blackwell, C. Bronk Ramsey, C. E. Buck, G. S. Burr, R. L. Edwards, M. Friedrich, P. M. Grootes, T. P. Guilderson, I. Hajdas, T. J. Heaton, A. G. Hogg, K. A. Hughen, K. F. Kaiser, B. Kromer, F. G. McCormac, S. W. Manning, R. W. Reimer, D. A. Richards, J. R. Southon, S. Talamo, C. S. M. Turney, J. van der Plicht and C. E. Weyhenmeyer (2009): IntCal09 and Marine09 radiocarbon age calibration curves, 0–50,000 years cal BP. In: Radiocarbon 51 (4), 1111–1150.

Reiss, S. (2005): Langfristige Wirkungen der Landnutzung auf den Stoffhaushalt in der Dithmarscher Geest seit dem Neolithikum. Diss. Univ. Kiel.

Rethemeier, J. (2014): Organic carbon transformation in agricultural soils: radiocarbon analysis of organic matter fractions and biomarker compounds. Diss. Univ. Kiel.

Richter, G. (1965): Bodenerosion. Schäden und gefährdete Gebiete in der Bundesrepublik Deutschland. Bad Godesberg (Forschungen zur Deutschen Landeskunde 152).

Riedel, W. (1997): Naturräumliche Voraussetzungen am Kammberg von Joldelund. In: Jöns, H., ed.: Frühe Eisengewinnung in

Joldelund, Kreis Nordfriesland. Ein Bezug zur Siedlungs- und Technikgeschichte Schleswig-Holsteins. Teil 1: Einführung, Naturraum, Prospektionsmethoden und archäologische Untersuchungen. Bonn (Universitätsforschungen zur prähistorischen Archäologie aus dem Institut für Ur- und Frühgeschichte der Universität Kiel 40), pp. 3–11.

Roberts, H. M. (2015): Luminescence dating, deep-sea marine and lacustrine. In: Rink, W. J. and J. W. Thompson, eds.: Encyclopedia of scientific dating methods. Dordrecht, pp. 409–413.

Robin, V., B.-H. Rickert, M. J. Nadeau and O. Nelle (2011): Assessing Holocene vegetation and fire history by a multiproxy approach: the case of Stodthagen Forest (Northern Germany). In: The Holocene 22 (3), pp. 337–346.

Rösener, W. (2010): Die Wüstungen des Spätmittelalters und der Einfluss der Klimafaktoren. In: Zeitschrift des Vereins für hessische Geschichte 115, pp. 57–77

Royal Society (2006): Science and the Public interest. Communicating the results of new scientific research to the public. London.

Säppälä, M. (1995): Deflation and redeposition of sand dunes in finnish Lapland. In: Quaternary Science Reviews 14, pp. 799–809.

Sauer, D., H. Sponagel, M. Sommer, L. Giani, R. Jahn and K. Stahr (2007): Podzol: soil of the year 2007: a review on its genesis, occurrence, and functions. In: Journal of Plant Nutrition and Soil Science 170 (5), pp. 581–597.

Schirmer, W. (1999): Dune phases and fossil soils in the European sand belt. In: Schirmer, W., ed.: Dunes and fossil soils. Münster (GeoArchaeoRhein 3), pp. 11–42.

Schlaak, N. (1999): Typical aeolian sand profiles and palaeosols of the Glien till plain in the northwest of Berlin. In: Schirmer, W., eds. (1999): Dunes and fossil soils. Münster (GeoArchaeoRhein 3), pp. 97–105.

Schleswig-Holsteinische Landesforsten (SHLF) (2014a): Die Orkane »Christian und Xaver«. Krisenmanagement in stürmischen Zeiten. In: lignatur 15, pp. 4–5.

Schleswig-Holsteinische Landesforsten (SHLF) (2014b): Starke Maschinen für starkes Holz: Orkanholzaufarbeitung in Gebieten mit hohem Starkholzanteil. In: lignatur 15, p. 6.

Schirmer, W. (1999): Dunes phases and soils in the European sand belt. In: Schirmer, W., eds. (1999): Dunes and fossil soils. Münster (GeoArchaeoRhein 3), pp. 11–42.

Schmidtchen, G. and H.-R. Bork (2003): Changing human impact during the period of agriculture in central Europe: the case study Biesdorfer Kehlen, Brandenburg, Germany. In: Lang, A., K. Hennrich and R. Dikau, eds.: Long-term hillslope and fluvial system modelling: concepts and case studies from Rhine river catchment. Berlin, pp. 183–200.

Schnepel, H. (1981): Dorfchronik Joldelund, Kolkerheide. Joldelund.

Schultz, A. (1978): Windschutz auf der nordfriesischen Geest. In: Jahrbuch der Schleswigschen Geest 26, pp. 29–38.

Schweingruber, F. H. (1990a): Mikroskopische Holzanatomie: Formenspektren mitteleuropäischer Stamm- und Zweighölzer zur Bestimmung von rezentem und subfossilem Material. Bern.

Schweingruber, F. H. (1990b): Anatomie europäischer Hölzer: ein Atlas zur Bestimmung europäischer Baum-, Strauch- und Zwergstrauchhölzer. Bern.

Schwertmann, U. (1964): Differenzierung der Eisenoxide des Bodens durch photochemische Extraktion mit saurer Ammoniumoxalat-Lösung. In: Zeitschrift für Pflanzenernährung, Düngung, Bodenkunde 105, pp. 194–202.

Scott, A. C., J. A. Cripps, M. E. Collinson and G. J. Nichols (2000): The taphonomy of charcoal following a recent heathland fire

and some implications for the interpretation of fossil charcoal deposits. In: Palaeogeography, Palaeoclimatology, Palaeoecology 164, pp. 1–31.

Sevink, J., E. A. Koster, B. van Geel and J. Wallinga (2013): Drift sands, lakes, and soils: the multiphase Holocene history of the Laarder Wasmeren area near Hilversum, the Netherlands. In: Geologie en Mijnbouw 92 (2/3), pp. 217–240.

Shao, Y. (2008): Physics and modelling wind erosion. Köln.

Sheppard, S. R. J. (2005a): Landscape visualisation and climate change: the potential for influencing perceptions and behaviour. In: Environmental Science and Policy 8, 637–654.

Sheppard, S. R. J. (2005b): Participatory decision support for sustainable forest management: a framework for planning with local communities at the landscape level in Canada. In: Canadian Journal of Forest Research 35, pp. 1–12.

Sheppard, S. R. J. (2005c): Validity, reliability and ethics in visualization. In: Bishop, I. D. and E. Lange, eds.: Visualization in landscape and environmental planning London, pp. 79–97.

Sheppard, S. R. J. (2001): Guidance for crystal ball gazers: developing a code of ethics for landscape visualization. In: Landscape and Urban Planning 54, pp. 183–199.

Sheppard, S. R. J. and J. Salter (2004): The role of visualization in forest planning, In: Evans, J. and J. Younguist, eds.: Encyplodedia of forest sciences, landscape and planning section. Vol. 1. Amsterdam, pp. 486–498.

Siart, C., S. Hecht, B. Brilmayer and I. Holzhauer (2011): Analysis and 3D visualization of Mediterranean subsurface karst features based on tomographic mapping (Zominthos, Central Crete). In: Zeitschrift für Geomorphologie 55 (Suppl. 3), pp. 315–335.

Statistikamt Nord (= Statistisches Amt für Hamburg und Schleswig-Holstein) (2005): Agrarstruktur in Schleswig-Holstein: Betriebsgrößenstruktur, Bodennutzung und Viehhaltung in den Gemeinden: Ergebnisse der Agrarstrukturerhebung 2003 (zugleich EG-Agrarstrukturerhebung): Statistischer Bericht C IV 9-4j/2003 S. Teil 1.1. Hamburg.

Statistikamt Nord (= Statistisches Amt für Hamburg und Schleswig-Holstein) (2009): Agrarstruktur in Schleswig-Holstein: Betriebsgrößenstruktur, Bodennutzung und Viehhaltung in den Gemeinden: Ergebnisse der Agrarstrukturerhebung 2005 (zugleich EG-Agrarstrukturerhebung): Statistischer Bericht C IV 9-4j/2007 S. Teil 1.1. Hamburg.

Statistikamt Nord (= Statistisches Amt für Hamburg und Schleswig-Holstein) (2013): Naturraum- und Gemeindeergebnisse in Schleswig-Holstein 2010: endgültige Ergebnisse der Landwirtschaftzählung 2010: Landwirtschaftliche Fläche je Betrieb in den Naturräumen Schleswig-Holsteins 2010: Statistischer Bericht C IV - LZ 2010. Teil 8: Naturräume und Gemeinden, Hamburg.

Stephan, H.-J. (2014): Climato-stratigraphic subdivision of the Pleistocene in Schleswig-Holstein, Germany and adjoining areas: status and problems. In: E&G. Eiszeitalter und Gegenwart. Quaternary Science Journal 63 (1), pp. 3–18.

Stock, C., I. D. Bishop, A. N. O'Connor, T. Chen, C. J. Pettit, J.-P. Aurambout (2008): SIEVE: collaborative decision-making in an immersive online environment. In: Cartography and Geographic Information Science 35 (2), pp. 133–144.

Stokes, S. (1999): Luminescence dating applications in geomorphological research. In: Geomorphology 29 (1–2), pp. 153–171.

Stout, J. E. (2012): A field study of wind erosion following a grass fire on the Llano Estacado of North America. In: Journal of Arid Environments 82, pp. 165–174.

Strehl, E. (1999): Erläuterungen zur Geologischen Karte von Schleswig-Holstein

1:25000, Drelsdorf, Jörl, Blatt 1320, 1321. Flintbek.

Stuiver, M. and H. A. Polach (1977): Discussion: reporting of 14C data. In: Radiocarbon 19 (3), pp. 355–363.

Suess, H.E. (1955): Radiocarbon concentration in modern wood. In: Science 122, pp. 415–417.

Szücs, L. (2014): Understanding landscape changes and cultural ecosystem services in a retro(per)spective. In: Wissen Hayek, U., P. Fricker and E. Buhmann, eds. (2014): Peer reviewed proceedings of digital landscape architecture 2014 at ETH Zurich. Berlin, pp. 352–361.

Talon, B. (2010): Reconstruction of holocene high-altitude vegetation cover in the french southern alps: evidence from soil charcoal. In: The Holocene 20, pp. 35–44.

Tamm, O. (1932): Über die Oxalatmethode in der chemischen Bodenanalyse. In: Meddelanden från Statens skogsförsöksanstalt 27 (1), pp. 1–20.

Teichmann, M. (2010): Visualisation in archaeology: an assessment of modelling archaeological landscapes using scientific and gaming software. In: International Journal of Humanities and Arts Computing 3 (1-2), pp. 101–125.

Tinner, W., S. Hofstetter, F. Zeugin, M. Conedera, T. Wohlgemuth, L. Zimmermann and R. Zweifel (2006): Long-distance transport of macroscopic charcoal by an intensive crown fire in the Swiss Alps: implications for fire history reconstruction. In: The Holocene 16, pp. 287–292.

Tolksdorf, J. F., K. Kaiser (2012): Holocene aeolian dynamics in the European sand-belt as indicated by geochronological data. In: Boreas 41 (3), pp. 408–421.

Tolksdorf, J. F., N. Klasen and A. Hilgers (2013): The existence of open areas during the Mesolithic: evidence from aeolian sediments in the ElbeJeetzel area, northern Germany. In: Journal of Archaeological Science 40, pp. 2813–2823.

Tomescu, A. M. F. (2005): Selective pollen destruction in archeological sediments at Grădiştea Coslogeni (Călăraşi county, Romania). In: Studii de Preistorie 2, pp. 181–186.

Tooth, S. (2015): Luminescence, geomorphological processes. In: Rink, W. J. and J. W. Thompson, eds.: Encyclopedia of scientific dating methods. Dordrecht, pp. 470–475.

Traub, K. P. and J. Kohlus (2006): GIS im Küstenzonenmanagement. Heidelberg.

Trimble, S. W. and S. W. Lund (1982): Soil conservation and the reduction of erosion and sedimentation in the Coon Creek basin, Wisconsin Washington (Geological Survey Professional Paper 1234).

Twiddle, C. L. (2012): Section 4.1.4: Pollen analysis. Not just a qualitative tool. In: Cook, S. J., L. E. Clarke, J. M. Nield, eds.: Geomorphological techniques. London. URL: http://www.geomorphology.org.uk/sites/default/files/flip_geom_tech/index.html#geomorph_techniques/page/1 (Stand: 03.07.2016).

Vernet, J.-L. (2002): Preface. In: Thiébault, S., eds.: Charcoal analysis: methodological approaches, palaeoecological results and wood uses. Proceedings 2nd International Meeting of Anthracology, Paris, Sept. 2000 (BAR International Series 1063), pp. v–vi.

Vandenberghe, D., C. Kasse, S. M. Hossain, F. de Corte, P. van den Haute, M. Fuchs and A. S. Murray (2004): Exploring the method of optical dating and comparison of optical and 14C ages of Late Weichselian coversands in the southern Netherlands. In: Journal of Quaternary Science 19, pp. 73–86.

Vandenberghe, J. (1991): Changing conditions of aeolian sand deposition durch the last glaciation period. In: Schirmer, W., ed.: Dunes and fossil soils. Münster (GeoArchaeoRhein 3), pp. 193–207.

van Breemen, N. and P. Buurmann (2002): Soil formation. Dordrecht.

van der Hammen, T. (1957): The stratigraphy of the Late-Glacial. In: Geologie en Mijnbouw 19 (7), pp. 250–254.

van der Hammen, T. (1951): Late-Glacial flora and periglacial phenomena in The Netherlands. In: Leidse Geologische Mededelingen 17, pp. 71–183.

van der Hammen, T. and B. van Geel (2008): Charcoal in soils of the Allerød-Younger Dryas transition were the result of natural fires and not necessary the effect of an extra-terrestrial impact. In: Netherlands Journal of Geosciences 87, pp. 359–361.

van Mourik, J. M., K. G. J. Nierop and D. A. G. Vandenberghe (2010): Radiocarbon and optically stimulated luminescence dating based chronology of a polycyclic driftsand sequence at Weerterbergen (SE Netherlands). In: Catena 80 (3), pp. 170–181.

van Geel, B., G. R. Coope and T. van der Hammen (1989): Palaeocology and stratigraphy of the Lateglacial type section at Usselo (the Netherlands). In: Review of Palaeobotany and Palynology 60 (1/2), pp. 25–130.

van Mourik, J. M., A. C. Seijmonsbergen, R. T. Slotboom and J. Wallinga (2012): Impact of human land use on soils and landforms in cultural landscapes on aeolian sandy substrates (Maashorst, SE-Netherlands). In: Quaternary International 265, pp. 74–89.

Walker, M. J. C. (2005): Quaternary dating methods. New York.

Wallinga, J. and A. C. Cunningham (2015): Luminescence dating, uncertainties and age range. In: Rink, W. J. and J. W. Thompson, eds.: Encyclopedia of scientific dating methods. Dordrecht, pp. 440–445.

Wallinga, J., F. Davids and J. W. A. Dijkmans (2007): Luminescence dating of Netherlands' sediments. In: Netherlands Journal of Geosciences 86 (3), pp. 179–196.

Warren, A., ed. (2003): Wind erosion on agricultural land in europe: research results for land managers: office for official publications of the european communities. Luxemburg.

Warren, A. and L. Bärring (2003): Wind erosion in European history. In: Warren, A., ed.: Wind erosion on agricultural land in Europe: research results for land managers. Office for Official Publications of the European Communities. Luxemburg, pp. 7–8.

Warkentin, B. P. (2006): Footprints in the soil: people and ideas in soil history. Amsterdam.

Webb, N. R. (1998): The traditional management of European heathlands. In: Journal of Applied Ecology 35 (6), pp. 987–990.

Wiechmann, H. (1981): Unterscheidung der Subtypen Humus-, Eisenhumus- und Eisenpodsol. In: Zeitschrift für Pflanzenernährung und Bodenkunde 144 (2), pp. 174–180.

Wiethold, J. (1998): Studien zur jüngeren postglazialen Vegetations- und Siedlungsgeschichte im östlichen Schleswig-Holstein (mit einem Beitrag von H. Erlenkeuser). Bonn (Universitätsforschungen zur prähistorischen Archäologie 45).

Willemse, N. W. and B. J. Groenewoudt (2012): Resilience of meta-stable landscapes? The non-linear response of late glacial aeolian landforms to prehistoric reclamation along dutch river valleys. In: eTopoi Journal for Ancient Studies, Special Vol. 3, pp. 245–255.

Winterbottom, S. J. and D. Long (2006): From abstract digital models to rich virtual environments: Landscape contexts in Kilmartin Glen, Scotland. In: Journal of Archaeological Science 33, pp. 1356–1367.

Wintle, A. G. (1997): Luminescence dating: laboratory procedures and protocols. In: Radiation measurements 27 (5/6), pp. 769–817.

Wintle A. G. and A. S. Murray (2006): A review of quartz optically stimulated luminescence characteristics and their relevance in single-aliquot regeneration dating protocols. In: Radiation Measurements 41 (4), pp. 369–391.

Wu, H., W. He and J. Gong (2010): A virtual globe-based 3D visualization and interactive framework for public participation in urban planning processes. In: Computer, Environment and Urban Systems 34 (4), pp. 291–298.

Yang, X., L. Scuderi (2010): Hydrological and climatic changes in deserts of China since the Late Pleistocene. Quaternary Research 73, 1–9.

Yang, X., L. Scuderi, P. Paillou, Z. Liu, H. Li and X. Ren (2011): Quaternary environmental changes in the drylands of China: a critical review. In: Quaternary Science Reviews 30, pp. 3219–3233.

Yang, X., H. Li and A. Conacher (2012): Large-scale controls on the development of sand seas in northern China. In: Quaternary International 250, pp. 74–83.

Zander, A. and A. Hilgers (2013): Potential and limits of OSL, TT-OSL, IRSL and pIRIR290 dating methods applied on a Middle Pleistocene sediment record of Lake El'gygytgyn, Russia. In: Climate of the Past 9, pp. 719–733.

Zeeberg, J. J. (1998): The European sand belt in eastern Europe: and comparison of Late Glacial dune orientation with GCM simulation results. In: Boreas 27, pp. 127–139.

Zuazo, V. H. D. and C. R. R. Pleguezuelo (2009): Soil erosion and run-off prevention by plant covers: a review. In: Lichtfouse, E., M. Navarrete, P. Debaeke, V. Souchere and C. Alberola, eds.: Sustainable agriculture. Dordrecht, pp. 785–811.

Zube, E. H., D. E. Simcox and C. E. Law (1987): Perceptual landscape simulations: history and prospects. In: Landscape Journal 6, pp. 62–80.

Appendix 11

Appendix 1: Photographs and drawings of dune profiles
Vertical sections and main physical and chemical pedological features

Appendix 2: Results of ^{14}C dating
Results of OSL dating and measurement report

Appendix 3: Results of palynological and anthracological analysis

Appendix 4: TIN-models of former dunes surfaces using ArcGIS 10.1

Appendix: 5: Results of 3D visualization using 3DsMax

Appendix 1

Photographs and drawings of dune profiles
Vertical sections and main physical and chemical pedological features

Profile 2
(54°38'45" N, 9°7'15" E)

Profile 1
(54°38'46" N, 9°7'16" E)

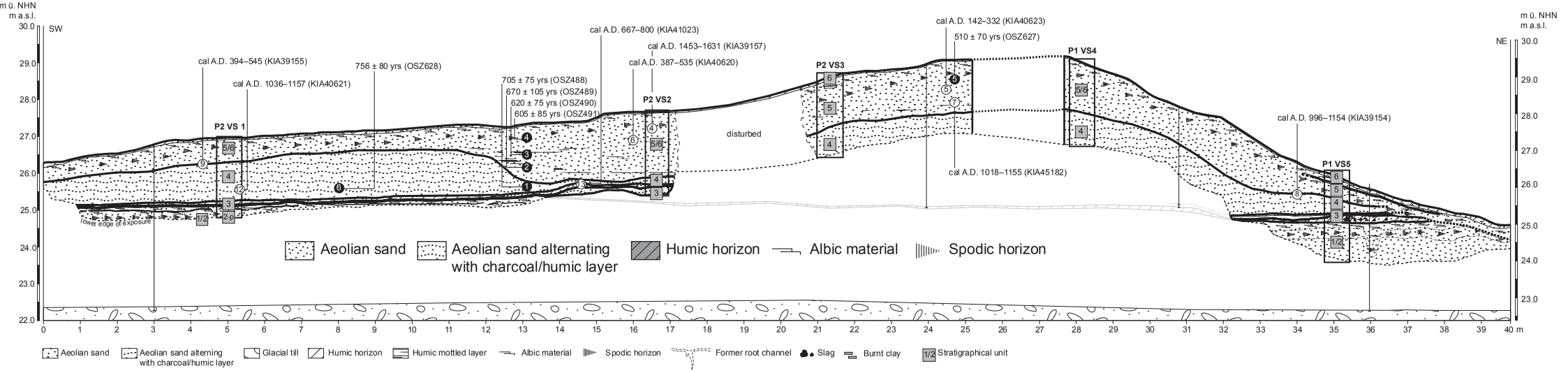

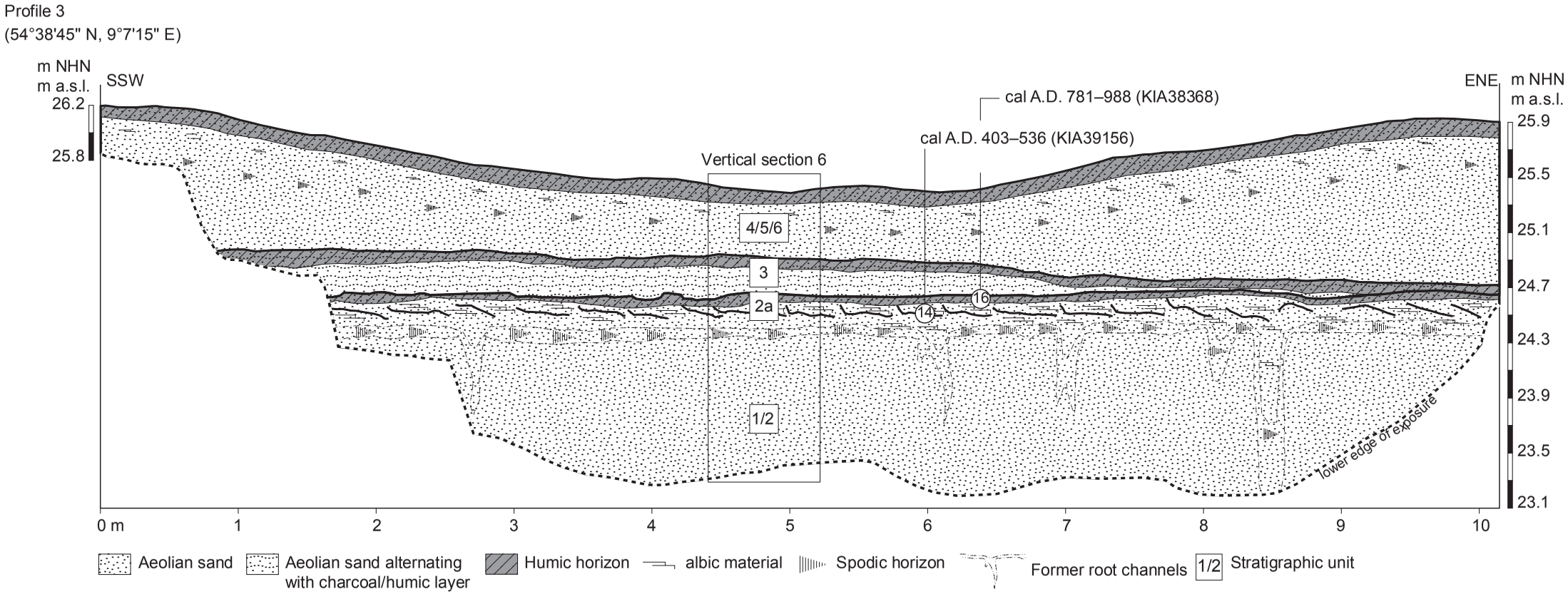
Profile 3
(54°38'45" N, 9°7'15" E)
m NHN
m a.s.l.
26.2
25.8
SSW
ENE
m NHN
m a.s.l.
25.9
25.5
25.1
24.7
24.3
23.9
23.5
23.1
cal A.D. 781–988 (KIA38368)
cal A.D. 403–536 (KIA39156)
Vertical section 6
4/5/6
3
2a
1/2
16
14
lower edge of exposure
0 m
1
2
3
4
5
6
7
8
9
10
Aeolian sand
Aeolian sand alternating with charcoal/humic layer
Humic horizon
albic material
Spodic horizon
Former root channels
1/2
Stratigraphic unit

Profile 4
(54°38'42" N, 9°7'13" E)

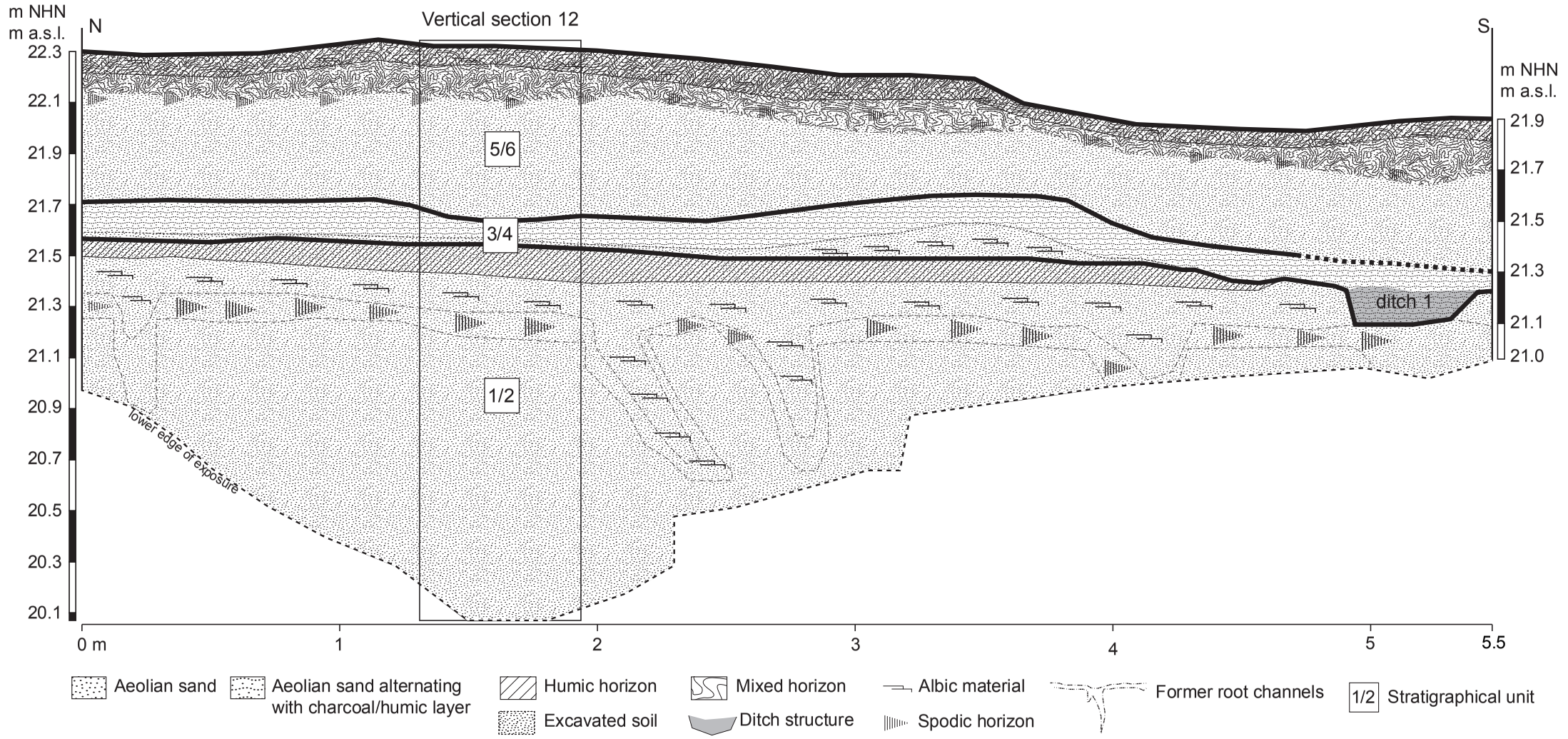

Profile 5
(54°38'40" N, 9°7'15" E)

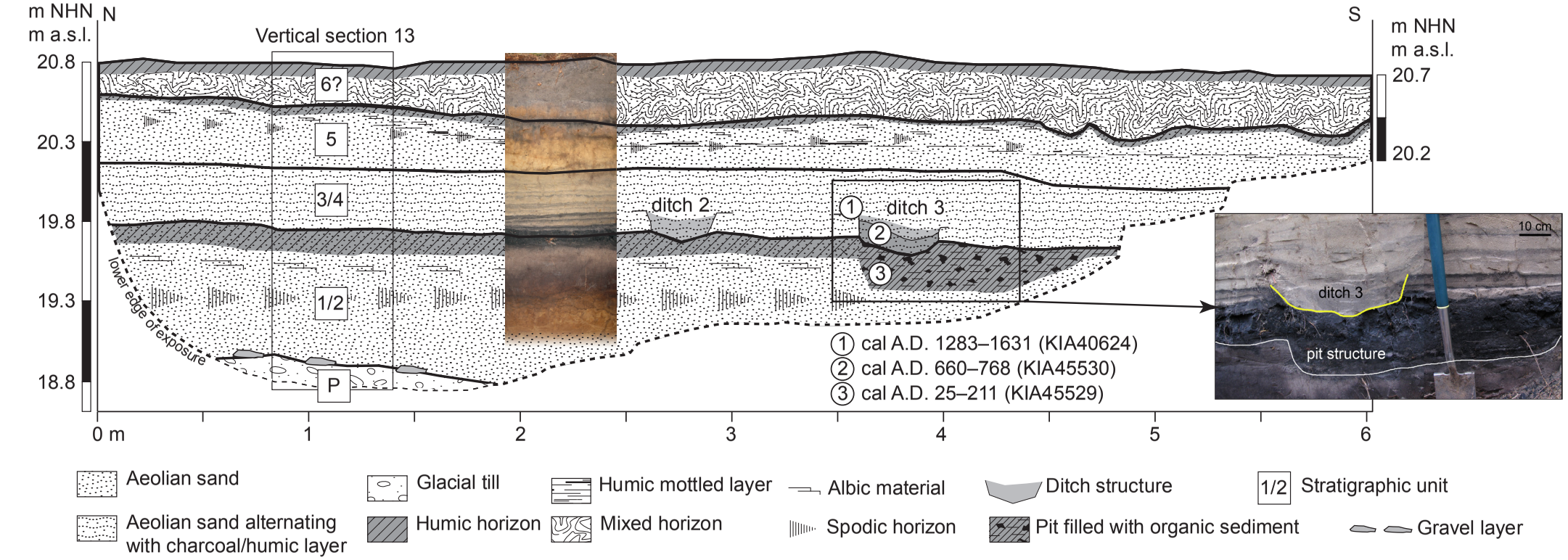

Profile 6, Vertical section 8
(54°38'46" N, 9°7'18" E)

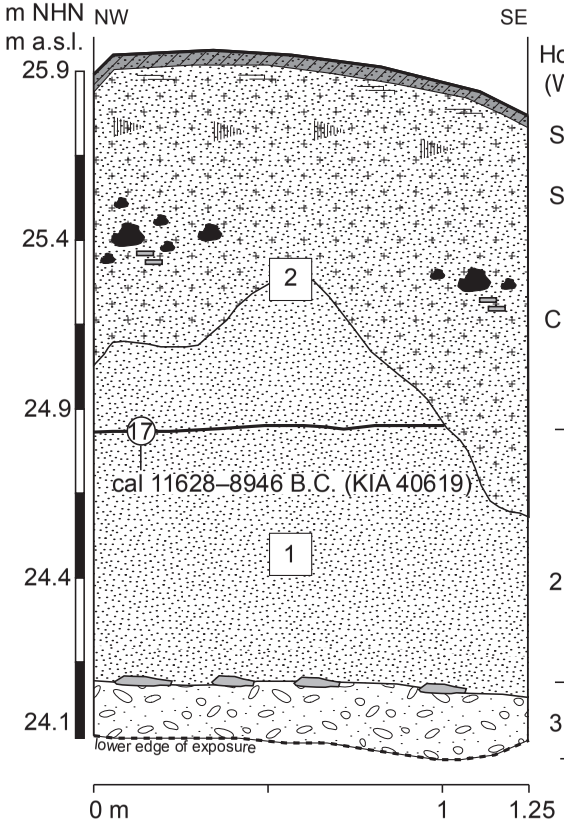

Horizon (WRB)	Aeolian unit	Depth (cm bgs)	Colour (Munsell)	Texture (< 2 mm)	G (wt.%)	COS (wt.%)	MS (wt.%)	FS (wt.%)	Silt (wt.%)	Clay (wt.%)	MS:FS	M (mm)	Md (mm)	So	pH ($CaCl_2$)	OM (%)	Fe_D (g/kg)	Fe_O (g/kg)	Fe_O:Fe_D
SP1	Unit 2	0-5	7.5YR 4/2	fSms	2.0	0.5	37.6	50.1	9.1	2.7	0.8	0.17	0.17	1.6	2.9	3.8	3.1	1.2	0.4
SP2	Unit 2	5-60	7.5YR 4/4	fSms	1.6	0.4	45.4	51.3	1.7	1.2	0.9	0.21	0.19	1.6	3.9	1.8	2.7	1.3	0.5
C	Unit 2	60-79	10YR 6/5	mSfs	0.0	0.9	51.5	44.1	0.9	2.5	1.2	0.23	0.21	1.6	4.5	0.1	0.5	0.2	0.4
	Unit 2	79-99	10YR 6/5	fSms	0.0	0.4	30.8	66.6	1.1	1.1	0.5	0.18	0.16	1.4	-	0.1	0.6	0.2	0.4
	Unit 1	99-158	2.5Y 7/4	fSms	0.0	0.1	30.1	68.1	0.3	1.3	0.4	0.18	0.17	1.4	4.5	0.1	0.4	0.2	0.4
2C		158-176	2.5YR 6/6	Sl2	11.8	4.2	36.7	40.8	11.7	6.6	0.9	0.15	0.17	2.0	3.8	0.1	1.2	0.3	0.2
3C																			

Note. Abbrevations: cm bgs = cm below ground surface; G = gravel, > 2mm; COS = coarse sand, < 2 mm; MS = medium sand, < 0.63 mm; FS = fine sand, < 0.2 mm; M = Mean; Md = Median; So = Sorting coefficient (Trask 1932); OM = organic matter content; SP = slag pit. Texture is given according to German Soil Systematics.

Aeolian sand
Aeolian sand alterning with charcoal/humic layer
Humic horizon
Glacial till
Gravel bed
Slag pit
Burnt clay
Slag
Albic material
Spodic horizon
1/2 Stratigraphic unit

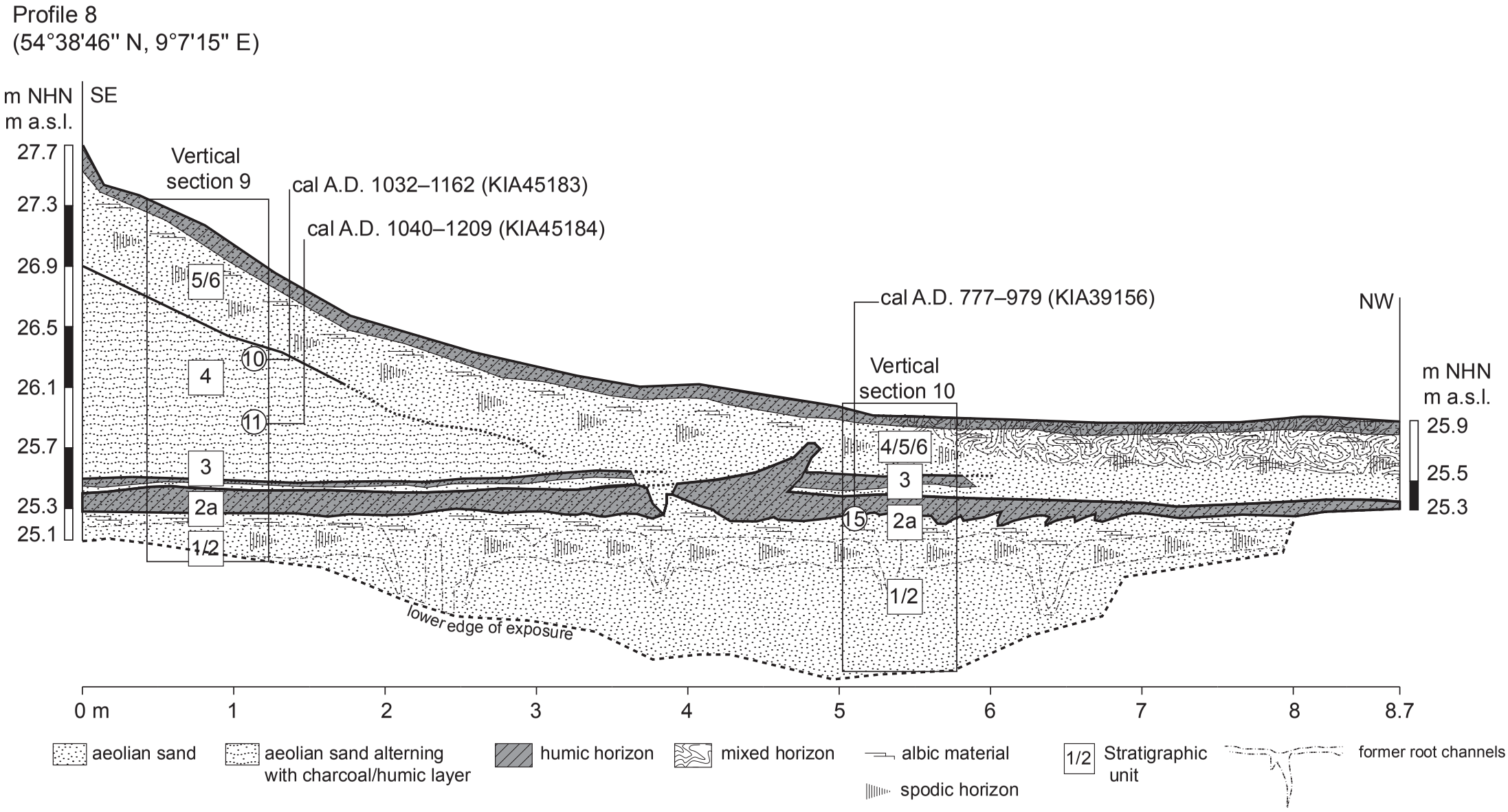
Profile 8
(54°38'46" N, 9°7'15" E)
m NHN
m a.s.l.
SE
27.7
27.3
26.9
26.5
26.1
25.7
25.3
25.1
Vertical
section 9
cal A.D. 1032–1162 (KIA45183)
cal A.D. 1040–1209 (KIA45184)
cal A.D. 777–979 (KIA39156)
NW
Vertical
section 10
m NHN
m a.s.l.
25.9
25.5
25.3
5/6
4
10
11
3
2a
1/2
4/5/6
3
15
2a
1/2
lower edge of exposure
0 m
1
2
3
4
5
6
7
8
8.7
aeolian sand
aeolian sand alterning
with charcoal/humic layer
humic horizon
mixed horizon
albic material
spodic horizon
1/2
Stratigraphic
unit
former root channels

Profile 9
(54°38'46" N, 9°7'13' E)

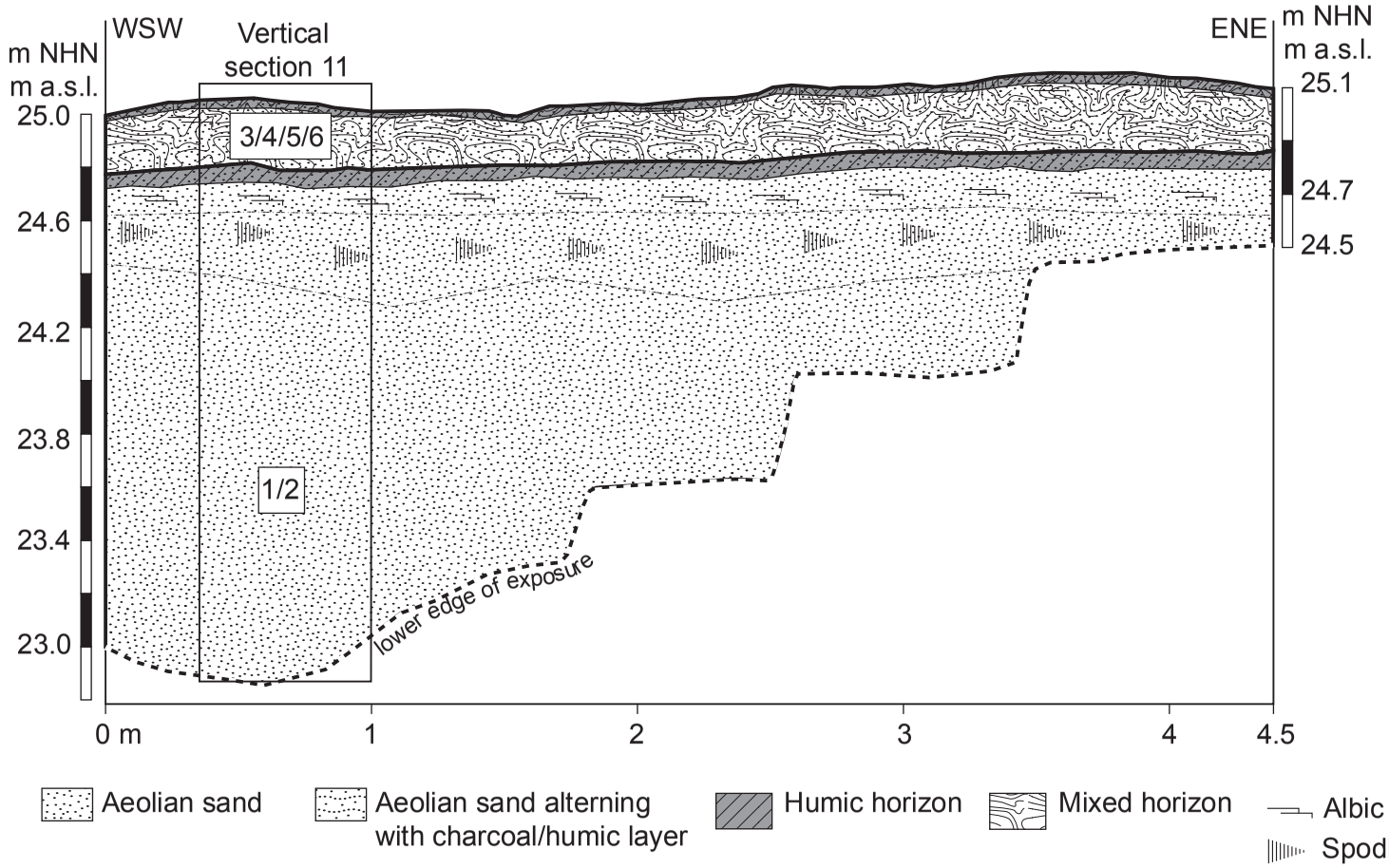

Profile 12
(54°38'45" N, 9°7'15" E)
26.2 m a.s.l.

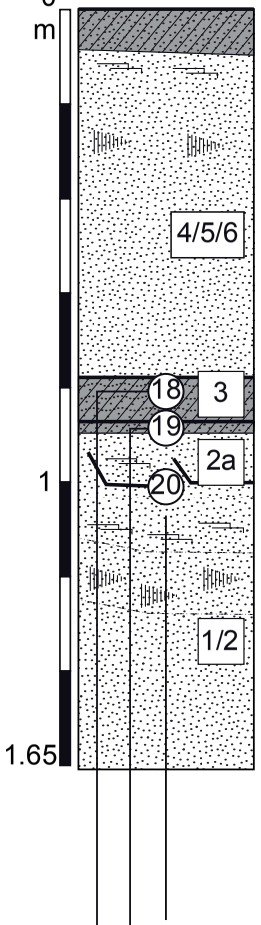

Vertical Section 7	Horizon (WRB)	Aeolian unit	Depth (cm bgs)	Colour (Munsell)	Texture (< 2 mm)	G (wt.%)	COS (wt.%)	MS (wt.%)	FS (wt.%)	Silt (wt.%)	Clay (wt.%)	MS:FS	M (mm)	Md (mm)	So	pH ($CaCl_2$)	OM (%)	Fe_D (g/kg)	Fe_O (g/kg)	Fe_O:Fe_D
	Ah	Unit 4/5/6	0-10	10YR 3/1	fSms	-	0.5	38.2	55.2	4.6	1.5	0.7	0.18	0.17	1.6	2.7	8.3	1.0	0.6	0.6
	E		10-15	7.5YR 5/1	fSms	-	0.4	41.5	53.6	2.2	2.3	0.8	0.19	0.18	1.6	2.9	2.7	0.6	0.2	0.4
	Bws		15-35	7.5YR 3/4	fSms	-	0.4	41.4	50.6	3.9	3.6	0.8	0.18	0.18	1.7	3.2	1.6	1.8	1.3	0.7
	C		35-76	10YR 6/6	mSfs	-	1.2	49.8	47.1	0.8	1.1	1.1	0.23	0.20	1.6	4.1	0.7	0.8	0.4	0.5
	2Ahb	Unit 3	76-86	10YR 5/3	fS	-	0.1	11.4	72.1	4.6	11.8	0.2	0.10	0.11	1.5	4.3	0.8	0.5	0.2	0.4
	3Ab	Unit 2a	86-88	10YR 2/1	mSfs	-	1.3	46.1	43.8	6.7	1.9	1.1	0.19	0.19	1.8	3.8	8.1	0.2	0.2	0.9
	4Apb		88-102	10YR 3/1	St2	-	1.1	38.4	44.9	8.4	7.0	0.9	0.16	0.17	1.8	3.9	4.5	0.7	0.5	0.7
	4Eb	Unit 1/2	102-122	2.5YR 4/1	mSfs	-	1.0	49.5	45.4	2.1	2.0	1.1	0.21	0.20	1.6	4.0	1.0	0.1	0.1	0.9
	4Bhb		122-133	7.5YR 5/2	mSfs	-	1.2	52.9	43.1	0.9	1.9	1.2	0.23	0.22	1.6	4.2	1.9	8.8	7.6	0.9
	4Bmsb		133-143	10YR 5/6	fSms	-	0.4	23.2	70.5	1.8	4.1	0.3	0.15	0.15	1.4	4.4	0.9	1.1	0.5	0.5
	4BC		143-165	10YR 6/6	St2	-	0.3	12.8	71.6	2.5	12.8	0.2	0.11	0.11	1.5	4.1	0.7	1.0	0.4	0.4

Note. Abbrevations: cm bgs = cm below ground surface; G = Gravel, > 2 mm; COS = coarse sand, < 2 mm; MS = medium sand, < 0.63 mm; FS = fine sand, < 0.2 mm; M = Mean; Md = Median; So = Sorting coefficient (Trask 1932); OM = organic matter content.Texture is given according to German Soil Systematics.

Aeolian sand
Aeolian sand alterning with charcoal/humic layer
Humic horizon
Albic material
Spodic horizon
1/2 Stratigraphic unit

Scaled drawing of profileG1–G5

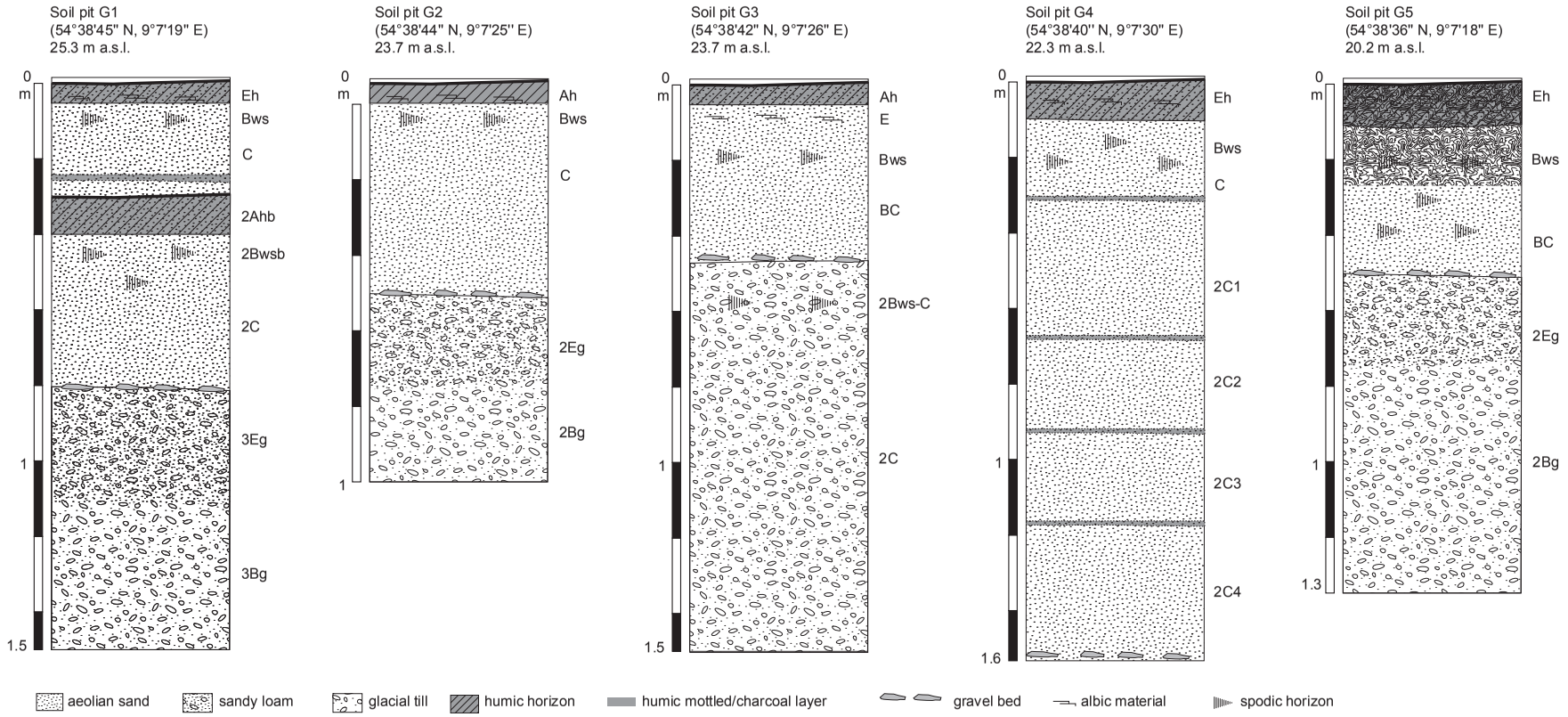

Scaled drawing of profile 12

Profile 12
(54°38'45" N, 9°7'15" E)
26.2 m a.s.l.

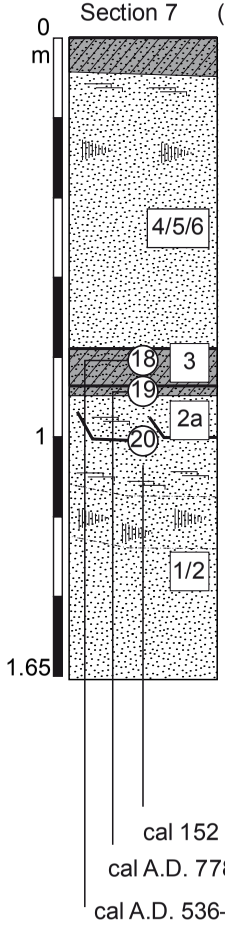

Vertical Section 7	Horizon (WRB)	Aeolian unit	Depth (cm bgs)	Colour (Munsell)	Texture (< 2 mm)	G (wt.%)	COS (wt.%)	MS (wt.%)	FS (wt.%)	Silt (wt.%)	Clay (wt.%)	MS:FS	M (mm)	Md (mm)	So	pH ($CaCl_2$)	OM (%)	Fe_D (g/kg)	Fe_O (g/kg)	Fe_O:Fe_D
	Ah	Unit 4/5/6	0-10	10YR 3/1	fSms	-	0.5	38.2	55.2	4.6	1.5	0.7	0.18	0.17	1.6	2.7	8.3	1.0	0.6	0.6
	E		10-15	7.5YR 5/1	fSms	-	0.4	41.5	53.6	2.2	2.3	0.8	0.19	0.18	1.6	2.9	2.7	0.6	0.2	0.4
	Bws		15-35	7.5YR 3/4	fSms	-	0.4	41.4	50.6	3.9	3.6	0.8	0.18	0.18	1.7	3.2	1.6	1.8	1.3	0.7
	C		35-76	10YR 6/6	mSfs	-	1.2	49.8	47.1	0.8	1.1	1.1	0.23	0.20	1.6	4.1	0.7	0.8	0.4	0.5
	2Ahb	Unit 3	76-86	10YR 5/3	fS	-	0.1	11.4	72.1	4.6	11.8	0.2	0.10	0.11	1.5	4.3	0.8	0.5	0.2	0.4
	3Ab	Unit 2a	86-88	10YR 2/1	mSfs	-	1.3	46.1	43.8	6.7	1.9	1.1	0.19	0.19	1.8	3.8	8.1	0.2	0.2	0.9
	4Apb		88-102	10YR 3/1	St2	-	1.1	38.4	44.9	8.4	7.0	0.9	0.16	0.17	1.8	3.9	4.5	0.7	0.5	0.7
	4Eb	Unit 1/2	102-122	2.5YR 4/1	mSfs	-	1.0	49.5	45.4	2.1	2.0	1.1	0.21	0.20	1.6	4.0	1.0	0.1	0.1	0.9
	4Bhb		122-133	7.5YR 5/2	mSfs	-	1.2	52.9	43.1	0.9	1.9	1.2	0.23	0.22	1.6	4.2	1.9	8.8	7.6	0.9
	4Bmsb		133-143	10YR 5/6	fSms	-	0.4	23.2	70.5	1.8	4.1	0.3	0.15	0.15	1.4	4.4	0.9	1.1	0.5	0.5
	4BC		143-165	10YR 6/6	St2	-	0.3	12.8	71.6	2.5	12.8	0.2	0.11	0.11	1.5	4.1	0.7	1.0	0.4	0.4

Note. Abbrevations: cm bgs = cm below ground surface; G = Gravel, > 2 mm; COS = coarse sand, < 2 mm; MS = medium sand, < 0.63 mm; FS = fine sand, < 0.2 mm; M = Mean; Md = Median; So = Sorting coefficient (Trask 1932); OM = organic matter content.Texture is given according to German Soil Systematics.

Aeolian sand
Aeolian sand alterning with charcoal/humic layer
Humic horizon
Albic material
Spodic horizon
1/2 Stratigraphic unit

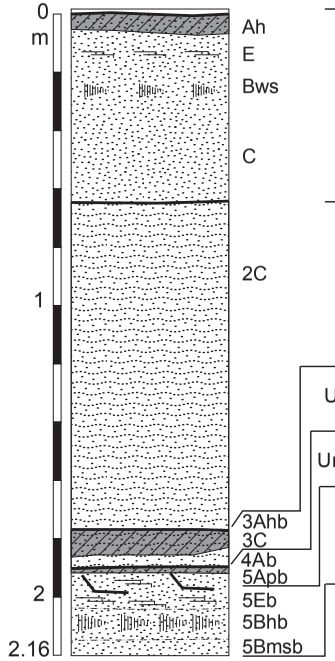

Horizon (WRB)	Aeolian unit	Depth (cm bgs)	Colour (Munsell)	Texture (< 2 mm)	G (wt.%)	COS (wt.%)	MS (wt.%)	FS (wt.%)	Silt (wt.%)	Clay (wt.%)	MS:FS	M (mm)	Md (mm)	So	pH ($CaCl_2$)	OM (%)	Fe_D (g/kg)	Fe_O (g/kg)	Fe_O:Fe_D	SBD (g/cm³)
Ah	Unit 5/6	0-6	7.5YR 4/1	fSms	0.0	0.2	34.8	58.7	2.5	3.7	0.6	0.18	167	1.5	2.7	5.5	1.0	0.4	0.5	-
E		6-15	7.5YR 5/2	fSms	0.0	0.2	38.2	58.6	1.4	1.5	0.7	0.19	173	1.5	2.9	2.0	1.0	0.5	0.4	-
Bws		15-35	7.5YR 3/4	fSms	0.0	0.1	37.0	60.5	0.6	1.8	0.6	0.19	173	1.5	3.2	1.3	1.6	1.2	0.8	1.6
C		35-63	10YR 6/5	mSfs	0.0	0.4	48.2	49.5	0.3	1.5	1.0	0.22	197	1.6	4.3	0.3	0.9	0.3	0.4	1.6
2C	Unit 4	63-90	10YR 6/5	fSms	0.0	0.7	43.8	53.9	0.3	1.3	0.8	0.22	0.19	1.5	4.4	0.3	0.9	0.5	0.6	1.6
		90-125	10YR 6/5	fSms	0.0	0.8	41.9	55.8	0.3	1.3	0.8	0.21	0.18	1.5	-	0.2	1.1	0.4	0.4	-
		125-150	10YR 6/5	fSms	0.0	0.1	46.1	51.9	0.5	1.5	0.9	0.22	0.19	1.5	-	0.2	1.0	0.4	0.4	-
		150-177	10YR 6/4	fSms	0.0	0.3	27.0	69.2	0.5	3.0	0.4	0.17	0.16	1.4	-	0.2	0.8	0.4	0.5	-
	Unit 3	177-187	-	-	-	-	-	-	-	-	-	-	-	-	-	-	-	-	-	-
		187-189	10YR 5/3	fSms	0.0	0.4	58.5	38.6	0.6	1.9	1.5	0.24	0.24	1.6	4.3	0.2	0.2	0.1	0.4	-
	Unit 2a	189-190	-	-	-	-	-	-	-	-	-	-	-	-	-	-	-	-	-	-
		190-195	10YR 4/1	mSfs	0.1	0.9	40.7	48.2	8.2	2.0	0.8	0.18	0.18	1.6	3.8	4.0	0.4	0.3	0.9	1.4
3Ahb	Unit 1/2	195-209	10YR 5/2	fSms	0.0	1.2	43.5	51.9	0.7	2.7	0.8	0.20	0.19	1.6	3.9	1.3	0.1	0.1	0.9	1.5
3C		209-214	10YR 3/1	mSfs	0.0	0.8	44.5	48.9	1.6	4.1	0.9	0.20	0.19	1.6	3.7	8.5	2.5	2.5	1.0	-
4Ab		214-216	7.5YR 3/4	fSms	0.0	0.7	43.4	52.9	1.3	1.7	0.8	0.21	0.19	1.6	4.1	1.3	2.0	1.8	0.9	-
5Apb																				
5Eb																				
5Bhb																				
5Bmsb																				

Note. Abbrevations: cm bgs = cm below ground surface; G = Gravel, > 2 mm; COS = coarse sand, < 2 mm; MS = medium sand, < 0.63 mm; FS = fine sand, < 0.2 mm; M = Mean; Md = Median; So = Sorting coefficient (Trask 1932); OM = organic matter content; SBD = soil bulk density. Texture is given according to German Soil Systematics.

Aeolian sand | Aeolian sand alternating with charcoal/humic layer | Humic horizon | Albic material | Spodic horizon

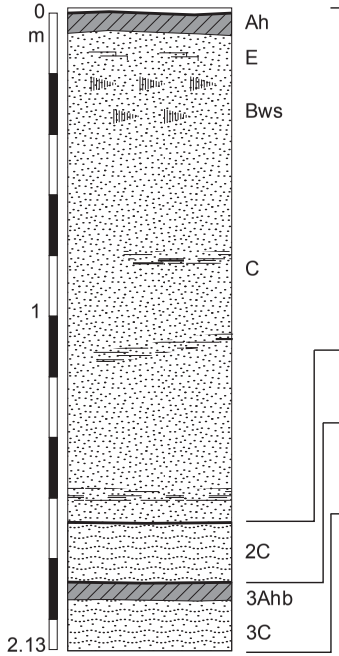

Horizon (WRB)	Aeolian unit	Depth (cm bgs)	Colour (Munsell)	Texture (< 2 mm)	G (wt.%)	COS (wt.%)	MS (wt.%)	FS (wt.%)	Silt (wt.%)	Clay (wt.%)	MS:FS	M (mm)	Md (mm)	So	pH ($CaCl_2$)	OM (%)	Fe_D (g/kg)	Fe_O (g/kg)	Fe_O:Fe_D
Ah	Unit 5/6	0-5	10YR 4/1	fSms	0.0	0.5	41.4	50.3	4.3	3.5	0.8	0.19	0.18	1.6	2.8	8.9	1.3	0.6	1.1
E		5-18	7.5YR 4/2	fSms	0.0	0.4	44.0	51.8	2.2	1.5	0.8	0.20	0.19	1.6	3.2	1.5	1.2	0.2	0.4
Bws		18-38	7.5YR 4/3	fSms	0.0	0.3	38.2	58.4	2.0	1.2	0.7	0.19	0.17	1.5	3.3	1.1	2.2	1.4	0.1
		38-78	10YR 6/5	mSfs	0.0	0.5	64.0	33.5	0.74	1.3	1.9	0.26	0.26	1.6	4.4	0.3	0.8	0.5	0.4
C		78-123	10YR 6/5	mSfs	0.0	0.4	65.1	32.3	0.3	1.9	2.0	0.26	0.26	1.4	-	0.2	1.0	0.3	0.4
		123-168	10YR 6/5	mSfs	0.0	2.2	62.4	33.6	0.2	1.6	1.9	0.26	0.26	1.4	-	0.2	0.6	0.3	0.5
2C	Unit 4	168-188	10YR 6/5	fSms	0.0	0.3	36.0	61.7	0.4	1.7	0.6	0.19	0.17	1.3	4.4	0.3	0.7	0.4	0.5
3Ahb	Unit 3	188-193	-	-	-	-	-	-	-	-	-	-	-	-	-	-	-	-	-
3C		193-213	10YR 6/5	fSms	0.0	0.1	40.5	57.8	0.3	1.3	0.7	0.20	0.18	1.5	4.3	0.2	0.6	0.4	0.6

Note. Abbrevations: cm bgs = cm below ground surface; G = Gravel, > 2 mm; COS = coarse sand, < 2 mm; MS = medium sand, < 0.63 mm; FS = fine sand, < 0.2 mm; M = Mean; Md = Median; So = Sorting coefficient (Trask 1932); OM = organic matter content. Texture is given according to German Soil Systematics.

Aeolian sand | Aeolian sand alternating with charcoal/humic layer | Humic horizon | Albic material | Spodic horizon

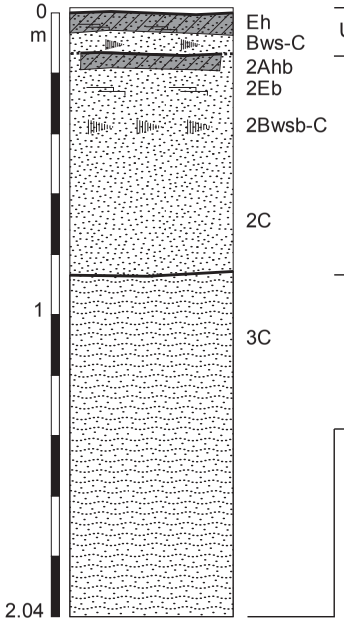

Horizon (WRB)	Aeolian unit	Depth (cm bgs)	Colour (Munsell)	Texture (< 2 mm)	G (wt.%)	COS (wt.%)	MS (wt.%)	FS (wt.%)	Silt (wt.%)	Clay (%)	MS:FS	M (mm)	Md (mm)	So	pH ($CaCl_2$)	OM (%)	Fe_D (g/kg)	Fe_O (g/kg)	Fe_O:Fe_D
Eh	Unit 6	0-8	10YR 4/2	fSms	0.0	0.2	43.0	49.0	0.3	7.4	0.9	0.19	0.18	1.6	3.6	2.8	2.0	1.2	0.6
Bws-C		8-13	7.5YR 4/3	fSms	0.0	0.1	39.7	58.7	0.3	1.2	0.7	0.20	0.18	1.5	3.0	0.9	1.9	0.7	0.4
2Ahb	Unit 5	13-19	7.5YR 4/3	mSfs	0.0	0.2	51.3	43.0	3.3	2.2	1.2	0.23	0.21	1.6	3.3	8.3	1.8	0.8	0.4
2Eb		19-29	7.5YR 4/1	fSms	0.0	0.3	46.7	50.5	1.8	0.7	0.9	0.21	0.19	1.6	3.0	1.8	1.3	0.6	0.5
2Bwsb-C		29-40	7.5YR 5/2	fSms	0.0	0.3	42.0	54.0	0.8	3.0	0.8	0.21	0.18	1.5	3.5	1.0	1.0	0.3	0.3
2C		40-89	10YR 6/5	mSfs	0.0	0.2	65.4	31.9	0.2	2.3	2.0	0.26	0.26	1.6	4.5	0.1	0.9	0.3	0.4
3C	Unit 4	89-160	10YR 6/5	mSfs	0.0	0.1	45.9	50.8	0.4	2.7	0.9	0.21	0.19	1.6	4.4	0.2	1.0	0.4	0.4
		160-204	10YR 6/4	mSfs	0.0	0.1	50.1	47.1	0.8	1.9	1.1	0.23	0.20	1.6	-	0.2	0.8	0.3	0.4

Note. Abbrevations: cm bgs = cm below ground surface; G = Gravel, > 2mm; COS = coarse sand, < 2 mm; MS = medium sand, < 0.63 mm; FS = fine sand, < 0.2 mm; M = Mean; Md = Median; So = Sorting coefficient (Trask 1932); OM = organic matter content; Texture is given according to German Soil Systematics.

Aeolian sand | Aeolian sand alternating with charcoal/humic layer | Humic horizon | Albic material | Spodic horizon

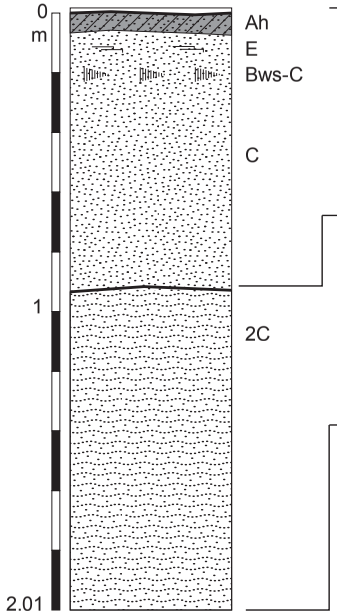

Vertical section 4	Horizon (WRB)	Aeolian unit	Depth (cm bgs)	Colour (Munsell)	Texture (< 2 mm)	G (wt.%)	COS (wt.%)	MS (wt.%)	FS (wt.%)	Silt (wt.%)	Clay (wt.%)	MS:FS	M (mm)	Md (mm)	So	pH ($CaCl_2$)	OM (%)	Fe_D (g/kg)	Fe_O (g/kg)	Fe_O:Fe_D
	Ah	Unit 5/6	0-6	10YR 4/1	fSms	0.0	0.1	39.7	55.3	2.9	2.0	0.7	0.20	0.18	1.5	2.8	6.6	1.5	0.5	0.4
	E		6-17	7.5YR 5/2	mSfs	0.0	0.0	48.3	45.7	0.5	5.5	1.1	0.22	0.20	1.6	3.1	1.6	1.2	0.4	0.4
	Bws-C		17-23	10YR 4/6	mSfs	0.0	0.1	48.4	48.1	0.9	2.5	1.0	0.22	0.20	1.6	3.9	0.6	1.4	0.5	0.4
	C		23-93	10YR 6/5	fSms	0.0	0.2	45.0	50.3	0.8	3.6	0.9	0.22	0.19	1.5	4.3	0.4	0.9	0.4	0.5
	2C	Unit 4	93-130	10YR 6/5	mSfs	0.0	1.2	50.8	44.2	0.3	3.6	1.1	0.23	0.21	1.6	4.4	0.2	1.0	0.3	0.4
			130-165	10YR 6/5	mSfs	0.0	0.8	57.0	37.7	0.6	3.8	1.5	0.24	0.23	1.6	-	0.2	0.8	0.3	0.4
			165-201	10YR 6/4	mSfs	0.0	0.2	51.7	44.1	0.3	3.7	1.2	0.23	0.21	1.6	-	0.2	0.9	0.4	0.4

Note. Abbrevations: cm bgs = cm below ground surface; G = Gravel, > 2mm; COS = coarse sand, < 2 mm; MS = medium sand, < 0.63 mm; FS = fine sand, < 0.2 mm; M = Mean; Md = Median; So = Sorting coefficient (Trask 1932); OM = organic matter content; Texture is given according to German Soil Systematics.

Aeolian sand | Aeolian sand alternating with charcoal/humic layer | Humic horizon | Albic material | Spodic horizon

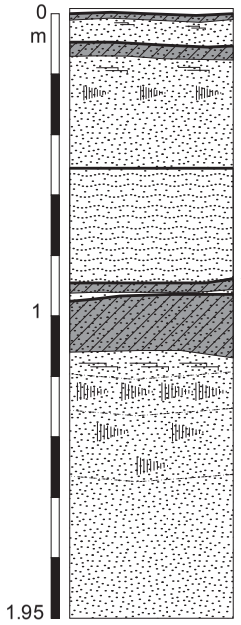

Horizon (WRB)	Aeolian unit	Depth (cm bgs)	Colour (Munsell)	Texture (< 2 mm)	G (wt.%)	COS (wt.%)	MS (wt.%)	FS (wt.%)	Silt (wt.%)	Clay (wt.%)	MS:FS	M (mm)	Md (mm)	So	pH ($CaCl_2$)	OM (%)	Fe_D (g/kg)	Fe_O (g/kg)	Fe_O:Fe_D
Ah	Unit 6	0-3	10YR 3/1	mSfs	0.0	0.3	48.9	45.6	2.9	2.3	1.1		0.20	1.6	2.7	8.1	1.7	0.7	0.4
E		3-6	10YR 4/1	mSfs	0.0	0.3	50.1	46.5	2.0	1.2	1.1		0.20	1.6	2.9	3.1	1.9	0.8	0.4
2Ahb	Unit 5	6-11	10YR 3/1	mSfs	0.0	0.4	44.5	46.6	3.2	5.3	1.0		0.19	1.6	2.8	7.2	1.5	0.6	0.4
2Eb		11-17	7.5YR 6/2	mSfs	0.0	0.1	50.7	4.0	0.3	2.8	1.1	0.22	0.20	1.6	3.1	1.2	1.2	0.4	0.3
2Bwsb-C		17-35	7.5YR 5/4	mSfs	0.0	0.5	57.1	40.3	0.3	1.7	1.4	0.22	0.23	1.6	3.4	0.7	1.7	0.8	0.5
2C		35-50	10YR 6/4	mSfs	0.0	2.1	52.9	41.7	0.6	2.7	1.3	0.19 0.19	0.22	1.6	3.8	0.3	1.2	0.4	0.3
3C	Unit 4	50-87	7.5YR 5/4	mSfs	0.0	0.4	54.9	42.3	0.6	1.7	1.3	0.24 0.23	0.22	1.6	4.3	0.2	0.8	0.3	0.4
4Ahb	Unit 3	87-89	-	-	-	-	-	-	-	-	-		-	-	-	-	-	-	-
4C		89-92	-	-	-	-	-	-	-	-	-		-	-	-	-	-	-	-
5Ahub	Unit 1/2	92-108	7.5YR 5/2	mSfs	0.1	0.8	50.8	43.6	3.0	1.9	1.2	0.23	0.21	1.6	4.2	0.7	2.5	0.5	0.2
5Eb		108-119	10YR 6/2	mSfs	0.2	1.0	48.9	46.1	2.0	1.9	1.1	-	0.20	1.6	4.1	0.3	0.4	0.3	0.9
5Bhb		119-126	7.5YR 2/2	fSms	0.0	0.6	42.4	53.4	0.6	2.9	0.8	0.22	0.18	1.5	3.8	1.6	3.2	2.6	0.8
5Bmsb		126-150	7.5YR 5/6	mSfs	0.0	1.1	50.5	46.2	0.3	1.9	1.1	0.22 0.21	0.21	1.6	4.1	1.1	2.0	2.1	1.0
5C		150-195	10YR 6/4	fS	0.0	0.4	12.0	80.5	3.4	3.7	0.1	0.23	0.11	1.4	4.4	0.2	0.8	0.3	0.4

Note. Abbrevations: cm bgs = cm below ground surface; COS = coarse sand, < 2 mm; MS = medium sand, < 0.63 mm; FS = fine sand, < 0.2 mm; M = Mean; Md = Median; So = Sorting coefficient (Trask 1932); OM = organic matter content; Texture given according to German Soil Systematics.

Aeolian sand | Aeolian sand alternating with charcoal/humic layer | Humic horizon | Albic material | Spodic horizon

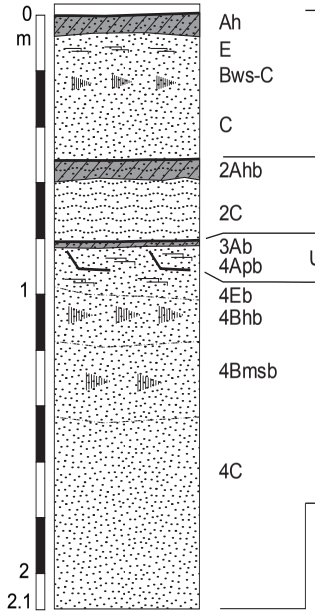

Horizon (WRB)	Aeolian unit	Depth (cm bgs)	Colour (Munsell)	Texture (< 2 mm)	G (wt.%)	COS (wt.%)	MS (wt.%)	FS (wt.%)	Silt (wt.%)	Clay (wt.%)	MS:FS	M (mm)	Md (mm)	So	pH ($CaCl_2$)	OM (%)	Fe_D (g/kg)	Fe_O (g/kg)	Fe_O:Fe_D	SBD (g/cm^3)
Ah	Unit 4/5/6	0-8	7.5YR 2/1	fSms	0.0	0.2	34.2	58.1	3.3	4.2	0.6	0.17	0.17	1.5	2.7	5.5	0.8	0.4	0.5	-
E		8-16	7.5YR 3/2	fSms	0.0	0.3	30.2	66.2	1.1	2.3	0.5	0.18	0.16	1.4	3.3	1.4	1.1	0.4	0.4	1.4
Bws-C		16-34	7.5YR 3/4	mSfs	0.0	0.4	51.1	45.5	0.9	2.2	1.1	0.23	0.21	1.6	3.8	0.7	1.3	0.7	0.5	1.5
C		34-52	10YR 4/6	fS	0.0	0.1	13.5	83.5	0.7	2.2	0.2	0.14	0.15	1.2	4.2	0.7	1.4	0.6	0.5	1.5
2Ahb	Unit 3	52-60	10YR 3/4	fS	0.0	0.3	18.6	74.6	3.9	2.67	0.2	0.13	0.13	1.5	4.1	1.0	1.7	0.8	0.5	-
		60-70	10YR 4/6	fSms	0.0	0.2	39.5	57.9	0.7	1.7	0.7	0.21	0.18	1.5	4.3	0.4	0.9	0.5	0.6	1.6
2C		70-80	10YR 4/6	fSms	0.0	0.1	27.9	69.5	0.8	1.7	0.4	0.17	0.16	1.3	-	0.4	1.3	0.7	0.6	-
3Ab	Unit 2a	80-82	-	-	-	-	-	-	-	-	-	-	-	-	-	-	-	-	-	-
4Apb		82-90	10YR 2/1	fSms	0.5	0.4	29.6	62.0	5.5	2.6	0.5	0.16	0.15	1.6	3.7	8.7	0.2	0.2	0.7	1.2
4Eb	Unit 1/2	90-102	10YR 5/1	mSfs	0.0	0.6	51.1	45.4	2.0	0.9	1.1	0.23	0.21	1.6	3.8	1.3	0.1	0.1	1.0	1.6
4Bhb		102-110	7.5YR 2/1	mSfs	0.0	1.1	48.3	41.6	2.4	6.5	1.2	0.21	0.20	1.6	3.7	7.8	4.1	4.5	1.1	
4Bmsb		110-134	7.5YR 3/3	fSms	0.0	0.4	42.8	53.4	1.7	1.6	0.8	0.20	0.18	1.6	4.2	1.0	1.4	0.9	0.6	1.4
4C		134-212	10YR 6/4	mSfs	0.0	0.1	70.1	28.2	1.0	0.7	2.5	0.27	0.28	1.5	4.3	0.1	0.6	0.1	0.2	1.5

Note. Abbrevations: cm bgs = cm below ground surface; G = Gravel, > 2 mm; COS = coarse sand, < 2 mm; MS = medium sand, < 0.63 mm; FS = fine sand, < 0.2 mm; M = Mean; Md = Median; So = Sorting coefficient (Trask 1932); OM = organic matter content; SBD = soil bulk density. Texture is given according to German Soil Systematics.

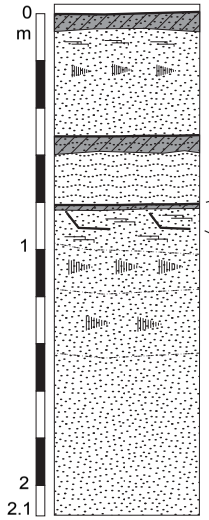

Horizon (WRB)	Aeolian unit	Depth (cm bgs)	Colour (Munsell)	Texture (< 2 mm)	G (wt.%)	COS (wt.%)	MS (wt.%)	FS (wt.%)	Silt (wt.%)	Clay (wt.%)	MS:FS	M (mm)	Md (mm)	So	pH ($CaCl_2$)	OM (%)	Fe_D (g/kg)	Fe_O (g/kg)	Fe_O:Fe_D	SBD (g/cm^3)
Ah	Unit 4/5/6	0-8	7.5YR 2/1	fSms	0.0	0.2	34.2	58.1	3.3	4.2	0.6	0.17	0.17	1.5	2.7	5.5	0.8	0.4	0.5	-
E		8-16	7.5YR 3/2	fSms	0.0	0.3	30.2	66.2	1.1	2.3	0.5	0.18	0.16	1.4	3.3	1.4	1.1	0.4	0.4	1.4
Bws-C		16-34	7.5YR 3/4	mSfs	0.0	0.4	51.1	45.5	0.9	2.2	1.1	0.23	0.21	1.6	3.8	0.7	1.3	0.7	0.5	1.5
C		34-52	10YR 4/6	fS	0.0	0.1	13.5	83.5	0.7	2.2	0.2	0.14	0.15	1.2	4.2	0.7	1.4	0.6	0.5	1.5
2Ahb	Unit 3	52-60	10YR 3/4	fS	0.0	0.3	18.6	74.6	3.9	2.67	0.2	0.13	0.13	1.5	4.1	1.0	1.7	0.8	0.5	-
		60-70	10YR 4/6	fSms	0.0	0.2	39.5	57.9	0.7	1.7	0.7	0.21	0.18	1.5	4.3	0.4	0.9	0.5	0.6	1.6
2C		70-80	10YR 4/6	fSms	0.0	0.1	27.9	69.5	0.8	1.7	0.4	0.17	0.16	1.3	-	0.4	1.3	0.7	0.6	-
3Ab	Unit 2a	80-82	-	-	-	-	-	-	-	-	-	-	-	-	-	-	-	-	-	-
4Apb		82-90	10YR 2/1	fSms	0.5	0.4	29.6	62.0	5.5	2.6	0.5	0.16	0.15	1.6	3.7	8.7	0.2	0.2	0.7	1.2
4Eb	Unit 1/2	90-102	10YR 5/1	mSfs	0.0	0.6	51.1	45.4	2.0	0.9	1.1	0.23	0.21	1.6	3.8	1.3	0.1	0.1	1.0	1.6
4Bhb		102-110	7.5YR 2/1	mSfs	0.0	1.1	48.3	41.6	2.4	6.5	1.2	0.21	0.20	1.6	3.7	7.8	4.1	4.5	1.1	
4Bmsb		110-134	7.5YR 3/3	fSms	0.0	0.4	42.8	53.4	1.7	1.6	0.8	0.20	0.18	1.6	4.2	1.0	1.4	0.9	0.6	1.4
4C		134-212	10YR 6/4	mSfs	0.0	0.1	70.1	28.2	1.0	0.7	2.5	0.27	0.28	1.5	4.3	0.1	0.6	0.1	0.2	1.5

Note. Abbrevations: cm bgs = cm below ground surface; G = Gravel, > 2 mm; COS = coarse sand, < 2 mm; MS = medium sand, < 0.63 mm; FS = fine sand, < 0.2 mm; M = Mean; Md = Median; So = Sorting coefficient (Trask 1932); OM = organic matter content; SBD = soil bulk density. Texture is given according to German Soil Systematics.

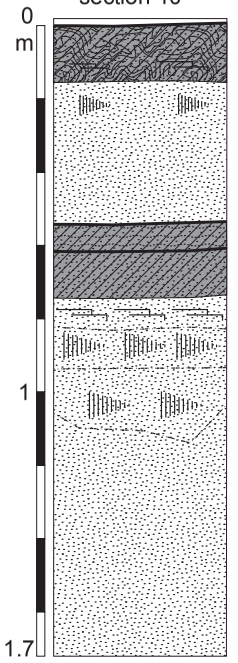

Horizon (WRB)	Aeolian unit	Depth (cm bgs)	Colour (Munsell)	Texture (< 2 mm)	G (wt.%)	COS (wt.%)	MS (wt.%)	FS (wt.%)	Silt (wt.%)	Clay (wt.%)	MS:FS	M (mm)	Md (mm)	So	pH ($CaCl_2$)	OM (%)	Fe_D (g/kg)	Fe_O (g/kg)	Fe_O:Fe_D
Ap	Unit 5/6	0-14	10YR 4/2	fSms	0.0	0.1	27.5	68.0	2.5	1.9	0.4	0.17	0.16	1.3	3.0	3.0	1.1	0.7	0.6
Bws		14-26	7.5YR 4/3	fSms	0.0	0.2	30.1	66.5	1.0	2.3	0.5	0.17	0.16	1.4	3.4	1.3	1.5	1.3	0.8
C		26-52	10YR 6/4	fSms	0.0	0.2	37.0	60.4	0.8	1.6	0.6	0.19	0.17	1.5	4.1	0.9	0.9	0.5	0.5
2Ahb	Unit 3	52-59	10YR 4/3	fS	0.0	0.1	23.1	71.7	2.8	2.2	0.3	0.15	0.15	1.4	4.1	1.5	1.1	0.7	0.7
3Apb		59-72	10YR 4/1	fSms	0.1	0.5	43.8	51.6	3.1	1.1	0.8	0.20	0.19	1.6	4.1	2.2	1.2	0.5	0.4
3Eb	Unit 1/2	72-80	10YR 6/2	mSfs	0.0	0.4	47.4	49.4	2.3	0.4	0.1	0.22	0.19	1.6	4.2	0.6	0.1	0.2	1.0
3Bhb		80-85	7.5YR 2/1	mSfs	0.0	0.3	54.2	43.8	0.6	1.1	1.2	0.23	0.22	1.6	4.0	4.5	6.0	5.5	0.9
3Bmsb		85-112	7.5YR 4/3	mSfs	0.0	0.3	49.5	48.3	0.7	1.1	1.0	0.22	0.20	1.6	4.4	0.6	0.9	0.6	0.7
3C		112-168	10YR 5/6	fSms	0.0	0.1	42.1	55.7	1.0	1.2	0.8	0.20	0.18	1.5	4.4	0.2	0.6	0.2	0.3

Note. Abbrevations: cm bgs = cm below ground surface; G = Gravel, > 2 mm; COS = coarse sand, < 2 mm; MS = medium sand, < 0.63 mm; FS = fine sand, < 0.2 mm; M = Mean; Md = Median; So = Sorting coefficient (Trask 1932); OM = organic matter content. Texture is given according to German Soil Systematics.

aeolian sand | aeolian sand alternating with charcoal/humic layer | humic horizon | mixed horizon | albic material | spodic horizon

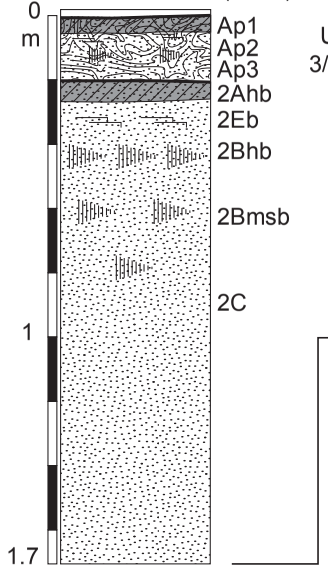

Horizon (WRB)	Aeolian unit	Depth (cm bgs)	Colour (Munsell)	Texture (< 2 mm)	G (wt.%)	COS (wt.%)	MS (wt.%)	FS (wt.%)	Silt (wt.%)	Clay (wt.%)	MS:FS	M (mm)	Md (mm)	So	pH ($CaCl_2$)	OM (%)	Fe_D (g/kg)	Fe_O (g/kg)	Fe_O:Fe_D
Ap1	Unit 3/4/5/6	0-4	10YR 4/1	fS	0.0	0.5	17.6	68.9	7.5	5.5	0.3	0.12	0.13	1.5	2.6	13.5	1.4	0.9	0.7
Ap2		4-13	7.5YR 4/3	fSms	0.0	0.4	28.3	66.6	3.8	0.9	0.4	0.16	0.15	1.5	3.0	3.1	1.8	1.7	0.9
Ap3		13-19	7.5YR 5/3	fSms	0.0	0.5	28.7	66.6	3.2	1.1	0.4	0.16	0.15	1.5	3.3	2.1	1.7	1.4	0.8
2Ahb	Unit 1/2	19-25	10YR 2/1	fSms	0.0	0.6	42.2	52.7	3.5	1.0	0.8	0.19	0.18	1.6	3.3	5.1	0.5	0.1	0.3
2Eb		25-38	7.5YR 5/2	fSms	0.0	0.5	43.9	52.8	2.5	0.3	0.8	0.20	0.19	1.6	3.7	0.9	0.8	0.7	0.9
2Bhb		38-46	10YR 3/1	fSms	0.0	0.4	43.5	52.5	1.1	2.5	0.8	0.21	0.19	1.6	3.6	8.3	0.1	0.1	1.0
2Bmsb		46-81	7.5YR 3/4	fSms	0.0	0.3	43.3	54.4	0.7	1.2	0.8	0.21	0.19	1.5	4.2	1.0	0.7	0.5	0.6
2C		81-172	10YR 5/3	mSfs	0.0	1.0	58.7	38.5	0.5	1.4	1.5	0.25	0.24	1.6	4.4	0.1	1.2	0.9	0.8

Note. Abbrevations: cm bgs = cm below ground surface; G = Gravel, > 2 mm, COS = coarse sand, < 2 mm; MS = medium sand, < 0.63 mm; FS = fine sand, < 0.2 mm; M = Mean; Md = Median; So = Sorting coefficient (Trask 1932); OM = organic matter content. Texture is given according to German Soil Systematics.

Aeolian sand | Aeolian sand alternating with charcoal/humic layer | Humic horizon | Albic material | Spodic horizon

Vertical Section 12

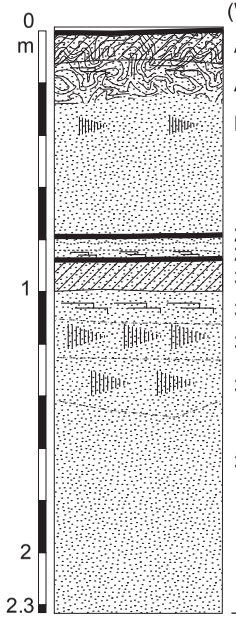

Horizon (WRB)	Unit	Depth (cm bgs)	Colour (Munsell)	Texture (< 2 mm)	G (wt.%)	COS (wt.%)	MS (wt.%)	FS (wt.%)	Silt (wt.%)	Clay (wt.%)	MS:FS	M (mm)	Md (mm)	So	pH ($CaCl_2$)	OM (%)	Fe_D (g/kg)	Fe_O (g/kg)	Fe_O:Fe_D
Ap1	Unit 5/6	0-8	10YR 4/1	fSms	0.0	0.3	23.0	66.8	2.7	7.1	0.3	0.15	0.15	1.4	2.8	16.1	1.9	0.9	0.5
Ap2		8-34	7.5YR 5/2	fS	0.0	0.3	22.1	73.8	2.2	1.6	0.3	0.16	0.15	1.3	3.1	3.3	1.1	0.8	0.7
Bws		34-43	7.5YR 4/3	fS	0.0	0.2	21.7	75.7	0.9	1.5	0.3	0.16	0.16	1.2	3.8	1.6	1.2	0.8	0.7
C		43-61	10YR 6/5	fSms	0.0	0.4	38.9	58.9	0.7	1.0	0.7	0.19	0.17	1.5	4.3	0.2	0.7	0.3	0.6
		61-79	10YR 6/5	fS	0.0	0.1	16.7	80.0	1.3	2.0	0.2	0.13	0.14	1.4	-	0.0	1.2	0.7	-
2Ab?	Unit 3/4	79-81	-	-	-	-	-	-	-	-	-	-	-	-	-	-	-	-	-
2C		81-85	10YR 6/5	fSms	0.0	0.1	38.0	59.6	0.9	1.3	0.6	0.19	0.17	1.5	4.0	0.5	0.7	0.5	0.7
3Ahb	Unit 1/2	85-99	10YR 3/1	mSfs	0.0	0.6	55.8	40.6	1.1	2.0	1.4	0.24	0.23	1.6	3.7	5.1	0.4	0.5	1.0
3Eb		99-113	7.5YR 6/2	mSfs	0.0	0.7	50.9	46.8	0.9	0.8	1.1	0.23	0.21	1.6	3.8	0.5	0.1	0.0	0.7
3Bhb		113-124	10YR 2/1	mSfs	0.0	0.7	46.9	49.3	0.7	2.4	1.0	0.22	0.19	1.6	3.6	9.4	0.4	0.3	0.8
3Bmsb		124-143	7.5YR 3/4	mSfs	0.0	1.2	49.7	46.6	1.0	1.6	1.1	0.22	0.20	1.6	4.1	1.1	1.3	1.1	0.8
3C		143-189	10YR 6/4	mSfs	0.0	0.9	54.2	43.7	0.2	1.1	1.2	0.24	0.22	1.6	4.3	0.1	0.4	0.2	0.5
		189-235	2.5Y 7/4	mSfs	0.0	0.7	50.8	46.9	0.3	1.3	1.1	0.23	0.21	1.6	-	0.1	0.3	0.2	-

Note. Abbrevations: cm bgs = cm below ground surface; G = Gravel, > 2 mm; COS = coarse sand, < 2 mm; MS = medium sand, < 0.63 mm; FS = fine sand, < 0.2 mm; M = Mean; Md = Median; So = Sorting coefficient (Trask 1932); OM = organic matter content. Texture is given according to German Soil Systematics.

Aeolian sand | Aeolian sand alternating with charcoal/humic layer | Humic horizon | Albic material | Spodic horizon

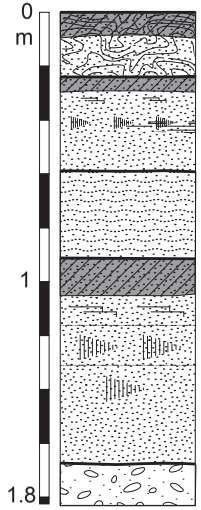

Vertical section 13	Horizon (WRB)	Unit	Depth (cm bgs)	Colour (Munsell)	Texture (< 2 mm)	G (wt.%)	COS (wt.%)	MS (wt.%)	FS (wt.%)	Silt (wt.%)	Clay (wt.%)	MS:FS	M (mm)	Md (mm)	So	pH ($CaCl_2$)	OM (%)	Fe_D (g/kg)	Fe_O (g/kg)	Fe_O:Fe_D	SBD (g/cm³)
	Ap1	6?	0-7	10YR 3/2	fSms	0.5	0.3	35.4	60.4	2.2	1.7	0.6	0.18	0.17	1.5	3.2	3.2	1.1	0.9	0.8	-
	Ap2		7-15	10YR 4/2	fSms	0.6	0.4	31.7	63.4	2.6	1.9	0.5	0.17	0.16	1.5	3.7	2.7	1.1	0.8	0.7	1.5
	Ap3		15-23	7.5YR 3/3	fS	0.1	0.1	22.7	74.5	1.9	0.8	0.3	0.16	0.15	1.3	4.9	1.1	1.0	1.0	1.0	-
	2Ahb	5	23-28	10YR 3/2	fSms	0.0	0.4	23.2	70.3	3.6	2.6	0.3	0.15	0.14	1.5	5.0	5.6	2.8	2.7	0.9	-
	2Eb		28-34	7.5YR 5/2	fSms	0.0	0.2	29.0	67.3	2.5	1.0	0.4	0.16	0.16	1.5	4.3	1.6	0.5	0.3	0.7	-
	2Bwsb		34-42	7.5YR 4/4	fSms	0.0	0.3	28.7	67.4	2.6	1.0	0.4	0.17	0.16	1.5	5.0	1.5	1.2	1.0	0.8	-
	2C		42-56	10YR 6/4	fSms	0.0	0.2	36.9	61.0	0.8	1.1	0.6	0.19	0.17	1.5	4.6	0.6	0.4	0.4	0.9	1.6
	3C	3/4	56-90	10YR 6/5	fSms	0.0	0.3	27.9	68.5	1.9	1.4	0.4	0.16	0.15	1.5	4.5	0.3	0.3	0.1	0.4	1.7
	4Ahb	1/2	90-104	10YR 2/1	fSms	0.0	0.9	35.5	50.0	7.5	6.1	0.7	0.16	0.16	1.8	3.9	11.4	1.4	1.2	0.9	1.1
	4Eb		104-116	7.5YR 5/2	fSms	0.0	0.5	30.5	62.8	5.1	1.1	0.5	0.16	0.15	1.6	4.0	1.2	0.1	0.2	1.2	1.6
	4Bhb		116-126	7.5YR 2/1	fSms	0.0	0.6	30.9	62.6	4.8	1.1	0.5	0.16	0.15	1.6	4.0	3.1	0.1	0.1	1.1	-
	4Bsb		126-146	7.5YR 3/4	fSms	0.0	0.3	38.2	55.3	4.8	1.4	0.7	0.17	0.16	1.7	4.1	3.4	0.2	0.1	0.4	1.5
	4C		146-166	10YR 5/6	mSfs	0.0	1.9	48.1	41.7	7.0	1.2	1.2	0.20	0.20	1.8	4.3	0.7	0.3	0.1	0.5	1.7
	5C	P	166-182	10YR 6/6	Su2	8.3	5.3	35.7	43.9	10.1	5.0	0.8	0.17	0.17	1.9	4.2	0.6	0.4	0.1	0.3	1.8

Note. Abbrevations: cm bgs = cm below ground surface; G = Gravel, > 2 mm; COS = coarse sand, < 2 mm; MS = medium sand, < 0.63 mm; FS = fine sand, < 0.2 mm; M = Mean; Md = Median; So = Sorting coefficient (Trask 1932); OM = organic matter content; SBD = soil bulk density. Texture is given according to German Soil Systematics.

Aeolian sand | Aeolian sand alternating with charcoal/humic layer | Glacial till | Humic mottled layer | Humic horizon | Mixed horizon | Albic material | Spodic horizon

Photograph of profile 1

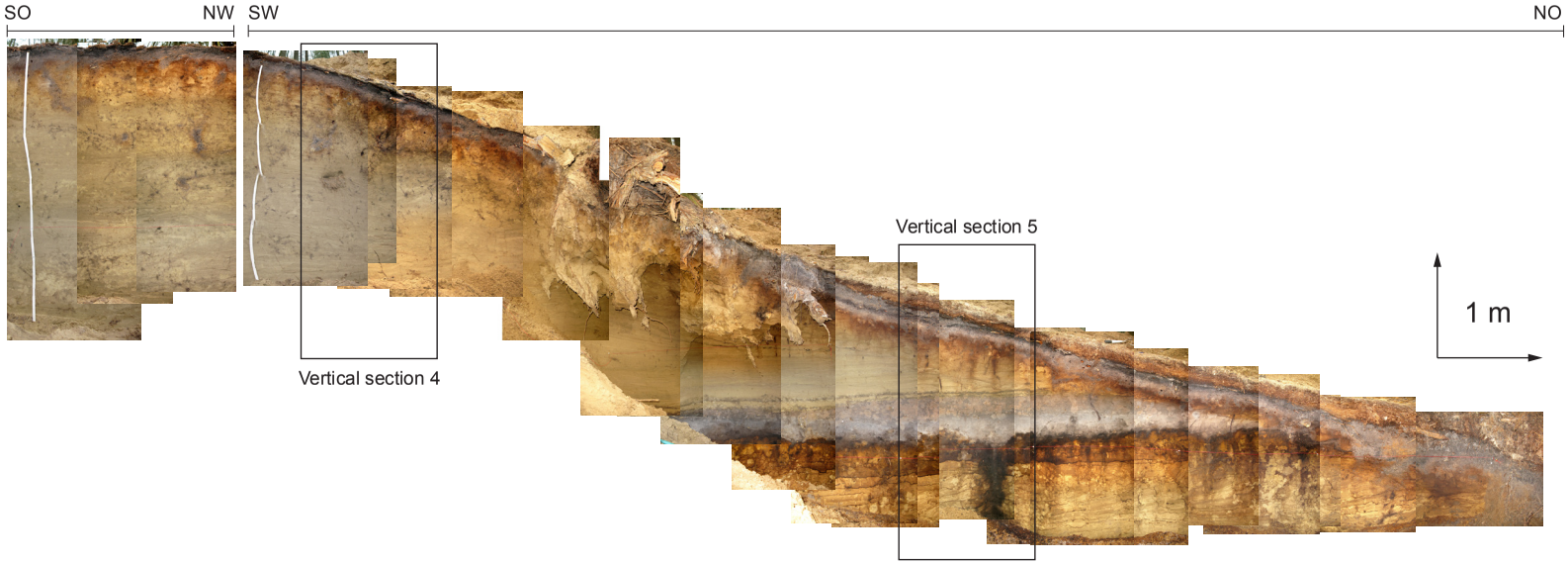

Photograph of profile 2

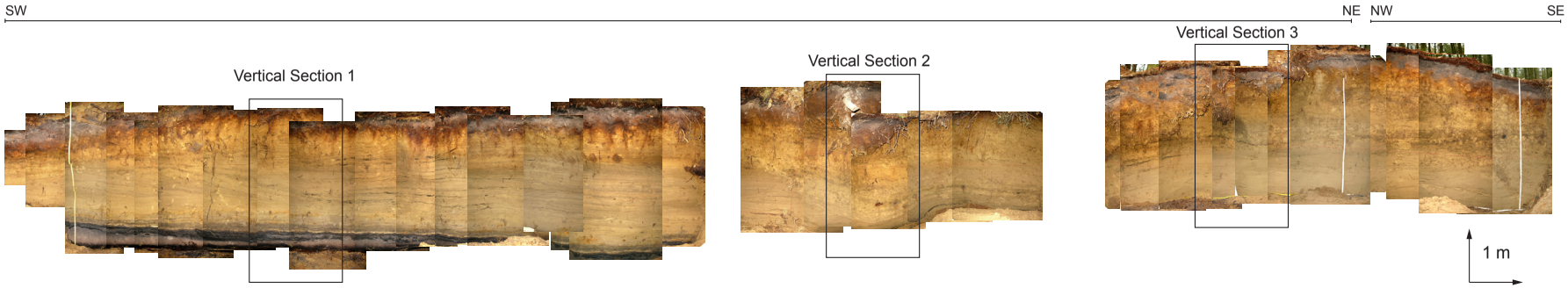

Photograph of profile 3

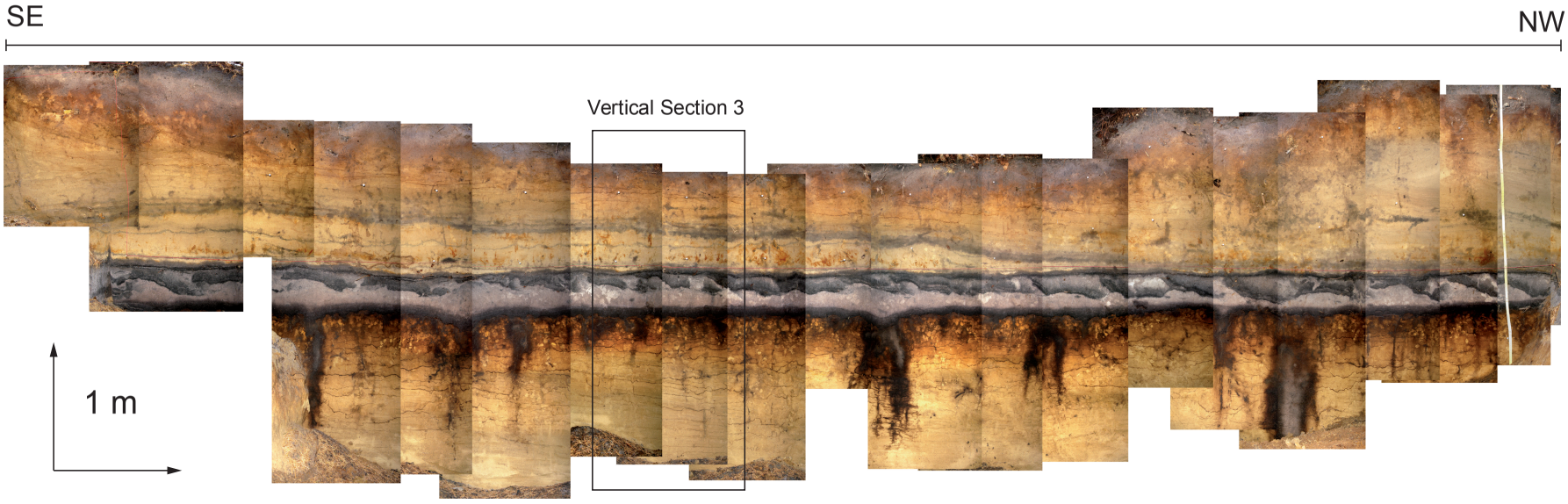

Photograph of profile 4

Photograph of profile 5

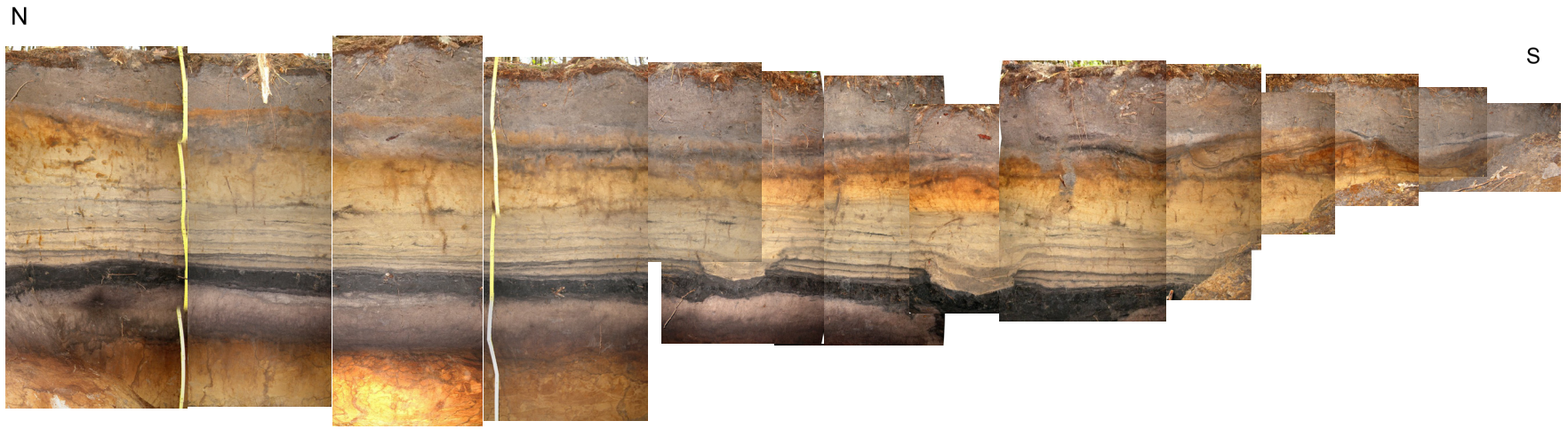

Photograph of profile 6

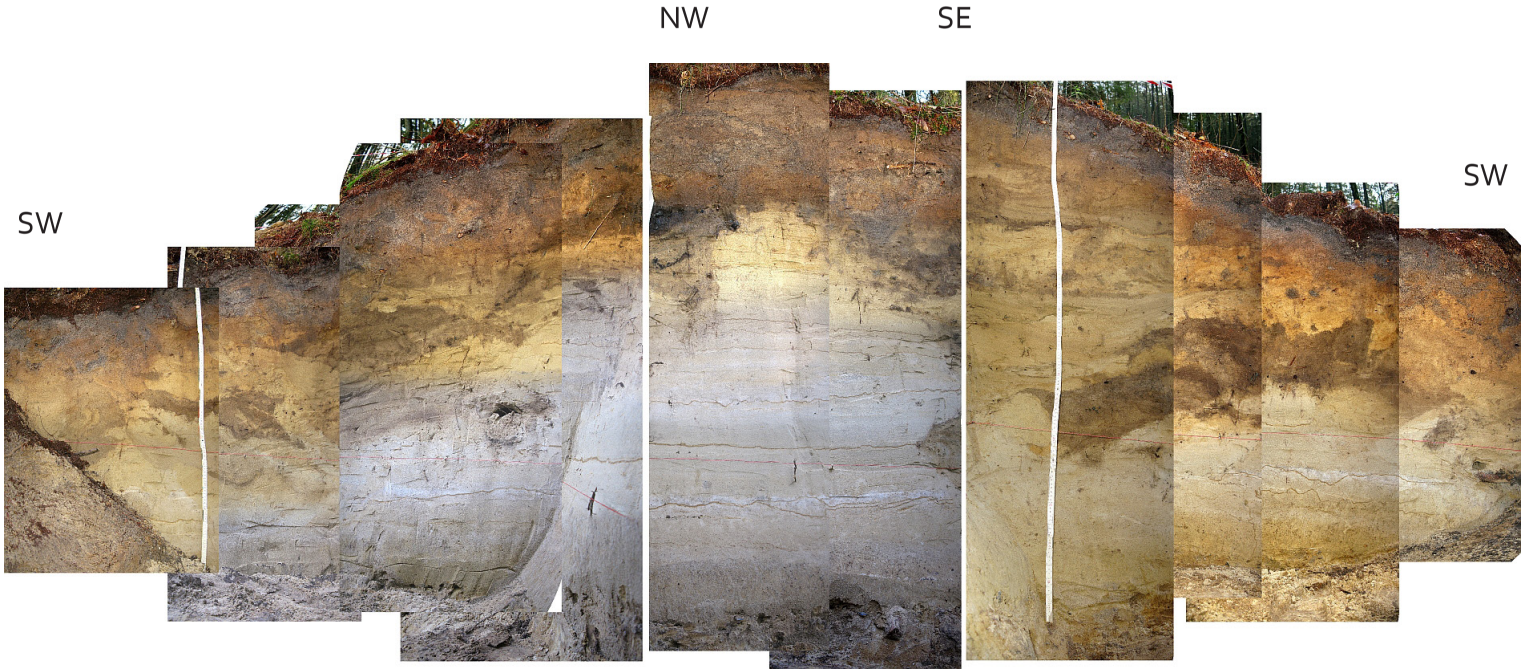

Photograph of profile 8

Appendix 2

Results of AMS ^{14}C dating
Results of OSL dating and measurement report

Radiocarbon dates calibrated with OxCal v.4.1.7. (Bronk Ramsey 2010) using IntCal13 calibration data (Reimer et al. 2013). Abbreviations: Exp.: exposure; M: matter type; C: charcoal; P: peat; SOM: soil organic matter; cf.: lat. confer (engl. compare)

No.	Exp./VS	Lab. ref.	M	Taxon	Context[b]	Depth (m)	$\delta^{13}C$(‰)	PMC (korrigiert)	Radiocarbon age (BP)	cal. BC/AD (2sigma) Int.Cal.13
1	P5 VS13	KIA40624	C	*Populus/Salix*	Unit 3/4, ditch	0.90	93.84 ± 1.06	-31.41 ± 0.51	510 ± 90	1283–1631 cal. AD
2	P5 VS13	KIA45530	P	-	Ditch (filling)	1.10	85.02 ± 0.28	-26-32 ± 0.38	1305 ± 25	660–768 cal. AD
3	P5 VS13	KIA45529	P	-	Ditch (filling)	1.20	78,91 ± 0,28	-25,91 ± 0,29	1905 ± 30	25–211 cal. AD
4	P2 VS2	KIA39157	C	*Quercus*	Unit 5/6	0.40	95.57 ± 0.26	-25.70 ± 0.15	365 ± 20	1453–1631 cal. AD
5	P2 VS3	KIA40623	C	*Quercus*	Unit 5/6	0.80	80.10 ± 0.20	-25.16 ± 0.15	1780 ± 20	142–332 cal. AD
6	P2 VS2	KIA40620	C	Ericaceae	Unit 5/6	0.80	81.73 ± 0.22	-26.32 ± 0.33	1620 ± 20	387–535 cal. AD
7	P2 VS3	KIA45182	C	*Fagus*	Unit 5/6	1.00	88.68 ± 0.28	-29.08 ± 0.08	965 ± 25	1018–1155 cal. AD
8	P1 VS5	KIA39154	C	*Fagus*	Unit 4	0.70	88.51 ± 0.26	-27.41 ± 0.20	980 ± 25	996–1154 cal. AD
9	P2 VS1	KIA39155	C	*Populus/Salix*	Unit 4	0.70	81.98 ± 0.35	-28.54 ± 0.26	1595 ± 35	394–545 cal. AD
10	P8 VS9	KIA45183	C	*Fagus*	Unit 4	0.80	89.13 ± 0.28	-25.06 ± 0.17	925 ± 25	1032–1162 cal. AD
11	P8 VS9	KIA45184	C	*Fagus*	Unit 4	1.40	89.39 ± 0.28	-28.26 ± 0.12	900 ± 25	1040–1209 cal. AD
12	P2 VS1	KIA40621	C	*Populus/Salix*	Unit 4	1.30	89.09 ± 0.22	-26.00 ± 0.18	930 ± 20	1036–1157 cal. AD
13	P2 VS2	KIA41023	C	*Betula*	Unit 3	2.00	85.43 ± 0.25	-28.35 ± 0.12	1265 ± 25	667–800 cal. AD
14	P3 VS6	KIA39156	C	Ericaceae	Unit 2-p	1.10	81.86 ± 0.26	-22.59 ± 0.17	1610 ± 25	395–536 cal. AD
15	P8 VS10	KIA38361	C	Ericaceae	Unit 2-p	0.70–0.90	86.79 ± 0.25	-25.83 ± 0.11	1140 ± 25	777–979 cal. AD
16	P3 VS6	KIA38360	C	Ericaceae	Unit 2-p	1.10–1.20	86.81 ± 0.27	-26.83 ± 0.22	1135 ± 35	777–986 cal. AD
17	P6 VS8	KIA40619[1]	C	c.f. *Alnus*	Unit 1	1.10	-	-	10600 ± 500	11600–8945 cal. BC
18	P12 VS7	KIA37875	SOM	-	Unit 3	0.90–1.00	83.12 ± 0.29	-26.55 ± 0.21	1485 ± 30	474–646 cal. AD
19	P12 VS7	KIA37876	SOM	-	Unit 2-p	1.00–1.01	86.56 ± 0.29	-27.19 ± 0.13	1160 ± 25	775–964 cal. AD
20	P12 VS7	KIA37877	SOM	-	Unit 2-p	1.16–1.17	77.65 ± 0.22	-30.69 ± 0.28	2030 ± 25	111 cal. BC–51 cal. AD

[1] Das Target des Laugenrückstands der Alnus Holzkohle-Probe KIA 40619, A06/SP02, lieferte einen 14C-Gehalt von ca. 27 pMC (Unsicherheit ca. 1,6 pMC) und damit ein berechnetes 14C-Alter rund 10 600 Jahre BP (Unsicherheit ca. 500 Jahre) und ein kalibriertes Alter rund 13 000 Jahre BP, gegen Ende des Allerøds/Anfang des Jüngeren Dryas. Die Kohlenstoffmenge (0,1 mg C) und die Ionenstromstärke (13 % des Normalstroms) sind jedoch zu gering für eine zuverlässige Messung. Das Alter deutet darauf hin, dass es sich bei dieser „Holzkohle" um altes umgelagertes Material handeln könnte.

Results of OSL dating

No.[a]	Exp.	Lab. ref.	Context[b]	Depth (m)	Water content (%)	U (ppm)	Th (ppm)	K (%)	D_{cosmic} (Gy/ka)	D_{total} (Gy/ka)	D_e (Gy)	OSL age (yr)
1	P2	OSZ488	5/6	1.60	0.12	0.43 ± 0.02	1.49 ± 0.07	0.82 ± 0.04	0.19 ± 0.01	1.14 ± 0.10	0.79 ± 0.05	705 ± 75
2	P2	OSZ489	5/6	1.40	0.10	0.37 ± 0.02	0.98 ± 0.05	0.61 ± 0.03	0.19 ± 0.01	0.90 ± 0.08	0.60 ± 0.08	670 ± 105
3	P2	OSZ490	5/6	1.15	0.06	0.29 ± 0.01	1.46 ± 0.07	0.69 ± 0.03	0.19 ± 0.01	1.02 ± 0.09	0.63 ± 0.05	620 ± 75
4	P2	OSZ491	5/6	0.40	0.07	0.52 ± 0.03	1.27 ± 0.06	0.76 ± 0.04	0.20 ± 0.01	1.12 ± 0.10	0.68 ± 0.07	605 ± 85
5	P2	OSZ627	5/6	0.45	0.10	0.39 ± 0.02	1.03 ± 0.05	0.71 ± 0.04	0.19 ± 0.01	1.00 ± 0.09	0.51 ± 0.05	510 ± 70
6	P2	OSZ628	4	1.40	0.10	0.35 ± 0.02	1.00 ± 0.05	0.62 ± 0.03	0.19 ± 0.01	0.90 ± 0.08	0.69 ± 0.04	765 ± 80

[a] refers to figure 2; [b] refers to units 1–6. Abbreviations: Exp.: Exposure; D_{cosmic}: Cosmic dose rate; D_{total}: Total dose rate; D_e: laboratory equivalent dose

Measurement report (source: University of Szeged, provided by Dr. Sipos György)

Results of SAR Test

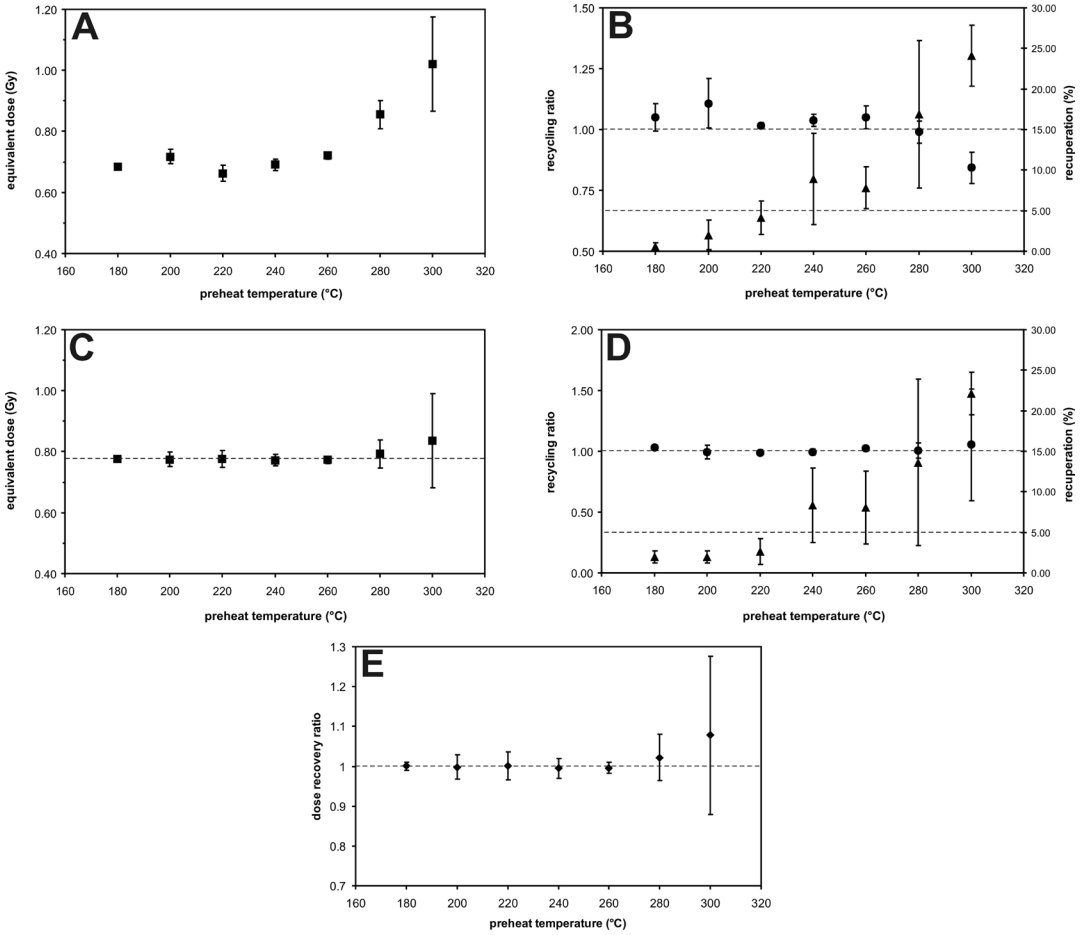

Figure 1: Results of preheat and dose recovery tests, sample **OSZ488**. Each point is the mean of three aliquots, error bars represent the standard deviation of values. **(A)** Equivalent dose of natural discs plotted against preheat temperature. Fairly uniform data were received between 180-260 ℃. **(B)** The change of recycling ratio (filled circle) and recuperation (filled triangle) with preheat temperature in the naturally irradiated samples. In an ideal situation recycling ratio equals 1.00 (marked by the upper dashed line). Note that the most precise results were received at 220 ℃. The malicious effect of recuperation can be disregarded if its value does not exceed 5 % marked by the lower dashed line). Until reaching 240 °C recuperation is well below the threshold. (C) Equivalent dose of artificially irradiated discs plotted against preheat temperature. The recovered dose was 0.78 Gy (marked by the dashed line). Note that the deviation of the average value from the known dose and the variation of individual results was very low in the 180-260 °C r egion. (D) The change of recycling ratio (filled circle) and recuperation (filled triangle) with preheat temperature in the artificially irradiated samples. Recycling ratios are close to unity, and recuperation does not exceed 5 % until reaching 260 °C. (E) Dose recovery at different temperatures (ratio of measured and given dose). Results suggest a high reproducibility of measurements in the 180-260 °C t emperature region. Diagrams indicate the applicability of the SAR protocol. Based on the results for the final measurements a 220 °C preheat temperature was appli ed.

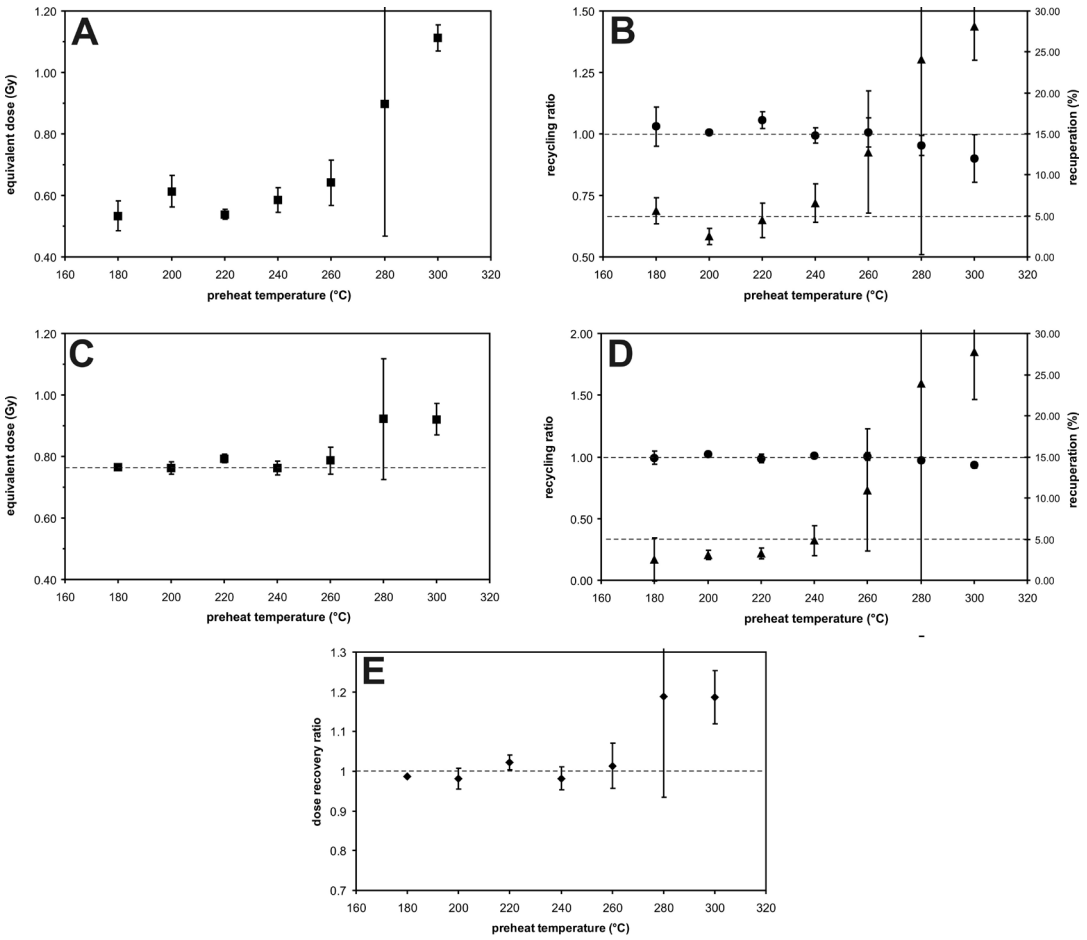

Figure 2: Results of preheat and dose recovery tests, sample **OSZ489**. Each point is the mean of three aliquots, error bars represent the standard deviation of values. **(A)** Equivalent dose of natural discs plotted against preheat temperature. Data show relatively low scatter between 180-260 °C **(B)** The change of recycling ratio (filled circle) and recuperation (filled triangle) with preheat temperature in the naturally irradiated samples. In an ideal situation recycling ratio equals 1.00 (marked by the upper dashed line). Note that the scatter of results is the lowest in the 200-240 °C temperature region. The malicious effect of recuperation can be disregarded if its value does not exceed 5 % (marked by the lower dashed line). Until reaching 240 °C recuperation is well below the threshold. (C) Equivalent dose of artificially irradiated discs plotted against preheat temperature. The recovered dose was 0.78 Gy (marked by the dashed line). Note that the deviation of the average value from the known dose and the variation of individual results was very low in the 180-260 °C region. (D) The change of recycling ratio (filled circle) and recuperation (filled triangle) with preheat temperature in the artificially irradiated samples. Recycling ratios are close to unity, and recuperation does not exceed 5 % until reaching 260 °C. (E) Dose recovery at different temperatures (ratio of measured and given dose). Results suggest a high reproducibility of measurements in the 180-240 °C temperature region. Diagrams indicate the applicability of the SAR protocol. Based on the results for the final measurements a 210 °C preheat tempera ture was applied.

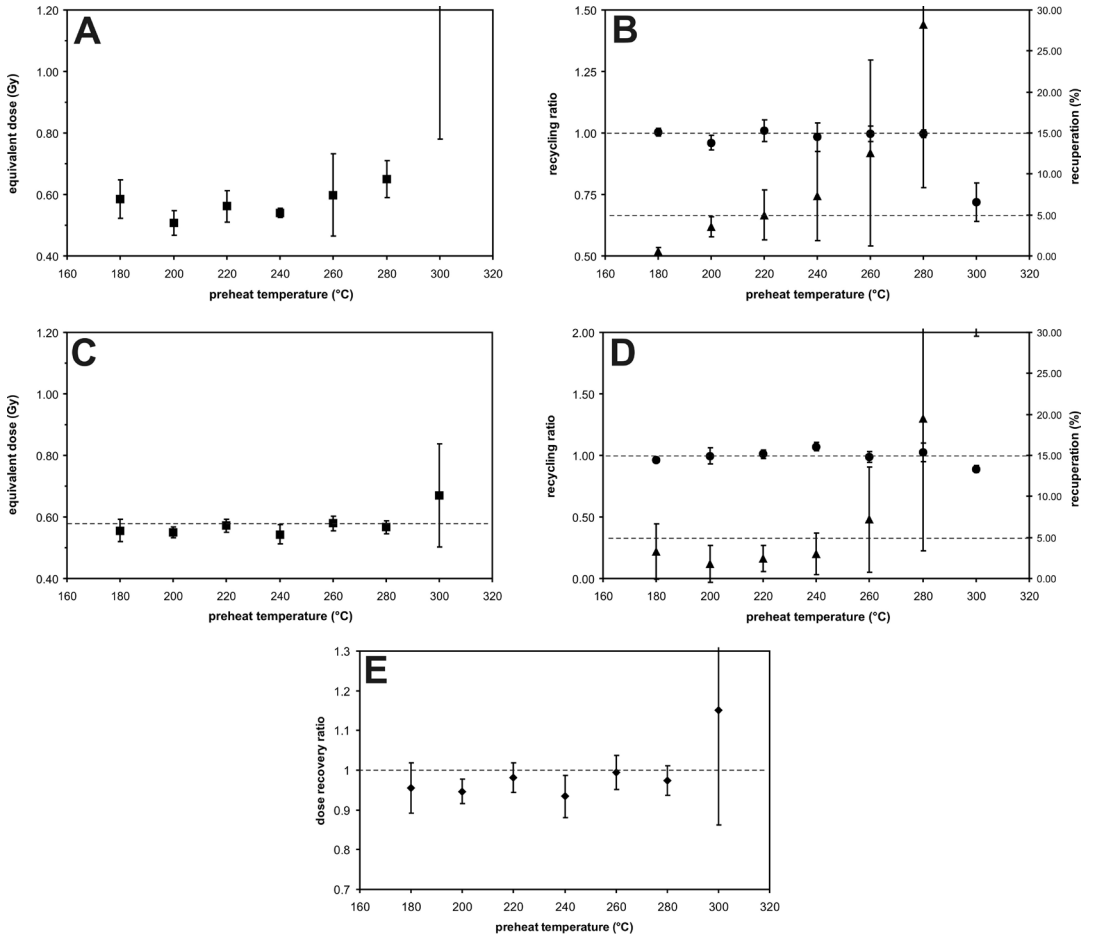

Figure 3: Results of preheat and dose recovery tests, sample **OSZ490**. Each point is the mean of three aliquots, error bars represent the standard deviation of values. **(A)** Equivalent dose of natural discs plotted against preheat temperature. Data show relatively low scatter between 180-240 °C. **(B)** The change of recycling ratio (filled circle) and recuperation (filled triangle) with preheat temperature in the naturally irradiated samples. In an ideal situation recycling ratio equals 1.00 (marked by the upper dashed line). Note that the scatter of results is low in the 180-280 °C temperature region. The malicious effect of recuperation can be disregarded if its value does not exceed 5 % (marked by the lower dashed line). Until reaching 240 °C recuperation is well below the threshold. (C) Equivalent dose of artificially irradiated discs plotted against preheat temperature. The recovered dose was 0.58 Gy (marked by the dashed line). Note that the deviation of the average value from the known dose and the variation of individual results was very low in the 180-280 °C region. (D) The change of recycling ratio (filled circle) and recuperation (filled triangle) with preheat temperature in the artificially irradiated samples. Recycling ratios are close to unity, and recuperation does not exceed 5 % until reaching 260 °C. (E) Dose recovery at different temperatures (ratio of measured and given dose). Results suggest a high reproducibility of measurements in the 180-280 °C temperature region. Diagrams indicate the applicability of the SAR protocol. Based on the results for the final measurements a 210 °C preheat tempera ture was applied.

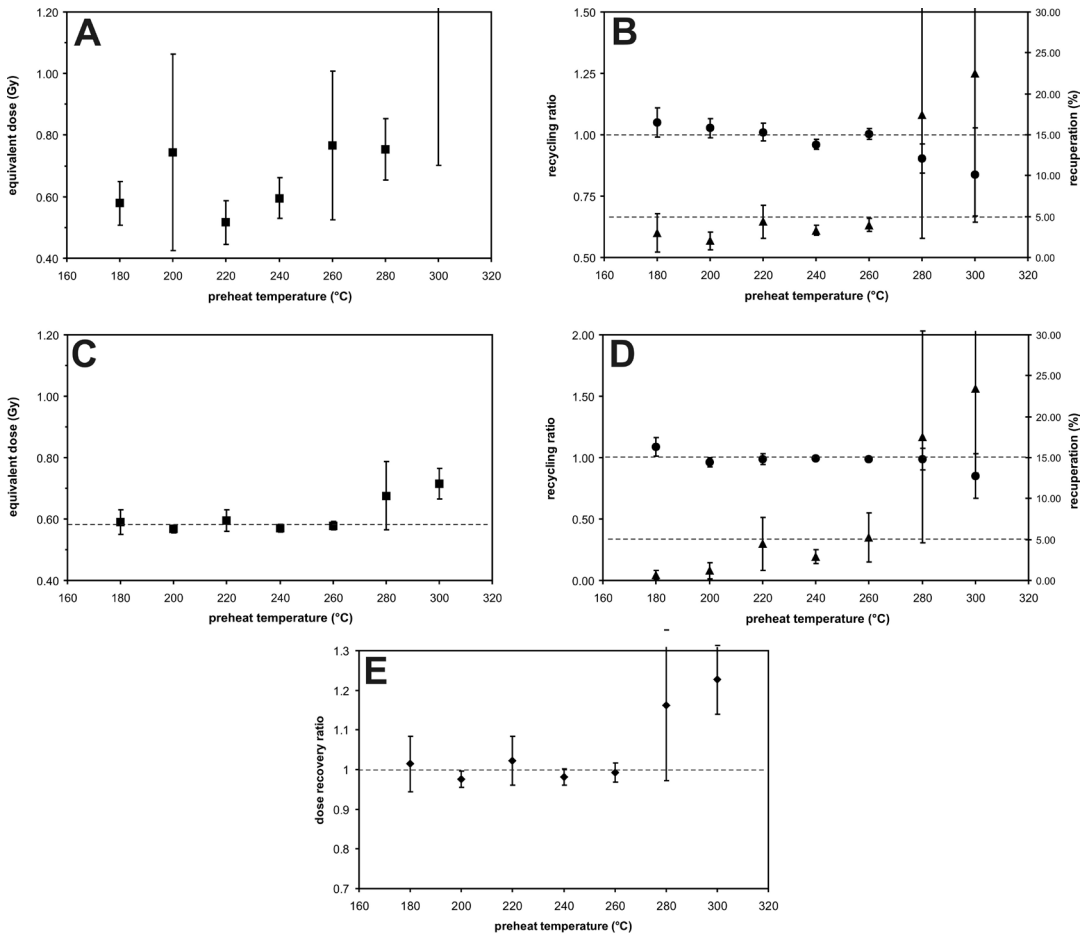

Figure 4: Results of preheat and dose recovery tests, sample **OSZ490**. Each point is the mean of 3 aliquots, error bars represent the standard deviation of values. **(A)** Equivalent dose of natural discs plotted against preheat temperature. Data show relatively low high scatter even at low temperatures. **(B)** The change of recycling ratio (filled circle) and recuperation (filled triangle) with preheat temperature in the naturally irradiated samples. In an ideal situation recycling ratio equals 1.00 (marked by the upper dashed line). Note that the scatter of results is acceptable in the 220-260 ℃ temperature region. The malicious effect of recuperation can be disregarded if its value does not exceed 5 % (marked by the lower dashed line). Until reaching 260 °C recuperation is well below the threshold. (C) Equivalent dose of artificially irradiated discs plotted against preheat temperature. The recovered dose was 0.58 Gy (marked by the dashed line). Note that the deviation of the average value from the known dose and the variation of individual results was low in the 180-260 °C region. (D) The change of recycling ratio (filled circle) and recuperation (filled triangle) with preheat temperature in the artificially irradiated samples. Recycling ratios are close to unity, and recuperation does not exceed 5 % until reaching 260 °C. (E) Dose recovery at different temperatures (ratio of measured and given dose). Results suggest a high reproducibility of measurements in the 180-280 °C temperature region, lowest variation was experienced at 240 °C. Diagrams indicate the applicability of the SAR protocol. Based on the results for the final measurements a 240 °C preheat temperature was applied.

SAR Measurements

Settings used throughout the measurements are shown in Table 1.

Table 1: Measurement parameters for the applied SAR sequences

step	1-6. cycles	7. cycle
1	Dose: 0; 0.39; 0.78; 1.16; 0; 0.78 Gy	Dose: 0.78 Gy
2	Preheat: 210 or 240 ℃ for 10s	Preheat: 210 or 24 0 ℃ for 10s
3	Stimulation: Blue LEDs, 40 s at 125 ℃	Stimulatio n: IR LEDs, 10 s at 50 ℃
4	Test Dose: 1.16 Gy	Stimulation: Blue LEDs, 10 s at 160 ℃
5	Cut heat: 160 ℃ for 0s	
6	Stimulation: Blue LEDs, 40 s at 125 ℃	
7	Stimulation: Blue LEDs, 40 s at 280 ℃	

In the 1st cycle the natural luminescence is measured (Fig 5), in the 2-4th cycles regeneration doses are added to set up the dose response curve, in the 5th cycle no dose is given to explore the effect of preheat and thermal transfer, in the 6th cycle one of the previous regeneration doses is administered again to determine the recycling ratio, in the 7th cycle after artificial dosing Infrared and Blue stimulations are used to identify any feldspar contamination. Test doses and responsive luminescence signals are applied for the normalisation of regenerative data, i.e. the sensitivity correction of the dose response curve (Figure 5).

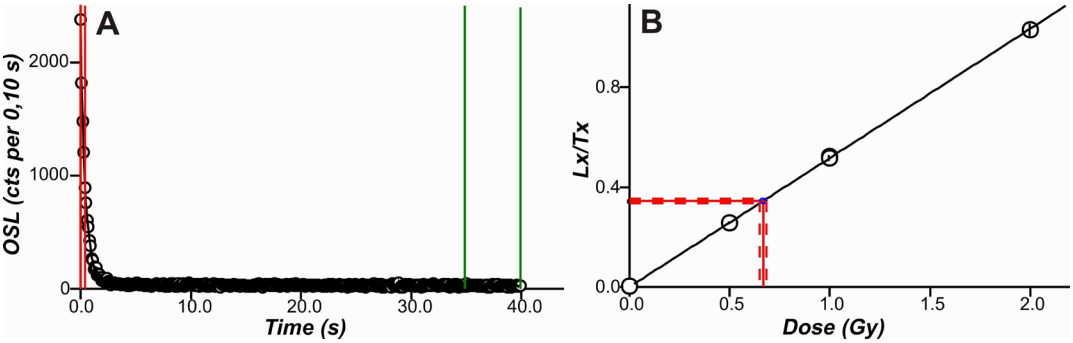

Figure 5.1: (A) Typical natural OSL decay curve of an aliquot bearing sample OSZ488. For the caculaions the first 0.5 s of the curve was applied, the last 5.0 s was taken as background. Note the sharp decay of the curve, which resembles a well behaving sample **(B)** Dose response curve for the same aliquot. Individual points mark the sensitivity corrected luminescence responses for regeneration doses. A linear fit was applied for determining the regression. Red lines refer to the natural luminescence projected onto the curve in order to calculate the naturally absorbed dose from the function of dose and luminescence.

The SAR protocol was run on 24-24 aliquots on each sample, setting up a dose response curve for each aliquot. Some aliquots were however rejected from equivalent dose calculations for the following reasons: the recycling ratio was outside 1.00±0.10 (referring to increased sensitivity change), the recuperation signal was over 5 % of the natural signal (referring to significant charge transfer), the error of the De was larger than 10 % (referring to deviation from linear fitting and error in sensitivity correction), or the IR/OSL ratio measured in the last cycle exceeded 0.05 (referring to feldspar contamination). Table 2 shows the results for each aliquot, and the equivalent dose values which were rejected due to failing the above criteria.

Table 2: Equivalent dose (D_e) data of the measured aliquots. Those aliquots which failed one of the criteria above (marked red) were excluded from further analysis.

aliq.	OSZ488					OSZ489					OSZ490					OSZ491				
	D_e (Gy)	criteria				D_e (Gy)	criteria				D_e (Gy)	criteria				D_e (Gy)	criteria			
		1	2	3	4		1	2	3	4		1	2	3	4		1	2	3	4
1	0.66 ± 0.02					0.58 ± 0.03					0.52 ± 0.04					0.65 ± 0.02				
2	0.77 ± 0.03					0.50 ± 0.03					0.47 ± 0.02					0.65 ± 0.02				
3	0.87 ± 0.03					0.49 ± 0.03					0.49 ± 0.02					0.48 ± 0.03				
4	0.60 ± 0.06					0.50 ± 0.02					0.49 ± 0.03					0.48 ± 0.02				
5	0.72 ± 0.03					0.52 ± 0.02					0.56 ± 0.03					1.30 ± 0.05				
6	0.70 ± 0.03					0.44 ± 0.02					0.54 ± 0.03					0.99 ± 0.04				
7	0.66 ± 0.05					0.49 ± 0.02					0.47 ± 0.03					0.59 ± 0.02				
8	0.74 ± 0.03					0.43 ± 0.02					0.49 ± 0.03					0.55 ± 0.04				
9	0.70 ± 0.03					0.54 ± 0.03					0.62 ± 0.03					0.60 ± 0.03				
10	0.71 ± 0.04					0.53 ± 0.02					0.51 ± 0.02					1.18 ± 0.04				
11	0.70 ± 0.02					0.61 ± 0.02					0.58 ± 0.03					0.55 ± 0.02				
12	0.65 ± 0.02					0.65 ± 0.02					0.51 ± 0.02					0.71 ± 0.04				
13	0.63 ± 0.03					0.53 ± 0.02					0.56 ± 0.02					0.65 ± 0.03				
14	0.73 ± 0.03					0.42 ± 0.01					0.49 ± 0.03					0.65 ± 0.04				
15	0.67 ± 0.02					0.46 ± 0.03					0.55 ± 0.02					0.60 ± 0.02				
16	1.07 ± 0.03					0.63 ± 0.02					0.78 ± 0.03					0.59 ± 0.02				
17	0.64 ± 0.02					0.55 ± 0.02					0.58 ± 0.02					0.71 ± 0.03				
18	0.72 ± 0.02					0.47 ± 0.02					0.49 ± 0.05					0.58 ± 0.02				
19	0.64 ± 0.02					0.51 ± 0.02					0.47 ± 0.03					0.61 ± 0.02				
20	0.69 ± 0.03					0.39 ± 0.02					0.53 ± 0.02					1.59 ± 0.05				
21	0.67 ± 0.04					0.54 ± 0.03					0.53 ± 0.02					0.57 ± 0.03				
22	0.68 ± 0.03					0.53 ± 0.03					0.59 ± 0.02					0.56 ± 0.03				
23	0.65 ± 0.03					0.38 ± 0.05					0.53 ± 0.02					0.69 ± 0.02				
24	0.69 ± 0.03					0.59 ± 0.02					0.61 ± 0.02					0.61 ± 0.03				

Results

Aliquots passing the rejection criteria were applied to calculate the final equivalent dose values. A probability density function was set up from aliquot data. Mean is the weighted mean, error is the weighted standard deviation of individual D_e values (Fig. 6-9). Some of the proper aliquots exhibited extraordinarily high D_e values. The reason for this can be some inherited OSL signals from older depositional phases, i.e. bleaching during the most recent sedimentation was not entirely adequate in case of certain grains. The problem seems however isolated, thus these aliquots were considered as outliers and excluded from later analysis (Fig. 6-9). Equivalent dose results applied later to age calculation are summarised in Table 3.

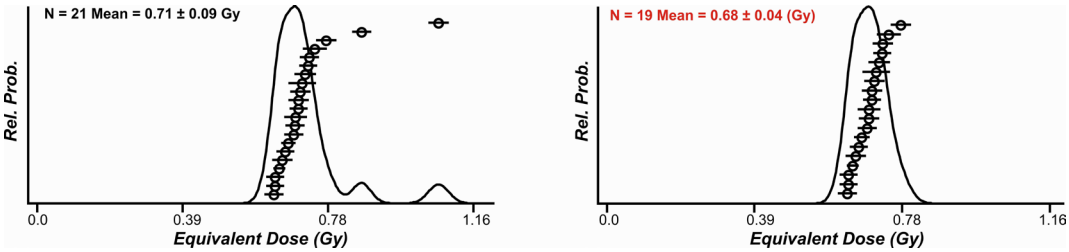

Figure 5: (A) distribution of D_e values of **OSZ488** aliquots passing the rejection procedure. Note the two outliers. **(B)** Refined probability density function by excluding outliers from the analysis. Finally 19 aliquots were applied, the weighted mean of their D_e values is 0.68 ± 0.04.

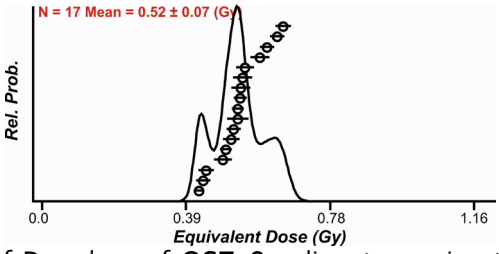

Figure 7: Distribution of D_e values of **OSZ489** aliquots passing the rejection procedure. Note that no true outliers could be identified. The separate peaks of the curve indicate that resetting during deposition was not entirely effective. In all 17 aliquots were applied, the weighted mean of their D_e values is 0.52 ± 0.07.

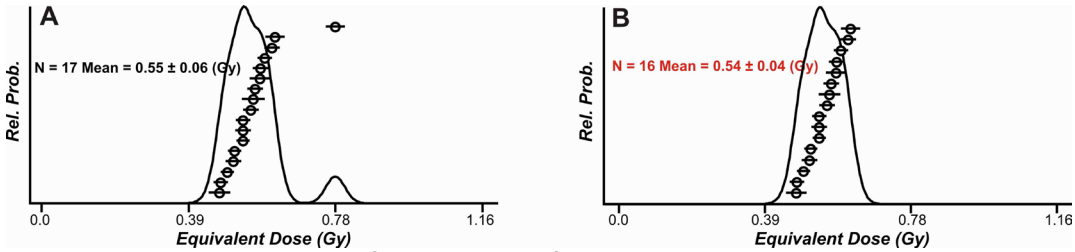

Figure 8: (A) distribution of D_e values of **OSZ490** aliquots passing the rejection procedure. Note the outlier. **(B)** Refined probability density function by excluding the outlier from the analysis. Finally 16 aliquots were applied, the weighted mean of their D_e values is 0.54 ± 0.04.

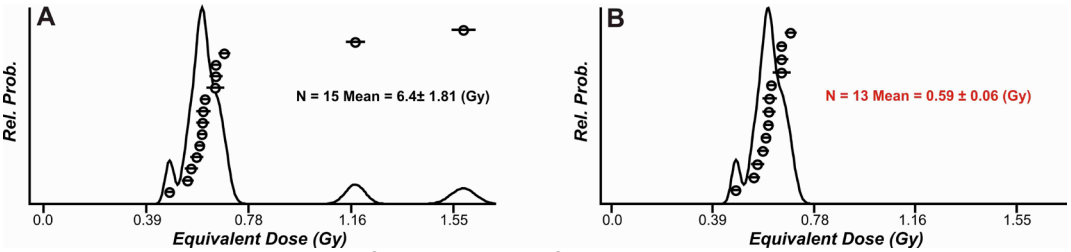

Figure 9: (A) distribution of D_e values of **OSZ491** aliquots passing the rejection procedure. Note the two outliers. **(B)** Refined probability density function by excluding outliers from the analysis. Finally 13 aliquots were applied, the weighted mean of their D_e values is 0.59 ± 0.06.

Appendix 3

Results of palynological and anthracological analysis

Results of anthracological analysis

	Vertical section	Aeolian unit	Quercus		Ericaceae		Fagus		Betula		Alnus		Corylus		Populus / Salix		Salix		Fraxinus		Pinus		other	indeterminata			sums		No. of taxa/ sample
			n	W [g]	n	W [g]	n	W [g]	n	W [g]	n	W [g]	n	W [g]	n	W [g]	n	W [g]	n	W [g]	n	W [g]	Taxon: n=1 (W [g])	dec.	conif.	id.	n	W [g]	
Profile 1	1	4/5	32	0.15	3	0.01	5	0.016	2	0.012	.	.	1	<0.001	.	.	.	.	.	.	.	.	.	2	.	.	45	0.198	5
	1	4/5	11	0.016	3	0.002	4	0.004	.	.	1	0.001	.	.	.	.	.	.	.	.	1	<0.001	Acer (0.003)	.	.	4	25	0.026	6
	1	4	20	0.033	.	.	1	<0.001	.	.	1	<0.001	.	.	.	.	.	.	.	.	.	.	Tilia (<0.001)	2	.	5	30	0.033	4
	1	4	10	--	.	.	.	.	.	.	.	.	.	.	.	.	.	.	.	.	.	.	.	1	.	4	15	0.006	1
	1	2	17	0.048	.	.	3	0.003	.	.	.	.	.	.	.	.	1	<0.001	.	.	.	.	.	.	.	3	25	0.068	4
	1	2	14	0.044	.	.	1	<0.001	.	.	1	0.005	.	.	.	.	.	.	.	.	.	.	.	2	.	.	18	0.054	3
	1	2	13	0.05	.	.	.	.	.	.	.	.	.	.	.	.	.	.	.	.	.	.	.	1	.	1	15	0.059	1
	1	2	9	0.009	.	.	.	.	.	.	.	.	.	.	.	.	.	.	.	.	.	.	.	3	.	.	12	0.010	1
	1; single finds	2, 3	12	0.098	.	.	.	.	.	.	.	.	.	.	.	.	.	.	.	.	.	.	.	.	.	.	12	0.098	1
Profile 2	2	4	17	0.06	.	.	.	.	.	.	1	0.001	.	.	.	.	.	.	.	.	.	.	.	1	.	1	20	0.061	2
	3	5	27	0.073	.	.	1	0.009	.	.	1	0.001	.	.	.	.	.	.	.	.	.	.	.	1	.	1	31	0.083	3
	3	4/5	13	0.044	.	.	.	.	.	.	.	.	1	<0.001	.	.	.	.	1	<0.001	.	.	.	2	.	3	20	0.044	3
	3	4	26	0.077	1	0.001	1	<0.001	.	.	.	.	.	.	.	.	.	.	.	.	.	.	Maloideae (0.004)	1	.	.	30	0.082	4
	3	5	2	--	.	.	.	.	.	.	.	.	.	.	.	.	.	.	.	.	.	.	.	.	.	.	2	--	1
	4	5	18	0.031	.	.	.	.	.	.	1	0.002	.	.	.	.	.	.	.	.	.	.	.	1	.	.	20	0.034	2
	4	5	28	0.228	2	0.001	.	.	.	.	.	.	.	.	.	.	.	.	.	.	.	.	.	.	.	.	30	0.229	2
	4	5	20	0.082	2	0.006	.	.	.	.	.	.	.	.	.	.	.	.	.	.	.	.	.	.	.	.	22	0.088	2
	4	5	31	0.124	.	.	.	.	.	.	.	.	.	.	.	.	.	.	.	.	.	.	.	.	.	.	31	0.124	1
	4	4	26	0.043	.	.	4	0.003	1	0.002	.	.	.	.	.	.	.	.	.	.	.	.	.	.	.	.	31	0.048	3
	4	3	16	0.029	1	--	.	.	4	0.005	.	.	.	.	.	.	.	.	2	0.003	.	.	.	.	.	2	25	0.038	4
	4	3	18	0.02	1	0.001	1	0.001	1	0.003	.	.	1	0.002	.	.	.	.	.	.	.	.	Tilia (0.001)	.	.	2	25	0.030	6
	5	4/5	36	0.21	1	0.009	2	0.015	1	0.01	.	.	.	.	1	0.013	.	.	.	.	.	.	.	.	.	.	41	0.257	5
	5	4	35	0.132	.	.	1	0.001	1	0.009	3	0.001	.	.	1	--	.	.	.	.	.	.	.	.	.	.	41	0.143	5
	5	4	44	0.217	1	<0.001	2	0.005	.	.	3	0.013	.	.	.	.	.	.	.	.	.	.	.	.	.	.	50	0.235	4
	5	4	32	0.077	1	--	1	0.001	3	0.009	.	.	1	0.001	.	.	.	.	.	.	.	.	.	.	.	2	40	0.092	5
	5	4	23	0.103	.	.	1	0.006	3	0.027	.	.	1	0.004	.	.	.	.	.	.	1	0.003	Lonicera (0.001)	.	.	.	30	0.144	6
	5	3/4	11	0.009	.	.	.	.	.	.	.	.	.	.	.	.	.	.	.	.	.	.	.	.	.	4	15	0.010	1
	5	3	.	.	10	0.009	.	.	.	.	.	.	.	.	.	.	.	.	.	.	.	.	.	.	.	.	10	0.009	1
Profile 3	6	4/5	24	0.054	1	0.003	2	0.001	1	<0.001	.	.	1	0.001	.	.	.	.	1	<0.001	.	.	.	.	.	.	30	0.059	6
	6	3	2	<0.001	.	.	1	<0.001	.	.	.	.	.	.	.	.	.	.	.	.	.	.	.	1	.	1	5	<0.001	2
	6	3	2	0.005	2	0.003	1	0.002	.	.	.	.	.	.	.	.	.	.	.	.	.	.	.	1	.	1	7	0.010	3
	6	2a	.	.	1	--	.	.	.	.	.	.	.	.	.	.	.	.	.	.	.	.	.	.	.	.	1	--	1
	6	2a	.	.	.	.	.	.	.	.	.	.	.	.	.	.	.	.	.	.	.	.	.	3	.	.	3	--	.
	6	2a	3	<0.001	114	0.362	.	.	.	.	.	.	.	.	.	.	.	.	.	.	.	.	.	2	.	1	120	0.365	2
	6	2a	.	.	78	0.371	.	.	.	.	.	.	.	.	.	.	.	.	.	.	.	.	.	.	.	.	78	0.371	1
P 4	12	3	8	0.013	5	0.01	.	.	.	.	.	.	.	.	.	.	.	.	.	.	.	.	.	3	.	4	20	0.023	2
P 5	12	4/5	24	0.098	2	0.005	2	0.004	2	.	1	0.005	1	<0.001	.	.	.	.	.	.	.	.	.	1	.	2	35	0.112	6
	13	ditch	1	<0.001	2	0.003	.	.	.	.	.	.	.	.	.	.	.	.	.	.	.	.	.	3	.	.	6	0.003	2
P 6	13	ditch	24	0.065	2	0.001	.	.	1	0.003	.	.	.	.	.	.	.	.	.	.	.	.	.	2	.	1	30	0.069	3
	13	4/5	22	0.02	1	<0.001	.	.	.	.	.	.	.	.	1	--	.	.	.	.	1	<0.001	.	.	.	3	28	0.020	4
P 8	8	1	.	.	.	.	.	.	5	--	cf.	--	.	.	.	.	1	--	.	.	1	--	.	5	3	1	17	--	4
	8; pit	2	5	0.064	.	.	.	.	.	.	.	.	.	.	.	.	.	.	.	.	.	.	.	.	.	.	5	0.064	5
Profile 8	9	4/5	12	0.025	.	.	2	0.008	.	.	1	0.001	.	.	.	.	.	.	.	.	.	.	.	.	.	2	17	0.034	3
	9	4	16	0.066	3	0.016	1	0.004	1	0.003	.	.	.	.	.	.	1	0.002	.	.	.	.	Acer (0.006)	3	.	2	28	0.097	6
	9	4	25	0.119	.	.	5	0.021	1	0.002	.	.	.	.	.	.	.	.	.	.	.	.	Maloideae (0.002)	3	.	.	35	0.144	4
	9	4	21	0.131	3	0.012	4	0.03	.	.	.	.	.	.	1	0.007	.	.	.	.	.	.	.	.	.	1	30	0.180	4
	9	4	16	0.057	1	<0.001	3	0.015	.	.	.	.	1	0.001	.	.	.	.	2	0.003	.	.	Acer (0.003), Maloideae (<0.001)	3	.	2	30	0.079	7
	9	3	.	.	5	0.011	.	.	.	.	.	.	.	.	.	.	.	.	.	.	.	.	.	5	.	.	10	0.011	1
	9	2a	38	0.121	84	0.442	.	.	.	.	.	.	.	.	.	.	.	.	.	.	.	.	.	.	.	.	122	0.563	2
Profile 11	7	5	2	<0.001	.	.	2	0.002	.	.	.	.	.	.	6	0.004	1	<0.001	.	.	.	.	bark (0.001)	3	.	2	17	0.008	4
	7	4/5	23	0.055	2	0.001	1	0.001	1	<0.001	.	.	2	<0.001	.	.	.	.	.	.	.	.	.	1	.	.	30	0.057	5
	7	4	16	0.052	.	.	.	.	.	.	.	.	1	0.003	.	.	.	.	.	.	.	.	Maloideae (0.001)	1	.	.	19	0.056	3
	7	4	12	0.009	1	<0.001	.	.	.	.	1	<0.001	.	.	.	.	.	.	.	.	.	.	Tilia (<0.001)	5	.	.	20	0.009	4
Total sum:			857	2.965	333	1.279	52	0.152	28	0.085	16	0.03	12	0.018	10	0.024	4	0.002	6	0.006	4	0.003	11; 0.021	62	3	55	1454	4.637	15
% of taxa-identified:			64.2	64.7	25.0	27.9	3.9	3.3	2.1	1.9	1.2	0.7	0.9	0.4	0.8	0.5	0.3	<0.1	0.5	0.1	0.3	0.1	0.9; 0.40				1333	4.585	

Results of pollen analysis

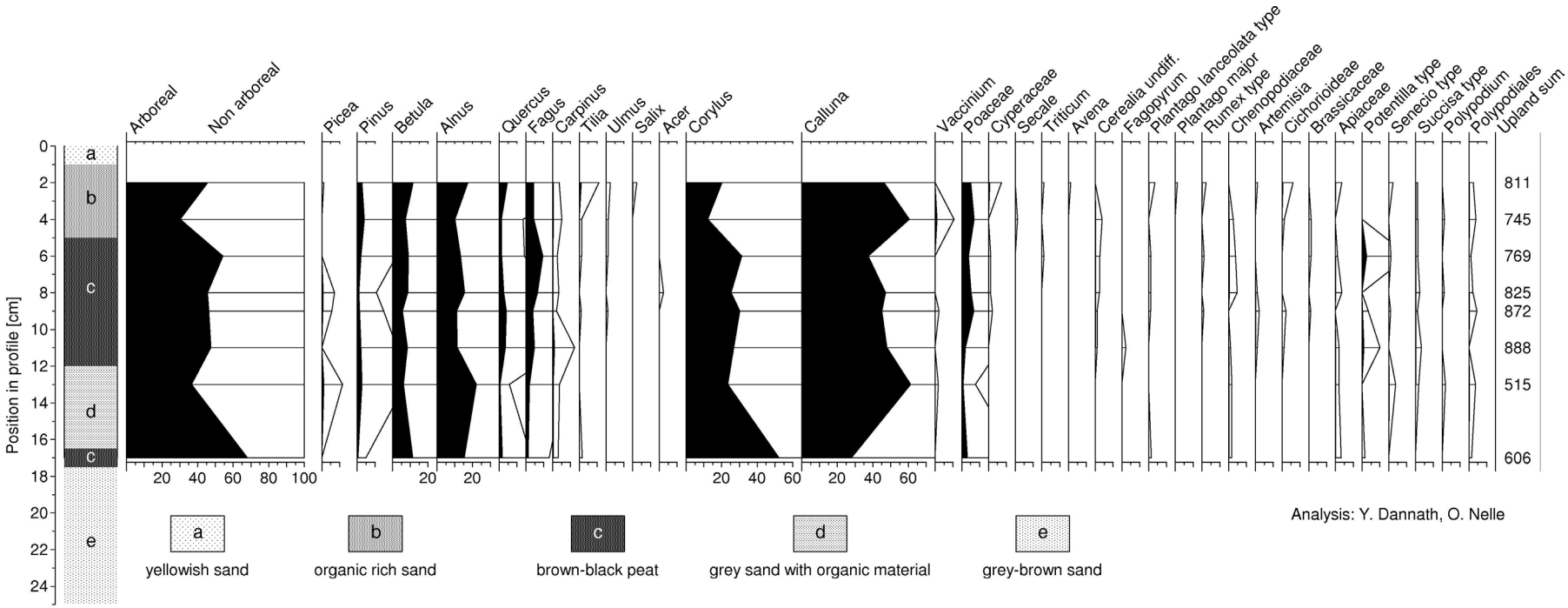

Appendix 4

TIN-models of former dunes surfaces using ArcGIS 10.1

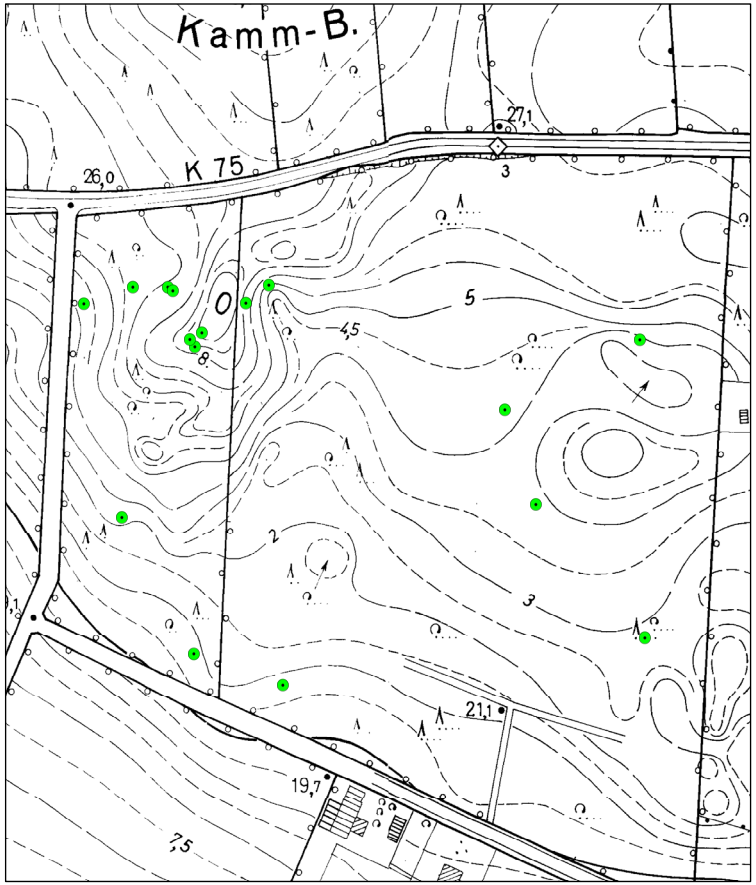

© GeoBasis-DE/LVermGeoSH
(www.LVermGeoSH.schleswig-hosltein.de) Source: DGK5

Legende

- Measured depth of stratigraphic unit P

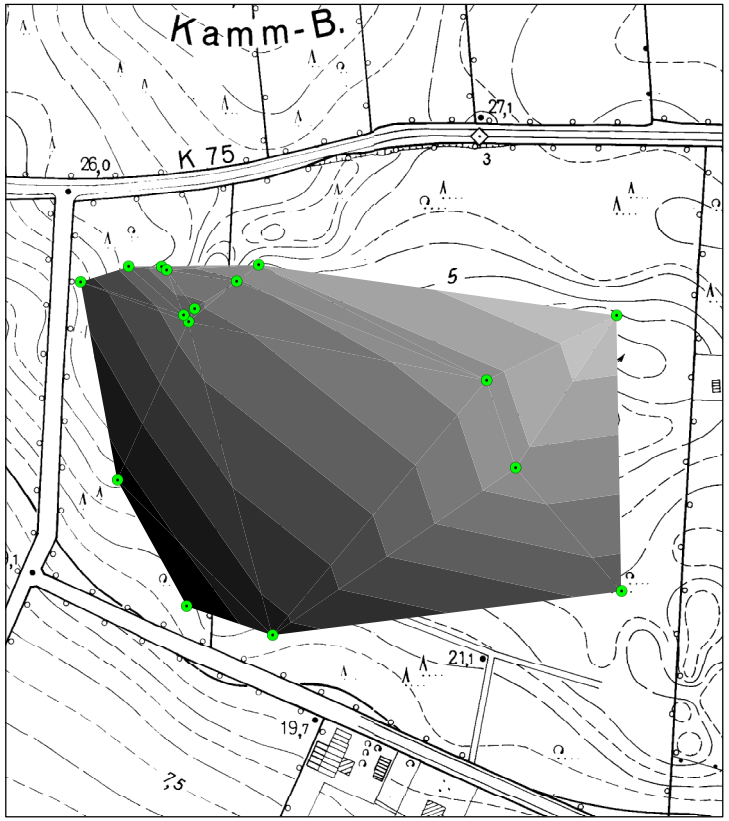

© GeoBasis-DE/LVermGeoSH
(www.LVermGeoSH.schleswig-hosltein.de) Source: DGK5

Legende

- Measured depth of stratigraphic unit P

Tin model of stratigraphic unit P
Elevation (m NHN)

- 24,6 - 25,3
- 23,9 - 24,6
- 23,2 - 23,9
- 22,5 - 23,2
- 21,8 - 22,5
- 21,2 - 21,8
- 20,5 - 21,2
- 19,8 - 20,5
- 19,1 - 19,8

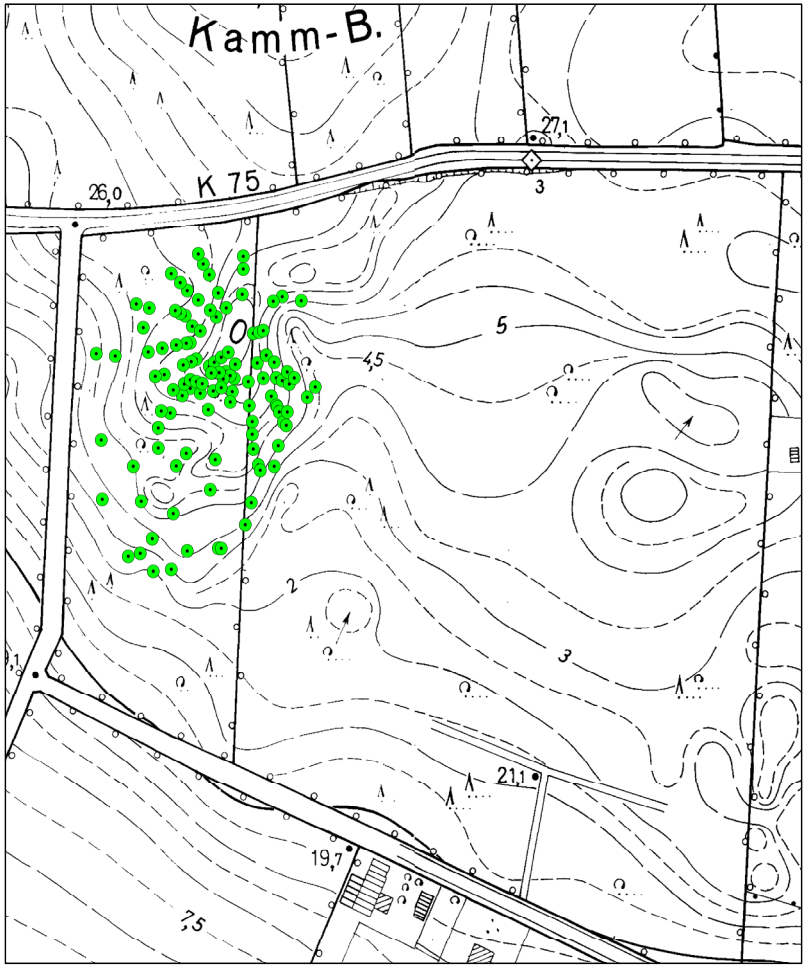

0 25 50 100 Meters

© GeoBasis-DE/LVermGeoSH
(www.LVermGeoSH.schleswig-hosltein.de) Source: DGK5

Legend

- Measured depth of stratigraphic unit 2

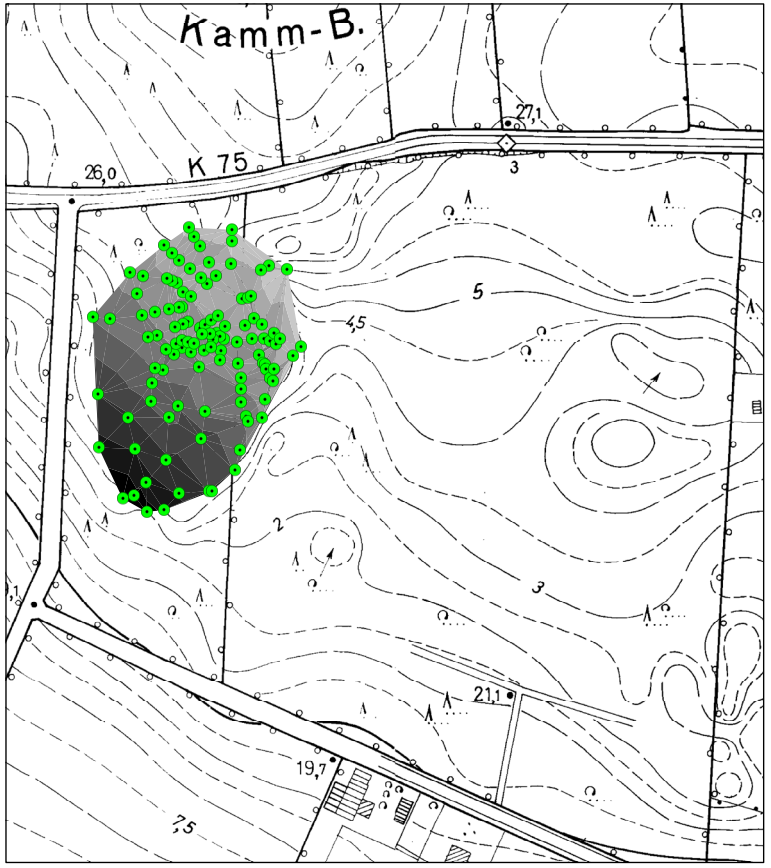

0 25 50 100 Meters

© GeoBasis-DE/LVermGeoSH
(www.LVermGeoSH.schleswig-hosltein.de) Source: DGK5

Legend

- Measured depth of stratigraphic unit 2

TIN model of stratigraphic unit 2

Elevation (m NHN)

25,9 - 26,5	23,6 - 24,2
25,3 - 25,9	23 - 23,6
24,7 - 25,3	22,5 - 23
24,2 - 24,7	21,9 - 22,5
	21,3 - 21,9

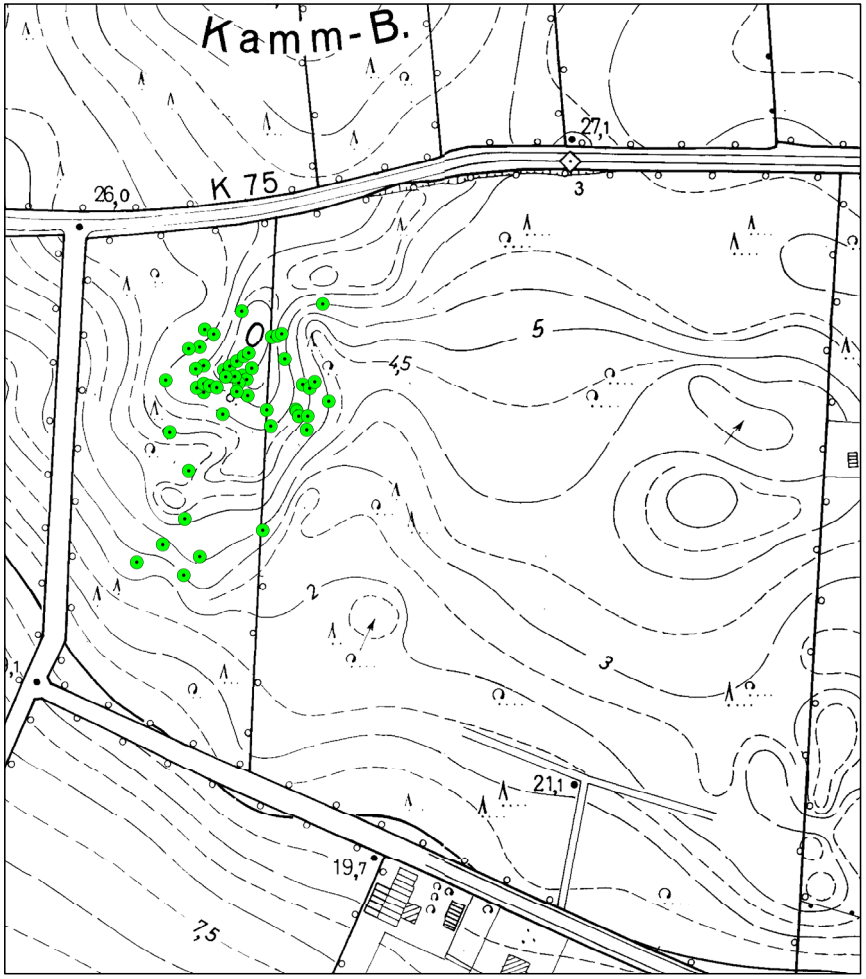

0 25 50 100 Meters

© GeoBasis-DE/LVermGeoSH
(www.LVermGeoSH.schleswig-hosltein.de) Source: DGK5

Legend

- Measured depth of stratigraphic unit 3

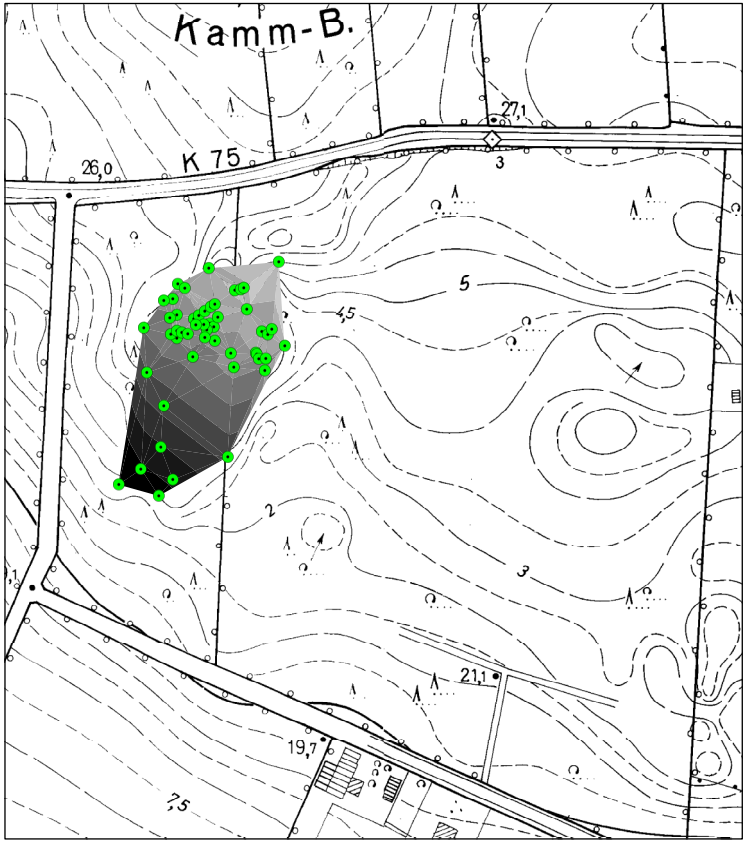

0 25 50 100 Meters

© GeoBasis-DE/LVermGeoSH
(www.LVermGeoSH.schleswig-hosltein.de) Source: DGK5

Legende

- Measured depth of stratigraphic unit 3

TIN model of stratigraphic unit 3
Elevation (m NHN)

25,8 - 26,5	24,5 - 25
25,4 - 25,8	24,1 - 24,5
25 - 25,4	23,6 - 24,1
	23 - 23,6
	22,4 - 23
	21,4 - 22,4

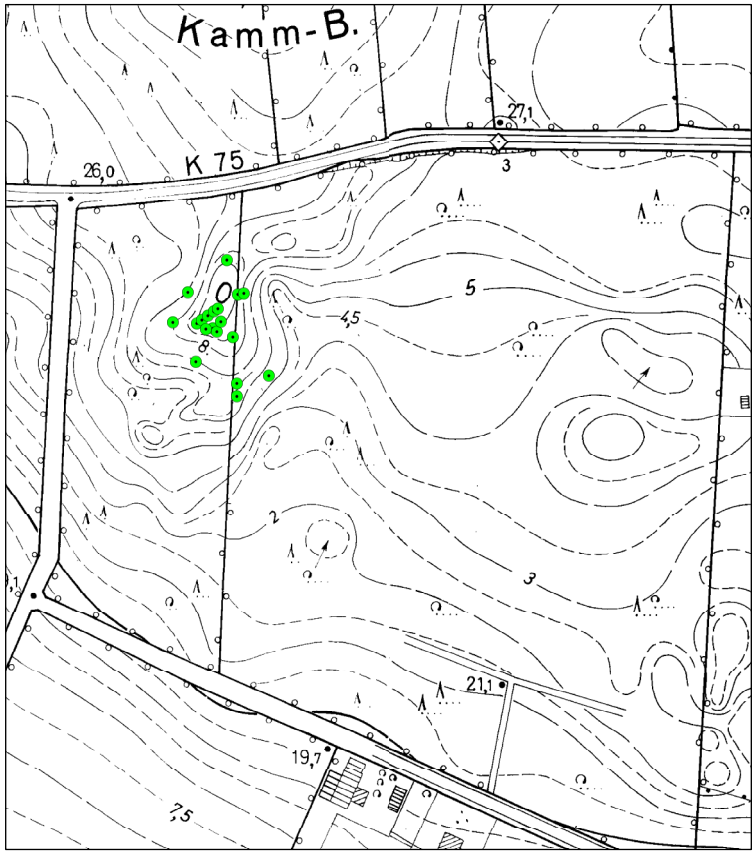

© GeoBasis-DE/LVermGeoSH
(www.LVermGeoSH.schleswig-hosltein.de) Source: DGK5

Legend

- Measured depth of stratigraphic unit 4

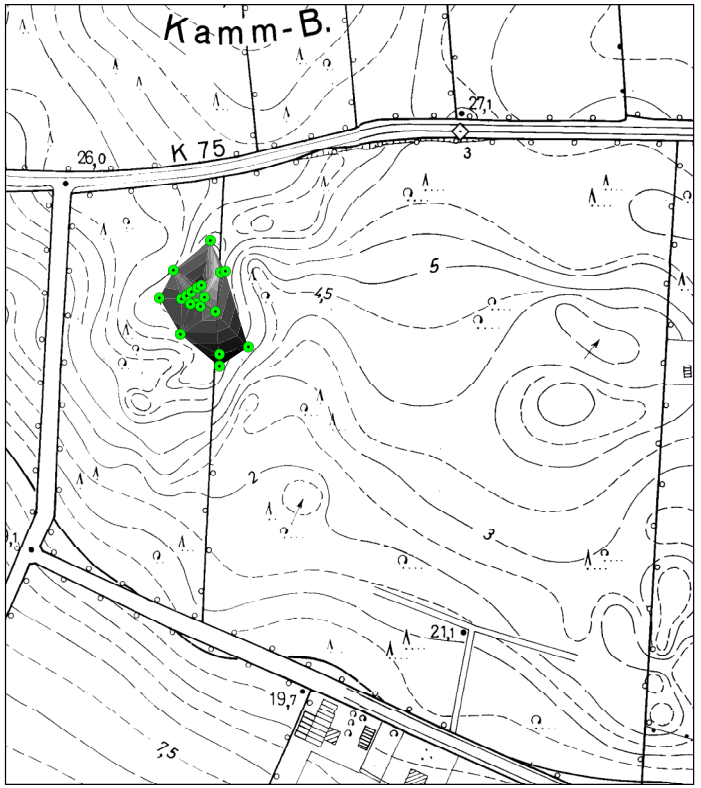

© GeoBasis-DE/LVermGeoSH
(www.LVermGeoSH.schleswig-hosltein.de) Source: DGK5

Legende

- Measured depth of stratigraphic unit 4

TIN model of stratigraphic unit 4

Elevation (m NHN)

- 27,4 - 27,7
- 27,1 - 27,4
- 26,8 - 27,1
- 26,5 - 26,8
- 26,2 - 26,5
- 25,9 - 26,2
- 25,5 - 25,9
- 25,2 - 25,5
- 24,9 - 25,2

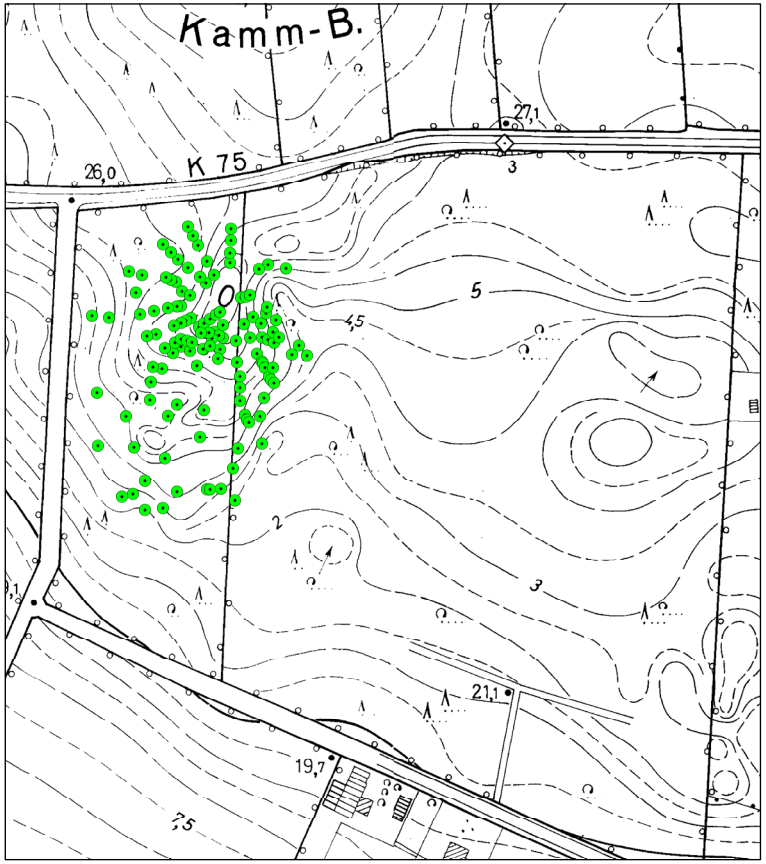

© GeoBasis-DE/LVermGeoSH
(www.LVermGeoSH.schleswig-hosltein.de) Source: DGK5

Legend

- Measured depth of stratigraphic unit 5/6

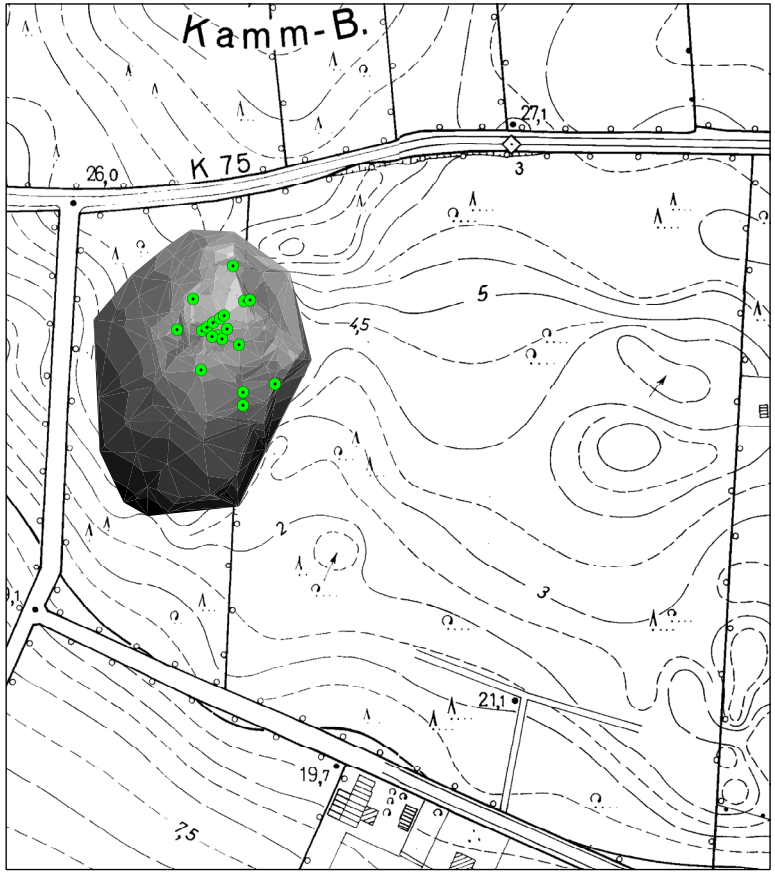

© GeoBasis-DE/LVermGeoSH
(www.LVermGeoSH.schleswig-hosltein.de) Source: DGK5

Legende

- Measured depth of stratigraphic unit 4

TIN model of stratigraphic unit 5/6

Elevation (m NHN)

- 27,8 - 28,5
- 27,1 - 27,8
- 26,4 - 27,1
- 25,6 - 26,4
- 24,9 - 25,6
- 24,2 - 24,9
- 23,4 - 24,2
- 22,7 - 23,4
- 22 - 22,7

Appendix 5

3D visualizations (referring to LUNGERSHAUSEN et al. 2013)

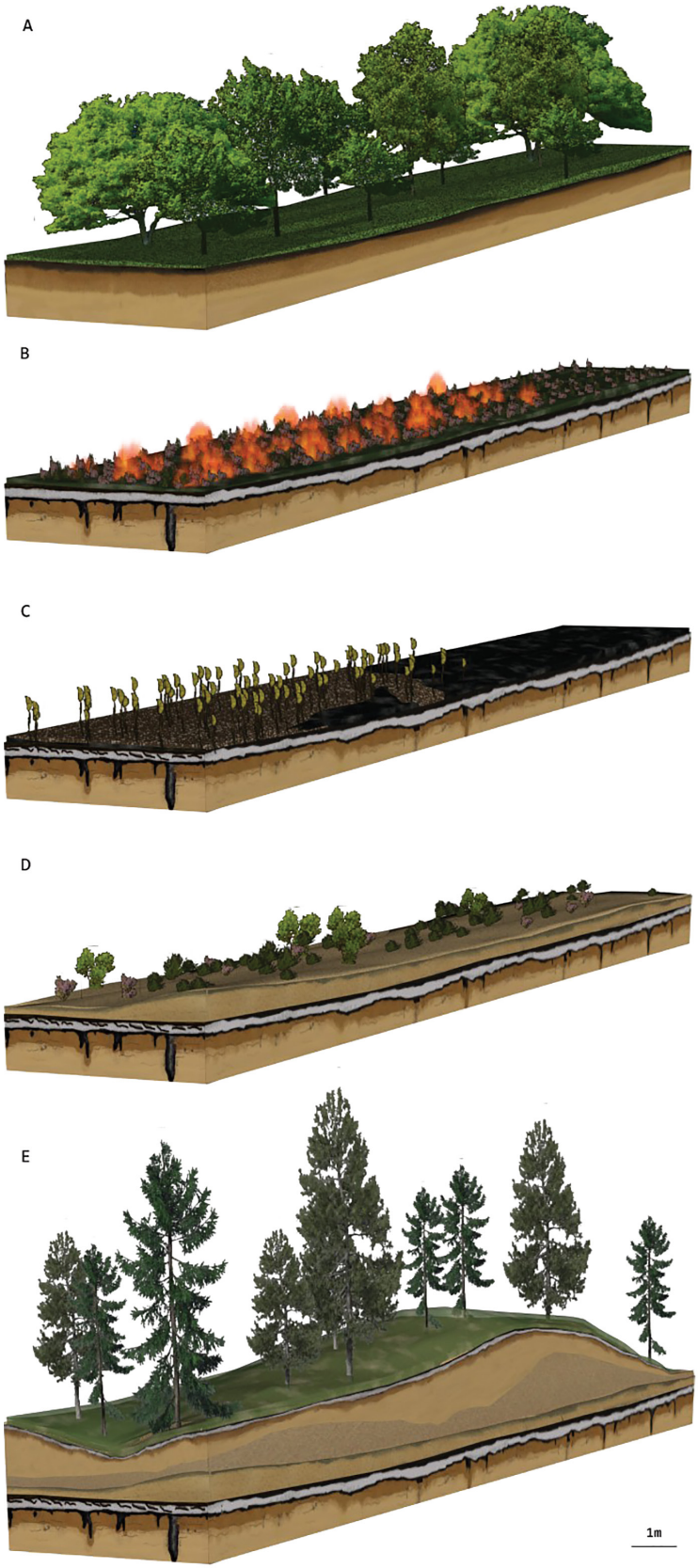
A
B
C
D
E
1m

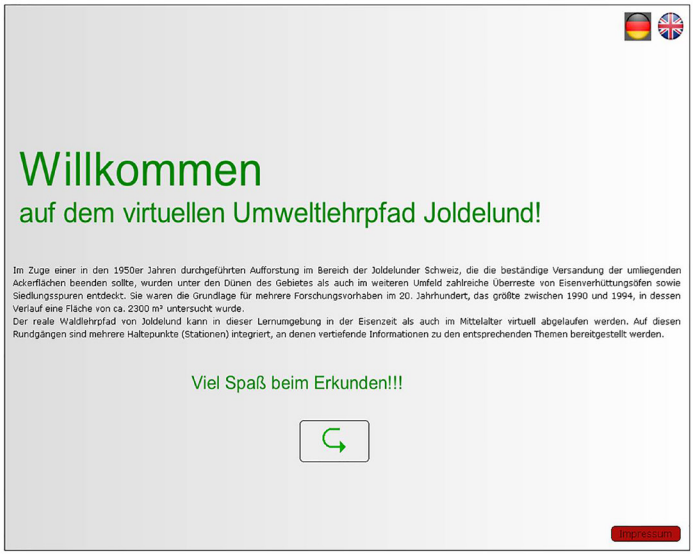

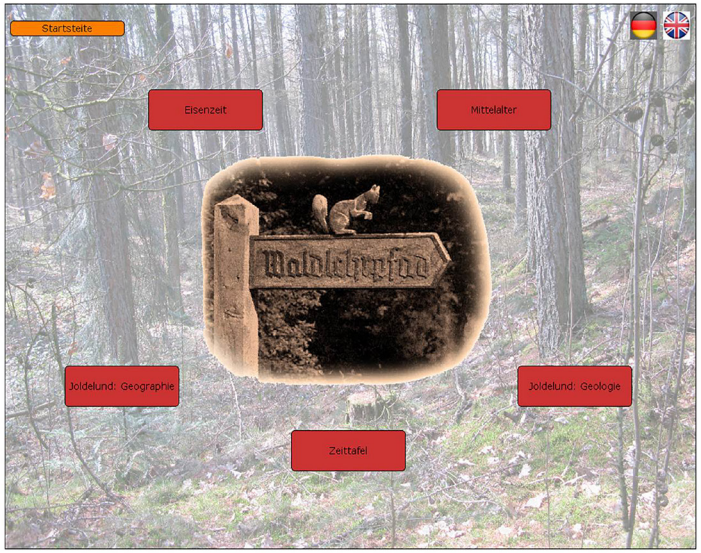

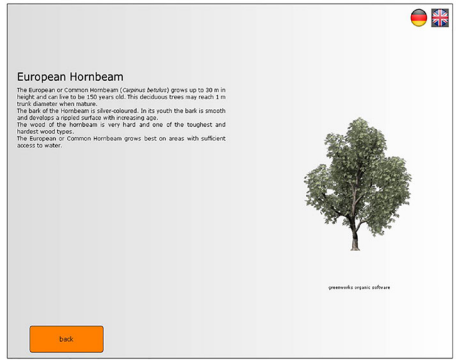

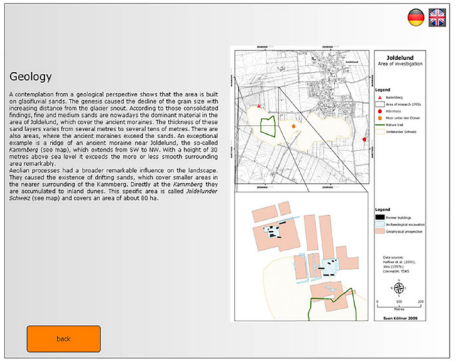

Learning environemtent with integrated regional visualisation created with Visual Nature Studio™2.86 (Source: S. Köllner)

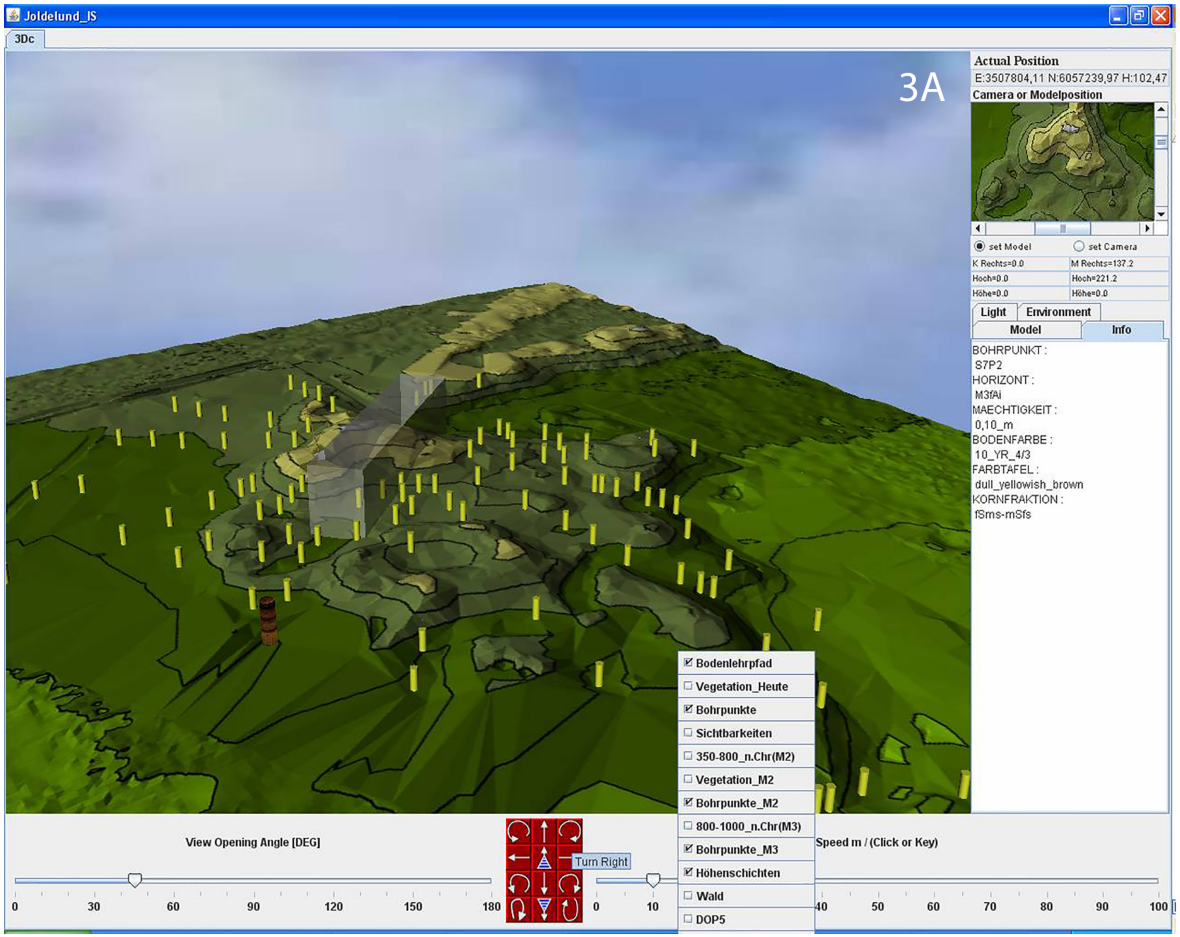

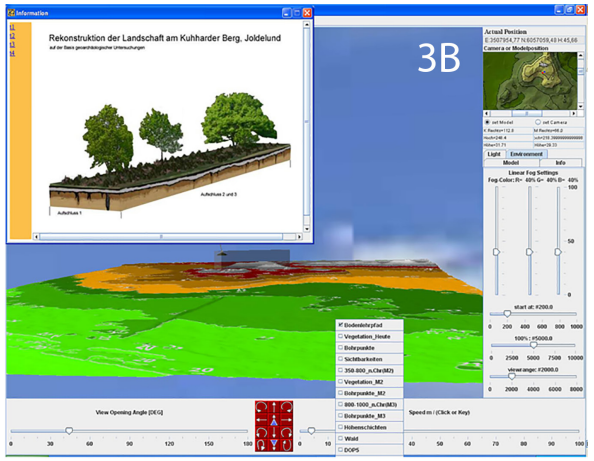

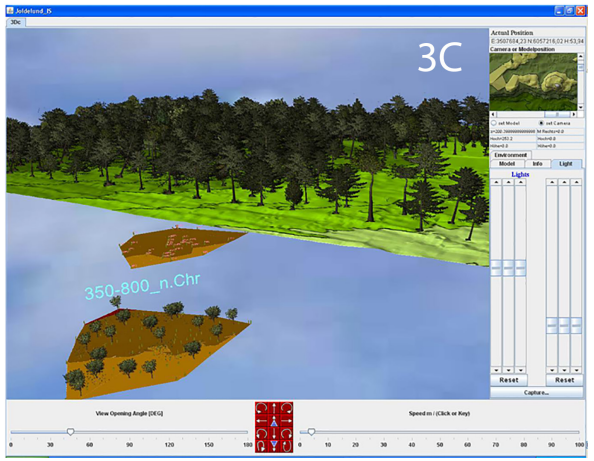

Screenshots of the 3D real-time environemtent a3dc

Lebenslauf

Anschrift:	Uta Lungershausen Leibnizstr. 15 55118 Mainz
Geburtsdatum, -ort:	29.07.1980, Schwerin
Nationalität:	Deutsch

Akademische Ausbildung

04/2008–09/2016	Promotion, Geographisches Institut, Christian-Albrechts-Universität zu Kiel
10/2001–02/2008	Diplomstudium der Geographie, Bodenkunde und Landschaftsentwicklung, Christian-Albrechts-Universität zu Kiel Abschluss: Diplom, Note: 1.3 Thema der Diplomarbeit: Die langfristige Veränderung der Insel Sylt – Visualisierung möglicher Entwicklungen, Note: 1.0
10/2000–09/2001	Diplomstudium der Geoökologie, Universität Potsdam